

Universidade Federal de Minas Gerais
Programa de Pós-Graduação em Engenharia Elétrica
Escola de Engenharia

Meshless Methods in Electromagnetic Wave Scattering

Williams Lara de Nicomedes

Belo Horizonte, February 2011

DISSERTAÇÃO DE MESTRADO Nº 651

MESHLESS METHODS IN ELECTROMAGNETIC WAVE SCATTERING

Williams Lara de Nicomedes

DATA DA DEFESA: 04/02/2011

Universidade Federal de Minas Gerais

Escola de Engenharia

Programa de Pós-Graduação em Engenharia Elétrica

**MESHLESS METHODS IN ELECTROMAGNETIC WAVE
SCATTERING**

Williams Lara de Nicomedes

Dissertação de Mestrado submetida à Banca Examinadora designada pelo Colegiado do Programa de Pós-Graduação em Engenharia Elétrica da Escola de Engenharia da Universidade Federal de Minas Gerais, como requisito para obtenção do Título de Mestre em Engenharia Elétrica.

Orientador: Prof. Fernando José da Silva Moreira

Belo Horizonte - MG

Fevereiro de 2011

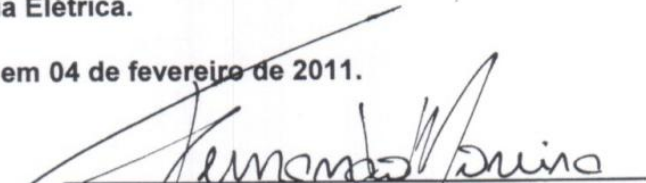
"Meshless Methods in Electromagnetic Wave Scattering"

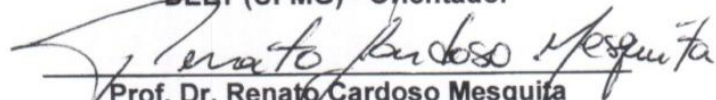
Williams Lara de Nicomedes

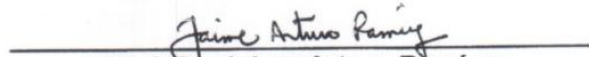
Dissertação de Mestrado submetida à Banca Examinadora designada pelo Colegiado do Programa de Pós-Graduação em Engenharia Elétrica da Escola de Engenharia da Universidade Federal de Minas Gerais, como requisito para obtenção do grau de Mestre em Engenharia Elétrica.

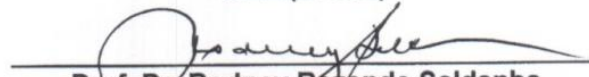
Aprovada em 04 de fevereiro de 2011.

Por:


Prof. Dr. Fernando José da Silva Moreira
DELT (UFMG) - Orientador


Prof. Dr. Renato Cardoso Mesquita
DEE (UFMG) - Co-Orientador


Prof. Dr. Jaime Arturo Ramírez
DEE (UFMG)


Prof. Dr. Rodney Rezende Saldanha
DEE (UFMG)

By nature, all men long to know.
Aristotle, *Metaphysics*, Book Alpha, 980a.

To my father, my mother and my brother (Head).

Abstract

This dissertation addresses the application of meshless techniques to a number of problems occurring in Electrical Engineering. These meshless methods are relatively new and innovative when compared to more traditional approaches like finite element, finite difference and moment methods. As a consequence, problems from many different areas are nowadays being attacked through the meshless procedures for the first time. Probably in the near future they will occupy a prominent place among the tools analysts, engineers, physicists and mathematicians resort to when faced by situations whose solution is not possible through analytical methods. However, lots of work and research still need to be done. In this dissertation, many aspects of the meshless methods in contexts such those of electrostatics, electromagnetic wave scattering and quantum mechanics will be clarified. Particular attention is paid to the implementation of the Meshless Local Petrov-Galerkin (MLPG) method, and to its variant, the Local Boundary Integral Equation (LBIE) method. Problems dealing with the scattering of waves by conducting and dielectric cylinders, photonic crystals, capacitors, and numerical solutions of Schrödinger equation (energy levels) are all addressed in detail. Themes like shape functions, integral equations, partial differential equations, boundary and interface conditions, boundary value and eigenvalue problems in two and three dimensions, among others, will be discussed in the pages to follow. The purpose of this dissertation is to expose and illustrate the concepts from meshless analysis that could serve as a basis for future works. By the end of the text, it is expected that a substantial insight into the mechanisms of meshless methods be gained by the reader.

Resumo

Esta dissertação versa sobre a aplicação de técnicas sem malha a vários problemas ocorrentes em Engenharia Elétrica. Esses métodos são relativamente novos e inovadores quando comparados com abordagens mais tradicionais como elementos finitos, diferenças finitas e o método dos momentos. Consequentemente, problemas de diversas áreas estão atualmente sendo atacados pelos métodos sem malha pela primeira vez. Provavelmente, no futuro eles ocuparão um lugar proeminente entre as ferramentas que analistas, engenheiros, físicos e matemáticos recorrerão quando se depararem com situações e problemas cuja solução seja impossível de ser encontrada através de métodos analíticos. Entretanto, muito trabalho e pesquisa ainda precisam ser feitos. Nesta dissertação, muitos aspectos dos métodos sem malha em contextos tais como eletrostática, espalhamento de ondas eletromagnéticas e mecânica quântica serão clarificados. Atenção particular é devotada à implementação do método MLPG (Meshless Local Petrov-Galerkin), e de uma sua variante, o método LBIE (Local Boundary Integral Equation). Problemas que lidam com o espalhamento de ondas por cilindros condutores bem como dielétricos, cristais fotônicos, capacitores e com a solução numérica da equação de Schrödinger (níveis de energia) serão todos tratados detalhadamente. Temas tais como funções de forma, equações integrais, equações diferenciais parciais, condições de contorno e interface, problemas de valor de contorno e problemas de autovalores em duas e três dimensões, entre outros, serão discutidos nas próximas páginas. O propósito da presente dissertação é expor e ilustrar conceitos da análise *meshless* que poderiam servir de base para trabalhos futuros. Ao final do texto, é esperado que o leitor tenha ganhado um *insight* substancial no que diz respeito aos mecanismos por detrás dos métodos sem malha.

Acknowledgements

This work could not have been brought to its full completion without the contributions of the individuals below. Each one gave a parcel of what proved to be absolutely fundamental to the production of this dissertation. They are:

Prof. Fernando Moreira, who gave me the opportunity to join his research group, and who willingly has arranged me scholarships (since the time I was an undergraduate!);

Prof. Renato Mesquita, who introduced me to the field of meshfree analysis (and this happened in a most unexpected way, since originally my research purposes were aimed at another direction);

Prof. Cassio Rego and Prof. Odilon Filho, who, through their classes, gave me a more profound knowledge of electromagnetic theory, so necessary for this work;

Prof. Reinaldo Palhares and all the CPDEE staff, who provided all the support for the academic activities throughout the Master's course.

To all of them... Thank you!

Agradecimentos

Este trabalho não poderia ter alcançado um patamar satisfatório sem a contribuição dos indivíduos listados abaixo. Cada um deu uma parcela que se revelou absolutamente fundamental para a produção desta dissertação. São eles:

Prof. Fernando Moreira, que permitiu que eu me associasse a seu grupo de pesquisa, e que benevolmente me tem conseguido bolsas de estudo (desde o tempo em que eu era um estudante de graduação!);

Prof. Renato Mesquita, que me apresentou ao campo de estudo dos métodos sem malha (e isso aconteceu de uma maneira totalmente inesperada, visto que primeiramente meus interesses de pesquisa estavam direcionados para um outro rumo);

Prof. Cássio Rego e Prof. Odilon Filho, que através de suas aulas, me proporcionaram acesso um conhecimento mais profundo sobre teoria eletromagnética, tão necessário para este trabalho);

Prof. Reinaldo Palhares e toda a equipe do CPDEE, que ofereceram todo o apoio para a realização das atividades acadêmicas durante o curso de mestrado.

A todos eles... Muito obrigado!

Resumo Estendido

Introdução

Os métodos sem malha (geralmente referenciados pelas expressões *meshless* ou *meshfree*) são uma família de procedimentos computacionais destinados à solução numérica de equações diferenciais parciais. Operacionalmente, tais métodos realizam as mesmas tarefas que métodos mais tradicionais, como o método de elementos finitos (FEM) e o método de diferenças finitas (FDTD), entre outros. Isto é, dada uma equação diferencial parcial, os métodos sem malha são aptos (ou pelo menos deveriam ser) a fornecer uma solução numérica para essa equação, da maneira mais acurada possível. Mas esses métodos resolvem equações de uma maneira bastante peculiar, baseando-se numa característica tão distinta que ela acabou por dar nome à inteira família de métodos: a completa ausência de malhas.

Mas o que viria a ser isso? O que seria uma malha? De maneira bastante informal (e sem qualquer intenção de expor definições e raciocínios rigorosos), uma malha seria uma subdivisão do domínio no qual uma dada equação deve ser resolvida. Uma equação diferencial deve ser satisfeita num domínio Ω , i.e., uma porção limitada do espaço uni, bi ou tridimensional. Ao se resolver essa equação num computador, os métodos tradicionais “quebram” o domínio Ω numa coleção de pedaços menores. O domínio pode ser subdividido de maneira regular, como no caso do FDTD, dando origem a uma malha estruturada, ou de maneira irregular (mas obviamente obedecendo a critérios específicos), originando uma malha irregular, prática comum no FEM.

Os métodos sem malha, por outro lado, não trabalham com subdivisões do domínio. Uma vez que Ω é definido, espalha-se sobre ele um conjunto de N pontos (chamados de *nós*), aos quais se associam certas funções, conhecidas como *funções de forma* (ou *de base*). A solução da equação para qualquer ponto $\vec{x} \in \Omega$ é então calculada como uma soma ponderada de funções de forma calculadas em \vec{x} . Em suma, isso seria a essência dos métodos sem malha. Não parece muito complicado, mas há um longo caminho a percorrer para se achar os pesos da soma ponderada citada acima. Há diversas maneiras de se calculá-los, cada uma dando origem a um diferente método (estamos a falar de uma família de métodos). Alguns são mais formidáveis do que outros, é claro, mas todos compartilham dessa mesma filosofia, que, aliás, é o tema do capítulo 2 dessa dissertação.

Os primeiros estudos a respeito dos métodos sem malha datam do início da última década. Ainda estão na sua “infância”, e ainda há muitos desafios que precisam ser explorados [Liu, 2003]. Praticamente todos eles são oriundos do campo da Mecânica Computacional, onde foram inicialmente (e ainda têm sido) aplicados a problemas de elasticidade, hidrodinâmica e mecânica dos sólidos, entre outros. Em Eletromagnetismo Computacional, por outro lado, os métodos sem malha são praticamente desconhecidos, mas este cenário está começando a mudar.

Dentre os membros da família, um em particular, o EFG (Element-Free Galerkin) tem sido empregado com sucesso [Parreira *et al.*, 2006], [Bottauscio *et al.*, 2006] e [Manzin e Bottauscio, 2008]. Entretanto, o EFG não é considerado como um método “verdadeiramente” sem malha pelo fato de depender de um procedimento que lembra muito uma divisão de domínio (e portanto uma malha!) durante o processo de cálculo [Liu, 2003]. Principalmente por causa disso, o principal objetivo desse trabalho é dissecar um outro método, o MLPG (Meshless Local Petrov-Galerkin), e tentar encontrar o maior número possível de aplicações a problemas tradicionais da engenharia elétrica. O MLPG, desenvolvido inicialmente por S. Atluri [Atluri and Shen, 2002] é verdadeiramente sem malha, e utiliza informações relativas à vizinhança de cada nó para se chegar à solução geral do problema. Ele parte do local (a versão do MLPG explorada neste trabalho emprega vizinhanças circulares em 2D e esféricas em 3D) para o global. Uma abordagem muito interessante, que será explicada um pouco mais nas próximas linhas (e no restante do trabalho).

Funções de Forma

De acordo com o que foi explicado acima, a principal noção que permeia os métodos sem malha é a aproximação da solução por uma soma ponderada de funções de forma (associadas a nós espalhados pelo domínio, e não a elementos). Dado um ponto \vec{x} pertencente ao domínio Ω , tem-se:

$$u^h(\vec{x}) = \sum_{i \in Neigh(\vec{x})} \phi_i(\vec{x}) \hat{u}_i \quad (1)$$

em que:

u^h é a versão discretizada (i.e., representada como uma soma de funções de forma) da solução u da equação diferencial parcial $\hat{A}u = f$ a ser resolvida numericamente (\hat{A} é um operador diferencial e f uma função conhecida, não necessariamente contínua);

$Neigh(\vec{x})$ representa o conjunto de nós que são aptos a influenciar o ponto \vec{x} ;

$\phi_i(\vec{x})$ representa uma função de forma associada ao nó i calculada em \vec{x} ;

\hat{u}_i é o *parâmetro nodal*, i.e., o peso associado ao nó i .

A noção geométrica associada à equação (1) acima é mostrada na Fig.3.1.

Dentre as propriedades que as funções de forma devem satisfazer, estão:

1 - Devem ser de suporte compacto (i.e., possuem valor diferente de zero apenas na vizinhança do nó ao qual está associada). Isso garante que somente os nós mais próximos do ponto \vec{x} onde se deseja calcular u^h contribuem com a soma ponderada (1). Essa característica leva naturalmente a sistemas lineares cujas matrizes são esparsas, de maneira análoga ao FEM;

2 - Todas as funções de forma que influenciam um ponto \vec{x} devem satisfazer a *partição da unidade*, i.e.,

$$\forall \vec{x} \in \bar{\Omega} \quad \sum_{i \in \text{Neigh}(\vec{x})} \phi_i(\vec{x}) = 1 \quad (2)$$

e também a propriedade da *reprodução do campo linear*:

$$\forall \vec{x} \in \bar{\Omega} \quad \sum_{i \in \text{Neigh}(\vec{x})} \phi_i(\vec{x}) x_i = x \quad (3)$$

$$\forall \vec{x} \in \bar{\Omega} \quad \sum_{i \in \text{Neigh}(\vec{x})} \phi_i(\vec{x}) y_i = y \quad (4)$$

$$\forall \vec{x} \in \bar{\Omega} \quad \sum_{i \in \text{Neigh}(\vec{x})} \phi_i(\vec{x}) z_i = z \quad (5)$$

As expressões (2) – (5) informam que as funções de forma conseguem aproximar uma função linear de maneira exata, i.e., se é sabido de antemão que a solução de uma equação diferencial é linear, então o erro cometido ao se aproximar a função u pela sua versão discretizada u^h é zero.

Há diferentes maneiras de se calcular as funções de forma ϕ_i . E aqui talvez resida o ponto fraco dos métodos sem malha. As funções de forma não possuem expressão analítica. Diferentemente do FEM, onde as funções de base N_i são conhecidas no interior de cada elemento, os métodos sem malha requerem a aplicação de métodos numéricos para sua determinação. Na abordagem *meshless*, pode-se dizer que o custo computacional para se construir uma malha não-estruturada é transferido para o cômputo das funções de forma.

Na quase totalidade dos problemas avaliados neste trabalho, a aproximação MLS (*Moving Least Squares*) foi empregada [Liu, 2003]. Funções de forma RPIM [Liu, 2003] foram empregadas apenas uma vez, na seção 5.4).

As funções de forma MLS se apoiam basicamente na geometria da distribuição nodal (i.e., posição dos nós no domínio Ω) e no domínio de influência associado aos nós:

- Cada nó é associado a um número real (problemas unidimensionais), a um par ordenado (bidimensionais), ou a uma trinca ordenada (tridimensionais), que localiza o nó no interior (ou na fronteira) do domínio Ω ;
- As funções de forma são capazes de influenciar (i.e., são diferentes de zero) apenas uma região na vizinhança de cada nó (apenas uma outra maneira de se dizer que as funções de forma são de suporte compacto). Há uma certa liberdade na escolha da forma dessas regiões. Neste trabalho, elas são círculos em 2D e esferas em 3D.

Portanto, para cada nó i (índice que varia de 1 a N , número total de nós espalhados por Ω) localizado em $\vec{x} = \vec{x}_i$, tem-se uma função de forma $\phi_i(\vec{x})$ que assume valores diferentes de zero na região

$$\Lambda_i = \{ \vec{x} \in \Omega : \|\vec{x} - \vec{x}_i\| \leq r_i \} \quad (2)$$

em que r_i é o raio da região (circular ou esférica) Λ_i . Visto que apenas os pontos $\vec{x} \in \Omega$ que se situam no interior de Λ_i podem ser influenciados pelo nó i , Λ_i recebe o nome de *domínio de influência* associado ao nó i .

Uma vez que a noção de influência tornou-se mais precisa através de (2), uma interpretação mais refinada de (1) seria: Dado o ponto \vec{x} no qual se deseja calcular u^h , toma-se toda a população nodal (índices i de 1 a N) e considera-se apenas aqueles para os quais $\vec{x} \in \Lambda_i$ (i.e., o nó i influencia \vec{x}). Esses nós formam o conjunto $Neigh(\vec{x})$. Mas e se porventura houvesse um ponto \vec{x} para o qual $Neigh(\vec{x}) = \emptyset$? Como se poderia construir uma aproximação para $u^h(\vec{x})$? Na verdade, tal cenário é inconsistente; o ponto \vec{x} estaria dentro de um ‘buraco de cobertura’. Se a abordagem *meshless* deve ter algum sentido para todos os pontos do domínio Ω , precisa-se garantir que

$$\Omega \cup \partial\Omega \subseteq \bigcup_{i=1}^N \Lambda_i \quad (3)$$

i.e., os domínios de influência de todos os nós devem formar uma cobertura para o domínio Ω (e para a sua fronteira $\partial\Omega$).

O processo para se calcular as funções de forma MLS é longo e tedioso. O Capítulo 3 é quase inteiramente devotado a ele. Nesta breve introdução, é suficiente dizer que, dado um ponto \vec{x} no qual se deseja calcular as funções de forma, tem-se:

$$\Phi(\vec{x}) = \mathbf{p}^T(\vec{x})\mathbf{A}^{-1}(\vec{x})\mathbf{B}(\vec{x}) \quad (4)$$

em que

$$\Phi(\vec{x}) = [\phi_{Neigh,1}(\vec{x}), \phi_{Neigh,2}(\vec{x}), \dots, \phi_{Neigh,n}(\vec{x})] \quad (5)$$

(*Neigh, 1* significa o primeiro elemento do conjunto $Neigh(\vec{x})$, *Neigh, 2* o segundo, e assim por diante, até o número de nós n que influenciam o ponto \vec{x} ; uma descrição detalhada do que realmente está por trás de $\mathbf{p}(\vec{x})$, $\mathbf{A}(\vec{x})$ e $\mathbf{B}(\vec{x})$ é dada no Capítulo 3, Seção 1). O procedimento para se calcular as funções de forma pode ser encarado como uma ‘caixa-preta’, i.e., informa-se as coordenadas do ponto \vec{x} e obtém-se como resultado um conjunto de funções de forma (5) pronto a ser utilizado em aproximações de u^h como em (1). O custo computacional associado é elevado, visto que, para cada ponto onde se deseja calcular as funções de forma, é fundamental o emprego de um algoritmo de busca (p.ex., baseado em *KdTrees*), além de inversões matriciais (apenas a aproximação MLS precisa de matrizes invertidas; tal procedimento é desnecessário no RPIM). O processo para o cálculo das derivadas parciais também pode ser considerado como uma ‘caixa-preta’. Neste caso, os cálculos vão um pouco mais além, e o procedimento retorna vetores como em (5), mas contendo os valores das derivadas das funções de forma associadas aos nós que influenciam o ponto \vec{x} (Capítulo 3, Seção 3).

Entretanto, há vantagens em se empregar a aproximação MLS. As funções de forma assim obtidas e suas derivadas são suaves, mesmo quando se empregam apenas termos lineares na base (no vetor \mathbf{p} ; no Capítulo 3, Seção 1, há uma discussão mais detalhada). Uma típica função de forma MLS pode ser vista na Figura 3.7, enquanto suas derivadas estão ilustradas nas Figuras 3.12 e 3.13.

Equações Integrais de Espalhamento Eletromagnético: Uma Primeira Aplicação para as Funções de Forma MLS

Embora os métodos sem malha terem sido originalmente propostos como uma alternativa ao método dos elementos finitos (FEM), que busca a solução de equações diferenciais parciais, a primeira oportunidade neste trabalho de aplicação das funções de forma veio de um campo totalmente diferente, a saber, da análise do espalhamento de ondas eletromagnéticas através de equações integrais.

As equações integrais da teoria eletromagnética geralmente são resolvidas através do método dos momentos (MoM) [Balanis, 1989], [Harrington, 1968]. Neste trabalho, o MoM foi adaptado de tal modo a empregar as funções de forma MLS no processo de discretização.

Na análise do espalhamento de ondas por objetos condutores (a única categoria aqui considerada), busca-se uma maneira de se determinar as correntes equivalentes \vec{J} que são induzidas na superfície do condutor, representado por $\partial\Omega$ (embora de acordo com o Capítulo 1 o mesmo símbolo também seja empregado para a fronteira do domínio onde uma equação diferencial deve ser resolvida, não há nenhum problema em empregá-lo também na abordagem via equações integrais, uma vez que $\partial\Omega$ aqui representa a ‘fronteira’, ou o contorno do objeto condutor, onde circulam as correntes equivalentes). Para problemas bidimensionais e polarização TM^z , tem-se

$$\forall \vec{x} \in \partial\Omega \quad E_z^i(\vec{x}) = \frac{\omega\mu_0}{4} \int_{\partial\Omega} J_z(\vec{x}') H_0^{(2)}(k\|\vec{x} - \vec{x}'\|) dl' \quad (6)$$

$$\forall \vec{x} \in \partial\Omega \quad (\hat{n} \times \vec{H}^i(\vec{x})) \cdot \hat{z} = J_z(\vec{x}) + \frac{jk}{4} \int_{\partial\Omega} J_z(x', y') H_1^{(2)}(kR) (\hat{n} \cdot \hat{R}) dl' \quad (7)$$

A equação (6) é a equação integral do campo elétrico (EFIE), e (7) é a equação integral do campo magnético (MFIE). Os campos incidentes $E_z^i(\vec{x})$ (componente z) e $\vec{H}^i(\vec{x})$ são funções conhecidas, assim como a geometria da superfície $\partial\Omega$ do condutor (em problemas 2D, uma curva fechada em \mathbb{R}^2). Uma completa dedução de (6) e (7) a partir das equações de Maxwell é dada na Seção 4.1.2.

O processo que leva à solução de (6) e (7) pode ser sucintamente descrito por:

- Espalha-se nós por todo o contorno $\partial\Omega$;
- Uma vez que as posições nodais tenham sido estabelecidas, constrói-se funções de forma MLS de acordo com o procedimento ‘caixa-preta’ (seção anterior);
- Aproxima-se a densidade de corrente $J_z(\vec{x})$ por uma soma ponderada de funções de forma [à maneira de (1)]:

$$J_z(\vec{x}) = \sum_{j=1}^N \phi_j(\vec{x}) \hat{u}_j \quad (8)$$

- Substitui-se (8) em (6) e/ou (7) e realiza-se as integrações numéricas ao longo de $\partial\Omega$. Isso leva a um sistema linear cujas incógnitas são os parâmetros nodais \hat{u}_j e cujo vetor é uma função do campo incidente (e portanto conhecido).

A qualidade dos resultados obtidos depende da geometria do condutor. Tal método se revelou preciso quando aplicado ao problema de espalhamento por um cilindro circular condutor perfeito. Entretanto, quando a seção reta do cilindro possui ‘lados’ (um quadrado, por exemplo), o método falha miseravelmente, porque a aproximação MLS não consegue produzir as funções de forma. Se os nós estiverem distribuídos ao longo de um lado do quadrado (de modo que uma de suas coordenadas, x ou y , tenha um valor fixo), a matriz A em (4) torna-se singular, o que impede que seja invertida.

Uma maneira de se contornar esse problema seria o emprego de um outro método para a construção de funções de forma, e que fosse apto a produzir resultados aceitáveis quando os nós estivessem distribuídos ao longo de uma linha (ou lado). A Seção 4.3 lida com o método IMLS (*Improved Moving Least Squares*), que emprega uma espécie de ortogonalização de Gram-Schmidt para a construção de funções para a base do MLS (vetor \mathbf{p}). O procedimento IMLS não necessita de inversão de matrizes, e produz bons resultados longe das quinas do cilindro condutor. O IMLS falha próximo aos vértices (ou quinas), o que resulta em um desempenho não muito satisfatório.

Entretanto, há uma maneira de se resolver as equações integrais (6) e (7) através de funções de forma MLS, tanto para geometrias circulares quanto para as que contém lados. A idéia é construir as funções de forma ao longo de uma linha, e depois definir uma transformação que mapeia os pontos dessa linha a pontos do contorno $\partial\Omega$. Esse processo funciona muito bem (Seção 4.4), e a ele foi dado o nome de *rubber band technique*, pelo fato de se parecer com o ato de esticar uma tira de borracha (que supostamente conteria as funções de forma) ao longo do contorno $\partial\Omega$.

O Método MLPG (Meshless Local Petrov-Galerkin)

O MLPG é o ponto central do presente trabalho, particularmente a sua aplicação a problemas de espalhamento eletromagnético. Esse método foi desenvolvido por S. Atluri [Atluri e Shen, 2002], inicialmente para a resolução de problemas modelados por equações diferenciais parciais em Mecânica Computacional. Esse método é considerado ‘verdadeiramente’ sem malha, uma vez que requer a integração de formas fracas apenas em domínios locais, na vizinhança de cada nó.

Em problemas de espalhamento de ondas eletromagnéticas monocromáticas em duas dimensões, as equações a serem resolvidas geralmente assumem a forma

$$\nabla \cdot \left(\frac{1}{p(\vec{x})} \nabla u(\vec{x}) \right) + k^2 q(\vec{x}) u(\vec{x}) = f(\vec{x}) \quad (9)$$

em que $u(\vec{x})$ representa a componente z do campo elétrico ou magnético (dependendo da polarização), enquanto $p(\vec{x})$ e $q(\vec{x})$ representam parâmetros materiais (permeabilidade magnética ou permissividade elétrica, também de acordo com a polarização). O termo k se

refere ao número de onda no espaço livre, e $f(\vec{x})$ é um termo que representa as fontes (excitação).

No MLPG, a equação (9), que envolve derivadas de segunda ordem da função u , não é resolvida diretamente; ela precisa ser antes colocada sob uma outra forma, a *forma fraca*, que envolve apenas derivadas de primeira ordem (enquanto (9) é conhecida como a *forma forte* do problema). Entretanto, a construção da forma fraca de (9) requer a introdução de um outro tipo de função, as *funções de teste* v . O processo geral de solução da equação (9) via MLPG pode ser descrito como:

- Espalha-se N nós através de todo o domínio Ω ;
- A cada um dos N nós se associa uma função de forma MLS ϕ_i ;
- A cada um dos N nós se associa uma função de teste v_i . As funções de teste também devem ser de suporte compacto (assim como as funções de forma). A região na vizinhança do nó i sobre a qual v_i é diferente de zero é chamada de domínio de teste Y_i ;
- Constrói-se a forma fraca de (9), usualmente uma expressão integral envolvendo u e v . A forma fraca é imposta N vezes, cada uma das quais devendo ser integrada em Y_i ;
- Em cada instância da forma fraca obtida de (9), substitui-se u pela aproximação (1). Tal procedimento leva a um sistema linear cuja matriz é esparsa, e cujas incógnitas são os parâmetros nodais \hat{u}_j .

Na versão do MLPG empregada neste trabalho, uma típica função de teste associada ao nó i é tal que

$$\nabla^2 v_i = -\delta(\vec{x} - \vec{x}_i) \quad (10)$$

$$v_i = 0, \quad \vec{x} \in \partial Y_i \quad (11)$$

Em duas dimensões, v_i é dada por

$$v_i(\vec{x}) = \frac{1}{2\pi} \ln \left(\frac{s_i}{\|\vec{x} - \vec{x}_i\|} \right) \quad (12)$$

E em três dimensões,

$$v_i(\vec{x}) = \frac{1}{4\pi} \left(\frac{1}{\|\vec{x} - \vec{x}_i\|} - \frac{1}{s_i} \right) \quad (13)$$

em que s_i é o raio do domínio de teste Y_i , que deve obrigatoriamente ser um círculo em problemas 2D (e esferas em problemas 3D), nessa versão apenas, conhecida como MLPG4 ou *Local Boundary Integral Equation Method* (LBIE).

No que diz respeito à forma fraca, há pelo menos duas maneiras de obtê-las: o método dos resíduos ponderados ou através da segunda identidade de Green. Uma vez que a forma fraca tenha sido obtida, ela requer a incorporação das condições de contorno, especificadas sobre a fronteira $\partial\Omega$. Como se trata de problemas de espalhamento, busca-se condições que representem o campo espalhado se afastado do objeto (*outward travelling waves*), i.e., as condições devem satisfazer, pelo menos num sentido aproximado, a condição de Sommerfeld:

$$\lim_{\rho \rightarrow \infty} \frac{\partial E_z^s}{\partial n} = -jkE_z^s \quad (14)$$

em que E_z^S representa a componente z do campo elétrico espalhado (as condições para o campo magnético H_z^S são análogas). Neste trabalho, foram empregadas as condições de contorno de radiação (*Radiation Boundary Conditions - RBC*) de Bayliss-Turkel de primeira (Seção 5.5) e de segunda ordem (Seção 5.3).

As condições de radiação podem ser impostas de duas maneiras: Diretamente na forma fraca (Seção 5.3) ou através do método da colocação (Seção 5.5). A primeira alternativa apresenta um desafio maior, visto que interseções entre o domínio Ω e os domínios de teste Y_i dos nós próximos a $\partial\Omega$ precisam ser encontradas. Já a segunda é muito simples de ser implementada, o que a torna mais eficiente. Ainda existe uma maneira de se lidar com (14), mas que não emprega RBC's aproximadas. Trata-se do método de expansão em autofunções, ou método *Unimoment* (Seção 5.4). Tal método foi originalmente proposto para a solução de problemas de espalhamento via elementos finitos [Chang e Mei, 1976]. Entretanto, ele foi aqui modificado de modo a incorporar o MLPG4/LBIE no lugar do FEM, com resultados bastante favoráveis.

Condições de Interface

Uma outra questão abordada neste trabalho diz respeito às condições de interface, que devem ser impostas quando algum parâmetro material [função $p(\vec{x})$ em (9)] é descrito por uma função descontínua. Essa questão é particularmente importante na análise do espalhamento de ondas eletromagnéticas com polarização TE^z . Para essa polarização, e se o domínio Ω for caracterizado por dois (ou mais) materiais com diferentes permissividades, ao longo da interface entre os dois materiais, as derivadas normais do campo magnético satisfazem à relação

$$\frac{1}{\varepsilon_r^-} \frac{\partial H_z^-}{\partial n} = \frac{1}{\varepsilon_r^+} \frac{\partial H_z^+}{\partial n} \quad (15)$$

em que H_z^- representa o campo magnético de um lado da interface, enquanto H_z^+ é o campo do outro lado; ε_r^- é a permissividade relativa de um lado da interface, enquanto ε_r^+ é a permissividade do outro lado. As derivadas em (15) são tomadas na direção normal à interface que separa os meios de permissividades diferentes. Não há uma maneira de inserir (15) diretamente na expressão para a forma fraca de (9). Entretanto, a Seção 5.5.1 apresenta um procedimento muito conveniente de tratar esse problema. As condições de interface são impostas diretamente no sistema matricial, via colocação, de um modo similar ao qual as condições de fronteira são impostas no contorno $\partial\Omega$. A idéia por trás desse procedimento foi inspirada por [Li *et al.*, 2003]. Resultados adicionais da aplicação dessa técnica a um problema tridimensional de eletrostática podem ser vistos na Seção 6.1.

Problemas de Autovalor: Cristais Fotônicos

Na análise de cristais fotônicos, há grande interesse na determinação da estrutura de *bandgap*. Tal estrutura diz respeito às frequências com as quais ondas eletromagnéticas (luz) podem se propagar no interior do cristal. A determinação das frequências que dão origem a

modos propagantes é um problema de autovalor; para cristais bidimensionais e assumindo ondas incidentes com polarização TM^z , o problema a ser resolvido é:

$$\nabla^2 E_z(\vec{x}) + \left(\frac{\omega}{c}\right)^2 \varepsilon_r(\vec{x}) E_z(\vec{x}) = 0 \quad (16)$$

sujeito às condições de contorno

$$E_z(\vec{x} + \vec{L}) = e^{-j\vec{K}\cdot\vec{L}} E_z(\vec{x}) \quad (17)$$

$$\frac{\partial E_z}{\partial n}(\vec{x} + \vec{L}) = e^{-j\vec{K}\cdot\vec{L}} \frac{\partial E_z}{\partial n}(\vec{x}) \quad (18)$$

em que \vec{L} é um vetor ligado às transformações de simetria do cristal (*lattice vector*). O problema (16)-(18) deve ser resolvido numa *célula unitária* Ω . (Os cristais fotônicos são estruturas periódicas. A menor unidade que, quando transladada dá origem ao cristal original, é geralmente chamada de célula unitária). Neste trabalho, considerou-se apenas células unitárias quadradas. As condições (17) e (18), impostas na fronteira de uma célula quadrada $\partial\Omega$ significam que o campo em um lado é igual ao campo no lado oposto, multiplicado por um fator de fase (no qual o vetor \vec{K} é o *vetor de Bloch*). O mesmo vale para a derivada normal do campo elétrico.

Para se resolver o problema (16) – (18), o campo elétrico E_z geralmente é representado como o produto de duas funções (teorema de Bloch):

$$E_z(\vec{x}) = e^{-j\vec{K}\cdot\vec{x}} u(\vec{x}) \quad (19)$$

onde $u(\vec{x})$ é agora uma função periódica na célula unitária, i.e.,

$$u(\vec{x} + \vec{L}) = u(\vec{x}) \quad (20)$$

$$\frac{\partial u}{\partial n}(\vec{x} + \vec{L}) = \frac{\partial u}{\partial n}(\vec{x}) \quad (21)$$

A substituição de (19) em (16) dá origem a uma nova equação diferencial:

$$-\nabla^2 u + j2\vec{K} \cdot \nabla u + \|\vec{K}\|^2 u = \left(\frac{\omega}{c}\right)^2 \varepsilon_r u \quad (22)$$

A transformação gerada pela aplicação do teorema de Bloch torna as coisas mais simples. Ao invés de se resolver o problema (16) – (18), resolve-se (20) – (22). A vantagem é que agora procura-se uma função $u(\vec{x})$ que seja periódica na célula unitária, sem qualquer referência a fatores de fase. Neste trabalho, uma maneira muito engenhosa de lidar com as condições (20) e (21) foi encontrada: o emprego de funções de forma periódicas, i.e., que atendam às mesmas condições de periodicidade (20) – (21). Como resultado, essas condições de contorno não precisam ser impostas; elas já estão embutidas nas funções de forma ϕ usadas na aproximação de $u(\vec{x})$. A construção de funções de forma periódicas é amplamente discutida na Seção 6.2, bem como a forma fraca de (22) e as matrizes que figuram no problema de autovalor associado. A partir daí, se obtém a estrutura de banda (*bandgap structure*) sem muito esforço.

Algumas Aplicações do MLPG em Mecânica Quântica

No mesmo espírito das seções anteriores, busca-se aqui soluções para problemas de autovalor provenientes da equação de Schrödinger em 2 e 3 dimensões

$$-\frac{\hbar^2}{2m}\nabla^2\psi(\vec{r}) + V(\vec{r})\psi(\vec{r}) = E\psi(\vec{r}) \quad (23)$$

Basicamente, dada uma distribuição de energia potencial $V(\vec{r})$ ($V: \mathbb{R}^3 \rightarrow \mathbb{R}$), as Seções 7.2 e 7.3 ilustram como encontrar os níveis de energia (autovalores) E . Todo o tratamento teórico é apresentado com detalhe, particularmente as estratégias para a construção da forma fraca da equação de Schrödinger a partir de (23). Comparações com os resultados de soluções analíticas demonstram a aplicabilidade do MLPG em problemas de mecânica quântica. O procedimento para construção de funções de forma periódicas do Capítulo 6 é aqui estendido com facilidade para três dimensões, para a resolução de um problema de determinação da estrutura de banda de sólidos (similar ao problema 2D para cristais fotônicos). Os resultados concordam muito bem com aqueles provenientes de um outro método numérico [Jun, 2004].

Por fim, a última seção do Capítulo 7 faz referência às primeiras incursões no emprego do MLPG4/LBIE em problemas dependentes do tempo. O objetivo é resolver a equação de Schrödinger não-linear dependente do tempo

$$i\frac{\partial\psi(\vec{x}, t)}{\partial t} + \nabla^2\psi(\vec{x}, t) = \alpha(\vec{x}, t) + \beta(\vec{x})|\psi(\vec{x}, t)|^p\psi(\vec{x}, t) \quad (24)$$

Na abordagem aqui empregada, a derivada temporal é discretizada através de um procedimento via diferenças finitas. Além disso, ao termo não-linear é dispensado um tratamento especial, baseado em iterações (*predictor-corrector*). Os resultados concordam muito bem com as soluções analíticas, e revelam que o MLPG4/LBIE também funciona corretamente ao ser aplicado a problemas que dependam do tempo.

Conclusões

O trabalho aqui apresentado cumpriu o seu papel de demonstrar a aplicabilidade dos métodos sem malha a vários problemas de interesse para a engenharia elétrica. Procurou-se demonstrar com clareza como os métodos funcionam. O custo de tal empreitada refletiu-se em exposições talvez demasiado longas, principalmente naquelas referentes à construção das formas fracas.

Partimos da definição de equações diferenciais, e o que representa um domínio no espaço. A partir daí, toda a idéia (ou filosofia) que permeia os métodos sem malha foi apresentada de uma maneira um tanto didática, através de uma analogia com a eletrostática (na qual as cargas eram representadas por nós, e os potenciais por elas produzido pela ação das funções de forma). Uma vez que o básico foi apresentado, todo o restante do trabalho é dedicado a refinar as ideias expostas aqui no Capítulo 2.

A construção das funções de forma é o tema do Capítulo 3. A aproximação MLS foi dissecada de uma maneira particularmente incisiva, com páginas e mais páginas demonstrando o processo por trás das funções de forma MLS. Apesar de poder ser encarado como um procedimento caixa-preta, muito *insight* pode ser obtido caso se conheça com detalhe como essas funções de forma são calculadas. O Capítulo 3 também faz uma breve referência às funções de forma RPIM, visto que são empregadas apenas uma única vez em todo o trabalho.

Uma vez que as funções de forma – componentes básicos na aproximação dos campos – foram definidas, prosseguiu-se na aplicação dessas funções ao processo de discretização de equações integrais do espalhamento eletromagnético. Os resultados foram muito bons, superando em precisão o método dos momentos, que é tradicionalmente empregado nessa categoria de problemas. Além disso, o Capítulo 4 discute as principais falhas do MLS na construção de funções de forma para objetos ‘quadrados’. Após muita discussão, uma maneira extremamente simples para resolver os problemas do MLS é apresentada ao final do capítulo.

O Capítulo 5, que trata de todo o desenvolvimento do MLPG aplicado a problemas de espalhamento, é o ponto central do trabalho. Diferentes estratégias para lidar com a imposição das condições de contorno foram abordadas. O método da colocação assume aí um destaque, em vista da facilidade com a qual pode ser efetivamente empregado.

Com a experiência dos capítulos anteriores, procede-se então a novas áreas de aplicação do MLPG a problemas tridimensionais (nos quais o método da colocação uma vez mais se revelou fundamental) e a problemas de autovalor provenientes da análise de cristais fotônicos e da mecânica quântica. Esse material, tema dos últimos dois capítulos, conclui a dissertação.

A principal intenção deste trabalho foi mostrar como o MLPG pode ser aplicado a problemas de espalhamento eletromagnético. O restante deve ser encarado como ‘subprodutos’ (*byproducts*), que foram obtidos à medida em que o tema principal era desenvolvido. Muitos temas foram aqui tratados pela primeira vez, e particular atenção foi devotada à exposição detalhada dos métodos. Isso levou, como já afirmado, a discussões um tanto prolongadas e a deduções que à primeira vista poderiam parecer desnecessárias. Mas isso já estava previsto; uma das intenções que tive ao produzir esse trabalho é que ele também servisse como uma espécie referência, onde tudo (ou quase) o que eu tivesse explorado sobre os métodos sem malha estivesse contido.

Uma vez que a aplicabilidade dos métodos sem malha a problemas foi demonstrada com sucesso, o próximo passo é o refinamento desses métodos. Resultados sobre erros, taxas de convergência e, sobretudo, comparações extensivas com o método dos elementos finitos, constarão na agenda dos trabalhos futuros. A fronteira foi aberta, e agora pode-se vislumbrar vários temas a serem abordados, como

- Problemas que envolvam grandezas vetoriais, e não apenas escalares;
- Problemas não-lineares (principalmente aqueles relacionados à não-linearidade de certos cristais fotônicos);
- Outras maneiras de se resolver problemas dependentes do tempo;
- Uso de PML’s (Perfectly Matched Layers) ao invés de condições de radiação (RBCs’);
- Esquemas mais eficientes para a integração numérica das formas fracas (de crucial importância ao se lidar com problemas grandes, que envolvam centenas de milhares de nós);

- Um tratamento matemático mais rigoroso (descrição mais detalhada dos espaços de funções e operadores que figuram nos métodos sem malha).

O futuro dos métodos *meshless* parece ser promissor em engenharia elétrica. Em vista da grande área que ainda resta para ser explorada, tudo indica que os próximos anos trarão surpresas agradáveis.

Contents

List of Symbols.....	XXV
Chapter 1 – Introduction.....	1
1.1 Preview.....	1
1.2 Some little information on the development of meshless methods.....	2
1.3 Survey of the chapters.....	3
1.4 Publications.....	4
Chapter 2 – The Philosophy of Meshless Methods.....	6
Chapter 3 - Shape Functions: The Building Blocks.....	15
3.1 The Moving Least Squares (MLS) Approximation.....	16
3.1.1 Examples of MLS shape functions.....	28
3.1.2 Some remarks regarding the MLS shape functions.....	30
3.2 Calculating the Derivatives of Shape Functions.....	32
3.2.1 MLS Shape Functions.....	32
Concluding Remarks.....	35
Chapter 4 - MLS Shape Functions and Integral Equations: A “Meshless Method of Moments”.....	36
4.1 A Brief on Maxwell’s Equations and Scattering Theory.....	37
4.1.1 Maxwell’s Equations and Interface Conditions. Time and Frequency Domains.....	37
4.1.2 Scattering Theory.....	41
4.1.3 Integral Equations.....	56
4.2 Meshless Analysis of Integral Equations. MLS Shape functions.....	52
4.2.1 Worked example: Scattering of a plane wave by a PEC circular cylinder.....	56
4.3 Meshless Analysis of Integral Equations. IMLS Shape functions.....	61
4.4 Meshless Analysis of Integral Equations. The “rubber band” technique.....	66
Concluding Remarks.....	69

Chapter 5 - The Meshless Local Petrov-Galerkin (MLPG) Method in Electromagnetic Wave Scattering.....	70
5.1 Helmholtz Equations.....	70
5.2 General Features of MLPG.....	72
5.3 Intersecting test domains and Radiation Boundary Conditions (RBC).....	76
5.4 Intersecting test domains and Eigenfunction Expansions (Unimoment).....	83
5.5 The Collocation Method.....	90
5.5.1 Interface conditions and the TE^z polarization.....	102
Concluding Remarks.....	108
Chapter 6 - The MLPG Method and other Applications: Three-Dimensional Electrostatics and Photonic Bandgap Crystals.....	109
6.1 Electrostatics.....	109
6.2 Eigenvalue Problems and Photonic Crystals.....	115
Concluding Remarks.....	127
Chapter 7 - Some Extensions of MLPG to Quantum Mechanics.....	128
7.1 Theoretical Motivation.....	128
7.1.1 Overview.....	128
7.1.2 Analytical solution to the harmonic oscillator potential.....	132
7.2 Two-dimensional examples.....	137
7.3 Three-dimensional examples.....	142
7.4 A nonlinear boundary value problem.....	146
Concluding Remarks.....	153
Chapter 8 – Conclusions.....	154
8.1 Summary.....	154
8.2 Future Work.....	155
Bibliography.....	156

List of Symbols

$a_j(\vec{x})$	j th unknown coefficient (MLS approximation, page 18)
$\mathbf{a}(\vec{x})$	unknown coefficients collected into a $m \times 1$ vector (MLS approximation, page 21)
$\mathbf{A}(\vec{x})$	one of the matrices involved in the MLS approximation (page 24)
\vec{A}	time-harmonic magnetic potential vector – spatial part (page 43)
$\mathbf{B}(\vec{x})$	one of the matrices involved in the MLS approximation (page 25)
c	speed of light in vacuum (page 117)
J	auxiliary real functional (MLS approximation, page 21)
$\vec{B}(\vec{x}, t)$	time-dependent magnetic flux density (page 37)
$\vec{B}(\vec{x})$	time-harmonic magnetic flux density – spatial part (page 39)
$\vec{D}(\vec{x}, t)$	time-dependent electric flux density (page 37)
$\vec{D}(\vec{x})$	time-harmonic electric flux density – spatial part (page 39)
$\vec{E}(\vec{x}, t)$	time-dependent electric field intensity (page 37)
$\vec{E}(\vec{x})$	time-harmonic electric field intensity – spatial part (page 39)
E_n	n th energy level (page 130)
E_z	z -component of the electric field – time-harmonic regime (page 71)
\hbar	reduced Planck's constant (page 129)
$\vec{H}(\vec{x}, t)$	time-dependent magnetic field intensity (page 37)
$\vec{H}(\vec{x})$	time-harmonic magnetic field intensity – spatial part (page 39)
$H_0^{(2)}$	zero-order Hankel function of the second type (page 44)
$H_p^{(2)}$	p -order Hankel function of the second type (page 85)
H_z	z -component of the magnetic field – time-harmonic regime (page 72)
j	imaginary number (page 39)
$\vec{J}(\vec{x}, t)$	time-dependent electric current density (page 37)
$\vec{J}(\vec{x})$	time-harmonic electric current density – spatial part (page 39)
\vec{J}_s	time-dependent electric surface current density (page 39)
\vec{J}_s	time-harmonic electric surface current density – spatial part (page 40)
k	wavenumber (page 43)

\vec{K}	the Bloch vector (page 117)
\ln	natural logarithm (page 76)
\vec{L}	the lattice vector (page 117)
\hat{n}	outward unit vector normal to a surface (page 38)
$Neigh(\vec{x})$	index set which collects the indices of all nodes able to influence point \vec{x} (page 10)
$p_j(\vec{x})$	j th term in the monomial basis (MLS approximation, page 18)
$\mathbf{p}(\vec{x})$	all monomial terms collected into a $m \times 1$ vector (MLS approximation, page 18)
\mathbf{P}	one of the matrices involved in the MLS approximation (page 24)
r_i	radius of the influence domain associated to node i (page 19)
s_i	radius of the test domain associated to node i (page 75)
u	scalar function (in \mathbb{R}^2 or \mathbb{R}^3) to be approximated (page 6)
u^h	discretized version of u (page 9)
\hat{u}_i	nodal parameter associated to node i (page 10)
$\hat{\mathbf{u}}$	vector collecting all n nodal parameters (page 25)
v_i	test function associated to node i (page 75)
\vec{x}	a point in \mathbb{R}^2 or \mathbb{R}^3 (page 6)
$w(t)$	weight (or window) function (MLS approximation, page 19)
$\mathbf{W}(\vec{x})$	diagonal matrix involved in the MLS approximation (page 24)
$\hat{\mathbf{z}}$	unit vector pointing at the z -direction (page 45)
Y_i	test domain associated to node i (page 74)
∂Y_i	Boundary of the test domain associated to node i (page 75)
$\boldsymbol{\gamma}(\vec{x})$	auxiliary vector employed in the derivatives of MLS shape functions (page 32)
δ_{IJ}	Kronecker delta (page 30)
ε	electric permittivity (page 37)
μ	magnetic permeability (page 38)
σ	electric conductivity (page 38)
Λ_i	influence domain associated to node i (page 10)
$\partial \Lambda_i$	boundary of the influence domain associated to node i (page 11)
$\rho(\vec{x}, t)$	time-dependent electric charge density (page 37)
$\rho(\vec{x})$	time-harmonic electric charge density – spatial part (page 39)
ρ_s	time-dependent electric surface charge density (page 39)
ρ_s	time-harmonic electric surface charge density – spatial part (page 40)
$\phi_i(\vec{x})$	a shape function associated to node i , evaluated at \vec{x} (page 10);
ϕ	scalar electric potential (page 43);

$\Phi(\vec{x})$	$1 \times n$ vector collecting the values of the shape functions evaluated at \vec{x} (page 26)
ψ_p	numerical modal basis functions (Unimoment, page 86);
ψ	time-independent quantum-mechanical wavefunction (page 129)
Ψ	time-dependent quantum-mechanical wavefunction (page 129)
ω	angular frequency (page 39)
Ω	domain in which the differential equation is stated (page 6)
$\partial\Omega$	Boundary of the domain Ω (page 7)
∇	the ‘grad’ operator (page 72)
$\nabla \times$	the ‘curl’ operator (page 37)
$\nabla \cdot$	the ‘div’ operator (page 37)
∇^2	the Laplacian operator (page 43)

Chapter 1

Introduction

1.1 Preview

THIS work is concerned with the application of meshless (or meshfree) methods to situations relevant to Electrical Engineering. As broad as this scope may appear at first, there is some kind of thread which links problems from contexts so different to each other like Electrostatics and Quantum Mechanics. It is just because of this issue that I have been able to investigate so many problems from different domains. After the reader finishes reading the text that I now lay before him, he will probably see this common link with his own eyes.

In writing this text, I strived to write it in a language as simple as possible. I tried to explain everything in words, down to the smallest details. In addition to this, this work is self-contained, insofar as I make no attempt to find out how methods other than those derived from the meshless framework would solve a certain kind of problem. As a consequence, the reader does not have to know how the Finite Element Method (FEM) or the Method of Moments (MoM) actually work in order to provide a solution to a given problem.

The purpose of this work is twofold. Firstly, it is the dissertation I shall submit to UFMG Electrical Engineering Graduate Program in order to earn a Master's degree. The other reason for my writing such a work is because I want to make some kind of reservoir, in which I would place everything concerning meshless methods I could put my hands on. So I want to assemble lots of things together, knowledge distilled from my reading of many papers and books related to mathematics, physics and engineering viewed from the viewpoint of the meshless techniques. I really do not want this to get lost, as the time passes and these ideas will no longer be fresh in my memory. Everything gathered at a single place and explained in a simple language. This is the sort of work I wish I had read when I first came to know about meshfree methods, two years ago. And now here it is.

This work moves around the numerical solution of problems described either by differential or by integral equations. I deal chiefly with the implementation of the meshless techniques applied to such problems. This is not a work on numerical analysis, in which the application of tools from Functional Analysis is of utmost importance. I shall deal with such advanced subjects (rigorous analysis of convergence rates, derivation of upper and lower bounds for solutions, theorems, stability of solutions, normed spaces and so on) in a future work. The reason why I have somehow postponed that is simple. Many of the techniques described in this work are here applied to problems from Electrical Engineering for the first time. There was no book or paper I could resort to in order to find something dealing with meshless methods in Electromagnetism in a simple way. So I had to begin from the scratch. I compare it to the sowing of a field. In order for it to produce something, the herbs must be removed, the soil be revolved, the seeds must be watered. All of this has to be carried out before the plants begin to bear fruit; actually, even before they are born! So with this work, which aims at cleaning the terrain for the development of future sophisticated applications and more rigorous mathematical analyses. In

order to investigate more advanced characteristics and implications of a method, we'd better figure out if the method works correctly first!

1.2 Some information on the development of meshless methods

The meshless methods comprise a large class of numerical procedures whose seminal idea underlying all its members is, as its name indicates, to be able to build numerical solutions to differential equations defined in a certain geometrical domain *without* the need of setting up a mesh or a grid in this domain. There are resemblances with FEM, to which meshfree methods aim to be an alternative. The most patent ones are: the operation with weak forms (the differential equation is converted into an integral expression involving the function to be approximated and test functions), the use of compactly supported shape functions, and the integration of the weak forms in local domains, which leads to global sparse matrices. The most striking difference from FEM is the complete absence of an underlying mesh; as there is no mesh, the concept of element loses its meaning. So the classical idea of an element with its 'connectivity array' linking nodes to edges is totally absent in the context of the meshless approach. This new technology offers the possibility of releasing the analyst from the burden of setting up an adequate mesh in favor of a more simplistic scenario, wherein only a simple cloud of nodes spread throughout the domain is necessary.

The first studies concerning the use of meshfree techniques were reported in the early past decade. These methods are in their infancy, and many challenges concerning them remain to be explored [Liu, 2003]. Meshless methods have successfully been applied in Computational Mechanics. Their use in areas such as Elastostatics and Hydrodynamics is well developed. In Computational Electromagnetics, otherwise, there are some appearances. Some papers dealing with meshless methods in Electrical Engineering are [Maréchal, 1998], [Cingoski *et al.*, 1998], [Viana and Mesquita, 1999], [Parreira *et al.*, 2006], [Bottauscio *et al.*, 2006] and [Manzin and Bottauscio, 2008]. However, in all these works (except [Viana and Mesquita, 1999]), a method called Element-Free Galerkin (EFG) is employed. EFG is not regarded as a true meshless method, because background cells are necessary to perform the numerical integrations [Liu, 2003].

On the other hand, a different method, called Meshless Local Petrov-Galerkin (MLPG), unlike EFG, is a true meshless method. The numerical integrations are carried out within certain local domains, which dismisses the use of any kind of background cells. MLPG was devised by S. Atluri within the framework of Mechanics [Atluri and Shen, 2002]. MLPG employs two kinds of functions, *shape functions* and *test functions*, which belong to two different function spaces. The shape functions are constructed numerically through procedures common to other meshless methods, whereas there are many choices available to the test functions. There are reports on the application of MLPG5 (the test function is a Heaviside function) to solve 2D electrostatic problems [Fonseca *et al.*, 2008]. Soares Jr. also solves problems concerning electromagnetic wave propagation in time-domain through MLPG, in which two choices for the test function have been taken: Heaviside step functions and Gaussian weight functions [Soares, 2009]. Y. Yu and Z. Chen, otherwise, use a meshless method whose formulation is quite different from MLPG (in fact, it resembles a time-domain finite-difference approach, based on collocation) in order to solve time-domain electromagnetic problems [Yu and Chen, 2009], [Yu and Chen, 2010]. In this work, we are particularly interested in MLPG4, whose test function is a solution

to Green's problem for Laplace's equation (reasons behind this choice will be addressed in later chapters).

1.3 Survey of the chapters

In this work, the meshless methods are going to be applied to a myriad of different problems. I decided to organize the information in seven chapters, as follows:

Chapter 1 – Introduction

A brief note stating the purposes of this work, and an account on the development of meshless methods. A list of publications is also provided.

Chapter 2 – The Philosophy of Meshless Methods

This chapter attempts to describe, in a rather informal way, the main ideas behind the meshless methods.

Chapter 3 – Shape Functions: The Building Blocks

It shows how the shape functions are constructed. These functions are fundamental to the meshless methods, because they are used to approximate the solution to the problems. They lack analytical expressions, and therefore some numerical schemes must be employed in order to build them. The Moving Least Squares (MLS) approximation is discussed in detail.

Chapter 4 – MLS Shape Functions and Integral Equations: A “Meshless Method of Moments”

This chapter describes the use of shape functions from the meshless methods in the discretization of integral equations. The theory of electromagnetic wave scattering is briefly revised. The chapter then illustrates how to discretize the electric field (EFIE) and magnetic field (MFIE) integral equations. Three different ways of doing that are analyzed.

Chapter 5 – The Meshless Local Petrov-Galerkin (MLPG) Method in Electromagnetic Wave Scattering

It deals with the implementation of MLPG to the differential equations arising in electromagnetic wave scattering. Both polarizations TM^z and TE^z are considered. Furthermore, there is an extensive discussion on the different ways to impose boundary conditions. The issue concerning the numerical treatment of the interface between two different materials (material discontinuity) is given its due attention.

Chapter 6 – The MLPG Method and other Applications: Three-Dimensional Electrostatics and Photonic Bandgap Crystals

This chapter extends the ideas developed in Chapter 5 to three-dimensional problems in Electrostatics. It also deals with eigenvalue problems, when the band structure of photonic crystals is considered. A handy procedure for constructing periodical shape functions is developed.

Chapter 7 – Some Extensions of MLPG to Quantum Mechanics

A little account on elementary Quantum Mechanics is provided at the beginning of the chapter, which then proceeds with the analytical solution of a problem (the quantum harmonic oscillator). This particular problem will be used as a basis for comparison with the numerical MLPG solutions. Two and three-dimensional problems illustrated by the time-independent Schrödinger equation are considered. The situation regarding the band structure of a three-dimensional crystal is also taken into account. The technique used to construct the periodic shape functions in Chapter 6 is extended here to three-dimensions. The last section of this chapter deals with the Nonlinear Schrödinger equation (NLS), whose characteristics – it is time-dependent and nonlinear – pose a challenge to MLPG4.

1.4 Publications

Much of what is discussed in the following pages actually came from some earlier works I had the opportunity to publish in the last two years. This dissertation comprises the bulk of the subjects I explored while in the Master's course. Almost everything has been assembled together and explained in detail. I decided to list the publications here and to leave them out from the Bibliography. In doing this, I avoid lots of self-reference, what would be unavoidable had I not taken this choice.

[1] Williams L. Nicomedes, Renato C. Mesquita, and Fernando J. S. Moreira "2D Scattering Integral Field Equation Solution through an IMLS Meshless-Based Approach", *IEEE Transactions on Magnetics*, v.46, p.2783 - 2786, 2010.

[2] Williams L. Nicomedes, Renato C. Mesquita, and Fernando J. S. Moreira, "An Integral Meshless-Based Approach in Electromagnetic Scattering", *The International Journal for Computation and Mathematics in Electrical and Electronic Engineering COMPEL* (Bradford), vol. 29, n°6, 2010.

[3] Williams L. Nicomedes, Renato C. Mesquita, and Fernando J. S. Moreira, "A Meshless Local Boundary Integral Equation Method for Three Dimensional Scalar Problems", *IEEE Transactions on Magnetics*, to be published.

[4] Williams L. Nicomedes, Renato C. Mesquita, and Fernando J. S. Moreira, "Meshless Local Petrov-Galerkin (MLPG) Methods in Quantum Mechanics", *The 14th International IGTE Symposium on Numerical Field Calculation in Electrical Engineering*, 2010, Graz, Austria.

[5] Williams L. Nicomedes, Renato C. Mesquita, and Fernando J. S. Moreira "A Meshless Local Boundary Integral Equation Method for Three Dimensional Scalar Problems", *14th Biennial IEEE Conference on Electromagnetic Field Computation, IEEE CEFC 2010*, 2010, Chicago.

[6] Williams L. Nicomedes, Renato C. Mesquita, and Fernando J. S. Moreira "2D Scattering Integral Field Equation Solution through an IMLS Meshless-Based Approach", *17th Conference*

on the Computation of Electromagnetic Fields - COMPUMAG 2009, 2009, Florianópolis, Brazil. Proceedings of the 17th Conference on the Computation of Electromagnetic Fields – COMPUMAG 2009., 2009. P.350 – 351.

[7] Williams L. Nicomedes, Renato C. Mesquita, and Fernando J. S. Moreira “The Unimoment Method and a Meshless Local Boundary Integral Equation (LBIE) Approach in 2D Electromagnetic Wave Scattering”, IMOC 2009 – *SBMO/IEEE MTT-S International Microwave and Optoelectronics Conference*, 2009, Belem, Brazil. Proceedings of the International Microwave and Optoelectronics Conference, 2009. P.514 – 518.

[8] Williams L. Nicomedes, Renato C. Mesquita, and Fernando J. S. Moreira "A Local Boundary Integral Equation (LBIE) Method in 2D Electromagnetic Wave Scattering, and a Meshless Discretization Approach", IMOC 2009 - *SBMO/IEEE MTT-S International Microwave and Optoelectronics Conference*, 2009, Belem, Brazil. Proceedings of the International Microwave and Optoelectronics Conference, 2009. p.133 – 137.

[9] Williams L. Nicomedes, Renato C. Mesquita, and Fernando J. S. Moreira "2D Scattering Analysis through Meshless Methods: A Comparison Between Two Different Shape Function Schemes", IMOC 2009 - *SBMO/IEEE MTT-S International Microwave and Optoelectronics Conference*, 2009, Belem, Brazil. Proceedings of the International Microwave and Optoelectronics Conference, 2009. p.368 – 372.

[10] Williams L. Nicomedes, Renato C. Mesquita, and Fernando J. S. Moreira "Electromagnetic Scattering Problem Solving by an Integral Meshless-Based Approach", *The 8th International Symposium on Electric and Magnetic Fields, EMF 2009*, 2009, Mondovi, Italy. Proceedings of the 8th International Symposium on Electric and Magnetic Fields, EMF 2009.

Chapter 2

The Philosophy of Meshless Methods

THIS work is concerned with the solution of physical models arising in the fields of classical electrodynamics and quantum mechanics. The language through which these models are expressed is, in the vast majority of situations, the language of partial differential equations (PDE's). Given the quantity we are interested in (e.g., scalar potentials, electric and magnetic fields, wavefunctions), a PDE expresses a relation among the derivatives of this quantity. Let us call u a certain quantity. u is represented as a function of space variables (x, y, z) and possibly of time t . Then a physical law, codified in the language of partial differential equations, reads as:

$$f_0(\vec{x}, t, u)u(\vec{x}, t) + \sum_i f_i(\vec{x}, t, u)\partial_i u(\vec{x}, t) = g(\vec{x}, t) \quad (2.1)$$

i.e., as a sum of terms each one of which is a product between a derivative of u and a factor f . These factors f_i can be real (or complex) numbers, functions of space and time (space, time or both) or even functions that, in addition to space and time also depend on the value of the function u (a feature that characterizes nonlinear equations). The partial derivatives ∂_i run through all independent variables involved in the equation:

$$\frac{\partial u}{\partial x}, \frac{\partial u}{\partial y}, \frac{\partial u}{\partial z}, \frac{\partial^2 u}{\partial x^2}, \frac{\partial^2 u}{\partial y^2}, \frac{\partial^2 u}{\partial z^2}, \frac{\partial^2 u}{\partial x \partial y}, \dots, \frac{\partial u}{\partial t}, \frac{\partial^2 u}{\partial t^2}, \dots \quad (2.2)$$

The derivative of highest order defines the order of the PDE. In this work, we shall deal with second-order PDE's (i.e., the derivative of highest order is the second one).

A PDE is stated at a domain, which is nothing else than a region of space. If this region is limited, we call it a bounded domain. Otherwise, if this region does not have a limit, the domain is referred to as an unbounded one. We are relying on an intuitive basis here. It should be noticed that what defines a domain is the range of the independent variables involved in the problem. If a problem is described by a PDE in three independent variables (x_1, x_2 and x_3) we can define the domain as a subset of \mathbb{R}^3 . Let us call Ω this domain. Then $\Omega \subseteq \mathbb{R}^3$. Ω is a set of ordered triples (x_1, x_2, x_3) whose elements satisfy a criterion. At first sight, it appears to be no connection to a physical region. But when we are interested in physical laws, the independent variables in the associated PDE are generally the space variables (x, y , and z). Then in specifying the domain of interest, we can state a criterion like this:

Let Ω be the set of ordered triples (x, y, z) , i.e., points in space, which are located inside a conducting sphere whose center is $(0,0,0)$ and whose radius is $R = 3$ units.

Or like this one:

Let Ω be the set of ordered triples (x, y, z) whose values are taken from an external source (e.g., a drawing, or a file).

Again on intuitive grounds, we already have the notion of what it is for something to be the *boundary* of the domain Ω . It is a place where the domain literally “ends”. From a more technical perspective, a boundary of Ω is a set of points which also satisfies a criterion. It is: A point \vec{x} is said to belong to the boundary of Ω if we can take a neighborhood of \vec{x} , it does not matter how small it is, that is not entirely contained in Ω . Or, there are both interior and exterior points for every neighborhood of \vec{x} . The boundary of Ω is represented as $\partial\Omega$. If the domain is unbounded, we consider as though its boundary were theoretically located at the infinite. Usually this is expressed as $-\infty < x < \infty$, $-\infty < y < \infty$, $-\infty < z < \infty$. But this is of no interest for us here: whenever a problem of this kind appears, we try to reduce the original unbounded domain to a bounded one. When we do this, we are *truncating* the domain, because it is by far easier to work with bounded domains rather than with unbounded ones.

The boundary $\partial\Omega$ is of utmost importance because in order to solve a PDE, we must know how our quantity u behaves over there. Later on we will come back to this issue.

Recapitulating: We picked up a quantity of interest (to us), considered it as a function u of space (and possibly time) and, through mathematics, we found out a PDE describing how u is related to its derivatives. We then chose a domain Ω where we want the solution of u to be calculated, and finally got the boundary $\partial\Omega$ together with information on the behavior of u over there. The next step amounts to nothing else than solving this PDE. But how?

There are many ways to solve a PDE, depending on the problem and on the equation under consideration. Some methods are able to express the solution of the PDE directly through a formula involving only the independent variables (an expression of the type $u = f(x, y, z, t)$, which allows for the determination of u at (x, y, z) and at time t by just plugging the values of x , y , z and t into f and by carrying out the required operations). Others express u as a series, i.e., an infinite sum of terms which depend upon (x, y, z, t) . These are the *analytical methods*, and the solutions for u derived from them are the *analytical solutions*. There are still other methods that express u as the integral of a function G (multiplied by other function, the *source term*) over some portion of the domain Ω . This is the method based on Green’s functions.

The analytical methods work well only for a small number of cases. They do a great job in equations stated at ‘regular’ domains (by ‘regular’ is meant domains akin to simple figures, like squares, circles, cubes, parallelepipeds, spheres). It should be noticed that there are a handful of analytical methods aimed at solving PDE’s: separation of variables, integral transforms, change of variables and superposition of solutions are just some examples. The problem with these methods is that, in addition to be applicable only on regular domains, in order to get the solution to the original PDE, one has to solve related subsequent partial or ordinary differential equations. But this sometimes can be quite a cumbersome task. For example, if one tries to solve Laplace’s equation in cylindrical coordinates, one has to solve first Bessel’s differential equation. But if the domain is not regular, how could these subsequent differential equations be solved (e.g., Laplace’s equation in a cylinder whose cross-section is neither a circle nor a rectangle)? A similar problem also happens when one tries to apply the method based on Green’s functions. In order to find Green’s function G , other PDE must be solved, in which the source term $g(\vec{x}, t)$ is substituted by a Dirac delta function. The same issue all over again: the solution to this new problem is usually cumbersome, and even impossible to solve analytically depending on the domain.

It seems that, although the analytical solutions are useful and provide insight into the form of u (by just seeing the form of u a skilled mathematician can deduce some important facts about the solution, like the behavior near the boundary, maxima and minima, how the solution decays with time, etc.), they can be obtained only for simple problems. The problems Science and Engineering are interested in are often by far more complicated: difficult PDE's, large and complex domains (some of them time-varying) and nonlinear problems constitute examples of cases where it would be virtually impossible to obtain analytical solutions. So, how to deal with these questions?

The answer to this problem is not a brand new one: numerical techniques. In situations where the tools of analysis often fail, mathematicians often turn to numerical algorithms in order to find approximate solutions to complex problems. In what regards partial differential equations, their study began systematically by Euler, d'Alembert, Lagrange and Laplace in the XVIII century, as a tool in the description of the mechanics of continuous media and in the analytical study of models in the physical science. In the XIX century, a large number of methods for solving PDE's were devised, which enhanced much of the Physics of the time (the solution of physical models), in addition to stimulate other areas of mathematics, like differential geometry, topology and analysis. In the 20th century, the digital computers came to the fore, and the scientific computing, which is concerned to the calculation of numerical solutions to PDE's (among other things), became one of the main features of modern technology [Brezis and Browder, 1998].

Nowadays, there is a multitude of these so-called methods of scientific computing aimed at finding numerical solutions to PDE's. Each one has its peculiar features, its advantages and its drawbacks. Meshless methods constitute a family of such methods, and it is a particular member, the MLPG, that this work will be focused on.

Given a domain Ω , we begin by spreading nodes throughout it. Nodes are simple points – a coordinate (x) in one-dimensional, ordered pairs (x, y) in two-dimensional or ordered triples (x, y, z) in three-dimensional problems. Figure 1 illustrates this: over there we can see many nodes scattered across Ω , and some at the boundary $\partial\Omega$. A general feature shared by meshless methods is that there is no need for this nodal arrangement to be uniform. The nodes can be spread in any way; even random distributions can be used. It is a common practice – based somehow on intuitive grounds – to place more nodes where the solution or its derivatives are expected to vary in a sudden way, e.g., near the edges of $\partial\Omega$ (if any) or near the interfaces between two regions characterized by different material properties. This looks rather obvious: the better the resolution, the better is the precision of the results. Actually, this can be proved through convergence studies, but as said earlier, this is not the main objective of the present work.

Now, suppose we want to find the value of the function u at a point $A \in \Omega$. Let the coordinates of A be represented by \vec{x} (i.e., $\vec{x} = (x_A)$ for 1D, $\vec{x} = (x_A, y_A)$ for 2D and $\vec{x} = (x_A, y_A, z_A)$ for 3D problems). But, as we have not solved the problem yet, there is no way to calculate this. The only data we can rely on at this stage is an unsolved differential equation and a set of nodes spread throughout Ω . So let us take the nodes only and see what we can do with them. Let us also assume another function u^h so that

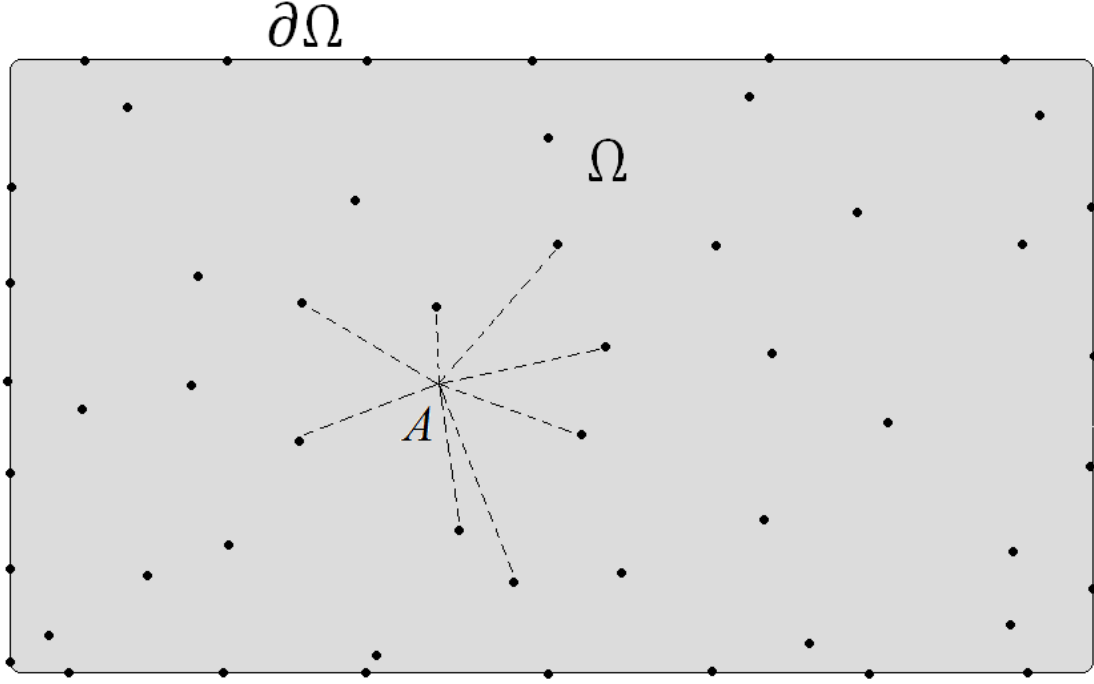


Fig.2.1. A geometrical domain Ω and its boundary $\partial\Omega$, in which there are many scattered nodes. Eight nodes act upon point $\vec{x} = A$. Nodes located too far away from point A are unable to transmit their influence to it.

$$u^h = a \text{ function dependent on the nodal distribution} \quad (2.3)$$

because the set of nodes is the only information we have access to other than the unsolved differential equation. Well, the real function u does not depend on the nodes, as it is the solution to an equation that has been derived from physical laws. Physical laws do not know of nodes, that are nothing else than a mathematical notion. So, in trying to find the function u at A , we have to give up calculating the real value of u . We now take a leap of faith, and hope that there could be some resemblance between the real u and the node-dependent function u^h , i.e., we approximate u by u^h :

$$u \sim u^h = a \text{ function dependent on the nodal distribution} \quad (2.4)$$

If there are N nodes spread throughout the domain Ω (and $\partial\Omega$), then u^h would theoretically depend on all nodes:

$$u^h = \sum_{i=1}^N \text{something dependent on node ' } i \text{ ' } \quad (2.5)$$

Keep Fig.2.1 in mind; we shall now proceed to form an analogy between “something dependent on node i ” and electrical charges. Suppose that at the location of each node i in Fig.2.1 (point \vec{x}_i), there is an electrical charge Q_i . Given these charges, we want to calculate the resulting electric potential at point $\vec{x} = A$. From electrostatics, we know that the electric potential at $\vec{x} = A$ is the sum of the contributions from all charges involved in the problem, and that the potential produced by a charge at a point is inversely proportional to the distance between the charge and the point, or

$$V = \sum_{i=1}^N \frac{1}{4\pi\epsilon} \frac{1}{\|\vec{x} - \vec{x}_i\|} Q_i = \sum_{i=1}^N \xi(\vec{x}, \vec{x}_i) Q_i \quad (2.6)$$

where ξ is a function dependent on the charge's location \vec{x}_i and on the point \vec{x} (where the potential shall be calculated), and ϵ is the electric permittivity (suppose the charges to be in the vacuum, just to keep things simple). In the analogy, each node, instead of a charge Q_i , is associated to a number \hat{u}_i , called the *nodal parameter* (which, differently from electrical charges, could be a complex number). So we can write (2.5) as

$$u^h = \sum_{i=1}^N \theta(\vec{x}, \vec{x}_i) \hat{u}_i \quad (2.7)$$

Equation (2.7) above tells us that u^h at $\vec{x} = A$ is given by the sum of the contributions of all nodes from Ω ($\theta(\vec{x}, \vec{x}_i) \hat{u}_i$ is “the thing dependent on node i ”). It is as though each node had a “charge \hat{u}_i ” and were able to extend its influence until $\vec{x} = A$ through the function $\theta(\vec{x}, \vec{x}_i)$. This picture seems nice but, if there are many nodes in Ω , then we need to take into account all N nodes of the domain each time we want to calculate u^h at a point \vec{x} . We can improve the situation if we modify the way a node is able to influence other points. Let us make a guess. What about if the function $\theta(\vec{x}, \vec{x}_i)$ that governs the nodal influence were chosen in such a way that, instead of influencing all space, like an electric charge does, a node at \vec{x}_i could influence only a small neighborhood around \vec{x}_i ? The obvious consequence is that the point $\vec{x} = A$ would be influenced only by neighbor nodes. Nodes located too far away from $\vec{x} = A$ could then be disregarded. Therefore we can rewrite (2.7) as

$$u^h = \sum_{i \in \text{Neigh}(\vec{x})} \theta_{mod}(\vec{x}, \vec{x}_i) \hat{u}_i \quad (2.8)$$

where $\text{Neigh}(\vec{x})$ is the set of the closest nodes to the point \vec{x} (whose number of elements is obviously smaller than N) and θ_{mod} is the modified function that governs the nodal influence.

Back to the analogy with electric charges, we can assume functions $\theta_{mod}(\vec{x}, \vec{x}_i)$ differing from $\xi(\vec{x}, \vec{x}_i)$ (in (6)) in two points:

First: $\theta_{mod}(\vec{x}, \vec{x}_i)$ does not extend throughout space indefinitely, but is a *compactly supported* function. It is able to carry the influence from node i only to those points \vec{x} located in a region surrounding \vec{x}_i . These influenced points \vec{x} comprise a set Λ_i , called the *influence domain* associated to node i . Outside the influence domain, $\theta_{mod}(\vec{x}, \vec{x}_i) = 0$.

Second: $\theta_{mod}(\vec{x}, \vec{x}_i)$ does not blow up when $\vec{x} = \vec{x}_i$. Otherwise, it takes on a finite maximum value there, and then decays to zero at the boundary of the influence domain Λ_i .

So, if $\theta_{mod}(\vec{x}, \vec{x}_i)$ is able to carry the influence from a node \vec{x}_i only to those points \vec{x} sufficiently close, then we are done: only few neighbor nodes are needed in the computation of u^h at \vec{x} . These functions $\theta_{mod}(\vec{x}, \vec{x}_i)$ satisfying both observations above are called *shape functions* (or basis functions) and are written as:

$$\theta_{mod}(\vec{x}, \vec{x}_i) = \phi_i(\vec{x}) \quad (2.9)$$

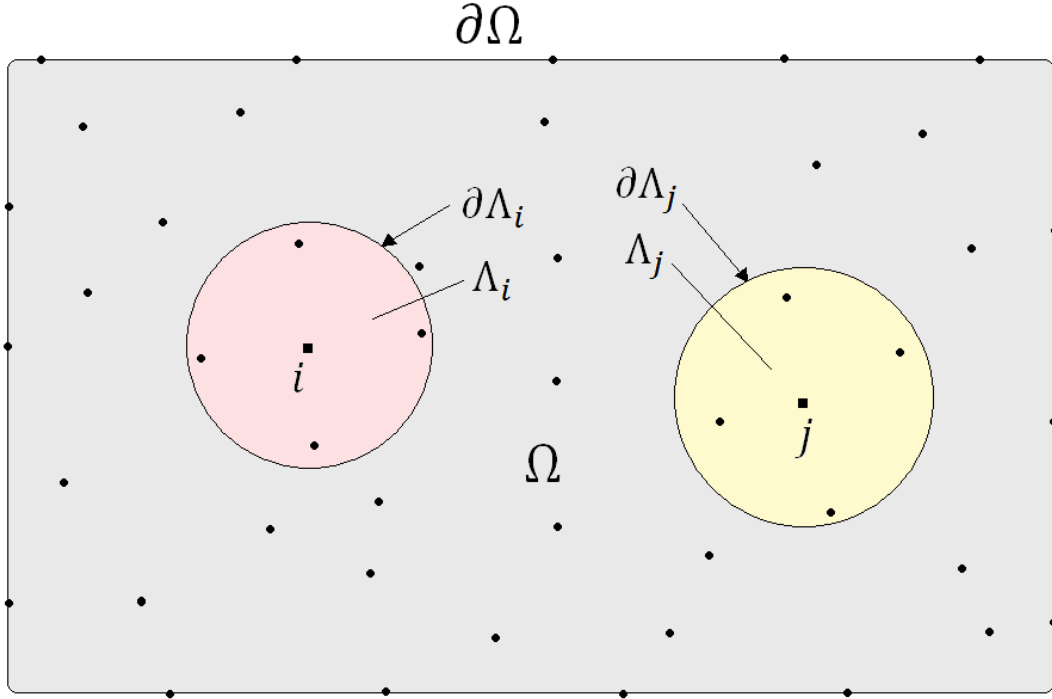


Fig.2.2. Node i is able to influence only the surrounding circular region, which is called its influence domain. It is represented by Λ_i and its boundary by $\partial\Lambda_i$. Likewise for node j , and for all other nodes in the domain Ω (whose influence domains are not represented in this figure).

where $\phi_i(\vec{x})$ stands for the shape function ϕ associated to node i (located at \vec{x}_i) evaluated at a point \vec{x} . The function u^h calculated at \vec{x} then reads:

$$u^h(\vec{x}) = \sum_{i \in \text{Neigh}(\vec{x})} \phi_i(\vec{x}) \hat{u}_i \quad (2.10)$$

Table I below sums up the analogy between electric charges and nodes. Electric charges act together to produce a potential, as do nodes when calculating a function at a point. It is as if the nodes had been assigned a special kind of charge that is able to influence only their surroundings, instead of the whole space.

TABLE I
ANALOGY BETWEEN NODES AND ELECTRIC CHARGES

Electrostatics	Meshless approximation
Electric charges at \vec{x}_i	Nodes at \vec{x}_i
Charge magnitude Q_i	Nodal parameter \hat{u}_i
Influence from a charge at \vec{x}_i extends indefinitely.	Influence from a node \vec{x}_i extends to the neighborhood Λ_i only.
The charges determine the electrostatic potential V at \vec{x}	The nodes determine the function u^h at \vec{x} .

So the nodes of the domain are able to extend their influence to neighboring regions only. In meshless methods, all N nodes must share the following property: it is mandatory for each one of the nodes in the domain to have an associated influence domain Λ (according to Fig.2.2).

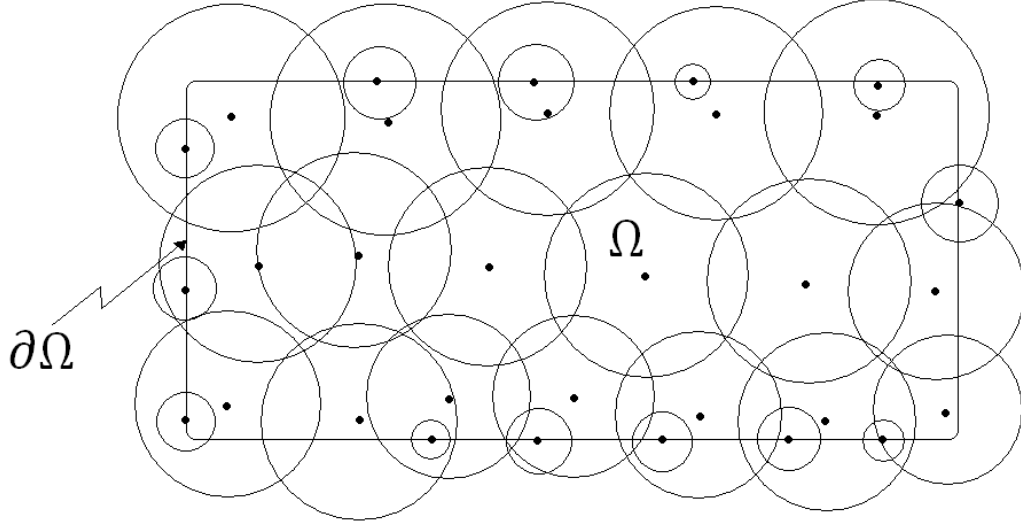


Fig.2.3. The union of all influence domains must cover the domain Ω (and its boundary $\partial\Omega$).

There are no specific forms that these domains have to satisfy, but squares and circles (or cubes or spheres in 3D problems) are usually employed. In what regards the influence of the nodes over the domain Ω , the following fundamental proposition must hold:

Proposition 2.1 *The union of all N influence domains Λ must cover the whole domain Ω (and its boundary $\partial\Omega$). Or:*

$$\Omega \subseteq \bigcup_{i=1}^N \Lambda_i \quad (2.11)$$

Figure 2.3 shows us what (2.11) means. Another way to state this proposition is to say that no holes can be left behind in the covering of Ω by the Λ 's. We saw earlier that the shape functions are compactly supported, i.e., they do not carry the influence from the nodes to every part of the domain. Let us suppose a scenario in which the proposition stated above does not hold, i.e., there is a hole. We have then a picture like that depicted in Fig.2.4. If we want to find u^h at a point in this hole, say, \vec{y} , we see straightforwardly that no node extends its influence until this point. This is the same as to say that there are no neighbor nodes influencing point \vec{y} , or:

$$Neigh(\vec{y}) = \emptyset \quad (2.12)$$

and therefore, the sum in (2.10) is meaningless. So it becomes impossible to find an approximation for u^h like (2.10). This situation is quite odd, because we want u^h everywhere inside (and at the boundary of) the domain Ω . For that reason, we must make sure that the aforementioned proposition is satisfied.

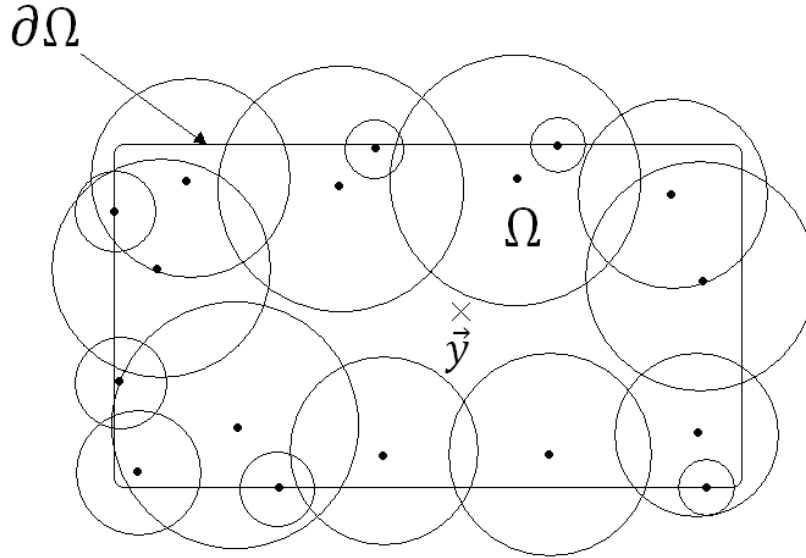


Fig.2.4. It is impossible for a function u^h to be calculated at point \vec{y} , as no node is able to extend its influence domain Λ until there.

A point of concern is that related to the intersection of the influence domains associated to two neighboring nodes. Take a look at Fig.2.5, and suppose we want to find out u^h at point \vec{z} . The influence domains Λ of the 3 nodes that influence \vec{z} overlap with each other. But in meshless methods, overlapping of influence domains is freely allowed. The 3 nodes in Fig.2.5 act on point \vec{z} , or, equivalently, point \vec{z} belongs to each one of the 3 influence domains that extend until \vec{z} . So, we have another proposition valid in meshless methods:

Proposition 2.2 *Influence domains of neighboring nodes can freely overlap, i.e., if i and j are two nodes, it may occur that*

$$\Lambda_i \cap \Lambda_j \neq \emptyset \quad (2.13)$$

By now, the main feature of meshless approximation should be apparent. If someone wants to calculate u^h at a point \vec{x} , than he first have to find all neighbor nodes that influence \vec{x} . This is a set of nodes hereby represented by $Neigh(\vec{x})$. $Neigh(\vec{x})$ can be structured in such a way that it returns the set of the closest nodes that influence point \vec{x} . Once this set is determined, then we proceed to the application of (2.10). But there are two questions of vital interest here, which seem to have been overrun. The first: What about the values of the nodal parameters \hat{u}_i ? Equation (2.10) is a weighted sum, but we do not know anything about the weights. How could it be that way? The second: How do we calculate the shape functions ϕ_i ?

Answer to the first: At this stage, we are at no position to tell this. We must wait until Chapter 5, which explains the method that shall be used to figure out the values of the nodal parameters (MLPG). But let us give a quick general picture about how they are obtained. It suffices to say that they are found through the solution of a linear system, and that, in order to set up this linear system one must rely on the application of formula (2.10) to the given differential equation many times, besides some more little calculations. It now becomes clear how important expression (2.10) is. It is extensively used throughout the process of finding u^h .

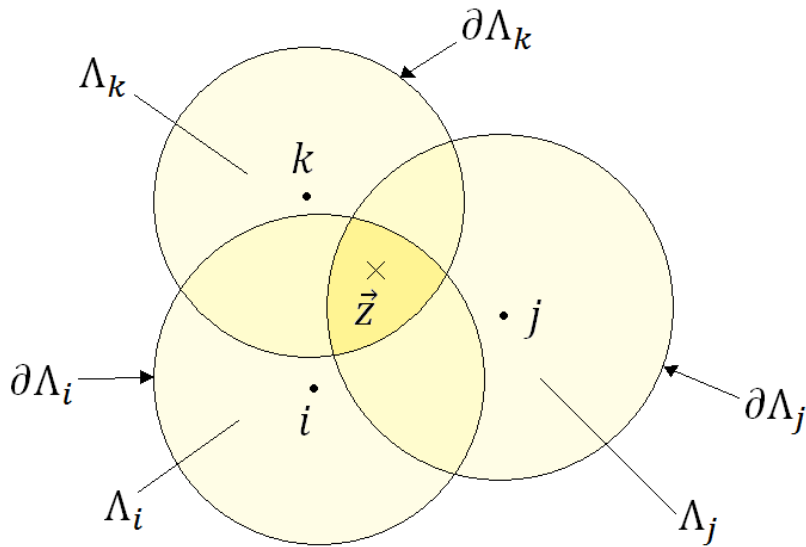


Fig.2.5. Nodes i, j and k extend their influence domain until point \vec{z} . There is no problem with the overlapping of neighboring influence domains.

Answer to the second: The shape functions lack analytical expressions. Given a node i (located at \vec{x}_i) and a point \vec{x} where a shape function must be calculated, there is no formula χ that takes the values of the coordinates of \vec{x}_i and \vec{x} and returns the value of the shape function. In other words, there is no way to express $\phi_i(\vec{x})$ as $\phi_i(\vec{x}) = \chi(\vec{x}_i, \vec{x})$. Numerical procedures must be relied upon in order to find out the shape functions. Curiously, the shape function associated to node i evaluated at \vec{x} also depends on the relative positions of neighboring nodes. There is a little bit of strangeness in the behavior of the shape functions; back to our analogy with electric charges, it is as though the influencing functions ξ depended on the neighbor charges. Or, as though the manner an electric charge influences a point depended on the relative positions of neighboring charges. Notwithstanding this issue, shape functions work very well in the approximating process. In the next chapter, we will be concerned to the numerical construction of these shape functions.

Let us finish this chapter with an overall view of the procedures for finding the solution to the differential equation, with the tools we have thus far. We expect to add (and refine) the steps in the next table as we move on.

THE MESHLESS PROCEDURE IN A NUTSHELL

Given a differential equation and a domain where it shall be solved:

First Step	Set up the domain Ω and its boundary $\partial\Omega$.
Second Step	Spread N nodes throughout the domain Ω and at its boundary $\partial\Omega$ as well.

Chapter 3

Shape Functions: The Building Blocks

As the last chapter made explicit, the shape functions play a fundamental role in the task of finding an approximation u^h for a function u (which is the solution to a differential equation). Indeed, whenever we want to know u^h at a point \vec{x} , we need first to determine a set of shape functions ϕ_i calculated at \vec{x} (according to equation 2.10). This chapter looks for a solution to one of the questions raised earlier: How do we calculate ϕ_i ?

Despite occupying such a prominent position in the meshless analysis of PDE's, the shape functions are not calculated directly. There are no expressions that return the value of these functions at some point \vec{x} in the domain. They must be determined numerically. Furthermore, a shape function associated to a node depends on the information concerning neighbor nodes. This is quite an odd situation: we have to rely on approximated things (ϕ) in order to calculate approximate functions (u^h). But, curiously enough, the method based on these shape functions proved to be a success. It is able to solve a PDE in the same way as FEM does, but without a mesh. The basis functions employed in FEM are really far simpler to deal with, but they happen to rely on a mesh in order to be constructed. It is known that to set up an adequate mesh sometimes reveals to be a rather difficult process, especially when it comes to 3D problems. In meshless methods, otherwise, there is just a cloud of nodes spread throughout the domain. There are neither meshes nor elements. But this extra ease comes in at the expense of a harsh numerical process in constructing the shape functions.

So, the challenge is to devise suitable shape functions using only scattered nodes without any connectivity among them. The development of effective methods for constructing shape functions is one of the hottest areas of research in the field of meshless methods. But we are not going to address these questions in this work. A thorough discussion of the different requirements and methods intended to find shape functions can be found in [Liu, 2003].

We have used two different approaches for constructing the shape functions. One of them, the Moving Least Squares approximation (MLS from now on) has been employed in almost the totality of the solved problems. In only one situation we have made use of the other, called the Radial Point Interpolation Method with Polynomial Reproduction (RPIM-PR), and, because of that, it will not be addressed here. Information on this particular method can be found in [Liu, 2003]. Both methods produce shape functions with their own features, which may be harnessed differently (e.g., the RPIM-PR interpolates a solution, whereas the MLS does not). It is reasonable at this point to mention a compulsory condition that the shape functions must satisfy, regardless of the method employed to build them: the *partition of unity*. Given any point \vec{x} in the domain, the sum of the shape functions acting on \vec{x} must be 1, or

$$\forall \vec{x} \in \bar{\Omega} \quad \sum_{i \in \text{Neigh}(\vec{x})} \phi_i(\vec{x}) = 1 \quad (3.1)$$

It means that the shape functions are able to approximate exactly the constant function $u = 1$ (if we take equation (2.10) and substitute all nodal parameters \hat{u}_i by 1, condition (1) above ensures that $u^h(\vec{x})$ equals 1 throughout the closure $\bar{\Omega}$ of the domain Ω , $\bar{\Omega} = \Omega \cup \partial\Omega$).

There are some other requirements that are not “compulsory” for example, we could want the shape functions to obey the *reproduction of the linear field* conditions. This is expressed as, assuming the coordinates to be represented in Cartesian coordinates $[(x, y, z)$ for a point \vec{x} and (x_i, y_i, z_i) for a node at $\vec{x}_i]$:

$$\forall \vec{x} \in \bar{\Omega} \quad \sum_{i \in \text{Neigh}(\vec{x})} \phi_i(\vec{x}) x_i = x \quad (3.2)$$

$$\forall \vec{x} \in \bar{\Omega} \quad \sum_{i \in \text{Neigh}(\vec{x})} \phi_i(\vec{x}) y_i = y \quad (3.3)$$

$$\forall \vec{x} \in \bar{\Omega} \quad \sum_{i \in \text{Neigh}(\vec{x})} \phi_i(\vec{x}) z_i = z \quad (3.4)$$

Expressions (3.1), (3.2), (3.3) and (3.4) point out that the shape functions are able to approximate exactly any linear function (i.e., any linear function can be exactly approximated at any point \vec{x} in the domain, or, more clearly, the expression (2.10) is exact whenever it happens to be applied to a linear function u).

It seems that there is a plenty of room to explore here. Other features can still be added to the shape functions, usually features that are natural to the problem being solved. This is a point that deserves much attention, as it can simplify matters in an astonishing way. As an example, if the solution is required to have periodic boundary conditions on $\partial\Omega$, things can be arranged in such a way that the numerical shape functions come out to be periodic. The boundary conditions then do not need to be imposed anymore: the periodicity has been embedded in the shape functions. Needless to say, the solution becomes simpler than imposing boundary conditions throughout $\partial\Omega$. In Chapter 6, which describes the meshless analysis of photonic crystals, this technique is used extensively. This process of enriching shape functions is akin to what sometimes happens in FEM. There, if we define vector basis functions \vec{N} such that $\nabla \cdot \vec{N} = 0$, then the solution expressed as a sum of basis functions will also exhibit a zero divergent. This is formidable when one is trying to find solutions to solenoidal fields. But enough of these details. Let us now concentrate on how the shape functions are constructed.

3.1 The Moving Least Squares (MLS) Approximation

Once we have got the nodes spread throughout Ω , each node is identified with an *index*, which is just a number used to label that node. Given a nodal distribution, there are different ways to ascribe indices to nodes. If the indices are represented by natural numbers, and the nodes by points in the real space, which are nothing else than ordered pairs (\mathbb{R}^2) or ordered triples (\mathbb{R}^3), then we can talk about different *numbering schemes*. A numbering scheme is a relation between indices and points, or a mapping between natural numbers (indices of the

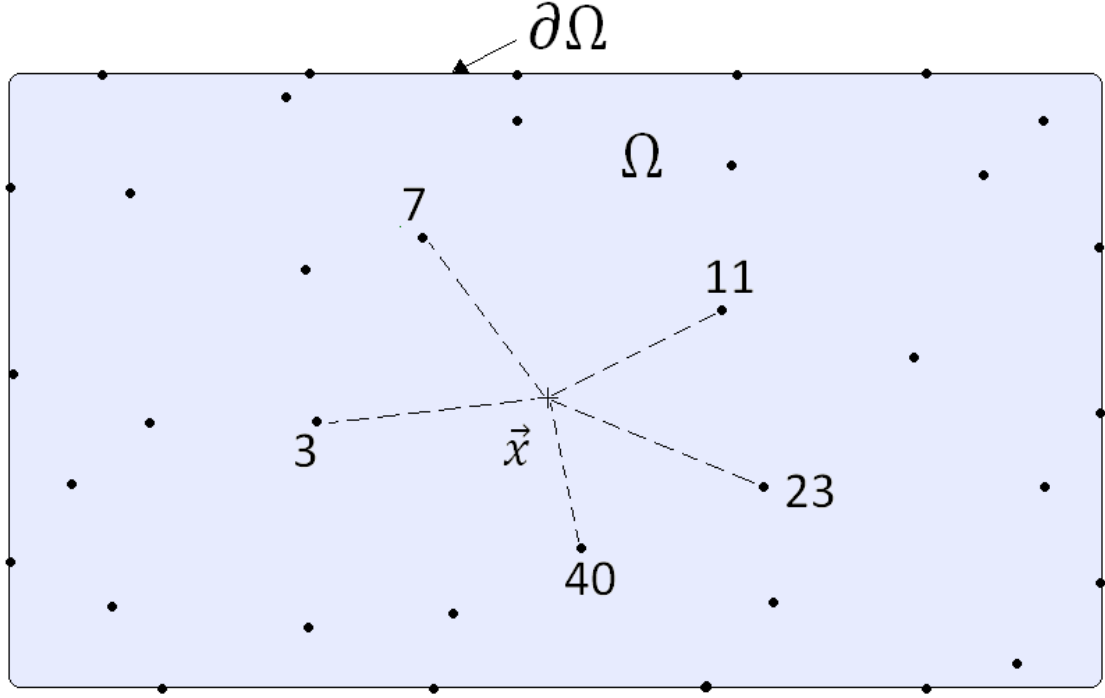


Fig.3.1. The set $Neigh(\vec{x})$, whose elements stand for nodes are able to extend their influence domains until \vec{x} .

nodes) and real vectors (the coordinates of the nodes, represented by vectors in \mathbb{R}^2 or \mathbb{R}^3). If we have a total of N scattered nodes, we can set up a map f that associates a vector to each index i , i.e., we can set up a map $f: \mathbb{N} \rightarrow \mathbb{R}^2$ or $f: \mathbb{N} \rightarrow \mathbb{R}^3$, if that is the case. The index i runs from 1 to N , and the real vectors comprise the coordinate set of all N nodes. Summing up, we can say that, given a node whose index is i , their coordinates are given by $f(i) = (x_i, y_i)$ (or $f(i) = (x_i, y_i, z_i)$). The map f can be established in many ways, and there is some research going on which aims to determine which numbering scheme is the most efficient. This is outside the scope of this work, but it suffices to say here that different numbering schemes lead to matrices with different sparsity patterns, and this has an impact on the numerical solution of the final linear system. References [Liu, 2003] and [Yavari *et al.*, 2001] address this issue.

Given a point \vec{x} , if we want to calculate the approximated function u^h at \vec{x} , expression (2.10) is needed (restated here for convenience):

$$u^h(\vec{x}) = \sum_{i \in Neigh(\vec{x})} \phi_i(\vec{x}) \hat{u}_i \quad (3.5)$$

Let us bear Fig.3.1 in mind. There we can see 5 nodes acting on point \vec{x} , which is the same as to say that the set $Neigh(\vec{x})$ has 5 elements. Let us suppose that their indices are 3, 7, 11, 23 and 40. Then

$$Neigh(\vec{x}) = \{3, 7, 11, 23, 40\} \quad (3.6)$$

The MLS approximation assumes that the function u^h at \vec{x} can be expressed as a sum of products, where each product is formed by 2 factors which depend on \vec{x} . We can state a proposition:

Proposition 3.1 (The MLS Approximation) *The function u^h evaluated at point \vec{x} is given by a sum of products, each one formed by two factors dependent on \vec{x} . Mathematically:*

$$u^h(\vec{x}) = \sum_{j=1}^m p_j(\vec{x})a_j(\vec{x}) \quad (3.7)$$

At first sight, this looks strange. We affirmed that u^h is given by (3.5), where neither the ϕ_i 's nor the \hat{u}_i 's are known, and now proposition 3.1 assumes u^h to be given by an entirely different way, with no mention to shape functions at all. It seems that we have two ways of approximating u^h , and at this point, we have no clue whatsoever about what the ϕ_i 's, the \hat{u}_i 's, the p_j 's and the a_j 's are. We are left with four unknown terms.

As mentioned in Chapter 1, the nodal parameters \hat{u} are the last things to be determined in the meshless solution of a problem. They are the unknowns of the final linear system, and can be used to approximate u^h [through (5)] only *after* the problem is entirely solved. So it is meaningless to rely upon them at this stage. Remember: we have not even defined the shape functions yet! What MLS approximation does, is essentially *to assume* that the p_j 's are known functions of \vec{x} . These known p_j 's are called *basis functions*, and are generally represented by monomials. If the point \vec{x} has coordinates (x, y) , then

$$\begin{aligned} p_1(\vec{x}) &= 1 \\ p_2(\vec{x}) &= x \quad p_3(\vec{x}) = y \\ p_4(\vec{x}) &= x^2 \quad p_5(\vec{x}) = xy \quad p_6(\vec{x}) = y^2 \end{aligned} \quad (3.8)$$

High order monomials (e.g., third order, fourth order, etc.) can also be employed. If $\vec{x} = (x, y, z)$:

$$\begin{aligned} p_1(\vec{x}) &= 1 \\ p_2(\vec{x}) &= x \quad p_3(\vec{x}) = y \quad p_4(\vec{x}) = z \\ p_5(\vec{x}) &= x^2 \quad p_6(\vec{x}) = y^2 \quad p_7(\vec{x}) = z^2 \quad p_8(\vec{x}) = xy \quad p_9(\vec{x}) = yz \quad p_{10}(\vec{x}) = xz \end{aligned} \quad (3.9)$$

If we assemble all monomial basis functions into a vector \mathbf{p} , then we can speak of a polynomial basis $\mathbf{p}(\vec{x})$:

$$\mathbf{p}(\vec{x}) = [p_1(\vec{x}), p_2(\vec{x}), \dots, p_m(\vec{x})]^T \quad (3.10)$$

A remarkable feature of MLS is that, if we assume that we know the monomial basis functions $p_j(\vec{x})$, then we can find the shape functions $\phi_i(\vec{x})$. This is achieved through the interplay of (3.5) and (3.7). Let us see how it can be accomplished.

After we have found all nodes acting on \vec{x} , we form slightly different MLS approximations for u^h : for each node $i \in Neigh(\vec{x})$, we substitute the monomial terms calculated at node i 's location \vec{x}_i for those calculated at \vec{x} , i.e., we form the approximation

$$u^h(\vec{x}, \vec{x}_i) = \sum_{j=1}^m p_j(\vec{x}_i)a_j(\vec{x}) \quad (3.11)$$

The unknown terms $a_j(\vec{x})$ are left untouched (still being calculated at \vec{x}). According to the situation depicted in Fig.3.1, we have a set of 5 “modified” approximations. They are:

$$S = \{u^h(\vec{x}, \vec{x}_3), u^h(\vec{x}, \vec{x}_7), u^h(\vec{x}, \vec{x}_{11}), u^h(\vec{x}, \vec{x}_{23}), u^h(\vec{x}, \vec{x}_{40})\} \quad (3.12)$$

Well, to each influencing node i we have an associated “modified” approximation $u^h(\vec{x}, \vec{x}_i)$. It seems pointless to build a set of approximations such as (3.12). We are interested in only one approximation, and the MLS formed a set S of approximations! There is a feeling that something has gone wrong here, but it has not. We are only halfway there. Let us proceed and consider the nodal parameters \hat{u}_i 's. Remember that, although we said earlier that it could be meaningless to employ the nodal parameters at this point, they actually do have some use here. They are unknown quantities, which contributes for rendering the procedure a little bit more obscure. Let us ignore this fact for a while and, given that each node i has its associated nodal parameter, we can form differences between the “modified” approximations and the \hat{u}_i 's. Let S now be given by

$$\forall i \in Neigh(\vec{x}) \quad S_i = (u^h(\vec{x}, \vec{x}_i) - \hat{u}_i) \quad (3.13)$$

where each element of the set is represented by S_i . According to the situation of Fig.3.1, we have 5 such differences, whose indices i involved are expressed in (3.6). If we can form differences, then we can form squares of differences. In modifying the S_i 's again, we get:

$$\forall i \in Neigh(\vec{x}) \quad S_i = (u^h(\vec{x}, \vec{x}_i) - \hat{u}_i)^2 \quad (3.14)$$

We are left with a set of real numbers, each of which represents a value dependent on points \vec{x} and \vec{x}_i . Adding still more complexity, we multiply each number in (3.14) by a weight function w , whose magnitude depends on the relative position of points \vec{x} and \vec{x}_i . This function must satisfy two criteria. First: The closer the distance between \vec{x} and \vec{x}_i is, the greater w becomes, until it reaches a maximum when $\vec{x} = \vec{x}_i$. Second: If the distance between \vec{x} and \vec{x}_i is larger than a given value r_i , then $w = 0$. Our new set of real numbers is:

$$\forall i \in Neigh(\vec{x}) \quad S_i = w\left(\frac{\|\vec{x} - \vec{x}_i\|}{r_i}\right) (u^h(\vec{x}, \vec{x}_i) - \hat{u}_i)^2 \quad (3.15)$$

The weight function w , sometimes called *window* function, can be chosen from a number of possibilities [Liu, 2003]. Some of them employed in this work are the *cubic spline*:

$$w(t) = \begin{cases} 2/3 - 4t^2 + 4t^3 & t \leq 1/2 \\ 4/3 - 4t + 4t^2 - 4t^3/3 & 1/2 < t \leq 1 \\ 0 & t > 1 \end{cases} \quad (3.16)$$

and also the *quartic spline*:

$$w(t) = \begin{cases} 1 - 6t^2 + 8t^3 - 3t^4 & 0 \leq t \leq 1 \\ 0 & t > 1 \end{cases} \quad (3.17)$$

The parameter r_i is somehow related to the size of node i 's influence domain Λ_i . If we consider the influence domains to be circles in two-dimensional and spheres and three-dimensional problems, then r_i is the radius of Λ_i . Figure 3.2 illustrates this: For a point A located at \vec{x}_A :

$$\|\vec{x}_A - \vec{x}_i\| \leq r_i \rightarrow \vec{x}_A \in \Lambda_i \quad (3.18)$$

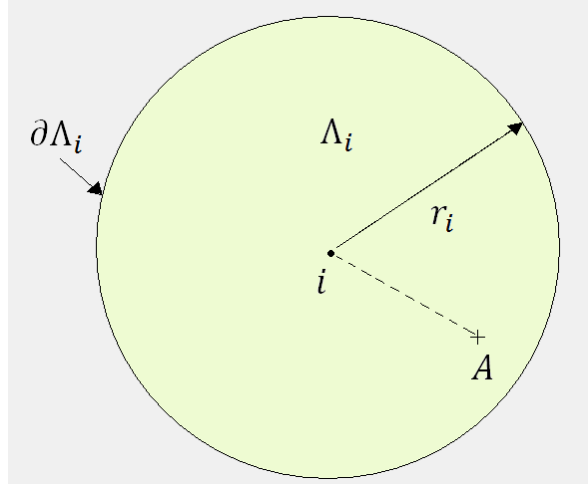


Fig.3.2. If the distance between node i (located at \vec{x}_i) and a point A (located at \vec{x}_A) is smaller than r_i , then point A belongs to node i 's influence domain Λ_i .

We can define the influence domain Λ_i of a node i as a set of points whose distances to \vec{x}_i are less than or equal to r_i :

$$\Lambda_i = \{ \vec{x} \mid \|\vec{x} - \vec{x}_i\| \leq r_i \} \quad (3.19)$$

where

$$\|\vec{x} - \vec{x}_i\| = \sqrt{(x - x_i)^2 + (y - y_i)^2} \quad (3.20)$$

in two dimensions and

$$\|\vec{x} - \vec{x}_i\| = \sqrt{(x - x_i)^2 + (y - y_i)^2 + (z - z_i)^2} \quad (3.21)$$

in three dimensions.

There is a certain freedom in defining the radii of the influence domains. It is possible for each node to have a different value for r , but, according to proposition 1.2, they must be taken so that the union of all Λ 's cover the computational domain Ω (and its boundary $\partial\Omega$) entirely.

Let us get back to expression (3.15). In order to fully specify our set of numbers, we plug (3.11) into (3.15):

$$\forall i \in Neigh(\vec{x}) \quad S_i = w \left(\frac{\|\vec{x} - \vec{x}_i\|}{r_i} \right) \left(\sum_{j=1}^m p_j(\vec{x}_i) a_j(\vec{x}) - \hat{u}_i \right)^2 \quad (3.22)$$

To recapitulate: we took a point \vec{x} , found the set of all nodes extending their influence domains until \vec{x} [i.e., the set $Neigh(\vec{x})$], and for each node i in $Neigh(\vec{x})$, we formed an expression S_i through (3.22) [which depends on \vec{x} , \vec{x}_i and on monomials $p_j(\vec{x}_i)$]. The nodal parameters \hat{u}_i are unknown. In the next step, we sum up the elements of S and hope that something interesting happens:

$$J = \sum_{i \in \text{Neigh}(\vec{x})} w \left(\frac{\|\vec{x} - \vec{x}_i\|}{r_i} \right) \left(\sum_{j=1}^m p_j(\vec{x}_i) a_j(\vec{x}) - \hat{u}_i \right)^2 \quad (3.23)$$

The weight function w is positive, according to (3.16) and (3.17), and the second term also, since it is the square of a quantity (the difference between $u^h(\vec{x}, \vec{x}_i)$ and \hat{u}_i). So we have a sum of positive terms, and therefore, J is always greater than (or equal) to zero. As said earlier, the nodal parameters will be determined only at the final stage of the meshless analysis, after the final linear system is solved. They have no role to play here. If we concentrate our attention on the unknown terms a_j 's, we can express (3.23) as

$$J(a_1(\vec{x}), \dots, a_m(\vec{x})) = \sum_{i \in \text{Neigh}(\vec{x})} w \left(\frac{\|\vec{x} - \vec{x}_i\|}{r_i} \right) \left(\sum_{j=1}^m p_j(\vec{x}_i) a_j(\vec{x}) - \hat{u}_i \right)^2 \quad (3.24)$$

i.e., J is a function of the unknown terms $a_1(\vec{x}), \dots, a_m(\vec{x})$. Because \vec{x} is known (the point at which we want to calculate the shape functions) as well as the location of the influencing nodes (points \vec{x}_i) and the monomial basis terms p_j , we can regard J as a function of the terms a_1, \dots, a_m (all calculated at \vec{x}). Then

$$J(a_1, a_2, \dots, a_m) = \sum_{i \in \text{Neigh}(\vec{x})} w \left(\frac{\|\vec{x} - \vec{x}_i\|}{r_i} \right) \left(\sum_{j=1}^m p_j(\vec{x}_i) a_j - \hat{u}_i \right)^2 \quad (3.25)$$

Equation (3.25) tells us that there is a map which associates a real number to a vector in \mathbb{R}^m . In other words, J is a *real functional*. The vector in \mathbb{R}^m is nothing else than the unknown terms $a_j(\vec{x})$ assembled together:

$$[a_1(\vec{x}), a_2(\vec{x}), \dots, a_m(\vec{x})]^T = \mathbf{a}(\vec{x}) \quad (3.26)$$

As we take different points \vec{x} , we get different vectors $\mathbf{a}(\vec{x})$ and therefore, different numbers $J(\mathbf{a})$.

Once we choose a point \vec{x} , how do we find the coefficients of the vector $\mathbf{a}(\vec{x})$? Remember that J is always greater than (or equal to) zero. No matter what values for the a_j 's we plug into (3.25), we always get a positive number. So it is reasonable to suppose the existence of a set of numbers a_j 's that, once plugged into (3.25), makes J assume its smallest value. So it seems that we have just found our answer: the coefficients of the vector \mathbf{a} are those that *minimize* the functional J . Looking at (3.25) as a function of several variables, we can find the a_j 's if, for each a_j , we impose $\partial J / \partial a_j = 0$. We can state this proposition through a conditional structure:

$$\forall j \in \mathbb{N} \left(j \leq m \rightarrow \frac{\partial J}{\partial a_j} = 0 \right) \quad (3.27)$$

i.e., for all natural numbers j , if j is less than or equal to m (the number of monomial terms in $\mathbf{p}(\vec{x})$) then $\partial J / \partial a_j = 0$.

Let us make explicit how to evaluate the a_j 's. It is a rather lengthy procedure, but it is at the same time quite a beautiful one. It is worth being described in detail. Beginning with $j = 1$, we have

$$\frac{\partial J}{\partial a_1} = 0 \quad (3.28)$$

Substituting (3.25) for J :

$$\frac{\partial}{\partial a_1} \left\{ \sum_{i \in \text{Neigh}(\vec{x})} w \left(\frac{\|\vec{x} - \vec{x}_i\|}{r_i} \right) \left(\sum_{j=1}^m p_j(\vec{x}_i) a_j - \hat{u}_i \right)^2 \right\} = 0 \quad (3.29)$$

As the weight function w is independent of a_1 , the derivative operator can be moved through it:

$$\sum_{i \in \text{Neigh}(\vec{x})} w \left(\frac{\|\vec{x} - \vec{x}_i\|}{r_i} \right) \frac{\partial}{\partial a_1} \left[\left(\sum_{j=1}^m p_j(\vec{x}_i) a_j - \hat{u}_i \right)^2 \right] = 0 \quad (3.30)$$

The chain rule of derivation:

$$\sum_{i \in \text{Neigh}(\vec{x})} w \left(\frac{\|\vec{x} - \vec{x}_i\|}{r_i} \right) 2 \left(\sum_{j=1}^m p_j(\vec{x}_i) a_j - \hat{u}_i \right) \frac{\partial}{\partial a_1} \left[\sum_{k=1}^m p_k(\vec{x}_i) a_k - \hat{u}_i \right] = 0 \quad (3.31)$$

When deriving the innermost term, it should be noticed that j is a dummy variable. Therefore, j can be freely substituted by another index, like k . We get:

$$\sum_{i \in \text{Neigh}(\vec{x})} w \left(\frac{\|\vec{x} - \vec{x}_i\|}{r_i} \right) 2 \left(\sum_{j=1}^m p_j(\vec{x}_i) a_j - \hat{u}_i \right) p_1(\vec{x}_i) = 0 \quad (3.32)$$

Factoring out the number '2' and rearranging the terms:

$$\sum_{i \in \text{Neigh}(\vec{x})} w \left(\frac{\|\vec{x} - \vec{x}_i\|}{r_i} \right) p_1(\vec{x}_i) \sum_{j=1}^m p_j(\vec{x}_i) a_j = \sum_{i \in \text{Neigh}(\vec{x})} w \left(\frac{\|\vec{x} - \vec{x}_i\|}{r_i} \right) p_1(\vec{x}_i) \hat{u}_i \quad (3.33)$$

In order to prevent the notation from becoming cluttered, the weight function w will henceforth be represented differently:

$$w \left(\frac{\|\vec{x} - \vec{x}_i\|}{r_i} \right) = w_i(\vec{x}) \quad (3.34)$$

Let us consider the left side of (3.33) first. Expanding it, we get:

$$\sum_{i \in \text{Neigh}(\vec{x})} w_i(\vec{x}) p_1(\vec{x}_i) [p_1(\vec{x}_i) \dots p_m(\vec{x}_i)] \begin{bmatrix} a_1 \\ \vdots \\ a_m \end{bmatrix} \quad (3.35)$$

Moving the factor $p_1(\vec{x}_i)$ into the vector that collects the p_j 's, there follows:

$$\sum_{i \in \text{Neigh}(\vec{x})} w_i(\vec{x}) [p_1(\vec{x}_i)p_1(\vec{x}_i) \dots p_1(\vec{x}_i)p_m(\vec{x}_i)] \begin{bmatrix} a_1 \\ \vdots \\ a_m \end{bmatrix} \quad (3.36)$$

The same reasoning applies to $j = 2$ (got from $\partial J / \partial a_2 = 0$):

$$\sum_{i \in \text{Neigh}(\vec{x})} w_i(\vec{x}) [p_2(\vec{x}_i)p_1(\vec{x}_i) \dots p_2(\vec{x}_i)p_m(\vec{x}_i)] \begin{bmatrix} a_1 \\ \vdots \\ a_m \end{bmatrix} \quad (3.37)$$

And likewise to $j = m$ (got from $\partial J / \partial a_m = 0$):

$$\sum_{i \in \text{Neigh}(\vec{x})} w_i(\vec{x}) [p_m(\vec{x}_i)p_1(\vec{x}_i) \dots p_m(\vec{x}_i)p_m(\vec{x}_i)] \begin{bmatrix} a_1 \\ \vdots \\ a_m \end{bmatrix} \quad (3.38)$$

We can gather the information concerning the left side of (3.33) for $1 \leq j \leq m$ and thence form a matrix:

$$\sum_{i \in \text{Neigh}(\vec{x})} w_i(\vec{x}) \begin{bmatrix} p_1(\vec{x}_i)p_1(\vec{x}_i) & \dots & p_1(\vec{x}_i)p_m(\vec{x}_i) \\ \vdots & \ddots & \vdots \\ p_m(\vec{x}_i)p_1(\vec{x}_i) & \dots & p_m(\vec{x}_i)p_m(\vec{x}_i) \end{bmatrix} \begin{bmatrix} a_1 \\ \vdots \\ a_m \end{bmatrix} \quad (3.39)$$

The set of influencing nodes $\text{Neigh}(\vec{x})$ has n nodes. However, in the summation expressed above, the index i does not run from 1 to n . As we saw earlier, there is a numbering scheme relating indices and nodes. In the scenario of Fig.3.1, i would take on the values from the set $\{3,7,11,23,40\}$, according to (3.6). Let us consider here an uppercase index I that runs from 1 to n . I is related to i in such a way that, when $i = 3$, then $I = 1$; when $i = 7$, then $I = 2$, and so forth. Rewriting (3.39):

$$\sum_{I=1}^n w_I(\vec{x}) \begin{bmatrix} p_1(\vec{x}_I)p_1(\vec{x}_I) & \dots & p_1(\vec{x}_I)p_m(\vec{x}_I) \\ \vdots & \ddots & \vdots \\ p_m(\vec{x}_I)p_1(\vec{x}_I) & \dots & p_m(\vec{x}_I)p_m(\vec{x}_I) \end{bmatrix} \begin{bmatrix} a_1 \\ \vdots \\ a_m \end{bmatrix} \quad (3.40)$$

Ignoring for now the vector $[a_1, \dots, a_m]^T$, the matrix multiplying it can be written as (after the summation on I has been carried out):

$$\begin{bmatrix} p_1(\vec{x}_1)w_1(\vec{x})p_1(\vec{x}_1) + \dots + p_1(\vec{x}_n)w_n(\vec{x})p_1(\vec{x}_n) & \dots & p_1(\vec{x}_1)w_1(\vec{x})p_m(\vec{x}_1) + \dots + p_1(\vec{x}_n)w_n(\vec{x})p_m(\vec{x}_n) \\ \vdots & \ddots & \vdots \\ p_m(\vec{x}_1)w_1(\vec{x})p_1(\vec{x}_1) + \dots + p_m(\vec{x}_n)w_n(\vec{x})p_1(\vec{x}_n) & \dots & p_m(\vec{x}_1)w_1(\vec{x})p_m(\vec{x}_1) + \dots + p_m(\vec{x}_n)w_n(\vec{x})p_m(\vec{x}_n) \end{bmatrix} \quad (3.41)$$

This is a $m \times m$ matrix. The element in line α ($1 \leq \alpha \leq m$) and column β ($1 \leq \beta \leq m$) is given by

$$A_{\alpha\beta} = p_\alpha(\vec{x}_1)w_1(\vec{x})p_\beta(\vec{x}_1) + \dots + p_\alpha(\vec{x}_n)w_n(\vec{x})p_\beta(\vec{x}_n) \quad (3.42)$$

Or in matrix form (This is a tricky step. Each element $A_{\alpha\beta}$ of matrix (3.41) is going to be represented by a product of matrices. Beware!):

$$A_{\alpha\beta} = [p_\alpha(\vec{x}_1), p_\alpha(\vec{x}_2), \dots, p_\alpha(\vec{x}_n)] \begin{bmatrix} w_1(\vec{x}) & 0 & \dots & 0 \\ 0 & w_2(\vec{x}) & \dots & \vdots \\ \vdots & \vdots & \ddots & \vdots \\ 0 & \dots & \dots & w_n(\vec{x}) \end{bmatrix} \begin{bmatrix} p_\beta(\vec{x}_1) \\ p_\beta(\vec{x}_2) \\ \vdots \\ p_\beta(\vec{x}_n) \end{bmatrix} \quad (3.43)$$

If an element $A_{\alpha\beta}$ is given by (3.43) above, then one can see that the whole matrix, which we will be called $\mathbf{A}(\vec{x})$ reads:

$$\mathbf{A}(\vec{x}) = \begin{bmatrix} p_1(\vec{x}_1) & \dots & p_1(\vec{x}_n) \\ \vdots & \ddots & \vdots \\ p_m(\vec{x}_1) & \dots & p_m(\vec{x}_n) \end{bmatrix} \begin{bmatrix} w_1(\vec{x}) & \dots & 0 \\ \vdots & \ddots & \vdots \\ 0 & \dots & w_n(\vec{x}) \end{bmatrix} \begin{bmatrix} p_1(\vec{x}_1) & \dots & p_m(\vec{x}_1) \\ \vdots & \ddots & \vdots \\ p_1(\vec{x}_n) & \dots & p_m(\vec{x}_n) \end{bmatrix} \quad (3.44)$$

If we call

$$\mathbf{P} = \begin{bmatrix} p_1(\vec{x}_1) & \dots & p_m(\vec{x}_1) \\ \vdots & \ddots & \vdots \\ p_1(\vec{x}_n) & \dots & p_m(\vec{x}_n) \end{bmatrix} \quad (3.45)$$

and

$$\mathbf{W}(\vec{x}) = \begin{bmatrix} w_1(\vec{x}) & 0 & \dots & 0 \\ 0 & w_2(\vec{x}) & \dots & \vdots \\ \vdots & \vdots & \ddots & \vdots \\ 0 & \dots & \dots & w_n(\vec{x}) \end{bmatrix} \quad (3.46)$$

then matrix $\mathbf{A}(\vec{x})$ can be written as

$$\mathbf{A}(\vec{x}) = \mathbf{P}^T \mathbf{W}(\vec{x}) \mathbf{P} \quad (3.47)$$

\mathbf{P} is a $n \times m$ matrix, and \mathbf{W} is a diagonal $n \times n$ matrix. Consequently, $\mathbf{A}(\vec{x})$ is a $m \times m$ matrix, as expected. So for $1 \leq j \leq m$ if we make $\partial J / \partial a_j = 0$, we get m expressions like (3.33). If we take the left sides of each one of these expressions and assemble into a matrix, we get the matrix \mathbf{A} . This is the meaning of matrix \mathbf{A} .

Let us get back now to the right side of (3.33). It is restated here for convenience:

$$\sum_{i \in \text{Neigh}(\vec{x})} w \left(\frac{\|\vec{x} - \vec{x}_i\|}{r_i} \right) p_1(\vec{x}_i) \hat{u}_i \quad (3.48)$$

Remember that we have arrived at this result by first considering the case in which $j = 1$. Rewriting (3.48) above and considering the index I instead of i (as explained earlier):

$$[p_1(\vec{x}_1)w_1(\vec{x}), \dots, p_1(\vec{x}_n)w_n(\vec{x})] \begin{bmatrix} \hat{u}_1 \\ \vdots \\ \hat{u}_n \end{bmatrix} \quad (3.49)$$

The case for $j = 2$ would read (got from $\partial J / \partial a_2 = 0$)

$$[p_2(\vec{x}_1)w_1(\vec{x}), \dots, p_2(\vec{x}_n)w_n(\vec{x})] \begin{bmatrix} \hat{u}_1 \\ \vdots \\ \hat{u}_n \end{bmatrix} \quad (3.50)$$

The case in which $j = m$ (got from $\partial J / \partial a_m = 0$) can be determined likewise:

$$[p_m(\vec{x}_1)w_1(\vec{x}), \dots, p_m(\vec{x}_n)w_n(\vec{x})] \begin{bmatrix} \hat{u}_1 \\ \vdots \\ \hat{u}_n \end{bmatrix} \quad (3.51)$$

Assembling the expressions from $1 \leq j \leq m$ [(3.49), (3.50), and (3.51)] together into a matrix, we get:

$$\begin{bmatrix} p_1(\vec{x}_1)w_1(\vec{x}) & p_1(\vec{x}_2)w_2(\vec{x}) & \cdots & p_1(\vec{x}_n)w_n(\vec{x}) \\ p_2(\vec{x}_1)w_1(\vec{x}) & p_2(\vec{x}_2)w_2(\vec{x}) & \cdots & p_2(\vec{x}_n)w_n(\vec{x}) \\ \vdots & \vdots & \ddots & \vdots \\ p_m(\vec{x}_1)w_1(\vec{x}) & p_m(\vec{x}_2)w_2(\vec{x}) & \cdots & p_m(\vec{x}_n)w_n(\vec{x}) \end{bmatrix} \begin{bmatrix} \hat{u}_1 \\ \hat{u}_2 \\ \vdots \\ \hat{u}_n \end{bmatrix} \quad (3.52)$$

If we express this as $\mathbf{B}(\vec{x})\hat{\mathbf{u}}$, where $\mathbf{B}(\vec{x})$ is a $m \times n$ matrix, one verifies that it can be written as

$$\mathbf{B}(\vec{x}) = \begin{bmatrix} p_1(\vec{x}_1) & p_1(\vec{x}_2) & \cdots & p_1(\vec{x}_n) \\ p_2(\vec{x}_1) & p_2(\vec{x}_2) & \cdots & p_2(\vec{x}_n) \\ \vdots & \vdots & \ddots & \vdots \\ p_m(\vec{x}_1) & p_m(\vec{x}_2) & \cdots & p_m(\vec{x}_n) \end{bmatrix} \begin{bmatrix} w_1(\vec{x}) & 0 & \cdots & 0 \\ 0 & w_2(\vec{x}) & \cdots & 0 \\ \vdots & \vdots & \ddots & 0 \\ 0 & 0 & 0 & w_n(\vec{x}) \end{bmatrix} \quad (3.53)$$

But if we take a look at (3.45) and (3.46), we conclude that

$$\mathbf{B}(\vec{x}) = \mathbf{P}^T \mathbf{W}(\vec{x}) \quad (3.54)$$

Expression (3.52) above is therefore equal to

$$\mathbf{B}(\vec{x})\hat{\mathbf{u}} = \mathbf{P}^T \mathbf{W}(\vec{x})\hat{\mathbf{u}} \quad (3.55)$$

where

$$\hat{\mathbf{u}} = [\hat{u}_1, \hat{u}_2, \dots, \hat{u}_n]^T \quad (3.56)$$

is a vector collecting all nodal parameters involved.

So for each j in (3.27), we get an expression like (3.33) (which was obtained from the case $j = 1$). For all j such that $1 \leq j \leq m$ we get a linear system [from (3.40), (3.41), (3.44) and (3.55)]:

$$\mathbf{A}(\vec{x}) \begin{bmatrix} a_1 \\ \vdots \\ a_m \end{bmatrix} = \mathbf{B}(\vec{x})\hat{\mathbf{u}} \quad (3.57)$$

or, invoking (3.26):

$$\mathbf{A}(\vec{x})\mathbf{a}(\vec{x}) = \mathbf{B}(\vec{x})\hat{\mathbf{u}} \quad (3.58)$$

which means that

$$\mathbf{a}(\vec{x}) = \mathbf{A}^{-1}(\vec{x})\mathbf{B}(\vec{x})\hat{\mathbf{u}} \quad (3.59)$$

We are almost there. We just have to remember two little things. First, if we take the fundamental “meshless approximation rule” (equation (3.5), restated again here):

$$u^h(\vec{x}) = \sum_{i \in \text{Neigh}(\vec{x})} \phi_i(\vec{x}) \hat{u}_i \quad (3.60)$$

and rewrite it using the indices I instead of i , we get

$$u^h(\vec{x}) = \sum_{I=1}^n \phi_I(\vec{x}) \hat{u}_I = \mathbf{\Phi}(\vec{x}) \hat{\mathbf{u}} \quad (3.61)$$

where $\mathbf{\Phi}(\vec{x}) = [\phi_1(\vec{x}), \phi_2(\vec{x}), \dots, \phi_n(\vec{x})]$ is a vector that collects the shape functions from all influencing nodes and $\hat{\mathbf{u}}$ is a vector of nodal parameters [according to (3.56)].

Second, if we take the MLS approximation rule (equation (3.7), restated here again)

$$u^h(\vec{x}) = \sum_{j=1}^m p_j(\vec{x}) a_j(\vec{x}) \quad (3.62)$$

And rewrite it using (3.10) and (3.26), we get

$$u^h(\vec{x}) = \mathbf{p}^T(\vec{x}) \mathbf{a}(\vec{x}) \quad (3.63)$$

From (3.61) and (3.63) there follows

$$\mathbf{\Phi}(\vec{x}) \hat{\mathbf{u}} = \mathbf{p}^T(\vec{x}) \mathbf{a}(\vec{x}) \quad (3.64)$$

But we already know vector $\mathbf{a}(\vec{x})$; it is given by (3.59). Therefore

$$\mathbf{\Phi}(\vec{x}) \hat{\mathbf{u}} = \mathbf{p}^T(\vec{x}) \mathbf{A}^{-1}(\vec{x}) \mathbf{B}(\vec{x}) \hat{\mathbf{u}} \quad (3.65)$$

In comparing both sides of equation (3.65) above, we finally arrive at the shape functions:

$$\mathbf{\Phi}(\vec{x}) = [\phi_1(\vec{x}), \phi_2(\vec{x}), \dots, \phi_n(\vec{x})] = \mathbf{p}^T(\vec{x}) \mathbf{A}^{-1}(\vec{x}) \mathbf{B}(\vec{x}) \quad (3.66)$$

Given a point \vec{x} , equation (3.66) shows how to calculate the shape functions associated to each one of the n nodes influencing \vec{x} . The last step is a translation from the indices I (which range from 1 to n) to the real indices i (n elements of the set $Neigh(\vec{x})$). In the scenario depicted in Fig.1, expression (3.66) would provide a vector of shape functions whose subscripts are the true indices of the influencing nodes, i.e.,

$$\mathbf{\Phi}(\vec{x}) = [\phi_3(\vec{x}), \phi_7(\vec{x}), \phi_{11}(\vec{x}), \phi_{23}(\vec{x}), \phi_{40}(\vec{x})] \quad (3.67)$$

We have seen in the last pages that many calculations are necessary in order to get the shape functions. But when it comes to their numerical implementation, one need not consider all that has been said so far concerning the ϕ 's. The process of calculating the shape functions at a point \vec{x} boils down to carrying out the matrix operations described by (3.66). One begins by first finding which nodes extend their influence domains until \vec{x} .

There are some ways in which such a task can be done, but in this work a *KdTree*-based search algorithm has been employed (the advantages of doing so are explained in [Parreira² *et al.*, 2006]). The coordinates of all nodes in the domain Ω are plugged into a tree (a sort of data structure). Given a point \vec{x} , one can then request the algorithm to return all neighbor nodes to \vec{x} . In other words, the search algorithm determines the set $Neigh(\vec{x})$. The version of this algorithm employed in this work is very quick, even if thousands of nodes are scattered throughout Ω . The impact of the speed in computing neighbor nodes on the CPU time performance has not been evaluated, because this kind of analysis would take us too far afield from the main theme of this

work. But it remains to be investigated in the future, when more detailed studies concerning the computational cost of meshless methods will be carried out.

Once the indices of the neighbor nodes are found, one then proceeds to the evaluation of (3.66). The polynomial basis $\mathbf{p}(\vec{x})$ is found through (3.10). The matrices $\mathbf{A}(\vec{x})$ and $\mathbf{B}(\vec{x})$ are calculated via matrices \mathbf{P} and $\mathbf{W}(\vec{x})$ (3.45 and 3.46). It can be seen that the whole procedure relies on calculations

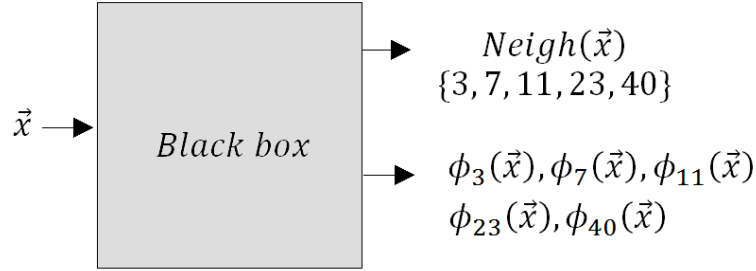


Fig.3.3. The procedure for finding which nodes influence point \vec{x} and their associated shape functions calculated at \vec{x} can be written in a simple piece of code, which resembles a kind of “black box”.

involving matrices $\mathbf{p}(\vec{x})$, \mathbf{P} and $\mathbf{W}(\vec{x})$, which by their turn depend on the coordinates of the point \vec{x} and on those of the influencing nodes. So everything amounts to mixing together the information concerning the coordinates of the nodes. After some calculations, one gets the shape functions ϕ 's.

Summing up, one can regard the implementation of shape functions as a “black box” procedure. The algorithm that determines the neighbor nodes (*KdTree*) and the numerical procedures for manipulating the matrices $\mathbf{p}(\vec{x})$, \mathbf{P} , and $\mathbf{W}(\vec{x})$ can all be assembled together in a separate piece of code (like a script in MATLAB). This black box takes in a point \vec{x} and returns the set of shape functions associated to all neighbor nodes that influence \vec{x} (together with their global indices, of course) calculated at \vec{x} . This is illustrated in Fig.3.3, for the scenario depicted in Fig.3.1.

Observation: Needless to say, given a point \vec{x} , only the shape functions whose indices are members of the set $Neigh(\vec{x})$ will be different from zero. This is a direct consequence from the fact that the shape functions are compactly supported. Nodes located too far away from \vec{x} are unable to extend their influence domains over there, and therefore, their associated shape functions are zero at \vec{x} . Mathematically, this can be expressed as:

$$\forall i (i \notin Neigh(\vec{x}) \rightarrow \phi_i(\vec{x}) = 0) \quad (3.68)$$

where the index i runs from 1 to the total number of nodes scattered throughout Ω , the antecedent of the conditional states that node i is not a neighbor to \vec{x} , and the consequent says that the shape function associated to node i is zero at \vec{x} . In the scenario of Fig.3.1, as $Neigh(\vec{x}) = \{3,7,11,23,40\}$, it means that, for example, $\phi_{55}(\vec{x}) = 0$, because $55 \notin Neigh(\vec{x})$.

3.1.1 Examples of MLS shape functions

It is now time to have a glance at how MLS shape functions look like. The first example illustrates the ϕ 's calculated for one-dimensional problems. The domain Ω is a straight line, extending from 0 to 1, or, $\Omega = [0,1]$. We took 11 nodes equally distributed across Ω , i.e., $x_1 = 0, x_2 = 0.1, x_3 = 0.2, \dots, x_{11} = 1$. The influence domains of the nodes (r_i) are set up in such a way that $r_i = 2d$, where d is the distance between two adjacent nodes (i.e., the *internodal* distance, equal to 0.1). Figures 3.4 and 3.5 illustrates the domain Ω and the MLS shape functions, respectively.

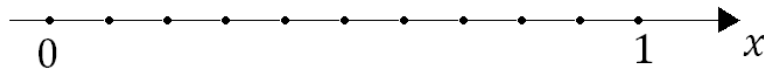


Fig.3.4. A one-dimensional domain Ω extending from $x = 0$ to $x = 1$. Eleven nodes have been equally scattered between the two extreme points.

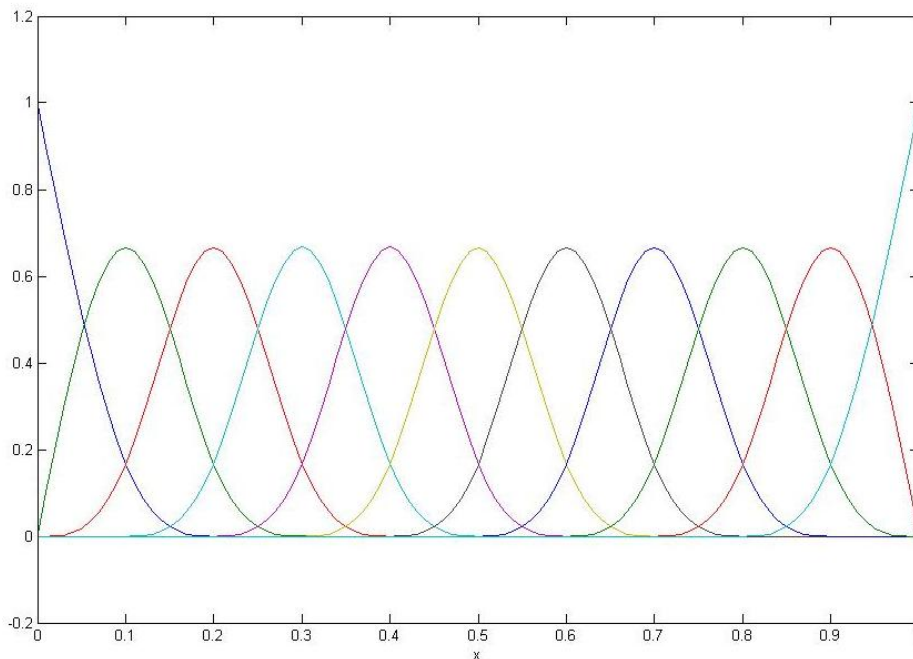


Fig.3.5. Eleven shape functions associated to the eleven nodes of Fig. 4.

The second example deals with two-dimensional shape functions, in which the domain Ω is now supposed to be a square, $\Omega = [0,1] \times [0,1]$. Nodes are scattered throughout Ω (and throughout its boundary $\partial\Omega$ as well), as in Fig.3.6. We can take a symmetrical distribution, say, 21 nodes along the x -direction and 21 along the y -direction. This amounts to $N = 441$ nodes in the domain. Suppose we want to evaluate the shape function associated to a node located at a node whose coordinates are $(0.55,0.65)$. The index of this node could be, for example, 287 (remember, different numbering schemes would lead to different global indices for the nodes). So we want to evaluate ϕ_{287} .

The first step is to define the size of the influence domains. We have employed $r_i = 2d$, where d is the internodal distance. This value has been employed for all nodes in Ω (this is not necessary, but it is simpler to write the code in this way). In the second step, we choose a square region larger than the influence domain Λ_{287} . This region is a sort of ‘window’ that will display the shape function ϕ_{287} . If ϕ_{287} is to be seen in its entirety, the window should be centered at \vec{x}_{287} , and its sides should be larger than r_{287} . As the third step, we scan all this window, i.e., we set up a fine grid of ‘observation’ points \vec{x} . To each one of these points \vec{x} , we apply the black box procedure, and verify if there is some value ascribed to node 287. Explaining in detail, it means that:

- (1) We take a \vec{x} and apply the black box procedure. This returns the set of shape functions influencing \vec{x} .
- (2) We verify if some of the influencing nodes is node 287 (the black box procedure determines the set $Neigh(\vec{x})$; we have just to look for 287 in the list of influencing nodes).
- (3) In the case that (2) turns out to be true, we ascribe the value ϕ_{287} to point \vec{x} . Otherwise, ϕ_{287} is made equal to zero (this is an equivalent way of saying that $287 \notin Neigh(\vec{x})$).
- (4) We return to (1) applied to a different point \vec{x} of the window and repeat the procedure.

This process is carried out for all observation points in the window region. It is obvious that, for those \vec{x} far from \vec{x}_{287} , ϕ_{287} will be zero there. This is what it means for any function to be compactly supported. As \vec{x} gets closer to \vec{x}_{287} , the shape function assumes higher values, until it reaches its peak when $\vec{x} = \vec{x}_{287}$. After we are done with this, we are ready to behold the graphical form of the MLS shape function associated to node 287. It is beautifully depicted in Fig.3.7.

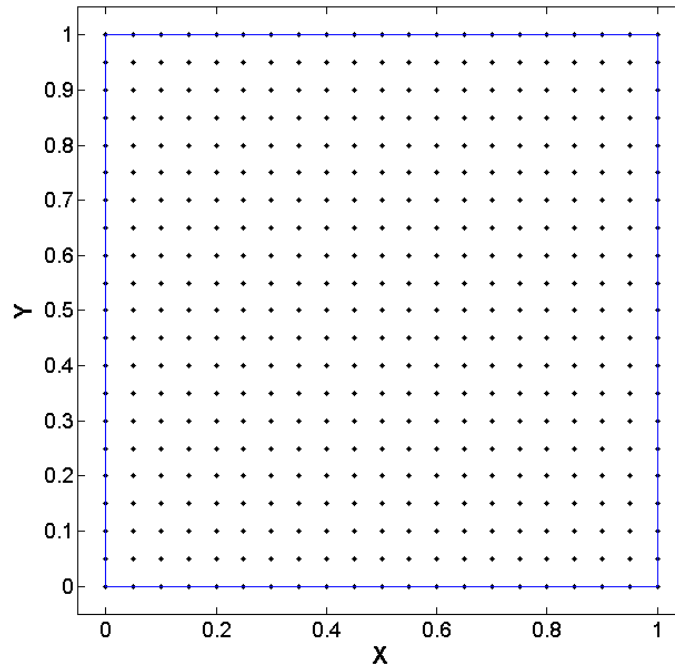


Fig.3.6. A square domain $\Omega = [0,1] \times [0,1]$, in which a nodal arrangement of 441 nodes (21×21) has been set up.

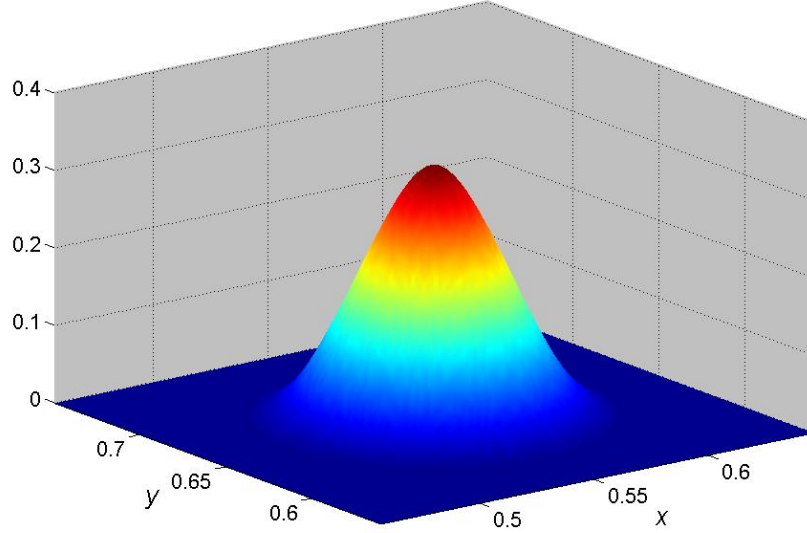


Fig.3.7. A MLS shape function associated to a node located at (0.55, 0.65).

Observation #1: Of course that such amount of work is not necessary in the meshless analysis of a problem. Only if someone is interested in the graphical forms of shape functions that he (or she) must perform all the aforementioned steps.

Observation #2: As it is impossible to visualize the shape functions constructed for three-dimensional problems, they are not illustrated here. But there is nothing special regarding them. They are constructed in the same way as two-dimensional shape functions are. All there is to do in order to find ϕ at a point \vec{x} is to make use of a *KdTree*-based search algorithm that supports points described by triples of real numbers [i.e., points like (x, y, z)] and of the three-dimensional analogues of matrices $\mathbf{p}(\vec{x})$, \mathbf{P} , and $\mathbf{W}(\vec{x})$.

3.1.2 Some remarks regarding the MLS shape functions

The shape functions in Figs.3.5 and 3.7 have been constructed using only linear terms in the vector $\mathbf{p}(\vec{x})$, i.e., $\mathbf{p}(\vec{x}) = [1, x]^T$ for the one-dimensional and $\mathbf{p}(\vec{x}) = [1, x, y]^T$ for the two-dimensional case. These figures reveal that the MLS shape functions are bell-shaped, despite the fact of employing only linear terms. This is in stark contrast with the FEM shape functions, which resembles triangles (one-dimensional) and pyramids (two-dimensional), if only linear terms are used. The extra degree of smoothness comes from the window function $w(t)$ [(16) and (17)]. If the shape functions are smooth, then their first derivatives are continuous. This feature turns out to be a great advantage when one is interested in the derivatives of the approximated function u^h . For instance, if the electrostatic potential is approximated by MLS shape functions, then the electric field is approximated by continuous functions (the first derivatives of the shape functions). The issue concerning the derivatives of the shape functions will be addressed a little bit later in this chapter (Section 3.3).

It can also be seen from Figs.3.5 and 3.7 that the MLS shape functions do not satisfy the Kronecker delta criterion, i.e., given two neighbor nodes I and J :

$$\phi_I(\vec{x}_J) \neq \delta_{IJ} \quad (3.69)$$

The most obvious consequence of (3.69) is that the nodal parameters (the \hat{u} 's) are not the values of the approximated function u^h at the nodes, i.e., for a node I :

$$u^h(\vec{x}_I) \neq \hat{u}_I \quad (3.70)$$

Let us see the impact this characteristic has on the meshless analysis via MLS shape functions. The approximated function u^h is approximated as (3.5) (restated again below):

$$u^h(\vec{x}) = \sum_{i \in \text{Neigh}(\vec{x})} \phi_i(\vec{x}) \hat{u}_i \quad (3.71)$$

If we number the nodes differently (as explained earlier), we get:

$$u^h(\vec{x}) = \sum_{I=1}^n \phi_I(\vec{x}) \hat{u}_I \quad (3.72)$$

where the index I now runs from 1 to n (the number of nodes in $\text{Neigh}(\vec{x})$). If the shape functions were to obey the Kronecker delta property, we would find that (after requiring u^h to be calculated at a node J);

$$u^h(\vec{x}_J) = \sum_{I=1}^n \phi_I(\vec{x}_J) \hat{u}_I = \sum_{I=1}^n \delta_{IJ} \hat{u}_I = \hat{u}_J \quad (3.73)$$

i.e., the approximated function at a node $u^h(\vec{x}_J)$ would be equal to the nodal parameter associated to that node \hat{u}_J . This has a little impact when one deals with a problem in which Dirichlet boundary conditions are imposed at some portion of the global boundary $\partial\Omega$. The consequence from the fact that MLS shape functions do not obey the Kronecker delta property will be treated later (Section 5.5), in the discussion of boundary conditions and collocation methods.

The last remark on MLS shape functions has to do with the matrix $\mathbf{A}(\vec{x})$, described by 3.47). According to (3.66), this matrix needs to be inverted in order to find the shape functions influencing a point \vec{x} . Can we take for granted that $\mathbf{A}(\vec{x})$ will always be non-singular, i.e., able to be inverted? The answer is negative. Sometimes, depending on the nodal distribution and on other factors, we can get singular matrices, which prevent us from getting the shape functions. This is a strong drawback of the MLS approximation.

According to [Liu, 2003], given a point \vec{x} , one of the requirements for avoiding the singularity of the \mathbf{A} matrices is to make sure that the number of nodes influencing \vec{x} (i.e., n), should be much greater than the number of monomial terms in the vector $\mathbf{p}(\vec{x})$ (i.e., m). In other words, one must guarantee that

$$n \gg m \quad (3.74)$$

There is a lot more to say about this, as the nodal distribution (topology) also has an influence on this issue. However, in the next chapter we will present a situation in which singular \mathbf{A} matrices occur frequently, and the ways we have found to overcome this issue.

3.2 Calculating the Derivatives of Shape Functions

If the shape functions themselves lack analytical expressions, so their derivatives. In the next lines we shall proceed to lay down methods for calculating first order derivatives of both MLS and RPIM-PR shape functions.

3.2.1 MLS Shape Functions

We follow a way suggested by G. R. Liu [Liu, 2003]. From (3.66) (restated below) we can express the $1 \times n$ vector of shape functions as

$$\Phi(\vec{x}) = [\phi_1(\vec{x}), \phi_2(\vec{x}), \dots, \phi_n(\vec{x})] = \mathbf{p}^T(\vec{x})\mathbf{A}^{-1}(\vec{x})\mathbf{B}(\vec{x}) \quad (3.75)$$

We write this as

$$\Phi(\vec{x}) = \mathbf{p}^T(\vec{x})\mathbf{A}^{-1}(\vec{x})\mathbf{B}(\vec{x}) = \boldsymbol{\gamma}^T(\vec{x})\mathbf{B}(\vec{x}) \quad (3.76)$$

where $\boldsymbol{\gamma}(\vec{x})$ is a $m \times 1$ vector. Or:

$$\mathbf{p}^T(\vec{x})\mathbf{A}^{-1}(\vec{x}) = \boldsymbol{\gamma}^T(\vec{x}) \quad (3.77)$$

Right multiplying both sides by $\mathbf{A}(\vec{x})$:

$$\mathbf{p}^T(\vec{x}) = \boldsymbol{\gamma}^T(\vec{x})\mathbf{A}(\vec{x}) \quad (3.78)$$

Taking the transpose at both sides:

$$(\mathbf{p}^T(\vec{x}))^T = (\boldsymbol{\gamma}^T(\vec{x})\mathbf{A}(\vec{x}))^T \quad (3.79)$$

Or:

$$\mathbf{p}(\vec{x}) = \mathbf{A}^T(\vec{x})\boldsymbol{\gamma}(\vec{x}) \quad (3.80)$$

We must remember that, according to (3.47),

$$\mathbf{A}(\vec{x}) = \mathbf{P}^T\mathbf{W}(\vec{x})\mathbf{P} = \mathbf{P}^T(\mathbf{W}(\vec{x})\mathbf{P}) \quad (3.81)$$

And therefore its transpose is given by

$$\mathbf{A}^T(\vec{x}) = (\mathbf{P}^T(\mathbf{W}(\vec{x})\mathbf{P}))^T = (\mathbf{W}(\vec{x})\mathbf{P})^T\mathbf{P} = \mathbf{P}^T\mathbf{W}^T(\vec{x})\mathbf{P} \quad (3.82)$$

However, according to (3.46), $\mathbf{W}(\vec{x})$ is a diagonal matrix, and therefore it is equal to its own transpose: $\mathbf{W}(\vec{x}) = \mathbf{W}^T(\vec{x})$. From this follows:

$$\mathbf{A}^T(\vec{x}) = \mathbf{P}^T\mathbf{W}(\vec{x})\mathbf{P} = \mathbf{A}(\vec{x}) \quad (3.83)$$

Equation (3.80) then writes

$$\mathbf{p}(\vec{x}) = \mathbf{A}(\vec{x})\boldsymbol{\gamma}(\vec{x}) \quad (3.84)$$

From now on, a subscript x will be a sign that we are calculating the partial derivatives with respect to the coordinate x . If we take (3.84):

$$\mathbf{p}_x(\vec{x}) = \mathbf{A}_x(\vec{x})\boldsymbol{\gamma}(\vec{x}) + \mathbf{A}(\vec{x})\boldsymbol{\gamma}_x(\vec{x}) \quad (3.85)$$

Finally

$$\boldsymbol{\gamma}_x(\vec{x}) = \mathbf{A}^{-1}(\vec{x})(\mathbf{p}_x(\vec{x}) - \mathbf{A}_x(\vec{x})\boldsymbol{\gamma}(\vec{x})) \quad (3.86)$$

Expression (3.76) then allows us to calculate the derivatives of the shape functions:

$$\boldsymbol{\Phi}_x(\vec{x}) = \boldsymbol{\gamma}_x^T(\vec{x})\mathbf{B}(\vec{x}) + \boldsymbol{\gamma}^T(\vec{x})\mathbf{B}_x(\vec{x}) \quad (3.87)$$

As the matrices $\mathbf{A}(\vec{x})$ and $\mathbf{B}(\vec{x})$ depend on matrices \mathbf{P} and $\mathbf{W}(\vec{x})$, and because \mathbf{P} does not depend on \vec{x} , the derivatives $\mathbf{A}_x(\vec{x})$ and $\mathbf{B}_x(\vec{x})$ can be calculated according to $\mathbf{W}_x(\vec{x})$. So almost everything boils down to calculating $\mathbf{W}_x(\vec{x})$, which is no more than to calculate the derivatives of window functions w (3.17) whose arguments are expressions (3.20) [or (3.21)] divided by the radius of the influence domain.

The first partial derivatives of MLS shape functions with respect to all directions/coordinates can therefore be summarized as:

$$\left[\frac{\partial \phi_1(\vec{x})}{\partial x}, \frac{\partial \phi_2(\vec{x})}{\partial x}, \dots, \frac{\partial \phi_n(\vec{x})}{\partial x} \right] = \boldsymbol{\gamma}_x^T(\vec{x})\mathbf{B}(\vec{x}) + \boldsymbol{\gamma}^T(\vec{x})\mathbf{B}_x(\vec{x}) \quad (3.88)$$

$$\left[\frac{\partial \phi_1(\vec{x})}{\partial y}, \frac{\partial \phi_2(\vec{x})}{\partial y}, \dots, \frac{\partial \phi_n(\vec{x})}{\partial y} \right] = \boldsymbol{\gamma}_y^T(\vec{x})\mathbf{B}(\vec{x}) + \boldsymbol{\gamma}^T(\vec{x})\mathbf{B}_y(\vec{x}) \quad (3.89)$$

$$\left[\frac{\partial \phi_1(\vec{x})}{\partial z}, \frac{\partial \phi_2(\vec{x})}{\partial z}, \dots, \frac{\partial \phi_n(\vec{x})}{\partial z} \right] = \boldsymbol{\gamma}_z^T(\vec{x})\mathbf{B}(\vec{x}) + \boldsymbol{\gamma}^T(\vec{x})\mathbf{B}_z(\vec{x}) \quad (3.90)$$

where the subscripts y and z refer to a derivative with respect to y and z , respectively. Figure 3.8 shows the derivatives for the one-dimensional shape functions from Fig.3.5, whereas Figs. 3.9 and 3.10 depict ϕ_x and ϕ_y for the MLS shape function of Fig.3.7.

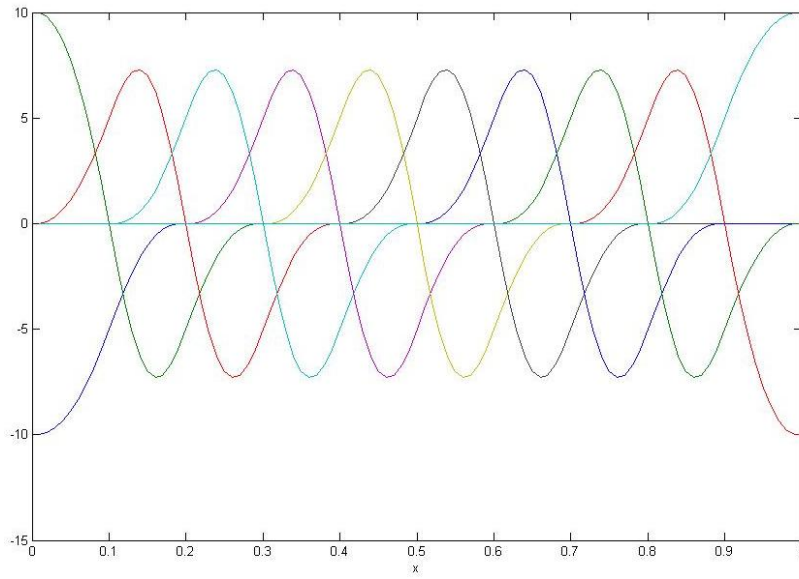


Fig.3.8. Derivative with respect to x for the one-dimensional shape functions of Fig.3.5.

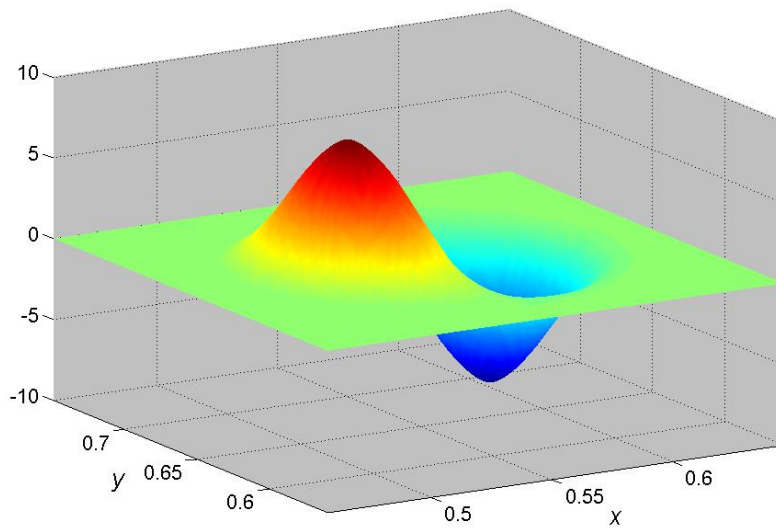


Fig.3.9. Partial derivative with respect to x for the MLS shape function of Fig.3.7.

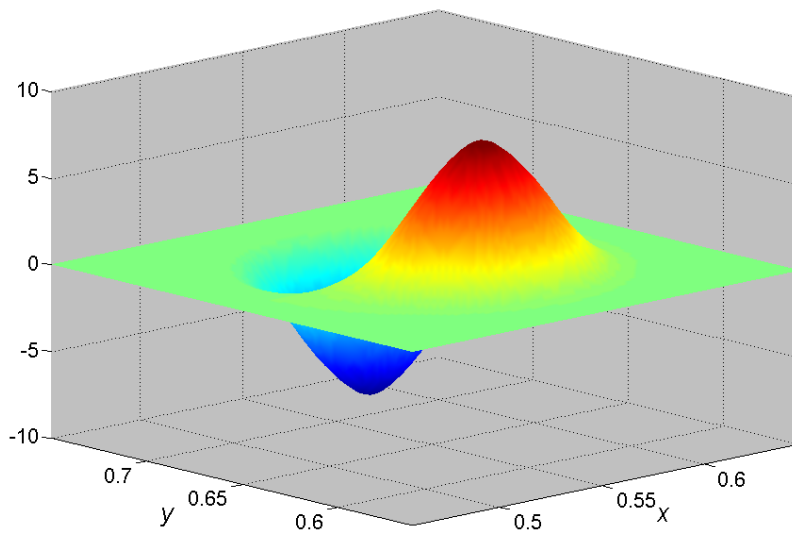


Fig.3.10. Partial derivative with respect to y for the MLS shape function of Fig.3.7.

Observation: The matrix calculations regarding the derivatives of shape functions [(3.88) - (3.90)] can be put into the same piece of code as that one used to calculate the shape functions themselves. This adds one more output to the black box in Fig.3.3.

Concluding Remarks

This is all we deemed necessary to know about shape functions in order to accomplish this work. Chapter 3 illustrated as carefully as possible the numerical procedure for constructing these functions through the MLS approximation. Now we know how to do this, our table can be updated.

THE MESHLESS PROCEDURE IN A NUTSHELL

Given a differential equation and a domain where it shall be solved:

First Step	Set up the domain Ω and its boundary $\partial\Omega$.
Second Step	Spread N nodes throughout the domain Ω and at its boundary $\partial\Omega$ as well.
Third Step	<ul style="list-style-type: none"> • To each node i, define the radius of its influence domain Λ_i (for the use in the MLS shape functions); • Make sure the influence domains cover the computational domain entirely.
Fourth Step	Numerical construction of the shape functions.

Chapter 4

MLS Shape Functions and Integral Equations: A “Meshless Method of Moments”

AFTER becoming acquainted with the topic on the construction of MLS shape functions, thoroughly explained in the last chapter, it is now time for us to seek some interesting applications for them.

The first kind of problem to which we had the opportunity to apply MLS shape functions is concerned to the scattering of electromagnetic waves. In scattering analyses, we suppose a pre-existing field, called the *incident field*, to be disturbed by some sort of object, the *scatterer*. The role to be played by the scatterer is to produce another field, called the *scattered field*, which is combined with the incident field in order to produce a *total field*.

In this work, however, we are not so much concerned to the physics behind scattering phenomena. Our attention will be shifted towards the mathematical models employed in the description of such phenomena. Given a physical problem (i.e., a scattering problem), we are interested solely in its abstracted mathematical form. In what regards physical descriptions, it suffices to say here that the underlying framework came entirely from Classical Electrodynamics (i.e., no quantum or relativistic accounts have been included in the models). For a detailed explanation of the physics of scattering phenomena, the reader can take a look at the references [Jackson, 1998], [Harrington, 2001], [Balanis, 1989] and [Rothwell and Cloud, 2001].

Once the mathematical form has been abstracted from the physical description, the next step aims at answering the question: How do we solve the mathematical problem?

The answer depends on *how* the problem has been translated from the physical realm to the “mathematical realm”. In what regards scattering phenomena, there are at least two ways in which the mathematical forms can be stated. Either differential equations or integral equations can be used for such a task. Both forms are equivalent, since they are derived from Maxwell equations (through different ways, obviously) and produce the same results. If one is interested in details, much insight on the mechanism of these two mathematical forms can be gained by reading Chapters 2 and 3 from the book by Mittra [Peterson *et al.*, 1998]. Chapter 2 discusses how to formulate scattering problems through integral equations, whereas Chapter 3 deals with differential equations.

In this chapter, we show how to solve, through meshless analysis, the 2D scattering problems expressed by integral equations. Such an attempt looks strange at first sight, since according to Chapter 1, meshless methods are an alternative to FEM in what regards problems described by PDE’s, not by integral equations. The most well-known method that deals with integral equations is the Method of Moments (MoM). What we are going to lay before the reader is, above all, how to employ the MoM with the meshless shape functions (intended to substitute those of FEM). As strange as it may appear, this strategy works well for a number of cases, except for those in which there are problems related to the singularity of the \mathbf{A} matrices arising

in the MLS approximation (according to Chapter 3). This issue happens if the scatterer has a flat side (like a square). Many attempts to overcome this issue were made. One of them, which resorts to a variant of the MLS, called IMLS (where the “I” stands for *improved*) substitutes some sort of orthogonal functions for the monomials in the vector $\mathbf{p}(\vec{x})$. However, IMLS did not work quite satisfactorily, with some undesirable oscillations coming in and disturbing the solution. But in the meanwhile, we have found so simple a way to deal with flat-side scatterers that it looks a little bit childish. Indeed, it somehow resembles the action of a stretching a rubber band. The details of this naïve procedure follow by the end of this chapter.

We would like to emphasize that the content of this chapter is to be considered just as a kind of test, intended to verify the applicability of the MLS shape functions. The meshless analysis of integral equations once was the direction our entire work would follow. But along the way we shifted our interest to the differential formulations in which meshless analysis was originally aimed to be employed, and then we stuck to them.

4.1 A Brief on Maxwell’s Equations and Scattering Theory

In this section, we present the basic equations that are going to be the subject of our analysis. After stating Maxwell’s equations, we derive the integral equations governing the scattering phenomena. More detailed discussion on this process can be found in [Peterson *et al.*, 1998] and [Balanis, 1989].

4.1.1 Maxwell’s Equations and Interface Conditions. Time and Frequency Domains.

The dynamics of the fields $(\vec{\mathcal{E}}, \vec{\mathcal{H}}, \vec{\mathcal{D}}, \vec{\mathcal{B}})$ is governed by Maxwell’s equations (written in SI units):

$$\nabla \times \vec{\mathcal{E}}(\vec{x}, t) = -\frac{\partial \vec{\mathcal{B}}(\vec{x}, t)}{\partial t} \quad (4.1)$$

$$\nabla \times \vec{\mathcal{H}}(\vec{x}, t) = \vec{\mathcal{J}}(\vec{x}, t) + \frac{\partial \vec{\mathcal{D}}(\vec{x}, t)}{\partial t} \quad (4.2)$$

$$\nabla \cdot \vec{\mathcal{D}}(\vec{x}, t) = \rho(\vec{x}, t) \quad (4.3)$$

$$\nabla \cdot \vec{\mathcal{B}}(\vec{x}, t) = 0 \quad (4.4)$$

where $\vec{\mathcal{E}}$ is the electric field intensity (volts/meter), $\vec{\mathcal{H}}$ is the magnetic field intensity (amperes/meter), $\vec{\mathcal{D}}$ is the electric flux density (coulombs/square meter), $\vec{\mathcal{B}}$ is the magnetic flux density (webers/square meters), $\vec{\mathcal{J}}$ is the electric current density (amperes/square meter) and ρ is the electric charge density (coulombs/cubic meter). All quantities depend on the spatial coordinates \vec{x} and on the time t . The fields are related to each other through the constitutive relations (which depend on the material media involved):

$$\vec{\mathcal{D}}(\vec{x}, t) = \hat{\epsilon}(\vec{x}, t)\vec{\mathcal{E}}(\vec{x}, t) \quad (4.5)$$

$$\vec{B}(\vec{x}, t) = \hat{\mu}(\vec{x}, t)\vec{H}(\vec{x}, t) \quad (4.6)$$

$$\vec{J}(\vec{x}, t) = \hat{\sigma}(\vec{x}, t)\vec{E}(\vec{x}, t) \quad (4.7)$$

In the general case, the quantities $\hat{\varepsilon}$, $\hat{\mu}$ and $\hat{\sigma}$ map vectors into vectors, so they are tensors that depend on space and time. However, for the purposes of this work, it suffices to consider them as scalars (ε , μ , σ) that at most depend on the spatial coordinates \vec{x} (we are not going to deal with time-varying media, at least for now). The first quantity ε is called the electric permittivity (farads/meter), and the second (μ) is the magnetic permeability (henries/meter). The third quantity (σ) is the electric conductivity (siemens/meter), and is linked the capacity of the medium to produce a conduction current in the presence of a field \vec{E} . In the situations coming from the scattering analysis carried out in this work, there are no references to this kind of current (also represented by $\vec{J}_c = \sigma\vec{E}$). Whenever a \vec{J} appears in the equations to follow, it is related to an electric current density that arises from other sorts of mechanism, like the matching of tangential components of the magnetic field at the interface between two media characterized by different material properties (induced currents).

The fields (unless stated otherwise) exist in a three-dimensional space. Let a region Ω in the space be filled in such a way that two sub-regions (Ω_1 and Ω_2) characterized by different material properties are separated by a surface S . For example, let us suppose Ω to be a cube $\Omega = [-1,1] \times [-1,1] \times [-1,1]$. We can take $\Omega_1 = [-1,1] \times [-1,1] \times [-1,0]$ (the bottom half) and $\Omega_2 = [-1,1] \times [-1,1] \times [0,1]$ (the upper half). The surface S that separates both sub-regions is the plane $S = [-1,1] \times [-1,1]$ at $z = 0$. To each point \vec{x} in the surface S , we can ascribe a unit normal vector \hat{n} , that happens to be equal to \hat{z} for this example. If we assume that the sub-region Ω_1 is characterized by the parameters $(\varepsilon_1, \mu_1, \sigma_1)$ and Ω_2 by $(\varepsilon_2, \mu_2, \sigma_2)$, then the boundary conditions to be satisfied by the fields are:

Media with finite conductivities (no sources \vec{J} or ρ)

$$\forall \vec{x} \in S \quad (\hat{n} \times (\vec{E}_2 - \vec{E}_1)) = \vec{0} \quad (4.8)$$

$$\forall \vec{x} \in S \quad (\hat{n} \times (\vec{H}_2 - \vec{H}_1)) = \vec{0} \quad (4.9)$$

$$\forall \vec{x} \in S \quad (\hat{n} \cdot (\vec{D}_2 - \vec{D}_1)) = 0 \quad (4.10)$$

$$\forall \vec{x} \in S \quad (\hat{n} \cdot (\vec{B}_2 - \vec{B}_1)) = 0 \quad (4.11)$$

Equation (4.8) above tells us that the tangential components of the electric field \vec{E} are continuous across the interface S . The second equation (4.9) expresses the same for the magnetic field \vec{H} , as long as there are no currents flowing along S or neither of the media is a perfectly electric conductor (PEC). Equation (4.10) says that the normal components of the electric flux density \vec{D} are continuous across S , as long as neither Ω_1 nor Ω_2 are filled with perfectly electric conductor materials and there are no electric charges on S . Finally, (4.11) states the continuity of the normal components of the magnetic flux density \vec{B} .

Media with infinite conductivities (eventually with sources \vec{J} or ρ)

Continuing our example, let us suppose that the medium in Ω_1 is a PEC. Therefore, there are no fields inside this sub-region, and the interface conditions now read:

$$\forall \vec{x} \in S \quad (\hat{\mathbf{n}} \times \vec{\mathcal{E}}_2) = \vec{0} \quad (4.12)$$

$$\forall \vec{x} \in S \quad (\hat{\mathbf{n}} \times \vec{\mathcal{H}}_2) = \vec{J}_s \quad (4.13)$$

$$\forall \vec{x} \in S \quad (\hat{\mathbf{n}} \cdot \vec{\mathcal{D}}_2) = \rho_s \quad (4.14)$$

$$\forall \vec{x} \in S \quad (\hat{\mathbf{n}} \cdot \vec{\mathcal{B}}_2) = 0 \quad (4.15)$$

The second equation (4.13) tells us about a surface current density that must flow along the surface of a PEC (sub-region Ω_1). The magnetic field cannot “die” suddenly when one travels from the exterior (Ω_1) to the interior (Ω_2) of a PEC; a surface current density \vec{J}_s (ampères/meter) must be the measure of the discontinuity of $\vec{\mathcal{H}}$. Equation (4.14) states that a surface charge density ρ_s (coulombs/square meter) must exist on the surface in order to account for the discontinuity of the electric flux density $\vec{\mathcal{D}}$.

Throughout this work, we are going to be concerned with electromagnetic fields whose temporal dependency is characterized by a sinusoidal behavior. They oscillate with a frequency f (measured in Hertz), which means that they come back to their original configuration each $T = 1/f$ seconds. The functions that describe fields that behave in such a way are usually separable, i.e., they are written as a product of two terms, the first of which depends on the spatial coordinates \vec{x} only, whereas the second term depends on time t solely. The term governing the temporal dependency is given by $e^{j\omega t}$, where $\omega = 2\pi f$ is the *angular frequency* (radians/second) and $j = \sqrt{-1}$. So the quantities $\vec{\mathcal{E}}, \vec{\mathcal{H}}, \vec{\mathcal{D}}, \vec{\mathcal{B}}, \vec{J}$ and ρ read as:

$$\vec{\mathcal{E}}(\vec{x}, t) = \text{Re}\{\vec{E}(\vec{x})e^{j\omega t}\} \quad (4.16)$$

$$\vec{\mathcal{H}}(\vec{x}, t) = \text{Re}\{\vec{H}(\vec{x})e^{j\omega t}\} \quad (4.17)$$

$$\vec{\mathcal{D}}(\vec{x}, t) = \text{Re}\{\vec{D}(\vec{x})e^{j\omega t}\} \quad (4.18)$$

$$\vec{\mathcal{B}}(\vec{x}, t) = \text{Re}\{\vec{B}(\vec{x})e^{j\omega t}\} \quad (4.19)$$

$$\vec{J}(\vec{x}, t) = \text{Re}\{\vec{J}(\vec{x})e^{j\omega t}\} \quad (4.20)$$

$$\rho(\vec{x}, t) = \text{Re}\{\rho(\vec{x})e^{j\omega t}\} \quad (4.21)$$

As the space-dependent quantities $\vec{E}, \vec{H}, \vec{D}, \vec{B}, \vec{J}$ and ρ may assume complex values, and in addition to their being multiplied by a complex term $e^{j\omega t}$, we must arrange so that the physical fields they describe come out as real quantities (i.e., described by real numbers). This is accomplished by taking the real part of the expression obtained from the product between the spatial and temporal terms (4.16) - (4.21). In Maxwell’s equations (4.1) and (4.2), there appear some derivatives with respect to time. If we substitute equations (4.16) - (4.21) above in Maxwell’s equations (4.1) - (4.4) and manipulate the real part $\text{Re}\{\cdot\}$ and time-derivative $\partial\{\cdot\}/\partial t$ operators, we find a new set of equations, in which the quantities $\vec{\mathcal{E}}, \vec{\mathcal{H}}, \vec{\mathcal{D}}, \vec{\mathcal{B}}, \vec{J}, \rho$ are replaced

by \vec{E} , \vec{H} , \vec{D} , \vec{B} , \vec{J} , ρ and the time derivative is changed to a product with the term $j\omega$. The new equations, whose terms are said to be in the *frequency domain*, are therefore written as

$$\nabla \times \vec{E}(\vec{x}) = -j\omega\vec{B}(\vec{x}) \quad (4.22)$$

$$\nabla \times \vec{H}(\vec{x}) = \vec{J}(\vec{x}) + j\omega\vec{D}(\vec{x}) \quad (4.23)$$

$$\nabla \cdot \vec{D}(\vec{x}) = \rho(\vec{x}) \quad (4.24)$$

$$\nabla \cdot \vec{B}(\vec{x}) = 0 \quad (4.25)$$

The set of equations above are easier to deal with than the set (4.1) - (4.4), as there are no references to time derivatives. However, care must be taken when one is solving for the real fields. As soon as one gets the complex fields \vec{E} , \vec{H} , \vec{D} , \vec{B} (sometimes they are said to be in *phasor* form), the real fields $\vec{\mathcal{E}}$, $\vec{\mathcal{H}}$, $\vec{\mathcal{D}}$, $\vec{\mathcal{B}}$ are obtained from them through a multiplication by $e^{j\omega t}$ and through the extraction of the real part (action of the $Re\{\cdot\}$), as shown in (4.16) - (4.19).

Observation: If the temporal variations are different from $e^{j\omega t}$, there are other techniques one can resort to. In the case the parameters ϵ and μ do not depend on the fields (linear problems), some kind of Fourier analysis can be employed. The sources \vec{J} and ρ are decomposed into components, each one depending on an angular frequency ω . These components are separately plugged into the equations (4.16) - (4.21). After the fields are solved for every component, they are summed up in order to form the total field. Needless to say this is quite a cumbersome process, as many components may be required to describe the fields with a reasonable accuracy. Instead of going through this large amount of work, numerical methods are often employed in order to tackle these situations (e.g., when one wants to find the fields produced by a pulse of current).

In the frequency domain, the boundary conditions remain unaltered:

Media with finite conductivities (no sources \vec{J} or ρ)

$$\forall \vec{x} \in S \quad (\hat{n} \times (\vec{E}_2 - \vec{E}_1)) = \vec{0} \quad (4.26)$$

$$\forall \vec{x} \in S \quad (\hat{n} \times (\vec{H}_2 - \vec{H}_1)) = \vec{0} \quad (4.27)$$

$$\forall \vec{x} \in S \quad (\hat{n} \cdot (\vec{D}_2 - \vec{D}_1)) = 0 \quad (4.28)$$

$$\forall \vec{x} \in S \quad (\hat{n} \cdot (\vec{B}_2 - \vec{B}_1)) = 0 \quad (4.29)$$

Media with infinite conductivities (eventually with sources \vec{J} or ρ)

If medium 1 is a PEC:

$$\forall \vec{x} \in S \quad (\hat{n} \times \vec{E}_2) = \vec{0} \quad (4.30)$$

$$\forall \vec{x} \in S \quad (\hat{n} \times \vec{H}_2) = \vec{J}_s \quad (4.31)$$

$$\forall \vec{x} \in S \quad (\hat{n} \cdot \vec{D}_2) = \rho_s \quad (4.32)$$

$$\forall \vec{x} \in S \quad (\hat{n} \cdot \vec{B}_2) = 0 \quad (4.33)$$

From now on, we will assume only fields with temporal variations dependent on $e^{j\omega t}$, and therefore only equations stated in the frequency domain are going to be considered.

4.1.2 Scattering Theory

When studying scattering phenomena, we begin by specifying a spatial region Ω (two or three-dimensional) in which there are elements relevant to our analysis. These elements are the incident fields and an object, called the scatterer. In the problems we are going to solve, we assume that none of the quantities involved depend on coordinate z , i.e., given a three-dimensional space (rectangular coordinates x , y and z), neither the fields nor the parameters (ε , μ) are functions of z . The region Ω we are interested in is then the plane XY , and the scatterer is an infinite cylinder. The parameters associated to the region Ω are those of the vacuum, i.e., $\varepsilon = \varepsilon_0 = 8.854 \times 10^{-12}$ F/m and $\mu = \mu_0 = 4\pi \times 10^{-7}$ H/m. Although the procedure developed in this chapter could also be applied to homogeneous dielectric scatterers (the method of moments applied to homogeneous dielectric scatterers, Chapter 2 of [Peterson *et al.*, 1998]), we will assume only PEC scatterers. The analysis of scattering by dielectric objects is postponed to later chapters, wherein a different method has been employed in their solution.

The incident fields are given, i.e., the expression governing them at all points $\vec{x} = (x, y)$ of the region Ω must be known at beforehand. These fields are produced by sources located elsewhere (where or how they are actually produced is irrelevant to our analysis). If we write the incident fields (and their associated sources) by a superscript i (for incident), then we can represent this situation schematically in Fig.4.1:

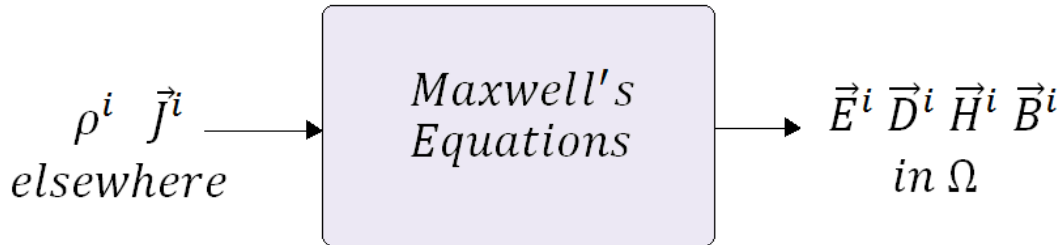


Fig.4.1. Sources ρ^i and \vec{J}^i located elsewhere produce the incident field.

The role to be played by the scatterer is to somehow disturb (or scatter) the incident field. Inside a PEC, the fields must vanish. As the incident fields must not “die” abruptly at the surface of the scatterer, Nature arranged things in such a way to bring about current and charge densities induced on the surface of the PEC. This is reflected in the interface conditions (4.31) - (4.32). However, these induced current and charge densities are sources, and, according to Maxwell's equations, they must generate electromagnetic fields. If we call them *scattered fields*, then we can label them by a superscript s (for scattered) and draw the scheme of Fig.4.2:

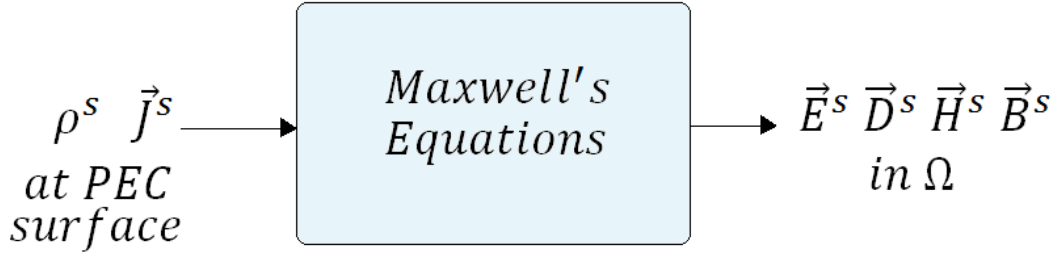


Fig.4.2. The scattered field is produced by sources ρ^s and \vec{J}^s induced on the PEC surface.

So the real scenario is depicted in Fig.4.3. The scattered fields produced by the induced current and charge densities add up to the incident fields, in order to produce a total field. The scattered fields are unknown, as their sources are. In order to find \vec{E}^s , \vec{H}^s , \vec{D}^s and \vec{B}^s , we must find \vec{J}^s and ρ^s first. However, these sources depend on no factors other than the geometry of the scatterer. And to make things simpler, the induced charge ρ^s does not need to be found. Only the induced current \vec{J}^s must be. Once the current flowing along the scatterer surface is found, we are finally able to calculate the scattered fields. The most important part is therefore the determination of the current density \vec{J}^s . Let us proceed to see how the equations governing it look like.

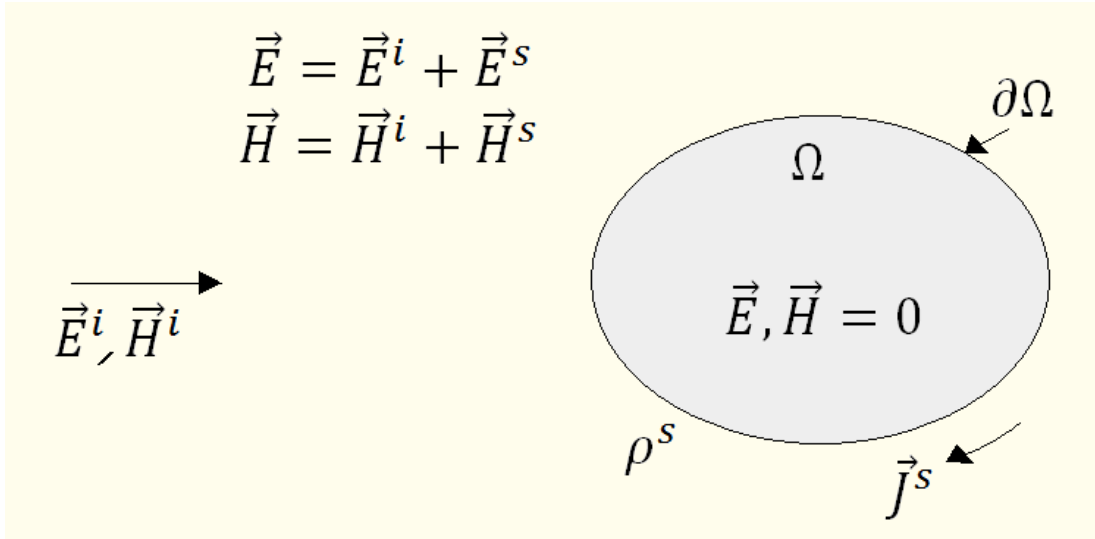


Fig.4.3. The scattered fields \vec{E}^s , \vec{H}^s combine on order to produce a total field \vec{E} , \vec{H} equal to zero inside Ω and equal to $\vec{E}^i + \vec{E}^s$, $\vec{H}^i + \vec{H}^s$ outside Ω .

As the sources \vec{J}^s and ρ^s produce the fields \vec{E}^s , \vec{H}^s , \vec{D}^s and \vec{B}^s in the vacuum, where $\varepsilon = \varepsilon_0$, $\mu = \mu_0$, $\vec{D}^s = \varepsilon_0 \vec{E}^s$ and $\vec{B}^s = \mu_0 \vec{H}^s$, the equations (4.22) - (4.25) can be written as (omitting the dependency on \vec{x}):

$$\nabla \times \vec{E}^s = -j\omega\mu_0 \vec{H}^s \quad (4.34)$$

$$\nabla \times \vec{H}^s(\vec{x}) = \vec{J}^s + j\omega\varepsilon_0 \vec{E}^s \quad (4.35)$$

$$\nabla \cdot \vec{E}^s = \rho^s / \varepsilon_0 \quad (4.36)$$

$$\nabla \cdot \vec{H}^s = 0 \quad (4.37)$$

Because the magnetic field intensity is solenoidal, it can be written as a curl of some vector $\vec{A}(x, y) = \vec{A}$ [Harrington, 2001]:

$$\vec{H}^s = \nabla \times \vec{A} \quad (4.38)$$

The vector \vec{A} is called the *magnetic vector potential*. Substituting (4.38) above in (4.34), we get

$$\nabla \times (\vec{E}^s + j\omega\mu_0\vec{A}) = \vec{0} \quad (4.39)$$

As the field $\vec{E}^s + j\omega\mu_0\vec{A}$ is irrotational, it can be written as a gradient of some scalar function ϕ (because of the vector identity $\nabla \times \nabla\phi = \vec{0}$). If $\nabla \times \nabla\phi = \vec{0}$, then obviously $\nabla \times \nabla(-\phi) = \vec{0}$. In Electrostatics it is customary to take the electric field as the negative of the electric potential. Following this trend, we can express $\vec{E}^s + j\omega\mu_0\vec{A}$ as the negative of a modified electric potential ϕ :

$$\vec{E}^s + j\omega\mu_0\vec{A} = -\nabla\phi \quad (4.40)$$

Substituting (4.38) in (4.35):

$$\nabla \times \nabla \times \vec{A} = \vec{j}^s + j\omega\varepsilon_0\vec{E}^s \quad (4.41)$$

From the vector identity

$$\nabla \times \nabla \times \vec{A} = \nabla\nabla \cdot \vec{A} - \nabla^2\vec{A} \quad (4.42)$$

we get

$$\nabla\nabla \cdot \vec{A} - \nabla^2\vec{A} = \vec{j}^s + j\omega\varepsilon_0\vec{E}^s \quad (4.43)$$

However, (4.40) tells us that $\vec{E}^s = -j\omega\mu_0\vec{A} - \nabla\phi$. Equation (4.43) above is then written as:

$$\nabla\nabla \cdot \vec{A} - \nabla^2\vec{A} = \vec{j}^s + j\omega\varepsilon_0(-j\omega\mu_0\vec{A} - \nabla\phi) \quad (4.44)$$

As $\omega^2\varepsilon_0\mu_0 = k^2$, where $k = 2\pi/\lambda$ is the *wavenumber* (radians/meter) and λ is the *wavelength* (meters). Rewriting (4.44):

$$\nabla^2\vec{A} + k^2\vec{A} = -\vec{j}^s + \nabla(\nabla \cdot \vec{A} + j\omega\varepsilon_0\phi) \quad (4.45)$$

According to Helmholtz's theorem, a vector field is unambiguously specified whenever its curl and its divergent are both known. The curl of \vec{A} is determined (4.38), so we are left with the task of choosing $\nabla \cdot \vec{A}$. There is some freedom on the choice of $\nabla \cdot \vec{A}$, but most books dealing with this subject [Balanis, 1989], seem to agree on a condition known as *Lorenz gauge*:

$$\nabla \cdot \vec{A} + j\omega\varepsilon_0\phi = 0 \quad (4.46)$$

which leads to an expression for $\nabla \cdot \vec{A}$:

$$\nabla \cdot \vec{A} = -j\omega\varepsilon_0\phi \quad (4.47)$$

Finally, the equation for the vector \vec{A} now becomes

$$\nabla^2 \vec{A} + k^2 \vec{A} = -\vec{j}^s \quad (4.48)$$

The current density \vec{j}^s along with suitable boundary radiation conditions suffice for the determination of \vec{A} . The radiation conditions which the vector \vec{A} is required to satisfy are those that resemble those of an outward propagating wave, i.e., a wave that moves away from the PEC scatterer. If such conditions are employed, then the derived fields \vec{E}^s and \vec{H}^s are shown to be in accordance with Sommerfeld's boundary conditions, which truly describe the behavior of scattered fields. There is a discussion of this subject in the Chapter 2 of [Harrington, 2001]. If \vec{j}^s is known, then the vector potential \vec{A} can be found everywhere as:

$$\vec{A}(\vec{x}) = \int_{\partial\Omega} \vec{j}^s(\vec{x}') \frac{1}{4j} H_0^{(2)}(k\|\vec{x} - \vec{x}'\|) dl' \quad (4.49)$$

Equation (4.49) holds true only for two-dimensional problems (the kind of problem we are dealing with). The potential vector and the current density both have the same direction. The integration is to be carried out at where the current \vec{j}^s exists, i.e., at the perimeter (boundary) $\partial\Omega$ of the PEC cross-section Ω . The term $H_0^{(2)}(k\|\vec{x} - \vec{x}'\|)/4j$ is the Green's function associated to the partial differential equation (4.48), i.e., if \vec{j}^s were equal to a Dirac delta located at \vec{x}' , then the potential vector \vec{A} at any point \vec{x} would be given by $H_0^{(2)}(k\|\vec{x} - \vec{x}'\|)/4j$. Equation (4.49) actually represents a convolution between the current distribution \vec{j}^s and Green's function (stated above). Given a point \vec{x} , (4.49) means that the potential vector \vec{A} at \vec{x} depends on the contribution of each point \vec{x}' where a current density \vec{j}^s is known to exist. Representing the points \vec{x} and \vec{x}' by Cartesian coordinates, (4.49) can be rewritten as

$$\vec{A}(\vec{x}) = \vec{A}(x, y) = \frac{1}{4j} \int_{\partial\Omega} \vec{j}^s(x', y') H_0^{(2)}(k\|\vec{x} - \vec{x}'\|) dl' \quad (4.50)$$

where $\|\vec{x} - \vec{x}'\|$ is the Euclidean distance between \vec{x} and \vec{x}' :

$$\|\vec{x} - \vec{x}'\| = \sqrt{(x - x')^2 + (y - y')^2} \quad (4.51)$$

The function $H_0^{(2)}$ that appears in (4.49) - (4.50) is a special function; it is known as *zero-order Hankel function of the second type*. For a detailed account of its properties, see [Balanis, 1989], and [Peterson *et al.*, 1998]. It suffices to say here that this function represents an outward travelling wave, i.e., a wave that propagates away from the PEC scatterer, and that it is defined as a combination of Bessel functions:

$$H_0^{(2)}(t) = J_0(t) - jY_0(t) \quad (4.52)$$

where $J_0(t)$ is the zero-order Bessel function of the first kind and $Y_0(t)$ is the zero-order Bessel function of the second type (which is singular at $t = 0$).

Once the potential vector \vec{A} is known from the current density \vec{j}^s through (4.49), then the scattered magnetic field can be found as $\vec{H}^s = \nabla \times \vec{A}$ (4.38). The potential ϕ comes from the Lorenz gauge condition (4.46):

$$\phi = -\frac{1}{j\omega\epsilon_0} \nabla \cdot \vec{A} \quad (4.53)$$

Finally, the scattered electric field is recovered from (4.40):

$$\vec{E}^s = -j\omega\mu_0\vec{A} + \frac{1}{j\omega\epsilon_0}\nabla\nabla\cdot\vec{A} = -j\omega\mu_0\vec{A} - \frac{j}{\omega\epsilon_0}\nabla\nabla\cdot\vec{A} \quad (4.54)$$

Observation: From the expression for \vec{A} , it can be easily verified that \vec{E}^s really satisfies Sommerfeld's radiation conditions. Just to keep things simple, let us assume that the current density \vec{J}^s is a Dirac delta placed at the origin of the Cartesian plane $\vec{x}' = (0,0)$, and that it is pointed towards the \hat{z} direction, i.e., $\vec{J}^s = \hat{z}\delta(\vec{x}')$. Under these circumstances, (4.49) becomes

$$\vec{A}(\vec{x}) = \hat{z}A_z(\vec{x}) = \frac{1}{4j}H_0^{(2)}(k\|\vec{x}\|) \quad (4.55)$$

The scattered electric field \vec{E}^s is derived from (4.54) above (A_z is not a function of z).

$$\vec{E}^s = -j\omega\mu_0\vec{A} + \frac{1}{j\omega\epsilon_0}\nabla\left(\frac{\partial A_z}{\partial z}\right) = -\hat{z}j\omega\mu_0A_z = -\hat{z}\frac{\omega\mu_0}{4}H_0^{(2)}(k\|\vec{x}\|) \quad (4.56)$$

So the z -component of the electric field is

$$E_z^s = -\frac{\omega\mu_0}{4}H_0^{(2)}(k\rho) \quad (4.57)$$

where $\rho = \|\vec{x}\|$ is the distance from point \vec{x} to the origin. For two-dimensional problems, Sommerfeld's radiation condition reads

$$\lim_{\rho\rightarrow\infty}\sqrt{\rho}\left(\frac{\partial}{\partial\rho} + jk\right)E_z^s = 0 \quad (4.58)$$

Inserting (4.57) into (4.58):

$$\lim_{\rho\rightarrow\infty}\sqrt{\rho}\left(\frac{\partial}{\partial\rho} + jk\right)\left(-\frac{\omega\mu_0}{4}H_0^{(2)}(k\rho)\right) = 0 \quad (4.59)$$

Ruling out $-\omega\mu_0/4$ we get

$$\lim_{\rho\rightarrow\infty}\sqrt{\rho}\left(\frac{\partial}{\partial\rho} + jk\right)H_0^{(2)}(k\rho) = 0 \quad (4.60)$$

Expanding (4.60):

$$\lim_{\rho\rightarrow\infty}\sqrt{\rho}\left(\frac{\partial H_0^{(2)}(k\rho)}{\partial\rho} + jkH_0^{(2)}(k\rho)\right) = 0 \quad (4.61)$$

The derivative of Bessel functions of any type Z and order p [including Hankel functions, as they are linear combinations of Bessel functions of first and second types, according to (4.52)] are given by [Balanis, 1989]:

$$\frac{d}{dt}(Z_p(\alpha t)) = -\alpha Z_{p+1}(\alpha t) + \frac{p}{t}Z_p(\alpha t) \quad (4.62)$$

The derivative of the Hankel function can then be found after substituting Z by $H^{(2)}$, p by 0, t by ρ and the partial derivative by a total derivative (because $H_0^{(2)}(k\rho)$ is a function of ρ only):

$$\lim_{\rho \rightarrow \infty} \sqrt{\rho} \left(-kH_1^{(2)}(k\rho) + jkH_0^{(2)}(k\rho) \right) = 0 \quad (4.63)$$

There is an asymptotic for the Hankel functions when their argument t is large [Balanis, 1989]:

$$H_p^{(2)}(t) \cong \sqrt{\frac{2}{\pi t}} e^{-j(t-p(\pi/2)-\pi/4)} \quad (4.64)$$

After some manipulations we arrive at:

$$\lim_{\rho \rightarrow \infty} \sqrt{\rho} \sqrt{\frac{2}{\pi k \rho}} e^{-j(k\rho-\pi/4)} k (-e^{j\pi/2} + j) = 0 \quad (4.65)$$

$$\lim_{\rho \rightarrow \infty} \sqrt{\frac{2k}{\pi}} e^{-j(k\rho-\pi/4)} (-e^{j\pi/2} + j) = 0 \quad (4.66)$$

However, $e^{j\pi/2} = j$, and the term in parentheses is zero. As the term depending on ρ is a complex exponential (unit modulus), we finally obtain an identity $0 = 0$. This means that the scattered electric field \vec{E}^s derived from \vec{A} satisfies Sommerfeld's radiation condition, as required.

As we are now equipped with the machinery of vector potentials and boundary conditions, we are ready to derive the integral equations that are going to be solved through a meshless method. This is the theme of the next section.

4.1.3 Integral Equations

As said earlier, we are dealing with three-dimensional problems in which there is a "privileged" direction along which no variable depends upon – the z -direction. The geometry of the scatterer does not varies with z , which means that it has a constant cross-section. Neither do the parameters ε and μ . These facts allow the original problem to be simplified. Actually, only what regards the plane XY is worth any consideration (any plane will serve our purposes, as long as they are all perpendicular to the z -axis; planes $z = -1$, $z = 0$, $z = 1$, etc. are all equivalent in this context).

In this scenario, there are two configurations the electromagnetic fields \vec{E}^s and \vec{H}^s can be in. One of them, called TM^z , has 3 field components: E_z , H_x and H_y . In TM^z , the electric field (both incident and scattered) points towards the z -direction, i.e., it is parallel to the PEC cylinder. The magnetic field lies in the XY plane. The other configuration, TE^z , is also characterized by 3 components: H_z , E_x and E_y . In TE^z , the magnetic field instead is parallel to the PEC cylinder.

The integral equations describing the fields in either TM^z or TE^z configurations differ from each other. Actually, there is some resemblance among them [Peterson *et al.*, 1998]. When one is interested in “mixed fields” (6 components, 3 for the electric and 3 for the magnetic fields), then the problem is broken up into two parts: one deals with the TM^z configuration (3 components) and with the TE^z configuration (the other 3 components) separately. After the solutions from both parts are available, they are added up in order to find the answer to the original “mixed” problem.

In this work, we are concerned with the TM^z configuration only. We derive the integral equations for the electromagnetic fields and then solve them for PEC scatterers. The integral equations for the TE^z configuration are similar to their TM^z counterpart. The duality principle can take one from the TM^z equations to the TE^z equations and from them back to the TM^z (although other quantities like the electric vector potential \vec{F} and the magnetic current density \vec{K} come up to the scene) [Peterson *et al.*, 1998].

The TM^z configuration is characterized by the fact that the current density induced on the PEC surface flows along the z -direction (i.e., it is directed parallel to the unit vector $\hat{\mathbf{z}}$, but does not vary with z , neither in magnitude nor in phase). Or

$$\vec{\mathbf{j}}^s(\vec{x}') = \hat{\mathbf{z}}J_z(\vec{x}') \quad (4.67)$$

The expression for the vector potential \vec{A} (4.49) becomes

$$\vec{A}(\vec{x}) = \vec{A}(x, y) = \frac{1}{4j} \int_{\partial\Omega} \hat{\mathbf{z}}J_z(x', y') H_0^{(2)}(k\|\vec{x} - \vec{x}'\|) dl' \quad (4.68)$$

Inserting (4.49) above in the expression (4.54) for the scattered electric field \vec{E}^s :

$$\begin{aligned} \vec{E}^s = & -j\omega\mu_0 \left(\frac{1}{4j} \int_{\partial\Omega} \hat{\mathbf{z}}J_z(x', y') H_0^{(2)}(k\|\vec{x} - \vec{x}'\|) dl' \right) - \\ & - \frac{j}{\omega\varepsilon_0} \nabla \cdot \left(\frac{1}{4j} \int_{\partial\Omega} \hat{\mathbf{z}}J_z(x', y') H_0^{(2)}(k\|\vec{x} - \vec{x}'\|) dl' \right) \end{aligned} \quad (4.69)$$

$$\begin{aligned} \vec{E}^s = & -\frac{\omega\mu_0}{4} \int_{\partial\Omega} \hat{\mathbf{z}}J_z(x', y') H_0^{(2)}(k\|\vec{x} - \vec{x}'\|) dl' - \\ & - \frac{1}{4\omega\varepsilon_0} \nabla \frac{\partial}{\partial z} \left(\int_{\partial\Omega} J_z(x', y') H_0^{(2)}(k\|\vec{x} - \vec{x}'\|) dl' \right) \end{aligned} \quad (4.70)$$

The last step is justified due to the fact that the second term inside the parentheses in (4.69) is a vector whose unique component points towards $\hat{\mathbf{z}}$. This allow us to substitute $\partial/\partial z$ for $\nabla \cdot$. As $J_z(x', y')$ does not depend on z , we can move $\partial/\partial z$ and place it just before $H_0^{(2)}(k\|\vec{x} - \vec{x}'\|)$ (i.e., the only term that depends on the observation coordinates \vec{x} and on the source coordinates \vec{x}' as well).

$$\vec{E}^s = -\frac{\omega\mu_0}{4} \int_{\partial\Omega} \hat{\mathbf{z}}J_z(x', y') H_0^{(2)}(k\|\vec{x} - \vec{x}'\|) dl' - \quad (4.71)$$

$$-\frac{1}{4\omega\epsilon_0}\nabla\left(\int_{\partial\Omega}J_z(x',y')\frac{\partial}{\partial z}H_0^{(2)}(k\|\vec{x}-\vec{x}'\|)dl'\right)$$

But

$$H_0^{(2)}(k\|\vec{x}-\vec{x}'\|)=H_0^{(2)}\left(k\sqrt{(x-x')^2+(y-y')^2}\right) \quad (4.72)$$

Therefore

$$\frac{\partial}{\partial z}H_0^{(2)}(k\|\vec{x}-\vec{x}'\|)=\frac{\partial}{\partial z}H_0^{(2)}\left(k\sqrt{(x-x')^2+(y-y')^2}\right)=0 \quad (4.73)$$

So the expression for \vec{E}^s in the TM^z configuration boils down to the first term

$$\vec{E}^s(\vec{x})=-\frac{\omega\mu_0}{4}\int_{\partial\Omega}\hat{\mathbf{z}}J_z(x',y')H_0^{(2)}(k\|\vec{x}-\vec{x}'\|)dl' \quad (4.74)$$

There are two unknowns in (74), namely \vec{E}^s and $J_z(x',y')$. One more relation is needed in order to solve it. The extra information is provided by the incident electric field \vec{E}^i (known) and the boundary condition (4.30), restated below:

$$\forall\vec{x}\in S\quad(\hat{\mathbf{n}}\times\vec{E}_2)=\vec{0} \quad (4.75)$$

In equivalent two-dimensional problems with PEC scatterers, the interface between two media S is just the perimeter (or contour) of the scatterer cross-section $\partial\Omega$. The total field in the medium external to the PEC (\vec{E}_2) is given by the sum of the incident and scatterer fields ($\vec{E}^i+\vec{E}^s$). So (4.75) is rewritten as

$$\forall\vec{x}\in\partial\Omega\quad(\hat{\mathbf{n}}\times(\vec{E}^i+\vec{E}^s))=\vec{0} \quad (4.76)$$

The normal $\hat{\mathbf{n}}$ to the interface S becomes a vector everywhere perpendicular to $\partial\Omega$. In this case, $\hat{\mathbf{n}}$ happens to be a unit vector on the XY plane (plane of the cylinder cross-section).

As explained earlier, in TM^z configuration, the electric field is required to point towards $\hat{\mathbf{z}}$ only (there is only one component for the electric field, i.e., E_z). Therefore, in TM^z analysis, incident fields with a z -component solely will be regarded. Just to remember, if the incident field happens to have other component in the XY plane, it is treated with other equations, derived from the TE^z configuration. So we assume the incident field to be

$$\vec{E}^i(\vec{x})=\vec{E}^i(x,y)=\hat{\mathbf{z}}E_z^i(x,y)=\hat{\mathbf{z}}E_z^i(\vec{x}) \quad (4.77)$$

Substituting (4.74) and (4.77) into (4.76), we get

$$\forall\vec{x}\in\partial\Omega\quad\left(\hat{\mathbf{n}}\times\left(\hat{\mathbf{z}}E_z^i(\vec{x})-\frac{\omega\mu_0}{4}\int_{\partial\Omega}\hat{\mathbf{z}}J_z(x',y')H_0^{(2)}(k\|\vec{x}-\vec{x}'\|)dl'\right)\right)=\vec{0} \quad (4.78)$$

Extracting the unit vector $\hat{\mathbf{z}}$ from the innermost parentheses:

$$\forall \vec{x} \in \partial\Omega \quad \left(\hat{\mathbf{n}} \times \hat{\mathbf{z}} \left(E_z^i(\vec{x}) - \frac{\omega\mu_0}{4} \int_{\partial\Omega} J_z(x', y') H_0^{(2)}(k\|\vec{x} - \vec{x}'\|) dl' \right) \right) = \vec{0} \quad (4.79)$$

As $\hat{\mathbf{n}}$ is perpendicular to $\hat{\mathbf{z}}$, the vector product $\hat{\mathbf{n}} \times \hat{\mathbf{z}}$ points toward a vector $\vec{\mathbf{t}}$ tangent to $\partial\Omega$ at every point $\vec{x} \in \partial\Omega$. Then

$$\forall \vec{x} \in \partial\Omega \quad \left(\hat{\mathbf{t}} \left(E_z^i(\vec{x}) - \frac{\omega\mu_0}{4} \int_{\partial\Omega} J_z(x', y') H_0^{(2)}(k\|\vec{x} - \vec{x}'\|) dl' \right) \right) = \vec{0} \quad (4.80)$$

The term in the right side is the null vector $\vec{0}$. As the product between the scalar 0 and any vector \vec{w} (particularly for $\vec{w} = \hat{\mathbf{t}}$) is the null vector $\vec{0}$ (i.e., $0\vec{w} = \vec{0}$), we conclude that the term inside the innermost parentheses must be equal to zero, which leads us to

$$\forall \vec{x} \in \partial\Omega \quad E_z^i(\vec{x}) = \frac{\omega\mu_0}{4} \int_{\partial\Omega} J_z(\vec{x}') H_0^{(2)}(k\|\vec{x} - \vec{x}'\|) dl' \quad (4.81)$$

Equation (4.81) above is the Electric Field Integral Equation (EFIE). It states that for any point at $\partial\Omega$, E_z^i is given by an integral over $\partial\Omega$ of the induced current density J_z multiplied by the Hankel function $H_0^{(2)}$. Once J_z is found, the scattered electric field \vec{E}^s at any point \vec{x} can be calculated through (4.74). The magnetic scattered field \vec{H}^s is found by first determining the potential vector \vec{A} and then taking $\vec{H}^s = \nabla \times \vec{A}$:

$$\vec{H}^s = \frac{1}{4j} \nabla \times \int_{\partial\Omega} \hat{\mathbf{z}} J_z(x', y') H_0^{(2)}(k\|\vec{x} - \vec{x}'\|) dl' \quad (4.82)$$

The integral equation (4.81) is not the only one that can be derived for the TM^z configuration. Had we begun our analysis from the magnetic fields, we would get a different equation that, differently from EFIE, does not relate the current density to the incident electric field, but to the incident magnetic field instead. This equation is called the Magnetic Field Integral Equation (MFIE). Let us proceed to verify how it is found out.

The boundary condition for the magnetic field (when the other medium is a PEC) is given by (31) (repeated here):

$$\forall \vec{x} \in S \quad (\hat{\mathbf{n}} \times \vec{H}_2) = \vec{J}_s \quad (4.83)$$

The interface S is the contour $\partial\Omega$, and the total external magnetic field \vec{H}_2 is the sum of the incident and scattered fields. Then

$$\forall \vec{x} \in \partial\Omega \quad (\hat{\mathbf{n}} \times (\vec{H}^i + \vec{H}^s)) = \vec{J}_s \quad (4.84)$$

This means that the tangential component of the total magnetic field at \vec{x} is equal to the surface current density evaluated at \vec{x} . Rewriting (4.84):

$$\forall \vec{x} \in \partial\Omega \quad \hat{\mathbf{n}} \times \vec{H}^i(\vec{x}) = \vec{J}_s(\vec{x}) - \hat{\mathbf{n}} \times \vec{H}^s(\vec{x}) \quad (4.85)$$

In the TM^z configuration, \vec{J}_s is given by (4.67). The scattered magnetic field \vec{H}^s is substituted by $\nabla \times \vec{A}$ in order to find

$$\forall \vec{x} \in \partial\Omega \quad \hat{n} \times \vec{H}^i(\vec{x}) = \hat{z}J_z(\vec{x}) - \hat{n} \times \nabla \times \vec{A}(\vec{x}) \quad (4.86)$$

After considering the expression for \vec{A} (4.50):

$$\forall \vec{x} \in \partial\Omega \quad \hat{n} \times \vec{H}^i(\vec{x}) = \hat{z}J_z(\vec{x}) - \frac{1}{4j} \hat{n} \times \nabla \times \int_{\partial\Omega} \hat{z}J_z(x', y') H_0^{(2)}(k\|\vec{x} - \vec{x}'\|) dl' \quad (4.87)$$

Taking the unit vector \hat{z} outside the integral:

$$\forall \vec{x} \in \partial\Omega \quad \hat{n} \times \vec{H}^i(\vec{x}) = \hat{z}J_z(\vec{x}) - \frac{1}{4j} \hat{n} \times \nabla \times \hat{z} \int_{\partial\Omega} J_z(x', y') H_0^{(2)}(k\|\vec{x} - \vec{x}'\|) dl' \quad (4.88)$$

A simple calculation shows us that

$$\nabla \times \hat{z} = \hat{x} \frac{\partial}{\partial y} - \hat{y} \frac{\partial}{\partial x} \quad (4.89)$$

Substituting:

$$\forall \vec{x} \in \partial\Omega \quad \hat{n} \times \vec{H}^i(\vec{x}) = \hat{z}J_z(\vec{x}) - \frac{1}{4j} \hat{n} \times \left(\hat{x} \frac{\partial}{\partial y} - \hat{y} \frac{\partial}{\partial x} \right) \int_{\partial\Omega} J_z(x', y') H_0^{(2)}(k\|\vec{x} - \vec{x}'\|) dl' \quad (4.90)$$

As the derivatives are taken in respect to the observation coordinates (x and y), and as the current density J_z does not depend on them (they depend on the source coordinates x' and y' instead), we are allowed to place them just before the Hankel function $H_0^{(2)}$:

$$\forall \vec{x} \in \partial\Omega \quad \hat{n} \times \vec{H}^i(\vec{x}) = \hat{z}J_z(\vec{x}) - \frac{1}{4j} \hat{n} \times \left(\hat{x} \int_{\partial\Omega} J_z(x', y') \frac{\partial}{\partial y} H_0^{(2)}(k\|\vec{x} - \vec{x}'\|) dl' - \hat{y} \int_{\partial\Omega} J_z(x', y') \frac{\partial}{\partial x} H_0^{(2)}(k\|\vec{x} - \vec{x}'\|) dl' \right) \quad (4.91)$$

Writing the vector $\vec{x} - \vec{x}'$ as

$$\vec{R} = \vec{x} - \vec{x}' = \hat{x}(x - x') + \hat{y}(y - y') \quad (4.92)$$

So that its modulus is $\|\vec{x} - \vec{x}'\| = \|\vec{R}\| = R$, (4.91) becomes

$$\forall \vec{x} \in \partial\Omega \quad \hat{n} \times \vec{H}^i(\vec{x}) = \hat{z}J_z(\vec{x}) - \frac{1}{4j} \hat{n} \times \left(\hat{x} \int_{\partial\Omega} J_z(x', y') \frac{\partial}{\partial y} H_0^{(2)}(kR) dl' - \hat{y} \int_{\partial\Omega} J_z(x', y') \frac{\partial}{\partial x} H_0^{(2)}(kR) dl' \right) \quad (4.93)$$

From the chain rule for differentiation it follows that

$$\frac{\partial}{\partial y} H_0^{(2)}(kR) = \frac{\partial H_0^{(2)}(kR)}{\partial(kR)} \frac{\partial(kR)}{\partial y} \quad (4.94)$$

and likewise for $\partial H_0^{(2)}(kR)/\partial x$. Substituting this in (4.93):

$$\forall \vec{x} \in \partial\Omega \quad \hat{\mathbf{n}} \times \vec{H}^i(\vec{x}) = \hat{\mathbf{z}}J_z(\vec{x}) - \quad (4.95)$$

$$-\frac{1}{4j} \hat{\mathbf{n}} \times \left(\hat{\mathbf{x}} \int_{\partial\Omega} J_z(x', y') \frac{\partial H_0^{(2)}(kR)}{\partial(kR)} \frac{\partial(kR)}{\partial y} dl' - \hat{\mathbf{y}} \int_{\partial\Omega} J_z(x', y') \frac{\partial H_0^{(2)}(kR)}{\partial(kR)} \frac{\partial(kR)}{\partial x} dl' \right)$$

From the expression (4.62) concerning the derivative of Hankel functions:

$$\frac{\partial H_0^{(2)}(kR)}{\partial(kR)} = -H_1^{(2)}(kR) \quad (4.96)$$

Then

$$\forall \vec{x} \in \partial\Omega \quad \hat{\mathbf{n}} \times \vec{H}^i(\vec{x}) = \hat{\mathbf{z}}J_z(\vec{x}) - \quad (4.97)$$

$$-\frac{1}{4j} \hat{\mathbf{n}} \times \left(\hat{\mathbf{x}} \int_{\partial\Omega} J_z(x', y') \left(-H_1^{(2)}(kR) \right) \frac{\partial(kR)}{\partial y} dl' - \hat{\mathbf{y}} \int_{\partial\Omega} J_z(x', y') \left(-H_1^{(2)}(kR) \right) \frac{\partial(kR)}{\partial x} dl' \right)$$

The remaining derivatives are calculated as

$$\frac{\partial(kR)}{\partial x} = \frac{\partial \left(k\sqrt{(x-x')^2 + (y-y')^2} \right)}{\partial x} = k \frac{(x-x')}{\sqrt{(x-x')^2 + (y-y')^2}} = k \frac{(x-x')}{R} \quad (4.98)$$

$$\frac{\partial(kR)}{\partial y} = \frac{\partial \left(k\sqrt{(x-x')^2 + (y-y')^2} \right)}{\partial y} = k \frac{(y-y')}{\sqrt{(x-x')^2 + (y-y')^2}} = k \frac{(y-y')}{R} \quad (4.99)$$

After retaining the terms in common and moving the unit vectors $\hat{\mathbf{x}}$ and $\hat{\mathbf{y}}$, (4.97) becomes

$$\forall \vec{x} \in \partial\Omega \quad \hat{\mathbf{n}} \times \vec{H}^i(\vec{x}) = \hat{\mathbf{z}}J_z(\vec{x}) - \quad (4.100)$$

$$-\frac{1}{4j} \hat{\mathbf{n}} \times \left(\int_{\partial\Omega} J_z(x', y') \left(-H_1^{(2)}(kR) \right) \left(\hat{\mathbf{x}}k \frac{(y-y')}{R} - \hat{\mathbf{y}}k \frac{(x-x')}{R} \right) dl' \right)$$

Placing the wavenumber k outside the integral, and moving the normal vector $\hat{\mathbf{n}}$, we get

$$\forall \vec{x} \in \partial\Omega \quad \hat{\mathbf{n}} \times \vec{H}^i(\vec{x}) = \hat{\mathbf{z}}J_z(\vec{x}) + \frac{k}{4j} \int_{\partial\Omega} J_z(x', y') H_1^{(2)}(kR) \hat{\mathbf{n}} \times \left(\hat{\mathbf{x}} \frac{(y-y')}{R} - \hat{\mathbf{y}} \frac{(x-x')}{R} \right) dl' \quad (4.101)$$

Writing the normal vector $\hat{\mathbf{n}} = \hat{\mathbf{x}}n_x + \hat{\mathbf{y}}n_y$, the vector product is

$$\hat{\mathbf{n}} \times \left(\hat{\mathbf{x}} \frac{(y-y')}{R} - \hat{\mathbf{y}} \frac{(x-x')}{R} \right) = \begin{vmatrix} \hat{\mathbf{x}} & \hat{\mathbf{y}} & \hat{\mathbf{z}} \\ n_x & n_y & 0 \\ (y-y')/R & -(x-x')/R & 0 \end{vmatrix} = \quad (4.102)$$

$$-n_x \frac{(x-x')}{R} - n_y \frac{(y-y')}{R} = -\hat{\mathbf{z}} \frac{1}{R} (\hat{\mathbf{x}}n_x + \hat{\mathbf{y}}n_y) \cdot (\hat{\mathbf{x}}(x-x') + \hat{\mathbf{y}}(y-y'))$$

where the dot \cdot stands for the scalar product between two vectors. Simplifying further:

$$-\hat{\mathbf{z}} \frac{1}{R} (\hat{\mathbf{x}} n_x + \hat{\mathbf{y}} n_y) \cdot (\hat{\mathbf{x}}(x-x') + \hat{\mathbf{y}}(y-y')) = -\hat{\mathbf{z}} \frac{1}{R} \hat{\mathbf{n}} \cdot \vec{R} = -\hat{\mathbf{z}} (\hat{\mathbf{n}} \cdot \hat{R}) \quad (4.103)$$

In (4.103) above, $\hat{R} = \vec{R}/R = \vec{R}/\|\vec{R}\|$ is a radial unit vector, i.e., a unit vector whose direction is the same as that of a line joining the origin (0,0) to point $(x,y) = \vec{x}$. The integral equation (4.101) becomes

$$\forall \vec{x} \in \partial\Omega \quad \hat{\mathbf{n}} \times \vec{H}^i(\vec{x}) = \hat{\mathbf{z}} J_z(\vec{x}) + \frac{k}{4j} \int_{\partial\Omega} J_z(x',y') H_1^{(2)}(kR) (-\hat{\mathbf{z}} (\hat{\mathbf{n}} \cdot \hat{R})) dl' \quad (4.104)$$

which can be written as

$$\forall \vec{x} \in \partial\Omega \quad \hat{\mathbf{n}} \times \vec{H}^i(\vec{x}) = \hat{\mathbf{z}} J_z(\vec{x}) + \hat{\mathbf{z}} \frac{jk}{4} \int_{\partial\Omega} J_z(x',y') H_1^{(2)}(kR) (\hat{\mathbf{n}} \cdot \hat{R}) dl' \quad (4.105)$$

The terms in the right side of (4.105) point towards the z-direction only, and so does the term in the left, as it can be easily verified. Indeed, in the TM^z configuration, the magnetic field lies in the plane XY, i.e., it is written as $\vec{H}^i = \hat{\mathbf{x}} H_x + \hat{\mathbf{y}} H_y$. Cross-multiplying it with the normal vector $\hat{\mathbf{n}}$ we readily discover that the term in the left side $\hat{\mathbf{n}} \times \vec{H}^i$ really points towards $\hat{\mathbf{z}}$ as well:

$$\hat{\mathbf{n}} \times \vec{H}^i(\vec{x}) = \begin{vmatrix} \hat{\mathbf{x}} & \hat{\mathbf{y}} & \hat{\mathbf{z}} \\ n_x & n_y & 0 \\ H_x^i & H_y^i & 0 \end{vmatrix} = \hat{\mathbf{z}} (n_x H_y^i - n_y H_x^i) \quad (4.106)$$

Bearing this observation in mind, we write the final form the MFIE shall assume:

$$\forall \vec{x} \in \partial\Omega \quad (\hat{\mathbf{n}} \times \vec{H}^i(\vec{x})) \cdot \hat{\mathbf{z}} = J_z(\vec{x}) + \frac{jk}{4} \int_{\partial\Omega} J_z(x',y') H_1^{(2)}(kR) (\hat{\mathbf{n}} \cdot \hat{R}) dl' \quad (4.107)$$

Now that we are in possession of both EFIE and MFIE, let us proceed to their numerical evaluation.

4.2 Meshless Analysis of Integral Equations. MLS Shape functions.

Because we are dealing with PEC's only, our region of interest reduces to the perimeter of the scatterer's cross-section. This looks reasonable, insofar as there are no fields inside a perfect conductor. As we know at beforehand that the fields are zero within the scatterer, then this region is summarily excluded from our analysis. An inspection at EFIE (4.81) and MFIE (4.107) reveals that the unknown current density is confined to the surface of the PEC only, which in equivalent two-dimensional problems happens to be a contour (the perimeter of the scatterer's cross-section). So there is no reason in considering the exterior region to the PEC (vacuum, or free space) either.

Commentary: From the last section, it can be seen that we had to go through a rather lengthy process in order to find out the integral equations governing the scattering of incoming waves. The information about induced current densities, the exterior medium and the scattered waves' sense of propagation (outward, as indicated by the Hankel functions of the second type) are all codified in two equations, namely, the EFIE and the MFIE. However, the situation depicted is a

relatively simple scattering problem - scattering by PEC objects. Had the problem involved media other than free space and dielectric objects, for example, other complications would arise, and the process of finding the integral equations would be more complex. Usually, one would have to use equivalence theorems in order to substitute objects for currents flowing along their surfaces, and there would appear artificial constructs like magnetic current densities \vec{K}^s [Peterson *et al.*, 1998]. Needless to say, the deduction of the integral equations could become much more complicated to that exposed in the last pages. One would end up with a pair of coupled equations in two unknowns (\vec{J}^s and \vec{K}^s). To make things worse, if there were many scatterers in the region, each one of them would have its associated current densities (\vec{J} and \vec{K}) flowing along their surfaces (after applying equivalence theorems [Peterson *et al.*, 1998]). As beautiful as the mathematical deduction of these integral equations can appear, no one could deny the huge effort carried out by the analyst in order to find them. However, although the integral equations look a little bit frightening, there is nothing more to do with them other than discretize them. Their solution is not that complicated; all we have to do is to approximate the unknown \vec{J} (or \vec{K} or both) by an expansion in shape functions. The burden of the work relies almost entirely on the analyst's shoulders. All that is left to the computer is to perform the numerical integrations out from the discretization process and to assemble (and solve) the resulting linear system. The purpose of this commentary is to point out that this complication in obtaining the integral equations is one of the reasons we gave up in pursuing further research in this area and decided to prioritize the approach based in differential equations. We are not saying that there are no difficulties associated with the differential approach – there are challenges as well – but it seems to explore more the processing power of the computer than the analytical skills of the programmer. When solving a scattering problem using FEM or MLPG, for example, all is needed is the knowledge of the governing differential equation and the boundary conditions. There is no need to resort to induced current densities or to equivalence theorems. Not even a knowledge of Hankel functions is required! This extra facility proves to be fundamental when it comes to the solution of problems related to the scattering of a wave by many bodies, as in the analysis of photonic crystals (Chapter 5).

Let Ω stand for the scatterer's cross-section. Its perimeter is then represented by $\partial\Omega$. In addition to this, let \vec{E}^i, \vec{H}^i be the incident field coming from the left (Fig.4.4. It could impinge on the PEC from whatever direction, but without loss of generality, it is represented graphically as a wave coming from the left). As the current density J_z (TMz polarization) exists only in $\partial\Omega$, we need to build shape functions that exist only in $\partial\Omega$ also. The first step is to spread nodes along $\partial\Omega$ (Fig.4.4).

Each node is characterized by its two Cartesian coordinates x and y . If we spread a total of N nodes, then from the index set

$$I = \{1,2,3,4, \dots, i, \dots, N\} \quad (4.108)$$

we can state the set of nodes (points) in $\partial\Omega$

$$\mathcal{N} = \{\vec{x} \in \partial\Omega \mid \exists i \in I(\vec{x} = \vec{x}_i)\} \quad (4.109)$$

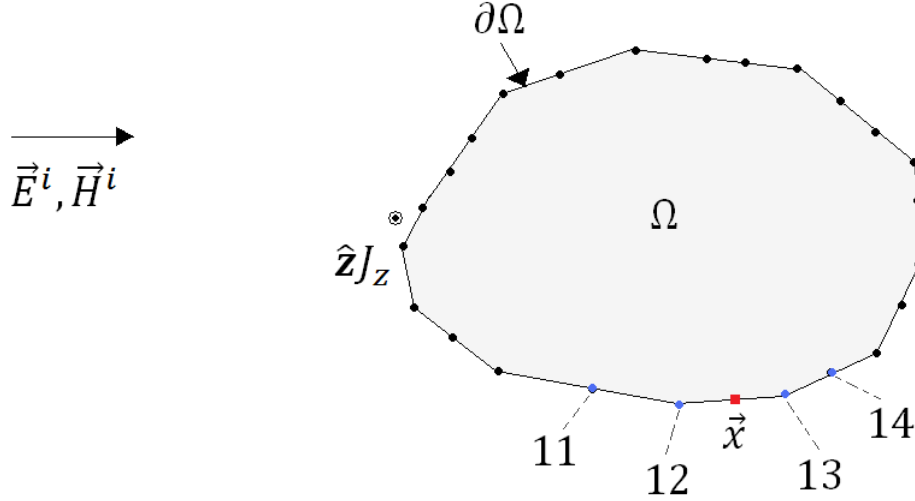


Fig.4.4. Nodes 11, 12, 13 and 14 extend their influence domains until point \vec{x} . This is the same as saying that $Neigh(\vec{x}) = \{11, 12, 13, 14\}$. The figure illustrates the scatterer's cross-section; therefore, the induced current density J_z which flows along the z -axis cannot be drawn.

i.e., the set \mathcal{N} is formed by all those points in the contour $\partial\Omega$ which have an associated index i . As only the N points located at \vec{x}_i are arbitrarily chosen by the programmer, the number of elements in \mathcal{N} is N . An obvious observation is that nodes located at some location \vec{x}_i should have a unique index i :

$$\forall \vec{x} \in \mathcal{N} (\exists! i \in I(\vec{x} = \vec{x}_i)) \quad (4.110)$$

i.e., a single node could not be labeled by two different indices i and j :

$$\forall \vec{x} \in \mathcal{N} \left(\exists i \in I(\vec{x} = \vec{x}_i) \wedge \left(\neg \exists j \in I(\vec{x} = \vec{x}_j \wedge i \neq j) \right) \right) \quad (4.111)$$

This proposition means that for each point \vec{x} in the set \mathcal{N} (set of nodes) there is an index i \vec{x} is associated to, and that there is not another index j different from i \vec{x} is associated to. Although this may seem obvious, it has tremendous consequences in the numerical solution of the integral equations. The contour $\partial\Omega$ is a closed curve. It means that it can be described by a parametrization $f(t)$:

$$f: [0, t_{max}] \rightarrow \partial\Omega \quad (4.112)$$

or to each value of the parameter t (ranging from $t = 0$ to $t = t_{max}$) is associated a point \vec{x} in $\partial\Omega$:

$$\forall t \in [0, t_{max}] \exists \vec{x} \in \partial\Omega (\vec{x} = f(t)) \quad (4.113)$$

where $\vec{x} = (x, y) = (x(t), y(t))$. However, in order to exactly describe a closed curve, the initial and final points must be equal:

$$f(t = 0) = f(t = t_{max}) \quad (4.114)$$

When spreading nodes along $\partial\Omega$, one must be sure we do not ascribe different indices to the endpoint (characterized either by $t = 0$ or by $t = t_{max}$). If this is ever done, to the same location (the endpoint), two different nodes (two different indices) will be ascribed. This

violates the proposition (4.111) and as a result, the resulting matrix will have two linearly dependent lines (actually, equal to each other, since the points for different indices have the same coordinates and therefore, the same values for any function dependent on them). The matrix will then be singular, which makes impossible the solution of the final linear system.

After the nodes have been spread, the next step is to determine their influence domains. Just to remember, according to explained in Chapter 2, each node i must have its associated influence domain Λ_i . In this context,

$$\Lambda_i = \{\vec{x} \in \partial\Omega \mid \|\vec{x} - \vec{x}_i\| \leq r_i\} \quad (4.115)$$

where r_i is the radius of node i 's influence domain. Also, the collection (union) of all influence domains must cover the entire region of interest (in this case, just the contour $\partial\Omega$):

$$\partial\Omega \subseteq \bigcup_{i \in I} \Lambda_i \quad (4.116)$$

This ensures that, to each point \vec{x} in $\partial\Omega$, there is at least one node which extends its influence domain until \vec{x} . Let \mathcal{L} be the set of all influence domains Λ_i , i.e., \mathcal{L} is a family of sets whose elements are the influence domains Λ_i (sets of points):

$$\mathcal{L} = \{\Lambda \mid \exists i \in I (\Lambda = \Lambda_i)\} = \{\Lambda_1, \Lambda_2, \dots, \Lambda_i, \dots, \Lambda_N\} \quad (4.117)$$

This claim can be stated as

$$\forall \vec{x} \in \partial\Omega (\exists \Lambda \in \mathcal{L} (\vec{x} \in \Lambda)) \quad (4.118)$$

If (4.118) above holds for all \vec{x} , then there are no holes left in $\partial\Omega$, and therefore the current density J_z can be approximated everywhere. Usually a single point \vec{x} is influenced by many nodes, i.e., many nodes extend their influence domains until \vec{x} . In Chapter 2, we called the set of indices whose associated influence domains included point \vec{x} as the set of neighbor nodes influencing \vec{x} , represented as $Neigh(\vec{x})$:

$$Neigh(\vec{x}) = \{i \in I \mid \vec{x} \in \Lambda_i\} \quad (4.119)$$

In Fig.4.4, it is shown the set of four nodes influencing a given point \vec{x} [$Neigh(\vec{x}) = \{11,12,13,14\}$].

According to Chapter 3, in order to build MLS shape functions, a monomial basis \mathbf{p} is required. We employ here a basis formed by linear terms only:

$$\mathbf{p}(\vec{x}) = [1, x, y]^T \quad (4.120)$$

Once the monomial basis is chosen, in order to find the nodes influencing \vec{x} and their associated shape functions, all there is to do is to go through the series of matrix calculations involving the matrices \mathbf{P} and $\mathbf{W}(\vec{x})$. The process illustrating the construction of the MLS shape functions will not be repeated here; the detailed information is available in Section 3.1. It suffices only to remember that it is a black box procedure. Given a point \vec{x} , you feed this information into the black box and recover all influencing nodes along with the shape functions calculated at \vec{x} .

However, there is one more requirement: the curve describing the contour $\partial\Omega$ is parametrized in such a way that its endpoints coincide, i.e., $f(t = 0) = f(t = t_{max})$. This means that both endpoints amount to the same physical location, and as expected, the physical quantity of interest – the current density J_z – must assume the same value at both endpoints as well:

$$J_z(t = 0) = J_z(t = t_{max}) \quad (4.121)$$

Things would be enormously simplified if this feature were embedded in the shape functions used to approximate J_z (yes, the current density is approximated by MLS shape functions, as the direction this discussion is taking will soon make explicit), i.e.,

$$\forall i \in I(\phi_i(t = 0) = \phi_i(t = t_{max})) \quad (4.122)$$

where ϕ_i is the shape function associated to node i . We have found a way to make the shape functions obey (4.122) above. However, it will be explained in the worked example below.

4.2.1 Worked example: Scattering of a TM^z plane wave by a PEC circular cylinder

The first problem which we tried to solve through meshless techniques was that concerned to the scattering of a plane wave by a PEC circular cylinder. The reason for such a choice is that this problem has analytical solution (i.e., there is an expression for J_z), which provided us a means to verify whether the numerical experiments are working suitably or not.

As we are dealing with a curve $\partial\Omega$ in two dimensions, it can be described by a single degree of freedom, i.e., only one parameter t suffices for describing all points in $\partial\Omega$. In the case of a circular PEC cylinder, $\partial\Omega$ is a circumference and the parameter t happens to be the polar angle φ (Fig.4.5).

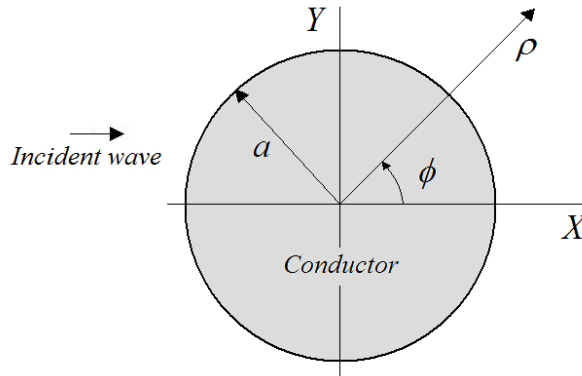


Fig.4.5. Scattering by a PEC circular cylinder. The contour $\partial\Omega$ is the circumference $\rho = a$ (polar coordinates). The parameter t that describes the curve $\partial\Omega$ is the polar angle φ .

Because every point in $\partial\Omega$ is situated at a distance a away from the origin, they can be written in polar coordinates as

$$\forall \vec{x} \in \partial\Omega (x = a \cos \varphi \text{ and } y = a \sin \varphi), \quad 0 \leq \varphi < 2\pi \quad (4.123)$$

i.e., the x -coordinate is given by $a \cos \varphi$ and the y -coordinate is given by $a \sin \varphi$. The radius of the cylinder is therefore given by a .

Inserting the values for x and y above in the monomial basis \mathbf{p} (4.120), we have:

$$\mathbf{p}(\vec{x}) = [1, a \cos \varphi, a \sin \varphi]^T = \mathbf{p}(\varphi) \quad (4.124)$$

The nodes have been spread uniformly throughout $\partial\Omega$ (this is not mandatory; a different nodal distribution could have been used). All influence domains Λ have the same radius (again, each influence domain could have its own value for the radius, but we preferred the simpler approach). These radii are chosen in such a way that a node is able to influence two other nodes ahead of it, and two nodes behind it. So given a point \vec{x} , all nodes influencing \vec{x} and their associated shape functions ϕ are calculated through the MLS procedure outlined in Chapter 3 (matrices \mathbf{P} , $\mathbf{W}(\vec{x})$, \mathbf{A} , etc.). Figure 4.6 illustrates a set of 10 shape functions associated to 10 nodes equally spread along $\partial\Omega$. As it can be seen, the parameter (polar angle φ) varies from 0 to 2π , as indicated. In order to produce Fig.4.6, many points \vec{x} have been spread throughout $\partial\Omega$, and to each one of them the set of influencing nodes ($Neigh(\vec{x})$) along with the shape functions calculated at \vec{x} have been determined. This process is akin to that used in producing the pictures for the two-dimensional MLS shape functions explained in chapter 2. Lots of information can be retrieved from Fig.4.6. First, the shape functions are compactly supported, being different from zero only at a certain region around the associated node. Second, to each point \vec{x} there are 3 to 4 nodes influencing it. Of course that, if the influence domains were larger, nodes distant from \vec{x} would be able to extend their influence until \vec{x} , what would lead to a greater amount of influencing nodes. Third, each shape function attains the maximum at its associated node, decays to zero at the first neighbor node, assume negative values and decays to zero at the second neighbor node. So the influence domain of a node acts on points located at distances smaller than the distance of two nodes ahead of the node (and two nodes behind the node as well). Finally, and surprisingly enough, we observe that the shape functions obey the Kronecker delta property. The MLS shape functions usually do not satisfy it (according to Chapter 3), but this behavior is likely due to the presence of trigonometric terms in the basis \mathbf{p} . Tests have been carried out, and the property of partition of unity proved to hold true everywhere in $\partial\Omega$. The obtained shape functions are therefore suitable to be used in the meshless discretization process.

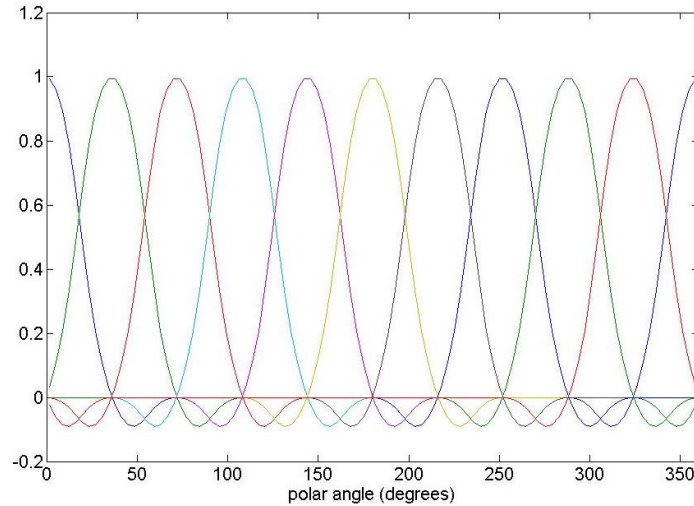


Fig.4.6. A set of 10 shape functions, associated to 10 nodes uniformly spread along $\partial\Omega$.

The next step is to approximate the unknown function J_z by an expansion in shape functions. For all points in $\partial\Omega$, the current density J_z at \vec{x} is expressed as:

$$\forall \vec{x} \in \partial\Omega \quad J_z(\vec{x}) = \sum_j \phi_j(\vec{x}) \hat{u}_j \quad (4.125)$$

where the index j runs through all nodes influencing \vec{x} . As nodes located far from \vec{x} do not contribute to the sum above, we can take all indices (from 1 to the number of nodes N):

$$\forall \vec{x} \in \partial\Omega \quad J_z(\vec{x}) = \sum_{j=1}^N \phi_j(\vec{x}) \hat{u}_j \quad (4.126)$$

We are now ready to deal the integral equations. The EFIE (restated below) is

$$\forall \vec{x} \in \partial\Omega \quad E_z^i(\vec{x}) = \frac{\omega\mu_0}{4} \int_{\partial\Omega} J_z(\vec{x}') H_0^{(2)}(k\|\vec{x} - \vec{x}'\|) dl' \quad (4.127)$$

According to (4.108), we have N unknowns in our problem, the N nodal parameters $\hat{u}_1, \dots, \hat{u}_N$. So we need N instances of the equation above, each one enforced at a different point \vec{x} . Nothing seems more natural than taking the location of each node i as *observation points*, i.e., we take N equations, each one enforced at \vec{x}_i :

$$\forall i \in I \quad E_z^{inc}(\vec{x}_i) = \frac{\omega\mu_0}{4} \int_{\partial\Omega} J_z(\vec{x}') H_0^{(2)}(k\|\vec{x}_i - \vec{x}'\|) dl' \quad (4.128)$$

where the superscript i in (4.127) that used to stand for the incident field has been replaced by 'inc', in order not to be confused by the index i . Substituting (4.126) for J_z we find

$$\forall i \in I \quad \sum_{j=1}^N \left(\frac{\omega\mu_0}{4} \int_{\partial\Omega} \phi_j(\vec{x}') H_0^{(2)}(k\|\vec{x}_i - \vec{x}'\|) dl' \right) \hat{u}_j = E_z^{inc}(\vec{x}_i) \quad (4.129)$$

As the indices i and j both run from 1 to N , the set of equations above can be written as a linear system:

$$\mathbf{K}^{EFIE} \hat{\mathbf{u}} = \mathbf{e}^{inc} \quad (4.130)$$

where the coefficients of the $N \times N$ matrix \mathbf{K}^{EFIE} are given by

$$K_{ij}^{EFIE} = \frac{\omega\mu_0}{4} \int_{\partial\Omega} \phi_j(\vec{x}') H_0^{(2)}(k\|\vec{x}_i - \vec{x}'\|) dl', \quad (4.131)$$

the j th component of the $N \times 1$ unknown vector $\hat{\mathbf{u}}$ is the nodal parameter \hat{u}_j and the i th component of the $N \times 1$ vector \mathbf{e}^{inc} is the incident electric field calculated at node i 's location:

$$e_i^{inc} = E_z^{inc} \quad (4.132)$$

The nodal parameters are solved through the solution of the linear system (4.130):

$$\hat{\mathbf{u}} = (\mathbf{K}^{EFIE})^{-1} \mathbf{e}^{inc} \quad (4.133)$$

Once the vector $\hat{\mathbf{u}}$ is found, the problem is finally solved. The current density at a given point \vec{x} in $\partial\Omega$ is given by (4.125), i.e., one must first find which nodes influence \vec{x} [the set $Neigh(\vec{x})$]

along with the influencing shape functions, and then add them up (weighted by the nodal parameters).

If the problem is not electrically large, i.e., if the radius a of the cylinder is smaller than the wavelength λ of the incident field, only the EFIE suffices for the solution. Otherwise, there appears some problems concerned to *resonances*. These problems arise out of the discretization process, and an extensive discussion on this topic would lead us too far astray from the purposes of this work. A thorough account of this phenomenon is found in [Peterson *et al.*, 1998]. It can be shown that the *spurious solutions* introduced by the resonances can be eliminated altogether by resorting to two extra steps:

- After discretizing the EFIE, do the same with the MFIE;
- Performing a weighted sum of the solutions provided by the EFIE and by the MFIE.

The MFIE is (restated below)

$$\forall \vec{x} \in \partial\Omega \quad (\hat{\mathbf{n}} \times \vec{H}^i(\vec{x})) \cdot \hat{\mathbf{z}} = J_z(\vec{x}) + \frac{jk}{4} \int_{\partial\Omega} J_z(\vec{x}') H_1^{(2)}(kR) (\hat{\mathbf{n}} \cdot \hat{\mathbf{R}}) dl' \quad (4.134)$$

Some issues concerning the discontinuity of the magnetic field at $\partial\Omega$ allows extra information to be extracted from the integral appearing in (4.134). The MFIE is usually written as

$$\forall \vec{x} \in \partial\Omega \quad (\hat{\mathbf{n}} \times \vec{H}^i(\vec{x})) \cdot \hat{\mathbf{z}} = \frac{1}{2} J_z(\vec{x}) + \frac{jk}{4} \int_{\partial\Omega \setminus \Delta\vec{x}} J_z(\vec{x}') H_1^{(2)}(kR) (\hat{\mathbf{n}} \cdot \hat{\mathbf{R}}) dl' \quad (4.135)$$

where the integration is no longer carried out at the closed curve $\partial\Omega$. A small segment of $\partial\Omega$ curve centered at the observation point \vec{x} – represented by $\Delta\vec{x}$ – is removed from the curve when the integration is performed. The result of this is that there appears a 1/2 coefficient multiplying $J_z(\vec{x})$. The derivation of (4.135) from (4.134) is presented in [Balanis, 1989]. We just take it for granted here.

Enforcing N instances of the MFIE at the N observation points (location of each node i) we get (after substituting ‘*inc*’ for ‘*i*’ in the left side):

$$\forall i \in I \quad (\hat{\mathbf{n}} \times \vec{H}^{inc}(\vec{x}_i)) \cdot \hat{\mathbf{z}} = \frac{1}{2} J_z(\vec{x}_i) + \frac{jk}{4} \int_{\partial\Omega \setminus \Delta\vec{x}_i} J_z(\vec{x}') H_1^{(2)}(kR) (\hat{\mathbf{n}} \cdot \hat{\mathbf{R}}) dl' \quad (4.136)$$

where $\vec{R} = \vec{x}_i - \vec{x}$ and $R = \|\vec{R}\|$. Inserting the expansion in shape functions (4.126) wherever J_z appears we arrive at

$$\forall i \in I \quad \sum_{j=1}^N \left(\frac{1}{2} \phi_j(\vec{x}_i) + \frac{jk}{4} \int_{\partial\Omega \setminus \Delta\vec{x}_i} \phi_j(\vec{x}') H_1^{(2)}(kR) (\hat{\mathbf{n}} \cdot \hat{\mathbf{R}}) dl' \right) \hat{u}_j = (\hat{\mathbf{n}} \times \vec{H}^{inc}(\vec{x}_i)) \cdot \hat{\mathbf{z}} \quad (4.137)$$

As in the case for the EFIE, we can arrange this set of equations into a linear system

$$\mathbf{K}^{MFIE} \hat{\mathbf{u}} = \mathbf{h}^{inc} \quad (4.138)$$

The coefficients of the $N \times N$ matrix \mathbf{K}^{MFIE} are given by

$$K_{ij}^{MFIE} = \frac{1}{2}\phi_j(\vec{x}_i) + \frac{jk}{4} \int_{\partial\Omega \setminus \Delta\vec{x}_i} \phi_j(\vec{x}') H_1^{(2)}(kR)(\hat{\mathbf{n}} \cdot \hat{\mathbf{R}}) dl' \quad (4.139)$$

the j th component of the $N \times 1$ unknown vector $\hat{\mathbf{u}}$ is again the nodal parameter \hat{u}_j and the i th component of the $N \times 1$ vector \mathbf{h}^{inc} is the expression below involving the incident magnetic field calculated at node i 's location:

$$h_i^{inc} = (\hat{\mathbf{n}} \times \vec{H}^{inc}(\vec{x}_i)) \cdot \hat{\mathbf{z}} \quad (4.140)$$

The current density J_z free from spurious solutions is therefore given by a linear combination of solutions provided by both EFIE (4.130) and MFIE (4.138):

$$(\alpha \mathbf{K}^{EFIE} + (1 - \alpha) \mathbf{K}^{MFIE}) \hat{\mathbf{u}} = (\alpha \mathbf{e}^{inc} + (1 - \alpha) \mathbf{h}^{inc}) \quad (4.141)$$

$$\hat{\mathbf{u}} = (\alpha \mathbf{K}^{EFIE} + (1 - \alpha) \mathbf{K}^{MFIE})^{-1} (\alpha \mathbf{e}^{inc} + (1 - \alpha) \mathbf{h}^{inc}) \quad (4.142)$$

This meshless discretization of integral equations worked well. In our simulation, we considered a relatively large cylinder whose radius a is equal to 10 wavelengths, or $a = 10\lambda$. In this scenario, applying only the EFIE does not provide accurate results, because of the issue regarding the spurious solutions. The combined equations above (4.142) therefore must be used. The incident field is a plane wave of unit amplitude ($E_0 = 1$) coming from the left:

$$E_z^{inc}(\vec{x}) = E_z^{inc}(x, y) = E_0 e^{-jkx} \quad (4.143)$$

This field becomes $e^{-jka \cos \varphi}$ in the contour $\partial\Omega$. The components x and y for the incident magnetic field can easily be retrieved from Maxwell's equations (Faraday law: $\nabla \times \vec{E}^{inc} = -j\omega\mu_0 \vec{H}^{inc}$). The frequency of the incident wave was set equal to 10^9 Hz. After spreading 250 nodes uniformly along $\partial\Omega$, we got the result illustrated by Figs.4.7 and 4.8, which show a comparison between the numerical and analytical results for the surface current density modulus (amplitude) and phase. The expression for the analytic solution is [Balanis, 1989]:

$$\forall \vec{x} \in \partial\Omega \quad J_z(\vec{x}) = J_z(\rho = a, \varphi) = \frac{2E_0}{\pi a \omega \mu_0} \sum_{n=-\infty}^{n=\infty} j^{-n} \frac{e^{jn\varphi}}{H_n^{(2)}(ka)} \quad (4.144)$$

In order to verify the convergence of the method, we defined the following norm to be used as a measure of the error between the numerical and analytical solutions:

$$norm = \sqrt{\frac{1}{2\pi a} \oint_{\partial\Omega} (J_{zAnalytical} - J_{zNumerical})^2 dl} \quad (4.145)$$

We run several cases, the number of nodes varying from 10 to 600. The numerical solution begins to converge when the number of nodes equals 100. Besides solving the problem through the aforementioned meshless technique, we have also solved the same problem numerically through the method of moments (MoM) with pulse expansion and impulse testing functions (point-matching). Figure 4.9 shows the error norm (4.145) for the meshless approach and for MoM as a function of h , where h is the distance between two consecutive nodes along the circular contour $\partial\Omega$.

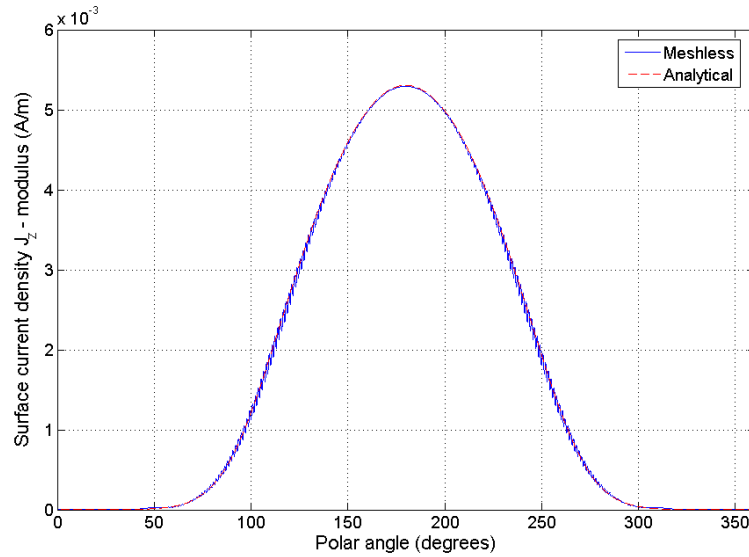


Fig.4.7. The modulus of J_z . Comparison between the numerical and analytical solutions.

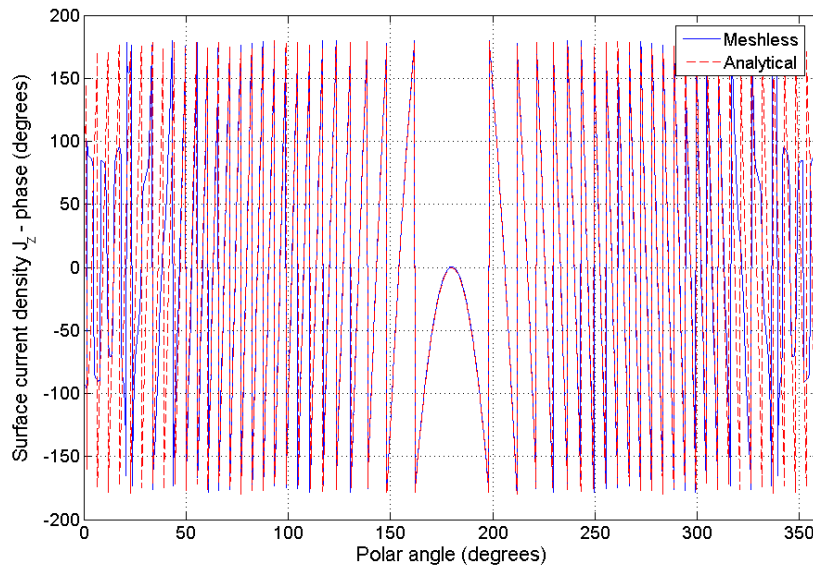


Fig.4.8. Phase of J_z . Comparison between the numerical and analytical solutions.

A linear regression applied to the rectilinear portion of the graph (abscissa between 0.8 and 1.1) shows that the convergence rates are approximately 3.07 for the meshless method and 2.66 for MoM.

4.3 Meshless Analysis of Integral Equations. IMLS Shape functions.

The MLS shape functions did a nice job when solving the problem for a circular cylinder, but, could they also be applied to non-circular geometries? Depending on the shape of the scatterer cross-section, the answer is no. The reason is that sometimes we get \mathbf{A} -matrices which are singular, what prevents them from being inverted (Chapter 3). Consequently, the shape functions calculated at a given point cannot be found. This phenomenon occurs for scatterers whose cross-section possesses a flat side, like a square or a rectangle. Let us illustrate

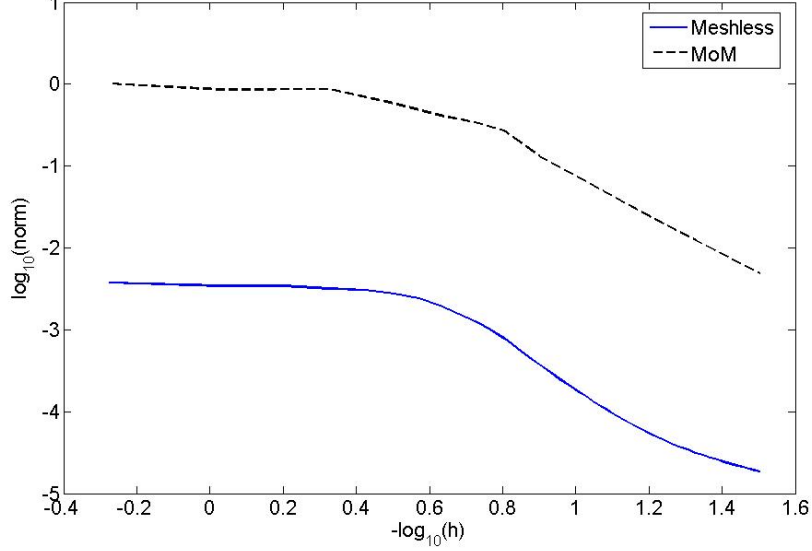


Fig.4.9. Convergence of the error norm for the meshless approach and for a MoM analysis employing pulse expansion functions and point-matching.

what happens if one tries to construct MLS shape functions for a square, i.e., the PEC contour $\partial\Omega$ is a square.

Suppose we want to calculate the shape functions influencing a point \vec{x} located in the midst of the upper face AB . After spreading the nodes along $\partial\Omega$, we determine which of them extend their influence domains until \vec{x} , i.e., we find the set $Neigh(\vec{x})$. The black box procedure for doing that relies on the matrices \mathbf{P} and $\mathbf{W}(\vec{x})$ (Section 3.1), repeated here for convenience:

$$\mathbf{P} = \begin{bmatrix} p_1(\vec{x}_1) & \cdots & p_m(\vec{x}_1) \\ \vdots & \ddots & \vdots \\ p_1(\vec{x}_n) & \cdots & p_m(\vec{x}_n) \end{bmatrix} \quad (4.146)$$

$$\mathbf{W}(\vec{x}) = \begin{bmatrix} w_1(\vec{x}) & 0 & \cdots & 0 \\ 0 & w_2(\vec{x}) & \cdots & \vdots \\ \vdots & \vdots & \ddots & \vdots \\ 0 & \cdots & \cdots & w_n(\vec{x}) \end{bmatrix} \quad (4.147)$$

If we employ a linear basis $\mathbf{p}(\vec{x}) = [p_1(\vec{x}), p_2(\vec{x}), p_3(\vec{x})]^T = [1, x, y]^T$, than a curious fact can be seen. As Fig.410 indicates, all nodes in $Neigh(\vec{x})$ lies on the line AB . So their y -coordinates are all equal to a given value, say, $y = c$. When we fill in the values for the matrix \mathbf{P} (4.146), we see that all elements in the first column are equal to 1 as expected, and also that all elements in third column are equal to c . Consequently, \mathbf{P} has two constant columns (the first, whose elements are 1 and the third). As the third column is a multiple of the first, \mathbf{P} has two linearly dependent columns. The matrix \mathbf{A} is given by (Section 3.1)

$$\mathbf{A}(\vec{x}) = \mathbf{P}^T \mathbf{W}(\vec{x}) \mathbf{P} \quad (4.148)$$

Because \mathbf{W} is diagonal (3.46), the product (4.148) has two linearly dependent columns as well. Therefore, \mathbf{A} is singular.

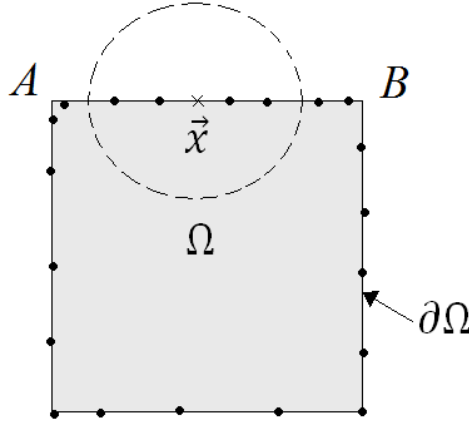


Fig.4.10. All nodes influencing \vec{x} (inside the dashed circle) have the same y -coordinate. A particular nodal configuration such as this one leads to singular \mathbf{A} -matrices in the traditional MLS procedure.

One way to solve that is to make the nodal influence domains bigger than the side of the rectangle, in order to assure that inside this domain there will be points distributed along two adjacent sides, i.e., whatever the point \vec{x} may be, the set $Neigh(\vec{x})$ will always have nodes from more than one side of the square. By doing this, both x and y will vary, \mathbf{P} will no longer have two linearly dependent columns and \mathbf{A} shall not be singular. But this does not seem to be a reasonable approach: one sees that as the influence domains become larger, the local perspective of the method is destroyed.

In order to deal with this situation, we decided to try another method for constructing MLS shape functions, called Improved Moving Least Squares (IMLS) approximation. At the time when this part of the work was carried out, the only paper addressing this technique we had access to was [Peng and Cheng, 2009]. The main characteristic of IMLS is that inversions of matrices are not necessary for calculating the shape functions. Hence, they can always be obtained, regardless of the geometry of the problem.

The IMLS shape functions are calculated as follows. Given a point \vec{x} in $\partial\Omega$, we find $Neigh(\vec{x})$. Now comes the novelty: the basis \mathbf{p} is no more given by $[1, x, y, \dots]^T$, but it is calculated recursively. Suppose any two functions defined for all \vec{x} in $\partial\Omega$, $f(\vec{x})$ and $g(\vec{x})$. The first step is to define a kind of inner product between these functions:

$$\langle f, g \rangle = \sum_{I=1}^n w \left(\frac{\|\vec{x} - \vec{x}_I\|}{r_I} \right) f(\vec{x}_I) g(\vec{x}_I) \quad (4.149)$$

The index I runs from 1 to the number n of nodes in $Neigh(\vec{x})$ (they are not the global indices, as explained in section 3.1), and w is the window function. In the IMLS, it is required that the terms of the basis \mathbf{p} be orthogonal to each other, *only at the nodal points*. The orthogonality condition is assured through the property ($k, j = 1, 2, \dots, m$):

$$\langle p_k, p_j \rangle = \sum_{I=1}^n w \left(\frac{\|\vec{x} - \vec{x}_I\|}{r_I} \right) p_k(\vec{x}_I) p_j(\vec{x}_I) = \begin{cases} A_k, & k = j \\ 0, & k \neq j \end{cases} \quad (4.150)$$

Bearing in mind the orthogonality at the nodal points, one forms the basis \mathbf{p} by requiring its first term to be equal to the unity everywhere, i.e.

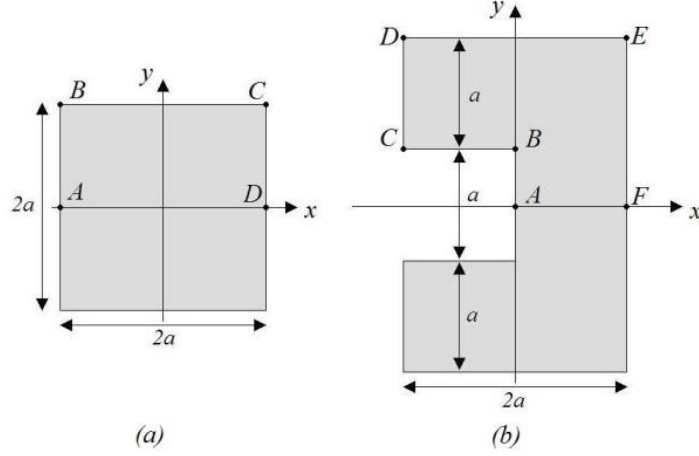


Fig.4.11. Non-circular cross sections ($a = \lambda/2\pi$).

$$p_1(\vec{x}) = 1 \quad (4.151)$$

The next terms are formed recursively:

$$p_i(\vec{x}) = r^{i-1} - \sum_{k=1}^{i-1} \frac{\langle r^{i-1}, p_k \rangle}{\langle p_k, p_k \rangle} p_k, \quad i = 2, 3, \dots, m \quad (4.152)$$

where r is the radial distance from the given point \vec{x} (i.e., $r = \sqrt{x^2 + y^2}$). If we go through the same process involving matrices $\mathbf{A}(\vec{x})$, $\mathbf{B}(\vec{x})$, \mathbf{P} and $\mathbf{W}(\vec{x})$ (expressions 3.45, 3.46, 3.47, 3.54, 3.55 and 3.58 from Chapter 3), working out the product of the matrix elements (in the same way as done in Chapter 3) and recalling the orthogonality conditions (4.150), the following linear system is obtained:

$$\begin{bmatrix} \langle p_1, p_1 \rangle & \cdots & 0 \\ \vdots & \ddots & \vdots \\ 0 & \cdots & \langle p_m, p_m \rangle \end{bmatrix} \begin{bmatrix} a_1(\vec{x}) \\ \vdots \\ a_m(\vec{x}) \end{bmatrix} = \begin{bmatrix} \langle p_1, \mathbf{u} \rangle \\ \vdots \\ \langle p_m, \mathbf{u} \rangle \end{bmatrix} \quad (4.153)$$

This system, when solved for \mathbf{a} gives:

$$\begin{bmatrix} a_1(\vec{x}) \\ \vdots \\ a_m(\vec{x}) \end{bmatrix} = \begin{bmatrix} \frac{1}{\langle p_1, p_1 \rangle} & \cdots & 0 \\ \vdots & \ddots & \vdots \\ 0 & \cdots & \frac{1}{\langle p_m, p_m \rangle} \end{bmatrix} \begin{bmatrix} \langle p_1, \mathbf{u} \rangle \\ \vdots \\ \langle p_m, \mathbf{u} \rangle \end{bmatrix} \quad (4.154)$$

Calling this new matrix $\bar{\mathbf{A}}(\vec{x})$ and as $(\langle p_1, \mathbf{u} \rangle, \dots, \langle p_m, \mathbf{u} \rangle) = \mathbf{B}(\vec{x})\mathbf{u}$, we have for the coefficients \mathbf{a} :

$$\mathbf{a}(\vec{x}) = \bar{\mathbf{A}}(\vec{x})\mathbf{B}(\vec{x})\mathbf{u} \quad (4.155)$$

which is an expression analogous to (3.59), but requires no matrix inversion. Once the inner products are always positive and different from zero, $\bar{\mathbf{A}}$ is always nonsingular, thus providing correct values for the coefficients \mathbf{a} . Expression (4.155) above is then substituted back in (3.63), and a comparison with (3.61) makes explicit the expression for the shape functions:

$$\Phi(\vec{x}) = [\phi_1(\vec{x}), \dots, \phi_N(\vec{x})] = \mathbf{p}^T(\vec{x})\bar{\mathbf{A}}(\vec{x})\mathbf{B}(\vec{x}) \quad (4.156)$$

In order to verify the feasibility of the IMLS method, we applied it to two cross-sectional geometries that could be “pathological” from the viewpoint of the MLS method, i.e., scatterers with flat sides (Fig.4.11). The parameter a was set equal to $\lambda/2\pi$, where λ is the wavelength. These problems illustrate the scattering of a TM^z plane wave of unit amplitude propagating in the direction x (e^{-jkx}). As these problems are not electrically large, only the EFIE suffices for their solution [solution provided by the system (4.130)].

The results of Figs.4.12 and 4.13 show that the meshless approach via IMLS shape functions provides reasonable results when compared to MoM, as long as the points of interest lie far away from the edges, where theoretically predicted singularities in the surface current density occur. We found that the IMLS shape functions go through strong peaks near the edges, thus providing very poor results there.

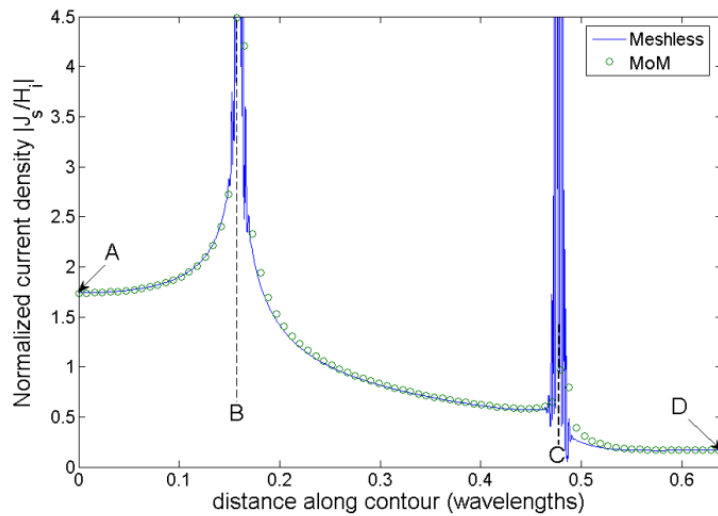


Fig.4.12. Normalized current density amplitude (J_z/H^i) along the perimeter section ABCD of Fig. 11a.

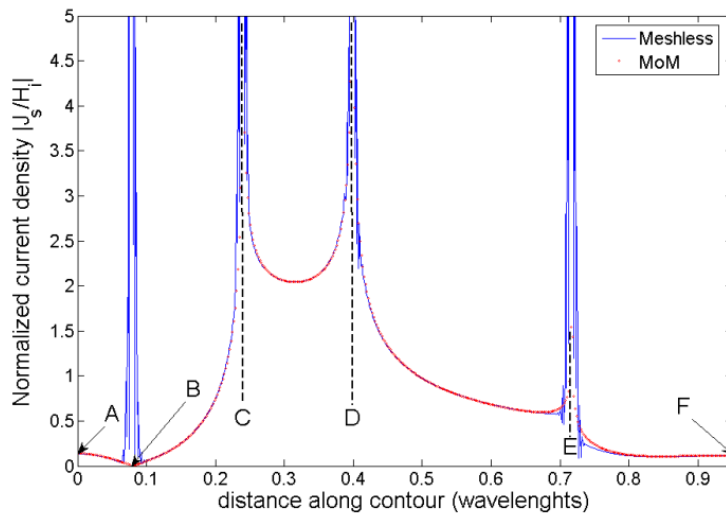


Fig.4.13. Normalized current density amplitude (J_z/H^i) along the perimeter section ABCDEF of Fig. 11b.

Commentary: This IMLS approach has not worked very well in the analyzed situations. Although the A -matrices are not singular, which allows the meshless analysis to be extended to cases involving flat-side scatterers, the peaks exhibited seem to jeopardize the precision of the solution near the edges. It is known that the solutions really blow up there, but even so, there is a feeling that things could have been better. We expect to find out reasons behind this behavior

in the future. By now, we can only speculate. In [Peng and Cheng, 2009], the IMLS procedure was applied to “full” two-dimensional problems, i.e., problems stated in a region Ω , and it seems that everything has gone on accordingly. However, in the cases we are studying, we have to restrict the nodal distribution to the contour $\partial\Omega$ only. Maybe using that machinery of inner products defined for two degrees of freedom (coordinates x and y), whereas the curve $\partial\Omega$ can be adequately described by only one degree of freedom (a parameter t), is what influenced the results in a negative way. In thinking about this, we soon came to realize that it really looks silly to employ the information provided by both coordinates x and y in the numerical construction of the shape functions. We have found that if the process is based on the *parameter* t (used to describe the points of $\partial\Omega$) rather than relying on points $(x, y) \in \partial\Omega$, the problems regarding the singular A -matrices and the oscillations both vanish. In the next section we exploit a new and much simpler way to deal with the kind of problem we are trying to solve. It is so simple that it looks rather childish.

4.4 Meshless Analysis of Integral Equations. The “rubber band” technique.

The method for constructing MLS shape functions which is going to be described is based in two steps:

- Construct periodic MLS shape functions in a one-dimensional interval T ;
- Take this interval as if it were a rubber band (or a kind of belt) and stretch it along the desired contour $\partial\Omega$.

This method had its origin in our struggle to answer the question: How do we construct consistent MLS shape functions for two-dimensional problems whose nodes exist along a contour $\partial\Omega$ only? Probably it will not be found in textbooks or papers dealing with meshless methods, because it was tailored for a specific situation (discretization of integral equations through meshless shape functions). Let us examine the details, as we show the application of this technique to the analysis of the TM^z scattering by an object whose contour is indicated in Fig.4.11b.

The parameter t describing $\partial\Omega$ ranges from 0 to L , where L is the perimeter (total length) of the curve $\partial\Omega$ (equal to $12a$ for this case):

$$T = \{t \in \mathbb{R} \mid 0 \leq t < L\} \tag{4.157}$$

(Remember, $t = 0$ and $t = L$ amount to the same physical location, and therefore the equality is excluded. We must take $t < L$ instead of $t \leq L$). We now must construct MLS shape functions on this one-dimensional interval T . However, if we apply the traditional MLS procedure, we get shape functions like those depicted in Fig.3.5 of Chapter 3, i.e., functions that are not periodic in T . This most important step on deriving periodic MLS shape functions is addressed now. Let the basis \mathbf{p} be composed of periodic functions in T :

$$\mathbf{p}(t) = [1, \cos 2\pi t/L, \sin 2\pi t/L]^T \tag{4.158}$$

This basis is periodic in the sense that $\mathbf{p}(0) = \mathbf{p}(L)$. We found that the periodicity of the basis is not sufficient to yield periodic shape functions in T . In the traditional MLS procedure, the distance between a point t and a node i in t_i is given by $|t - t_i|$. We modified this by considering also the *complementary distance* $L - |t - t_i|$ and by taking the smallest of them:

$$d_i = \min\{|t - t_i|, (L - |t - t_i|)\} \quad (4.159)$$

Figure 4.14 illustrates what (4.159) above means. The node i is located close to the beginning of the interval (i.e., $t = 0$), whereas the point t lies by the end of T (i.e., $t = L$). In the traditional MLS approach, the shape function ϕ_i associated to node i (at t_i) would not be able to influence point t , because it is too far away. But it should, because the points t and t_i are physically close to each other! Remember, the points $t = 0$ and $t = L$ amount to the same physical point. The traditional MLS shape function ϕ_i “die” at $t = 0$. It does not “extend its leg” until point t because this point does not belong to node i ’s influence domain. Here one can see the fundamental role played by the complementary distance. When it is considered, the point t is now considered to be an element of Λ_i , and node i is now able to extend its influence until point t (through the other way around).



Fig.4.14. A node located at t_i is unable to extend its influence domain Λ_i until the point t . But it should, because they are physically close to each other. When an expression that takes the complementary distance into account is employed in the numerical calculation of the shape functions, this problem is solved. The influence domain Λ_i now includes point t (the portion of the interval denoted by the dashed line has now been incorporated in Λ_i).

The result of implementing both modifications (4.158) and (4.159) in the MLS numerical procedure is found in Fig.4.15.

Because the interval T is nothing more than a piece of a straight line, pathological shape functions will never appear. This is the simplest kind of interval, and one must be sure that singular \mathbf{A} -matrices and oscillations are unlikely to occur (as long as only well behaved functions are incorporated into the basis \mathbf{p}). The fact that the shape functions assume negative values is probably due to the inclusion of trigonometric terms in the basis \mathbf{p} (4.158).

Observation: The inclusion of trigonometric terms in the basis has been motivated by the earlier work on the scattering by a circular cylinder. However, the periodicity there was assured because we used two parameters (values for x and y) and Euclidean distance in the calculation of the shape functions. Therefore, a point close to the endpoint ($t = L$) would be automatically influenced by a node close to the origin ($t = 0$). The situation is quite different here, as the shape functions relies on a single parameter (value for t). The periodicity must be enforced through the inclusion of the complementary distance.

Once the periodic shape functions are constructed, we must map each point t in the interval to a point in the contour $\partial\Omega$. There is a map f

$$f: T \rightarrow \partial\Omega \quad (4.160)$$

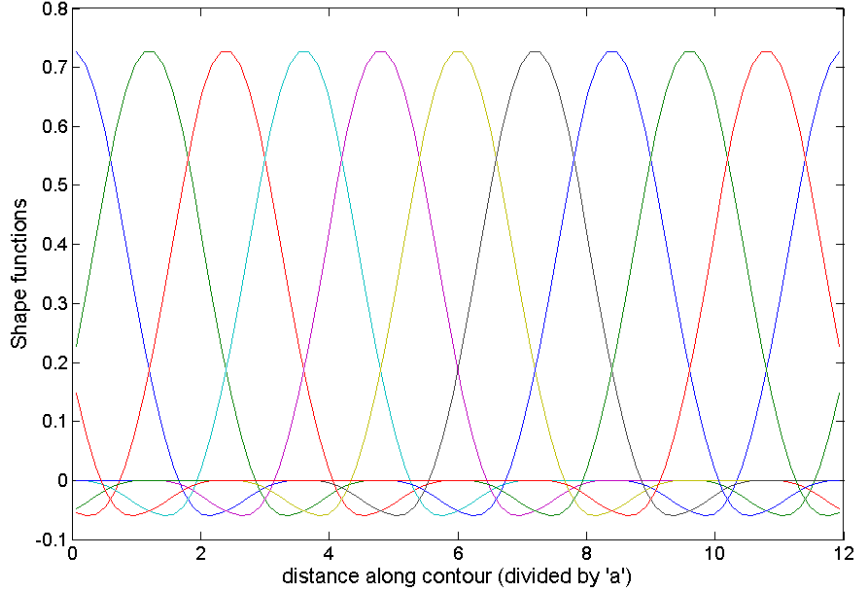


Fig.4.15. A set 10 shape functions constructed via the rubber band technique. For the scatterer of Fig.4.11b, the parameter t ranges from 0 to $12a$, where $a = \lambda/2\pi$. The simulation employed waves of frequency 10^9 Hz, which amounts to $\lambda = 0.3$ meter, and therefore $a = 0.0477$ meter. Because the scatterer is symmetric with respect to the a horizontal line $y = 0$ (Fig.4.11b), only a half of the problem was shown in Fig.4.13 (which explains $6 a/\lambda = 0.9549$, the final abscissa there).

that relates a parameter t to a point \vec{x} in $\partial\Omega$, or:

$$\forall t \in T \exists \vec{x} \in \partial\Omega (\vec{x} = f(t)) \quad (4.161)$$

The action of the map is quite like if the shape functions were built in a rubber band, which is stretched and wrapped around the contour $\partial\Omega$. Hence the name we decided to call this technique. Because the stretchings occur only in the horizontal direction, and never in the vertical one, the amplitudes of the shape functions are preserved. So they will never assume high values (towards infinity), maintaining their original range of values. Another useful comparison that conveys the same idea is this: we construct the shape functions along a belt (the interval T , whose length is L) which a person then wears around his waist (the contour $\partial\Omega$). The whole procedure is summarized as follows:

- Define an interval T ranging from 0 to L (total length of $\partial\Omega$);
- Spread nodes along T (at points t_i);
- Incorporate (4.158) and (4.159) into the MLS procedure and construct the periodic shape functions in the interval T first;
- Trough the map f , associate each value of the parameter t to a point in the perimeter of the scatterer cross-section ($\partial\Omega$).

So to each point \vec{x} , there is an associated parameter t which by its turn is associated to a set of influencing nodes $Neigh(t)$ (nodes whose shape functions extend their influence until t). Once we are done with this process, we discretize the EFIE in the usual way. The result is seen in Fig.4.16 below, where the peaks from Fig.4.13 have disappeared.

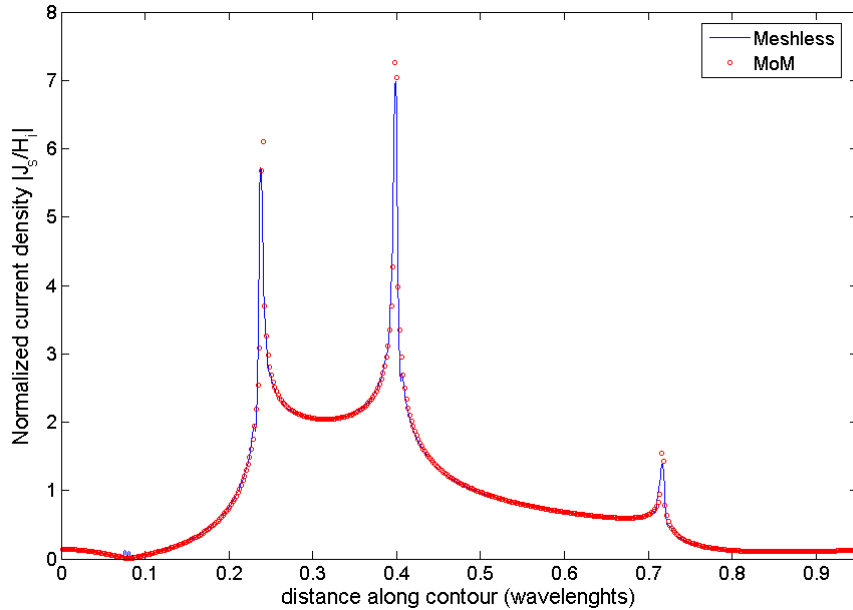


Fig.4.16. The scattering of a plane wave by the object depicted in Fig.4.11b. The problem has been solved through shape functions numerically constructed through the rubber-band technique.

Concluding Remarks

This is all we have done concerning the analysis of the scattering integral equations through meshless shape functions. Despite of its experimental character, much was learned. We now move on and delve into an authentic meshless method, the Meshless Local Petrov-Galerkin method. As this chapter is a little bit disconnected from the main theme of this work, i.e., the solution of differential equations, our table describing the overall procedures is left unchanged.

THE MESHLESS PROCEDURE IN A NUTSHELL

Given a differential equation and a domain where it shall be solved:

First Step	Set up the domain Ω and its boundary $\partial\Omega$.
Second Step	Spread N nodes throughout the domain Ω and at its boundary $\partial\Omega$ as well.
Third Step	<ul style="list-style-type: none"> • To each node i, define the radius of its influence domain Λ_i; • Make sure the influence domains cover the computational domain entirely.
Fourth Step	Numerical construction of the shape functions.

Chapter 5

The Meshless Local Petrov-Galerkin (MLPG) Method in Electromagnetic Wave Scattering

THE Meshless Local Petrov-Galerkin Method (MLPG, from now on), is a true meshless method aimed at solving partial differential equations. It shares some resemblances with FEM, as both deal with weak forms (i.e., the original PDE of a given order is restated as an integral expression involving lower-order derivatives) and sparse stiffness matrices. In this work, and particularly in this chapter, we are going to study second-order PDE's, stated at two-dimensional regions Ω (also called the computational domain). The problems are “fully” two-dimensional, meaning that nodes are spread throughout the region Ω and along its boundary $\partial\Omega$ as well (Differently from the last chapter, where we had considered nodes along $\partial\Omega$ only!).

The MLPG is based in a differential approach (like FEM), rather than an integral approach (as developed in the last chapter). This means that we begin to work with the differential equation and, after converting it quickly to a weak form, we are ready to perform the numerical integrations and assemble the global matrix. When it comes to be used in the study of electromagnetic wave scattering (the subject of this work), the most striking difference is that all that lengthy development of integral equations dealing with potential vectors, equivalent sources and Hankel functions is utterly unnecessary. Either for simple problems like the scattering by a single dielectric cylinder or for more complex situations involving scattering by dozens of objects, the formulation of the problem remains the same.

Electromagnetic wave propagation and scattering are modeled by Helmholtz differential equation, a second order PDE which is derived from Maxwell's equations. In the kind of problems we are concerned with, the scatterers are no longer PEC materials, but dielectric ones. We also are not going to deal with magnetic materials, what is not an oversimplification, because the mathematical form of a problem describing the scattering of the electric fields by dielectric materials and that of a problem describing the scattering of magnetic fields by magnetic materials are similar. They are dual problems. Difficulties arise when there are “mixed” situations, like the scattering of magnetic fields by dielectric materials or their dual counterpart (electric fields and magnetic materials). We address this delicate situation, which translates in the form of certain interface conditions that the fields must satisfy, by the end of this chapter. Let us now take a quick look at Helmholtz equations.

5.1 Helmholtz Equations

Considering again only temporal variations of the type $e^{j\omega t}$, Maxwell's equations become:

$$\nabla \times \vec{E}(\vec{x}) = -j\omega\vec{B}(\vec{x}) \quad (5.1)$$

$$\nabla \times \vec{H}(\vec{x}) = \vec{J}(\vec{x}) + j\omega\vec{D}(\vec{x}) \quad (5.2)$$

$$\nabla \cdot \vec{D}(\vec{x}) = \rho(\vec{x}) \quad (5.3)$$

$$\nabla \cdot \vec{B}(\vec{x}) = 0 \quad (5.4)$$

Since we are dealing with isotropic materials, the constitutive equations become

$$\vec{D}(\vec{x}, t) = \varepsilon_0 \varepsilon_r(\vec{x}) \vec{E}(\vec{x}, t) \quad (5.5)$$

$$\vec{B}(\vec{x}, t) = \mu_0 \mu_r(\vec{x}) \vec{H}(\vec{x}, t) \quad (5.6)$$

In these studies, there are no role to be played neither by the charge density ρ nor by the relative permeability μ_r . Therefore, we make $\rho = 0$ and $\mu_r = 1$. In addition to this, the problems we are going to solve also do not take into account any real current density \vec{J} . However, we leave this term in (5.2) just to illustrate the application of MLPG to situations involving sources (Section 5.5). The ε_r in (5.5) is the relative dielectric permittivity, and it is assumed to be 1 at any point \vec{x} in the free space. Our new set of equations is

$$\nabla \times \vec{E}(\vec{x}) = -j\omega\mu_0 \vec{H}(\vec{x}) \quad (5.7)$$

$$\nabla \times \vec{H}(\vec{x}) = \vec{J}(\vec{x}) + j\omega\varepsilon_0\varepsilon_r(\vec{x}) \vec{E}(\vec{x}) \quad (5.8)$$

$$\nabla \cdot \vec{E}(\vec{x}) = 0 \quad (5.9)$$

$$\nabla \cdot \vec{H}(\vec{x}) = 0 \quad (5.10)$$

Applying the curl operator ($\nabla \times$) to both sides of (5.7) we get (omitting the dependency on \vec{x} by now):

$$\nabla \times \nabla \times \vec{E} = -j\omega\mu_0 \nabla \times \vec{H} \quad (5.11)$$

Substituting (5.8) for $\nabla \times \vec{H}$ we arrive at

$$\nabla \times \nabla \times \vec{E} = -j\omega\mu_0 \vec{J} + \omega^2\mu_0\varepsilon_0\varepsilon_r \vec{E} \quad (5.12)$$

Because of the vector identity $\nabla \times \nabla \times \vec{E} = \nabla \nabla \cdot \vec{E} - \nabla^2 \vec{E}$ and of (5.9), we can rewrite (5.12) as $\nabla^2 \vec{E} + k^2 \varepsilon_r \vec{E} = j\omega\mu_0 \vec{J}$. In the TM^z polarization (field components given by E_z , H_x and H_y), our quantity of interest is E_z . Therefore we have the scalar Helmholtz equation for the electric field:

$$\nabla^2 E_z + k^2 \varepsilon_r E_z = j\omega\mu_0 J_z \quad (5.13)$$

The TE^z polarization (field components H_z , E_x and E_y) are treated best when there is a single scalar equation for H_z . As ε_r is a nonzero function, we rewrite (5.8) as

$$\frac{1}{\varepsilon_r} \nabla \times \vec{H} = \frac{1}{\varepsilon_r} \vec{J} + j\omega\varepsilon_0 \vec{E} \quad (5.14)$$

Taking the curl from both sides:

$$\nabla \times \left(\frac{1}{\varepsilon_r} \nabla \times \vec{H} \right) = \nabla \times \left(\frac{1}{\varepsilon_r} \vec{J} \right) + j\omega\varepsilon_0 \nabla \times \vec{E} \quad (5.15)$$

Substituting (5.7) for $\nabla \times \vec{E}$:

$$\nabla \times \left(\frac{1}{\epsilon_r} \nabla \times \vec{H} \right) = \nabla \times \left(\frac{1}{\epsilon_r} \vec{J} \right) + k^2 \vec{H} \quad (5.16)$$

We have

$$\nabla \times \left(\frac{1}{\epsilon_r} \nabla \times \vec{H} \right) = \begin{bmatrix} 0 \\ 0 \\ -\frac{\partial}{\partial x} \left(\frac{1}{\epsilon_r} \frac{\partial H_z}{\partial x} \right) - \frac{\partial}{\partial y} \left(\frac{1}{\epsilon_r} \frac{\partial H_z}{\partial y} \right) \end{bmatrix} = \begin{bmatrix} 0 \\ 0 \\ -\nabla \cdot \left(\frac{1}{\epsilon_r} \nabla H_z \right) \end{bmatrix} \quad (5.17)$$

and

$$k^2 \vec{H} = \begin{bmatrix} 0 \\ 0 \\ H_z \end{bmatrix} \quad (5.18)$$

If we allow the current \vec{J} to have only components J_x and J_y [in the case of a component J_z ever appears, then it gives origin to a TM^z field and therefore are treated through (5.13)], the term $\nabla \times (\vec{J}/\epsilon_r)$ has only a z-component. Therefore, equating the z-components of (5.16) we arrive at the scalar Helmholtz equation for the magnetic field:

$$\nabla \cdot \left(\frac{1}{\epsilon_r} \nabla H_z \right) + k^2 H_z = - \left(\nabla \times \left(\frac{1}{\epsilon_r} \vec{J} \right) \right) \cdot \hat{z} \quad (5.19)$$

However, in the subsequent problems, there we will never assume any current \vec{J} for the TE^z polarization, and then (5.19) above amounts to

$$\nabla \cdot \left(\frac{1}{\epsilon_r} \nabla H_z \right) + k^2 H_z = 0 \quad (5.20)$$

It is worthwhile to note that Helmholtz equations for both polarizations can be written as

$$\nabla \cdot \left(\frac{1}{p(\vec{x})} \nabla u(\vec{x}) \right) + k^2 q(\vec{x}) u(\vec{x}) = f(\vec{x}) \quad (5.21)$$

For TM^z polarization, u is the z-component of the electric field E_z , p is the relative magnetic permeability μ_r (equal to 1 everywhere) and q is the relative electric permittivity ϵ_r . For TE^z polarization, u is the z-component of the magnetic field H_z , p is the relative electric permittivity ϵ_r and q is the relative magnetic permeability μ_r (equal to 1 everywhere). In both cases, k is the free-space wavenumber ($k = 2\pi/\lambda$, λ is the free-space wavelength), and f is the source term.

5.2 General Features of MLPG

Our domain of interest is represented by a two-dimensional region Ω along with its boundary $\partial\Omega$. Differently from what was developed in the last chapter, the contour of the scatterer does not coincide with $\partial\Omega$. In the majority of cases, the scatterer will be located entirely within Ω . Given this region Ω , what really indicates if a point \vec{x} is inside a scatterer S is

the value of the relative permittivity ε_r calculated at \vec{x} . Usually, the scatterers are immersed in a medium whose properties resemble those of the free space (at least in this work). So we can say that:

$$\forall \vec{x} \in \bar{\Omega} (\varepsilon_r(\vec{x}) \neq 1 \rightarrow \vec{x} \in S) \quad (5.22)$$

i.e., if $\varepsilon_r(\vec{x}) \neq 1$, then the point \vec{x} is located in the interior of a scatterer. Another way of looking at (5.22) above is that a scatterer S is a set of points in the domain whose permittivity is different from 1. In (22), $\bar{\Omega} = \Omega \cup \partial\Omega$.

After we define our domain Ω , with different regions standing for the scatterer S (Fig. 5.1), the next step is to spread nodes throughout the computational domain.

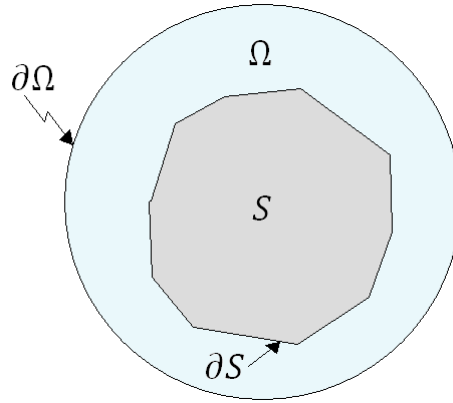


Fig.5.1. The computational domain Ω and the global boundary $\partial\Omega$. The scatterer is represented by the region S , whose boundary is ∂S .

Figure 5.2 illustrates a nodal distribution. If we spread N nodes throughout $\bar{\Omega}$, we take indices from the set of integers

$$I = \{1, 2, 3, 4, \dots, i, \dots, N\} \quad (5.23)$$

and associate a node to each one of them

$$\mathcal{N} = \{\vec{x} \in \bar{\Omega} \mid \exists i \in I (\vec{x} = \vec{x}_i)\} = \{\vec{x}_i \mid i \in I\} \quad (5.24)$$

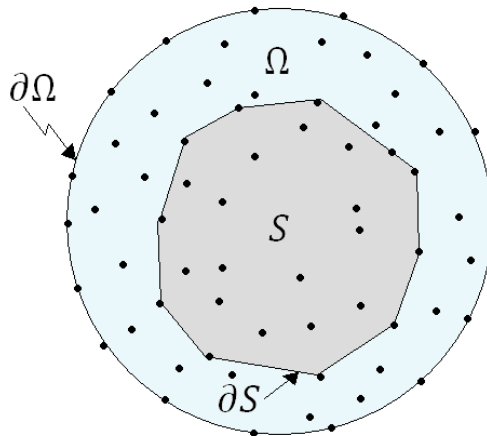


Fig.5.2 A nodal distribution set up in the domain of Fig.5.1.

According to what has been said earlier, to each node i we define an MLS influence domain Λ_i (with radius r_i):

$$\Lambda_i = \{\vec{x} \in \bar{\Omega} \mid \|\vec{x} - \vec{x}_i\| \leq r_i\} \quad (5.25)$$

which is the support of node i 's shape function ϕ_i . Besides that, the union of all influence domains Λ_i must cover the computational domain Ω entirely, i.e., given the family \mathcal{L} of influence domains

$$\mathcal{L} = \{\Lambda \mid \exists i \in I(\Lambda = \Lambda_i)\} = \{\Lambda_1, \Lambda_2, \dots, \Lambda_i, \dots, \Lambda_N\} \quad (5.26)$$

then

$$\bar{\Omega} \subseteq \bigcup \mathcal{L} = \bigcup_{i \in I} \Lambda_i \quad (5.27)$$

A particular feature of MLPG is that this method employs two kinds of domains. In addition to the influence domains Λ , there are the *test domains*, also called *sub-domains*, and represented by Y . To each node i , we associate a test domain Y_i , i.e., there is also a family \mathcal{Y} of test domains

$$\mathcal{Y} = \{Y \mid \exists i \in I(Y = Y_i)\} = \{Y_1, Y_2, \dots, Y_i, \dots, Y_N\} \quad (5.28)$$

The test domains, unlike the influence domains, do not necessarily cover the whole computational domain $\bar{\Omega}$. The reasons for that shall be explained later. The purpose of introducing test domains is that they are the field upon which another different function acts, called the *test function* v_i .

The Helmholtz equation (5.21) holds everywhere in Ω :

$$\forall \vec{x} \in \Omega \quad \nabla \cdot \left(\frac{1}{p(\vec{x})} \nabla u(\vec{x}) \right) + k^2 q(\vec{x}) u(\vec{x}) = f(\vec{x}) \quad (5.29)$$

In order to solve (5.29), we convert it from a second-order differential equation which holds everywhere in Ω to a set of N integral expressions holding in each one of the test domains Y_i . These integral expressions are known as weak forms. We get a weak form for the test domain Y_i by first multiplying (5.29) by the test function v_i and integrating over Y_i :

$$\forall i \in I \quad \int_{Y_i} \left(\nabla \cdot \left(\frac{1}{p(\vec{x})} \nabla u(\vec{x}) \right) + k^2 q(\vec{x}) u(\vec{x}) \right) v_i dA = \int_{Y_i} f(\vec{x}) v_i dA \quad (5.30)$$

The function $u(\vec{x})$ is expanded in shape functions as

$$u(\vec{x}) = \sum_{j \in \text{Neigh}(\vec{x})} \phi_j(\vec{x}) \hat{u}_j \quad (5.31)$$

After that, from the interplay of indices i and j , we get a linear system whose matrix (stiffness matrix) is sparse, which can be readily solved. In essence, this is the MLPG method. Let us now take a closer look at the details of how such a task is accomplished.

In the version of MLPG employed in this work, the test domains are required to be circles (two-dimensional problems) or spheres (three-dimensional problems):

$$\forall i \in I \quad Y_i = \{\vec{x} \in \bar{\Omega} \mid \|\vec{x} - \vec{x}_i\| \leq s_i\} \quad (5.32)$$

The radii s of the test domains usually differ from each other. They are not constrained to be all equal or to assume the same value as the radii of the influence domains. So each node i has an associated influence domain (Λ_i , radius r_i) and an associated test domain (Y_i , radius s_i). According to Chapter 2, the influence domain is related to a kind of “charge” a node has and whose combined influences are used to calculate the function of interest (u). The test domain can also be related to some sort of “charge”, which produces a field (described by the test function) that by its turn is not used to approximate anything. It is a kind of field entirely particular to the node, whose sole purpose is to restrict the differential equation to a region around the node only. It is because of this particularity that the test domains can overlap with each other. For two neighbor nodes i and j :

$$\|\vec{x}_i - \vec{x}_j\| < s_i + s_j \rightarrow Y_i \cap Y_j \neq \emptyset \quad (5.33)$$

The meaning of (5.33) is expressed in Fig. 5.3.

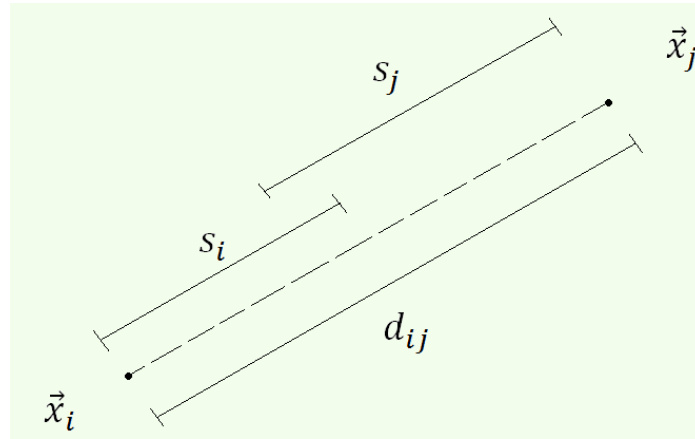


Fig.5.3 Node i 's test domain Y_i has a radius s_i , whereas Y_j has a radius s_j . If $s_i + s_j$ is greater than the distance between the nodes $d_{ij} = \|\vec{x}_i - \vec{x}_j\|$, then the test domains overlap with each other. Just imagine tracing two circles in the figure above. Take a compass, place its needle at the point \vec{x}_i and trace a circumference with radius s_i . Do the same with point \vec{x}_j and radius s_j . The two resulting circles will clearly overlap.

This is in stark contrast with FEM, where the integrations of the weak forms are traditionally carried out in non-overlapping elements, i.e., triangles (two-dimensional problems) and tetrahedrons (three-dimensional problems).

As we said earlier, in each test domain Y_i subsists a test function v_i . There is a lot of freedom in what test function one can choose [Atluri and Shen, 2002]. In this work, we decided to use the solution to Green's problem for the Laplace's equation as the test function. In addition to this, we also require the test function v_i to vanish at the test domain boundary ∂Y_i . Our test function is then characterized by

$$\forall \vec{x} \in Y_i \quad \nabla^2 v_i = -\delta(\vec{x} - \vec{x}_i) \quad (5.34)$$

and

$$\forall \vec{x} \in \partial Y_i \quad v_i = 0 \quad (5.35)$$

The reason for such a choice is that if the medium is homogeneous in respect to the parameter $p(\vec{x})$ in (5.21) (like what happens for the relative permittivity ε_r in the TM^z scattering), the resulting weak form (5.30) can be simplified. The solution to (5.34) and (5.35) is

$$v_i(\vec{x}) = \frac{1}{2\pi} \ln \left(\frac{s_i}{\|\vec{x} - \vec{x}_i\|} \right) \quad (5.36)$$

for two-dimensional problems and

$$v_i(\vec{x}) = \frac{1}{4\pi} \left(\frac{1}{\|\vec{x} - \vec{x}_i\|} - \frac{1}{s_i} \right) \quad (5.37)$$

for three-dimensional problems. When the test functions (5.36) or (5.37) are employed, the method we are studying is referred to as MLPG4 or Local Boundary Integral Equation Method (LBIE) [Atluri and Shen, 2002].

So, given a domain Ω , the first steps of MLPG4 are:

- Spread nodes throughout $\bar{\Omega}$;
- To each node i , associate an influence domain Λ_i with radius r_i ;
- Make sure that the “no-hole” condition is satisfied

$$\bar{\Omega} \subseteq \bigcup_{i \in I} \Lambda_i$$

- Construct a shape function (MLS) associated to each node i (whose compact support is Λ_i);
- To each node, associate a test domain Y_i with radius s_i ;
- Define a test function v_i acting on Y_i .

Having defined the basic steps, lets us move on and take a look at how MLPG4 is actually employed in electromagnetic wave scattering problems.

5.3 Intersecting test domains and Radiation Boundary Conditions (RBC)

We are interested here in the problem of the TM^z scattering of an incoming wave by a dielectric cylinder whose arbitrary cross-section is represented by S . For reasons that shall become clearer as our discussion evolves, the dielectric is surrounded by a circular boundary, as depicted in Fig.5.4. The bulk of the computational domain Ω includes both regions where the relative permittivity is equal to 1 (free space) and where it assumes other values (inside the scatterer). The equation describing the problem is

$$\forall \vec{x} \in \Omega \quad \nabla^2 E_z + k^2 \varepsilon_r E_z = 0 \quad (5.38)$$

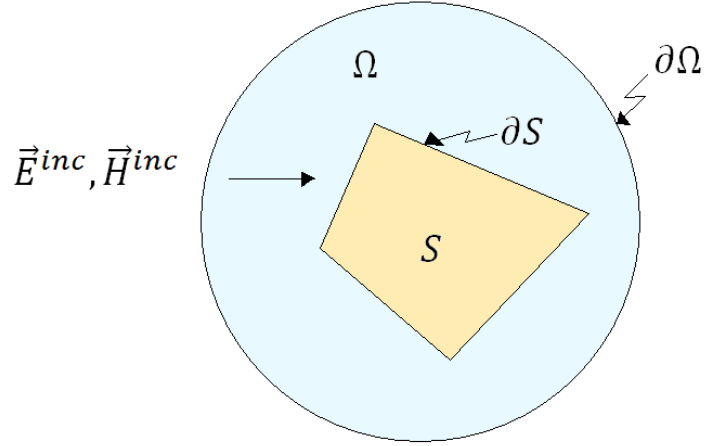


Fig.5.4 The dielectric scatterer S is located inside the computational domain Ω . The TM^z incident wave comes from the left.

(as there are no current whatsoever in $\bar{\Omega}$). After all steps discussed hitherto have been completed (nodes, domains, influence and test functions), we now derive the weak forms for (5.38). For the sake of generality, let us study here the most difficult case, i.e., that of a node i whose test domain Y_i intersects the global boundary $\partial\Omega$, as illustrated by Fig. 5.5.

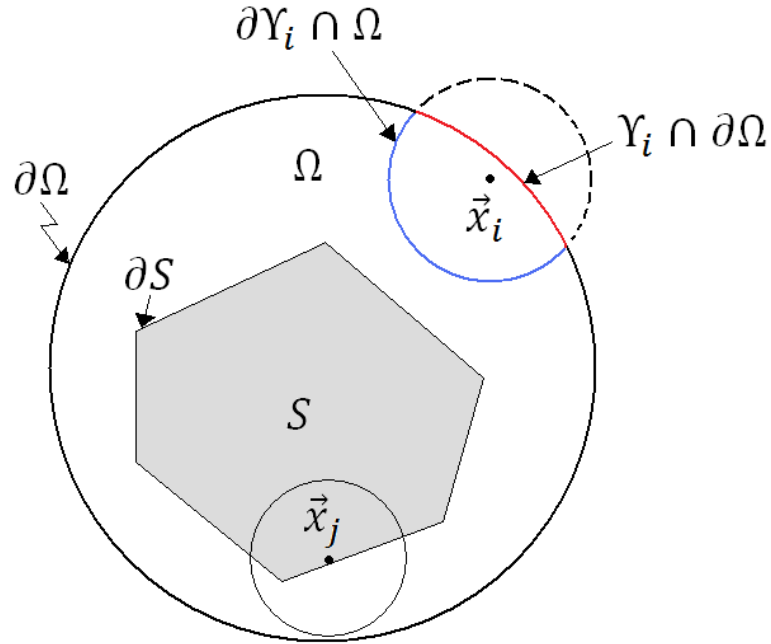


Fig.5.5. The problem domain Ω and the global boundary $\partial\Omega$. The irregular shaded area S is the scatterer cross-section, characterized by a relative permittivity ϵ_r . Node j 's (located at \vec{x}_j) test domain Λ_j (the circle around \vec{x}_j) does not intersect $\partial\Omega$. The situation is different for node i , as its test domain intersects the global boundary. Y_i is a circle centered in \vec{x}_i . Because the region limited by the dashed curve is outside the computational domain, it is summarily excluded. So we are left with the task of finding the intersection between Ω and Y_i . This new region where the weak form is imposed is limited by the curves $\partial Y_i \cap \Omega$ (blue) and $Y_i \cap \partial\Omega$ (red).

The second Green's identity for scalar fields is

$$\iint_R (u\nabla^2 v - v\nabla^2 u) dA = \oint_{\partial R} \left(u \frac{\partial v}{\partial n} - v \frac{\partial u}{\partial n} \right) dl \quad (5.39)$$

If we substitute the electric field E_z for the function u and the test function v_i for the function v we get:

$$\forall i \in I \quad -\alpha(\vec{x}_i)E_z(\vec{x}_i) + \iint_R k^2 \varepsilon_r E_z v_i dS = \oint_{\partial R} E_z \frac{\partial v_i}{\partial n} dl - \oint_{\partial R} v_i \frac{\partial E_z}{\partial n} dl \quad (5.40)$$

where the information concerning $\nabla^2 E_z$ came from (5.38) and that regarding $\nabla^2 v_i$ came from (5.34). According to Fig. 5.5, the integrations are to be performed at the intersection between the test domain Y_i and the computational domain Ω :

$$R = Y_i \cap \Omega \quad \text{and} \quad \partial R = (\partial Y_i \cap \Omega) \cup (Y_i \cap \partial \Omega) \quad (5.41)$$

The factor α in (5.40) arises in the integration of the delta function. It is equal to 1 for every \vec{x}_i (location of node i) inside the domain; however, if \vec{x}_i is exactly at the global boundary Γ , then α is proportional to the internal angle at \vec{x}_i (for example, if \vec{x}_i were located at the corner of a square, α would be $1/4$; were it to be located at wedge with internal angle equal to θ radians, α would be $\theta/2\pi$). For a circular boundary, α is approximately equal to $1/2$. Because ∂R is composed of two parts, we work out expression (5.40), which becomes

$$\begin{aligned} \forall i \in I \quad -\alpha(\vec{x}_i)E_z(\vec{x}_i) + \iint_{Y_i \cap \Omega} k^2 \varepsilon_r E_z v_i dS &= \int_{\partial Y_i \cap \Omega} E_z \frac{\partial v_i}{\partial n} dl - \int_{\partial Y_i \cap \Omega} v_i \frac{\partial E_z}{\partial n} dl \\ &+ \int_{Y_i \cap \partial \Omega} E_z \frac{\partial v_i}{\partial n} dl - \int_{Y_i \cap \partial \Omega} v_i \frac{\partial E_z}{\partial n} dl \end{aligned} \quad (5.42)$$

The second line integral is zero, because it depends on v_i evaluated at a portion of ∂Y_i (5.35). So we obtain:

$$\begin{aligned} \forall i \in I \quad -\alpha(\vec{x}_i)E_z(\vec{x}_i) + \iint_{Y_i \cap \Omega} k^2 \varepsilon_r E_z v_i dS &= \int_{\partial Y_i \cap \Omega} E_z \frac{\partial v_i}{\partial n} dl \\ &+ \int_{Y_i \cap \partial \Omega} E_z \frac{\partial v_i}{\partial n} dl - \int_{Y_i \cap \partial \Omega} v_i \frac{\partial E_z}{\partial n} dl \end{aligned} \quad (5.43)$$

Because the last two line integrals are evaluated at a portion of the global boundary $\partial \Omega$, E_z and $\partial E_z / \partial n$ are respectively the Dirichlet and Neumann conditions prescribed at the global boundary $\partial \Omega$ (if they were known). So we get

$$\begin{aligned} \forall i \in I \quad -\alpha(\vec{x}_i)E_z(\vec{x}_i) + \iint_{Y_i \cap \Omega} k^2 \varepsilon_r E_z v_i dS &- \int_{\partial Y_i \cap \Omega} E_z \frac{\partial v_i}{\partial n} dl \\ &= \int_{Y_i \cap \partial \Omega} E_z \frac{\partial v_i}{\partial n} dl - \int_{Y_i \cap \partial \Omega} v_i \frac{\partial E_z}{\partial n} dl \end{aligned} \quad (5.44)$$

This is the weak form that each node i in the problem gives rise to. If j happens to be an interior node whose test domain does not intersect $\partial \Omega$ (like \vec{x}_j in Fig. 5.5), there is no integration along the global boundary, and therefore the terms which depend on $\partial \Omega$ are discarded.

As it can be seen, in (5.44) there is no information about the incident field E_z^{inc} . Besides that, there is no information about the boundary conditions that must be imposed on $\partial \Omega$. A kind of

radiation boundary condition (RBC) has to be employed in order to provide this missing information.

RBC's are imposed in a contour located a certain distance away from the scatterer. In Fig.5.5, the irregular shaded area represents the cross-section S of the scatterer, which is composed of a dielectric material with relative permittivity ϵ_r . The circular line corresponding to the global boundary $\partial\Omega$ is the contour along which the RBC shall be imposed. It is seen that the global boundary comprises a certain space of the exterior medium (ϵ_0) surrounding the scatterer.

This type of boundary conditions is needed because the formulation based on Helmholtz differential equation only is not able to distinguish between outward-looking and inward-looking solutions. Strictly speaking, when a scattering problem is solved through (5.38), there is no means to distinguish between the two linearly independent solutions which represent waves coming onto the scatterer (like those represented by the zero-order Hankel functions of the first type in analytical solutions, $H_0^{(1)}$) and going away from the scatterer (represented by Hankel functions of the second type, $H_0^{(2)}$). In other words, RBC's simulate the Sommerfeld boundary conditions:

$$\lim_{\rho \rightarrow \infty} \frac{\partial E_z^S}{\partial n} = -jkE_z^S \quad (5.45)$$

where E_z^S is the scattered field.

As discussed in [Peterson *et al.*, 1998], RBC's can be exact, i.e., they simulate (5.45) exactly in a finite radius. But this approach is nonlocal; i.e., the normal derivative of the field at one point of the global boundary depends on an integral of the tangential field along the whole boundary. When exact RBC's are imposed at a finite distance, the aforementioned integral leads to fully populated matrices, thus making no sense in using them. To overcome this problem, a number of *approximate* RBC's were developed in the past. One of them is the second-order Bayliss-Turkel RBC, suited for circular global boundaries. The Bayliss-Turkel conditions are obtained from an asymptotic expansion of the scattered field E_z^S [Peterson *et al.*, 1998]. Using polar coordinates (ρ, φ) to locate a point at the global boundary $\partial\Omega$, they are

$$\frac{\partial E_z^S}{\partial n} = \frac{\partial E_z^S}{\partial \rho} = \beta_1(\rho)E_z^S + \beta_2(\rho)\frac{\partial^2 E_z^S}{\partial \phi^2} \quad (5.46)$$

where the coefficients β_1 and β_2 are given in terms of the finite boundary radius:

$$\beta_1(\rho) = \frac{-jk - \frac{3}{2\rho} + \frac{j3}{8k\rho^2}}{1 - \frac{j}{k\rho}} \quad (5.47)$$

and

$$\beta_2(\rho) = \frac{\frac{-j}{2k\rho^2}}{1 - \frac{j}{k\rho}} \quad (5.48)$$

Adding the term $\partial E_z^{inc}/\partial \rho$ at both sides of (5.46):

$$\frac{\partial E_z^s}{\partial n} + \frac{\partial E_z^{inc}}{\partial n} = \beta_1(\rho)E_z^s + \beta_2(\rho)\frac{\partial^2 E_z^s}{\partial \phi^2} + \frac{\partial E_z^{inc}}{\partial n} \quad (5.49)$$

Noting that E_z is the sum of the incident and scattered fields (i.e., $E_z = E_z^{inc} + E_z^s$), adding and subtracting the following term at the right side

$$\beta_1(\rho)E_z^{inc} + \beta_2(\rho)\frac{\partial^2 E_z^{inc}}{\partial \phi^2} \quad (5.50)$$

there follows

$$\frac{\partial E_z}{\partial n} = \beta_1(\rho)E_z + \beta_2(\rho)\frac{\partial^2 E_z}{\partial \phi^2} + f(E_z^{inc}) \quad (5.51)$$

where $f(E_z^{inc})$ is a function of the incident field:

$$f(E_z^{inc}) = \frac{\partial E_z^{inc}}{\partial n} - \beta_1(\rho)E_z^{inc} - \beta_2(\rho)\frac{\partial^2 E_z^{inc}}{\partial \phi^2} \quad (5.52)$$

Substituting (5.51) in (5.44) we get

$$\begin{aligned} \forall i \in I \quad & -\alpha(\vec{x}_i)E_z(\vec{x}_i) + \iint_{Y_i \cap \Omega} k^2 \varepsilon_r E_z v_i dS - \int_{\partial Y_i \cap \Omega} E_z \frac{\partial v_i}{\partial n} dl = \\ & \int_{Y_i \cap \partial \Omega} E_z \frac{\partial v_i}{\partial n} dl - \int_{Y_i \cap \partial \Omega} v_i \left(\beta_1(\rho)E_z + \beta_2(\rho)\frac{\partial^2 E_z}{\partial \phi^2} + f(E_z^{inc}) \right) dl \end{aligned} \quad (5.53)$$

This expression can be further simplified; the second derivative with respect to ϕ can be replaced by a simpler term. As the line integral in which it figures is evaluated along a portion of the global boundary where the radius ρ is a constant, all terms are functions of the ϕ solely. After some manipulations, which involve integration by parts, and reorganizing (5.54), we get the final expression:

$$\begin{aligned} \forall i \in I \quad & \alpha(\vec{x}_i)E_z(\vec{x}_i) - \iint_{Y_i \cap \Omega} k^2 \varepsilon_r E_z v_i dS + \int_{\partial Y_i \cap \Omega} E_z \frac{\partial v_i}{\partial n} dl + \\ & + \int_{Y_i \cap \partial \Omega} \left(E_z \frac{\partial v_i}{\partial n} - \beta_1 E_z v_i + \beta_2 \frac{\partial E_z}{\partial \phi} \frac{\partial v_i}{\partial \phi} \right) dl = \int_{Y_i \cap \partial \Omega} f(E_z^{inc}) v_i dl \end{aligned} \quad (5.54)$$

If the incident field is a plane wave coming from the left:

$$E_z^{inc}(x, y) = e^{-jkx} \rightarrow E_z^{inc}(\rho, \phi) = e^{-jk\rho \cos \phi} \quad (5.55)$$

expression (5.52) becomes:

$$f(E_z^{inc}) = -[\beta_1 + (1 + \beta_2\rho)jk \cos \phi - \beta_2 k^2 \rho^2 \sin^2 \phi] e^{-jk\rho \cos \phi} \quad (5.56)$$

In order to discretize the weak form (5.54), we express the electric field E_z as a weighted sum of shape functions:

$$\forall \vec{x} \in \bar{\Omega} \quad E_z(\vec{x}) = \sum_{m \in \text{Neigh}(\vec{x})} \phi_m(\vec{x}) \hat{u}_m \quad (5.57)$$

If we number the nodes differently (as explained in Section 3.1):

$$\forall \vec{x} \in \bar{\Omega} \quad E_z(\vec{x}) = \sum_{j=1}^n \phi_j(\vec{x}) \hat{u}_j \quad (5.58)$$

where the index j now runs from 1 to n (the number of nodes in $\text{Neigh}(\vec{x})$). After inserting (5.58) in (5.54) we get

$$\begin{aligned} \forall i \in I \quad & \sum_{j=1}^n \left(\alpha(\vec{x}_i) \phi_j(\vec{x}_i) - \iint_{\Upsilon_i \cap \Omega} k^2 \varepsilon_r \phi_j v_i dS + \int_{\partial \Upsilon_i \cap \Omega} \phi_j \frac{\partial v_i}{\partial n} dl \right) \hat{u}_j + \\ & + \sum_{j=1}^n \left(\int_{\Upsilon_i \cap \partial \Omega} \left(\phi_j \frac{\partial v_i}{\partial n} - \beta_1 \phi_j v_i + \beta_2 \frac{\partial \phi_j}{\partial \phi} \frac{\partial v_i}{\partial \phi} \right) dl \right) \hat{u}_j = \int_{\Upsilon_i \cap \partial \Omega} f(E_z^{\text{inc}}) v_i dl \end{aligned} \quad (5.59)$$

The form of the final linear system has now become apparent. It is

$$\mathbf{K} \hat{\mathbf{u}} = \mathbf{h} \quad (5.60)$$

where the elements of the stiffness matrix \mathbf{K} are

$$\begin{aligned} K_{ij} = & \alpha(\vec{x}_i) \phi_j(\vec{x}_i) - \iint_{\Upsilon_i \cap \Omega} k^2 \varepsilon_r \phi_j v_i dS + \int_{\partial \Upsilon_i \cap \Omega} \phi_j \frac{\partial v_i}{\partial n} dl + \\ & + \int_{\Upsilon_i \cap \partial \Omega} \left(\phi_j \frac{\partial v_i}{\partial n} - \beta_1 \phi_j v_i + \beta_2 \frac{\partial \phi_j}{\partial \phi} \frac{\partial v_i}{\partial \phi} \right) dl \end{aligned} \quad (5.61)$$

and the components of the source vector \mathbf{h} are

$$h_i = \int_{\Upsilon_i \cap \partial \Omega} f(E_z^{\text{inc}}) v_i dl \quad (5.62)$$

Observation #1: According to (5.36), the test functions v_i are characterized by a singularity at $\vec{x} = \vec{x}_i$. So care must be taken when performing the numerical integrations. One must make sure that none of the points used in the Gaussian integration coincides with \vec{x}_i .

Observation #2: The derivatives of the shape functions with respect to the polar angle that describes the global boundary $\partial \Omega$ are actually quite easy to calculate. Remember that the MLS procedure is a black box that returns the values of the shape functions and of their derivatives at any point we specify (Section 3.1). So for a point \vec{x} in $\partial \Omega$, we are given the values for $\partial \phi_j / \partial \varphi$ and $\partial \phi_j / \partial \varphi$. We also know that for a point \vec{x} in the global boundary, it is represented by the vector $\vec{x} = [x, y]^T = [a \cos \varphi, a \sin \varphi]^T$ where a is the radius of $\partial \Omega$. The derivative we are looking for can actually be retrieved from the chain rule for differentiation:

$$\frac{\partial \phi_j}{\partial \varphi} = \frac{\partial \phi_j}{\partial x} \frac{\partial x}{\partial \varphi} + \frac{\partial \phi_j}{\partial y} \frac{\partial y}{\partial \varphi} = -\frac{\partial \phi_j}{\partial x} a \sin \varphi + \frac{\partial \phi_j}{\partial y} a \cos \varphi \quad (5.63)$$

Observation #3: The element located at the i th row and at the j th column is given by (5.61). It can be seen that the integrations are carried out at the test domain (and at its boundary) associated to node i . If the shape function ϕ_j is unable to influence any point in Y_i , then K_{ij} will be zero. Hence

$$Y_i \cap \Lambda_j = \emptyset \rightarrow K_{ij} = 0 \quad (5.64)$$

i.e., whenever the intersection between the test domain Y_i and the influence domain Λ_j is the null set, the element K_{ij} will be zero. Therefore, the matrix \mathbf{K} will be sparse, as the influence domains Λ_j associated to nodes located far away from node i are unable to extend their influence domains until any point in Y_i . Figure 5.6 below illustrates the intersection between Y_i and Λ_j .

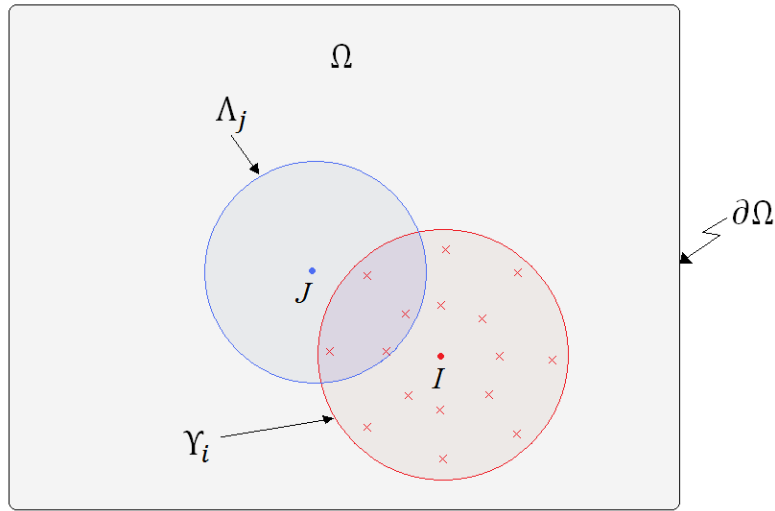


Fig.5.6 Two nodes i and j in the computational domain Ω . Node j is able to act on node i 's test domain, because $Y_i \cap \Lambda_j$. The element K_{ij} of the stiffness matrix is calculated taking into account the interaction between nodes i and j . When evaluating the integrals numerically, Gaussian points are spread throughout the test domain Y_i (red points). The integrals are then approximated by sums of expressions calculated at these points. Node j 's shape function ϕ_j is able to influence some of them (because they are located inside the influence domain Λ_j). Were node j located further away from node i in such a way that $Y_i \cap \Lambda_j = \emptyset$, then obviously $K_{ij} = 0$. Thus the fact that matrix \mathbf{K} is sparse becomes evident.

Once the nodal parameters are found, the total field E_z can be calculated everywhere in the domain through application of (5.57). To verify the precision of the method, we have applied it to the scattering analysis of a plane wave by a dielectric circular cylinder, a problem which is known to possess analytical solution [Balanis, 1989]. The global boundary is a circumference located at a distance 1.5 times greater than the cylinder radius. The results we have got are very precise, which can still be improved by adding more nodes or refining the numerical integration schemes. Figures 5.7 and 5.8 show the amplitude and phase for the scattering of a unit plane wave by a circular dielectric cylinder of radius $\lambda/2\pi$ and relative permittivity $\epsilon_r = 2 - j10$ (complex permittivity, which simulates a lossy dielectric). The total electric field E_z has been calculated along the dashed line that passes through the center of the cylinder. Approximately 300 nodes have been spread across the domain Ω (considering its boundary $\partial\Omega$ as well).

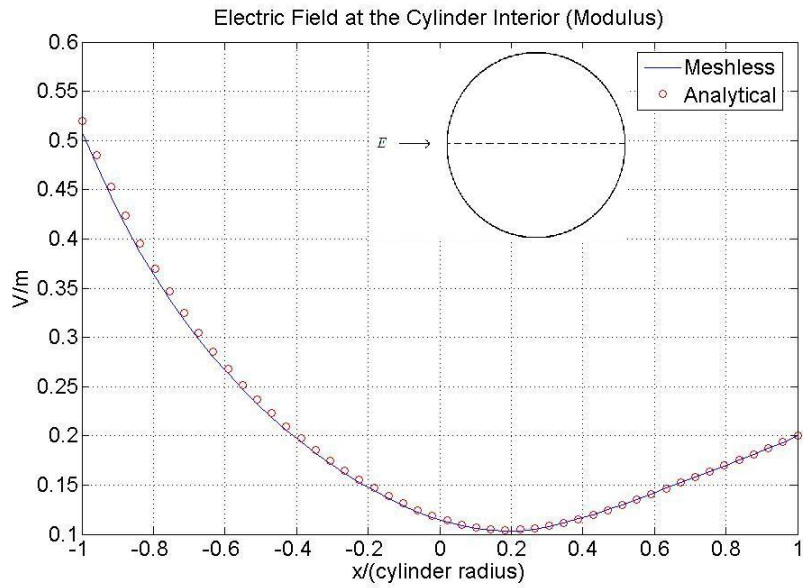


Fig.5.7. Electric field calculated along the dashed line (modulus). Dimension x is normalized with respect to the cylinder radius.

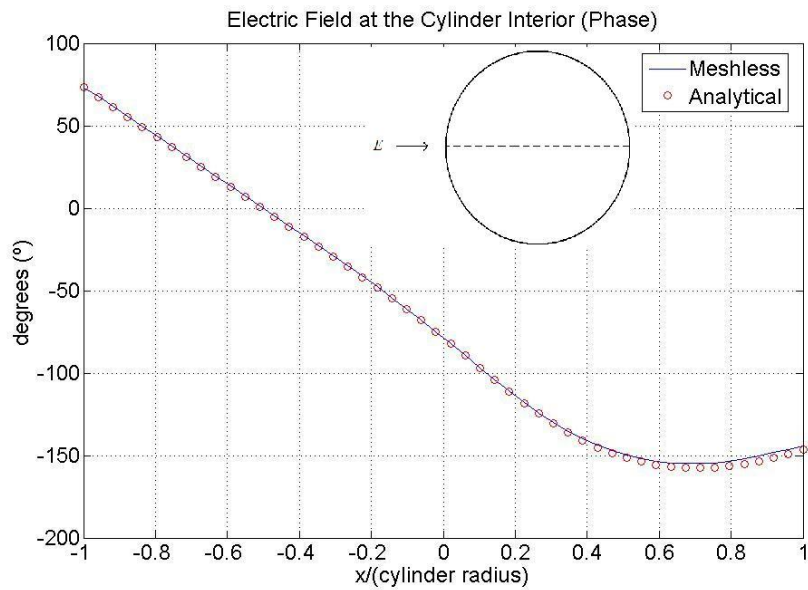


Fig.5.8. Electric field calculated along the dashed line (phase). Dimension x is normalized with respect to the cylinder radius.

5.4 *Intersecting test domains and Eigenfunction Expansions (Unimoment)*

When solving Helmholtz differential equation stated in a domain Ω , we found out that, in order to correctly simulate outward travelling waves, some sort of radiation boundary condition (RBC) had to be imposed on the global boundary $\partial\Omega$. The main point of concern is that the boundary $\partial\Omega$ must be imposed at a certain distance away from the scatterer (object upon which the wave impinges). As a consequence, a region surrounding the scatterer must also be

taken into account when solving Helmholtz equation. The size of the problem therefore becomes larger. This issue also happens if someone tries to use the Finite Element Method (FEM) in this formulation. Figure 9 below illustrates what has just been said.

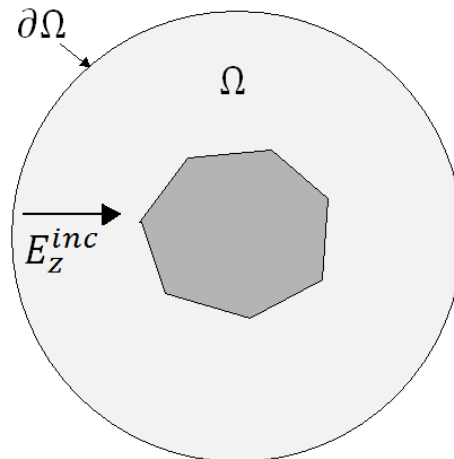


Fig.5.9. The scatterer (shaded region) must be surrounded by a layer of air, what causes the global boundary $\partial\Omega$ to be placed away from it.

In Fig.5.9, the scatterer is represented by a shaded region. A circular contour $\partial\Omega$ is placed away from the scatterer. The region in which the problem must be solved corresponds to all the interior of $\partial\Omega$, i.e., the domain Ω . The drawback with this formulation is that the radiation boundary conditions that simulate outward travelling waves are not exact, i.e., they are approximate. And, to make things worse, the further from the scatterer they are placed, the more precise they are. So if one wants accurate results, then one must place the boundary $\partial\Omega$ far away from the scatterer. The question is that, as $\partial\Omega$ is placed further and further away, the interior region Ω becomes larger and larger. In order to describe Ω appropriately, if MLPG is used, more nodes must be spread and the process must be carried out at a larger area. This is a waste of computational resources, because in problems of this sort, the electric (or magnetic field) close to the scatterer is what really matters. It seems to be no reason to calculate things that are not going to be used at all.

Looking for another formulation for the scattering problem, we have found that a hybrid method could do well without relying on radiation boundary conditions. So we blended the meshless LBIE (MLPG4) with eigenfunction expansions in order to correctly describe outward travelling waves.

The procedure that are going to be our object of study is a “meshless variant” of Unimoment method, which was devised by K. Mei [Chang and Mei, 1976] as a hybrid method intended to solve the scattering fields by dielectric bodies in unbounded domains. In two-dimensional analyses, the main idea is to set up a mathematical circle around the scatterer, thus splitting the problem into two regions: an interior and an exterior. The fields in the exterior region are expressed as a sum of Hankel functions, representing outward-travelling waves. The fields in the interior, by their turn, are given by a sum of solutions obtained through FEM. Once these interior solutions are formed, one imposes the continuity of the fields and of their normal derivatives along the mathematical circle, matching both problems at this boundary. The solutions of the interior and the exterior problems may then be expressed as sum of modal solutions, with Hankel functions in the exterior and numerical basis functions in the interior.

In the “meshless variant” of Unimoment method, instead of FEM, one uses the Meshless Local Petrov-Galerkin (MLPG) as a tool for calculating the numerical solutions to the interior problem. There are some advantages for doing this. Furthermore, the main feature of the hybrid method is that, as radiation boundary conditions are not imposed, the circle that divides the domain can be brought closer to the scatterer.

Given a scatterer with its characteristic cross section (shaded region in Fig.5.9), we set up a circumference $\partial\Omega$ surrounding it, thus dividing the space in two domains: the exterior (region I) and the interior (region II). The scatterer is to be entirely located inside region II, as in Fig.5.10.

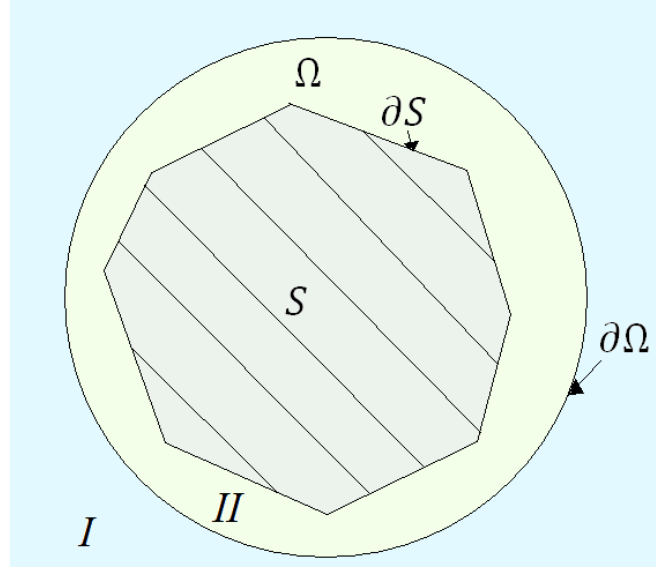


Fig.5.10. The circular boundary $\partial\Omega$ divides the domain in two regions: exterior (I) and interior (II). Region I (light blue) is related to the free space (air) only. The approximation there is made through a sum of Hankel functions. Region II (light green) encompasses the scatterer S and a small layer of air around it. The approximation is expressed as a sum of numerical basis (modal) functions ψ_p . The solutions in both regions are to be matched in $\partial\Omega$. The shaded area represents the cylinder cross-section.

For a TM^z incident wave, in which the electric field has only the z -component, we can write (in polar coordinates ρ and φ):

$$E_z^I(\rho, \varphi) = E_z^{inc}(\rho, \varphi) + E_z^S(\rho, \varphi) \quad (5.65)$$

for the total field in region I, as a sum of the incident and scattered fields. The scattered field E_z^S is expressed as an infinite sum of Hankel functions of the second type; but only those whose index vary from $-P$ to P will be taken into account:

$$E_z^S(\rho, \varphi) = \sum_{p=-P}^P A_p H_p^{(2)}(k\rho) e^{jp\varphi} \quad (5.66)$$

where the coefficients A_p remain to be evaluated. The wavenumber $k = 2\pi/\lambda$ is related to the exterior medium. The total field in region II is expressed by a sum of numerical basis functions:

$$E_z^{II}(\rho, \varphi) = \sum_{p=-P}^P B_p \psi_p(\rho, \varphi) \quad (5.67)$$

where B_p are coefficients to be determined and ψ_p are the numerical basis functions, or ‘modal solutions’.

The next step is to impose the continuity of the total field along both sides of the mathematical boundary $\partial\Omega$. Supposing this boundary to be located at a radius $\rho = a$, we arrive at two conditions:

$$\forall \vec{x} \in \partial\Omega \quad E_z^{inc}(\vec{x}) + E_z^S(\vec{x}) = E_z^{II}(\vec{x}) \quad (5.68)$$

$$\forall \vec{x} \in \partial\Omega \quad \frac{\partial E_z^{inc}(\vec{x})}{\partial n} + \frac{\partial E_z^S(\vec{x})}{\partial n} = \frac{\partial E_z^{II}(\vec{x})}{\partial n} \quad (5.69)$$

From the above expressions one sees that the infinite sum was replaced by a finite sum, with terms whose indices range from $-P$ to P , and there are no clue about the form of the numerical solutions ψ_n . They will then assumed to be solutions to the homogeneous Helmholtz equation:

$$\nabla^2 \psi_p(\vec{x}) + k^2 \varepsilon_r(\vec{x}) \psi_p = 0 \quad (5.70)$$

where the relative permittivity ε_r can be a function of position, $\varepsilon_r(\vec{x})$. Now comes one of the main features of the method: for each p , the Helmholtz equation (5.70) shall be subject to a characteristic Dirichlet condition enforced at the boundary $\partial\Omega$ ($\rho = a$). A linearly independent set of Dirichlet conditions is set up, i.e., for each p , one chooses the associated condition from the set

$$\{e^{-jP\varphi}, e^{-j(P-1)\varphi}, \dots, 1, \dots, e^{jP\varphi}, \dots, e^{j(P-1)\varphi}, e^{jP\varphi}\} \quad (5.71)$$

So, for a given p , taking (5.70) together with the associated Dirichlet condition $e^{jp\varphi}$ one finds the interior solution ψ_p throughout the interior domain (region II). After doing that for p ranging from $-P$ to P , the whole set of ‘modal’ interior solutions is formed. The equations (5.68) and (5.69) are then taken into account; when they are finally solved, the coefficients A_p and B_p of the field expansions are determined. The total interior field is thus given by (5.67).

In order to enforce (5.68) and (5.69) at the boundary $\rho = a$, we multiply these equations by a test function and integrate along the $\partial\Omega$ (as the radius is constant, it boils down to an integration in the polar angle φ). Taking the test function as $e^{-jq\varphi}$, where q ranges from $-P$ to P , keeping in mind that the numerical basis functions ψ_p vary as $e^{jp\varphi}$ at the boundary, and resorting to the identity

$$\int_0^{2\pi} e^{jp\varphi} e^{-jq\varphi} d\varphi = \int_0^{2\pi} e^{j(p-q)\varphi} d\varphi = 2\pi \delta_{pq} = \begin{cases} 2\pi, & p = q \\ 0, & p \neq q \end{cases} \quad (5.72)$$

we arrive at two expressions relating the coefficients A_p and B_p . After some manipulations, these expressions can be put in matrix form:

$$\begin{bmatrix} \mathbf{M}_1 & \mathbf{M}_2 \\ \mathbf{M}_3 & \mathbf{M}_4 \end{bmatrix} \begin{bmatrix} \mathbf{b} \\ \mathbf{a} \end{bmatrix} = \begin{bmatrix} \mathbf{f}_1 \\ \mathbf{f}_2 \end{bmatrix} \quad (5.73)$$

where each of the square submatrices \mathbf{M} has the size $(2P + 1)$, and $\mathbf{b}, \mathbf{a}, \mathbf{f}_1$ and \mathbf{f}_2 are vectors whose size is also $(2P + 1)$. The total system therefore has the size $(4P + 2)$. $\mathbf{M}_1, \mathbf{M}_2$ and \mathbf{M}_4 are diagonal matrices. Their elements are given by

$$[\mathbf{M}_1]_{rr} = 2\pi \quad (5.74)$$

$$[\mathbf{M}_2]_{rr} = -2\pi H_r^{(2)}(ka) \quad (5.75)$$

$$[\mathbf{M}_4]_{rr} = -2\pi \left. \frac{\partial H_r^{(2)}(k\rho)}{\partial n} \right|_{\rho=a} \quad (5.76)$$

\mathbf{M}_3 is a full matrix with elements:

$$[\mathbf{M}_3]_{rs} = \int_0^{2\pi} \left. \frac{\partial \psi_s}{\partial n} \right|_{\rho=a} e^{-jr\varphi} d\varphi \quad (5.77)$$

The indices range from $-P \leq r \leq P$ and $-P \leq s \leq P$. The vectors \mathbf{f}_1 and \mathbf{f}_2 have components:

$$[\mathbf{f}_1]_r = \int_0^{2\pi} E_z^{inc} \Big|_{\rho=a} e^{-jr\varphi} d\varphi \quad (5.78)$$

$$[\mathbf{f}_2]_r = \int_0^{2\pi} \left. \frac{\partial E_z^{inc}}{\partial n} \right|_{\rho=a} e^{-jr\varphi} d\varphi \quad (5.79)$$

The coefficients of the modal expansions (5.66) and (5.67) are given by the vectors $\mathbf{a}^T = [A_{-P}, \dots, A_P]$ and $\mathbf{b}^T = [B_{-P}, \dots, B_P]$, solutions to (5.72).

The procedure for solving Helmholtz equation (5.70) is the same as that one employed in the last section. The only difference is that Dirichlet boundary conditions are employed instead of radiation boundary conditions. After spreading the nodes throughout the computational domain, setting up the influence and test domains, and defining the shape and test functions, we take Green's second identity (5.39) and substitute ψ_p for u and v_i for v , thus obtaining

$$\forall i \in I \quad -\alpha(\vec{x}_i)\psi_p(\vec{x}_i) + \iint_R k^2 \varepsilon_r \psi_p v_i dS = \oint_{\partial R} \psi_p \frac{\partial v_i}{\partial n} dl - \oint_{\partial R} v_i \frac{\partial \psi_p}{\partial n} dl \quad (5.80)$$

Illustrating again the most difficult case for a node whose test domain Y_i intersects the global boundary $\partial\Omega$, i.e., letting the integration region R be defined by (5.41), restated here for convenience:

$$R = Y_i \cap \Omega \quad \text{and} \quad \partial R = (\partial Y_i \cap \Omega) \cup (Y_i \cap \partial\Omega) \quad (5.81)$$

Working out expression (5.81):

$$\begin{aligned} \forall i \in I \quad -\alpha(\vec{x}_i)\psi_p(\vec{x}_i) + \iint_{Y_i \cap \Omega} k^2 \varepsilon_r \psi_p v_i dS &= \int_{\partial Y_i \cap \Omega} \psi_p \frac{\partial v_i}{\partial n} dl - \int_{\partial Y_i \cap \Omega} v_i \frac{\partial \psi_p}{\partial n} dl \\ &+ \int_{Y_i \cap \partial\Omega} \psi_p \frac{\partial v_i}{\partial n} dl - \int_{Y_i \cap \partial\Omega} v_i \frac{\partial \psi_p}{\partial n} dl \end{aligned} \quad (5.82)$$

The second line integral is zero, as it depends on v_i evaluated at a portion of ∂Y_i (5.35):

$$\forall i \in I \quad -\alpha(\vec{x}_i)\psi_p(\vec{x}_i) + \iint_{Y_i \cap \Omega} k^2 \varepsilon_r \psi_p v_i dS = \int_{\partial Y_i \cap \Omega} \psi_p \frac{\partial v_i}{\partial n} dl \quad (5.83)$$

$$+ \int_{\Upsilon_i \cap \partial\Omega} \psi_p \frac{\partial v_i}{\partial n} dl - \int_{\Upsilon_i \cap \partial\Omega} v_i \frac{\partial \psi_p}{\partial n} dl$$

The term ψ_p (in the second line integral) actually stands for the Dirichlet condition on $\partial\Omega$. It is one of the elements from the set (5.71), namely, $e^{-jp\varphi}$. So, after rearranging the terms, the weak form (5.83) assumes its final form:

$$\begin{aligned} \forall i \in I \quad \alpha(\vec{x}_i) \psi_p(\vec{x}_i) - \iint_{\Upsilon_i \cap \Omega} k^2 \varepsilon_r \psi_p v_i dS + \int_{\partial\Upsilon_i \cap \Omega} \psi_p \frac{\partial v_i}{\partial n} dl - \int_{\Upsilon_i \cap \partial\Omega} v_i \frac{\partial \psi_p}{\partial n} dl \quad (5.84) \\ = - \int_{\Upsilon_i \cap \partial\Omega} e^{-jp\varphi} \frac{\partial v_i}{\partial n} dl \end{aligned}$$

Looking for a discretized version of (5.84), we express the modal solution ψ_p as a weighted sum of shape functions:

$$\forall \vec{x} \in \bar{\Omega} \quad \psi_p(\vec{x}) = \sum_{m \in \text{Neigh}(\vec{x})} \phi_m(\vec{x}) {}^p \hat{u}_m \quad (5.85)$$

Numbering the nodes differently (as explained in Section 3.1):

$$\forall \vec{x} \in \bar{\Omega} \quad \psi_p(\vec{x}) = \sum_{j=1}^n \phi_j(\vec{x}) {}^p \hat{u}_j \quad (5.86)$$

where the index j now runs from 1 to n (the number of nodes in $\text{Neigh}(\vec{x})$). After inserting (5.86) in (5.84) we get

$$\begin{aligned} \forall i \in I \quad \sum_{j=1}^n \left(\alpha(\vec{x}_i) \phi_j(\vec{x}_i) - \iint_{\Upsilon_i \cap \Omega} k^2 \varepsilon_r \phi_j v_i dS + \int_{\partial\Upsilon_i \cap \Omega} \phi_j \frac{\partial v_i}{\partial n} dl - \int_{\Upsilon_i \cap \partial\Omega} v_i \frac{\partial \phi_j}{\partial n} dl \right) {}^p \hat{u}_j \\ = - \int_{\Upsilon_i \cap \partial\Omega} e^{-jp\varphi} \frac{\partial v_i}{\partial n} dl \quad (5.87) \end{aligned}$$

The form of the final linear system is readily retrieved:

$${}^p \mathbf{K} {}^p \hat{\mathbf{u}} = {}^p \mathbf{h} \quad (5.88)$$

where the elements of the stiffness matrix ${}^p \mathbf{K}$ are given by

$${}^p K_{ij} = \alpha(\vec{x}_i) \phi_j(\vec{x}_i) - \iint_{\Upsilon_i \cap \Omega} k^2 \varepsilon_r \phi_j v_i dS + \int_{\partial\Upsilon_i \cap \Omega} \phi_j \frac{\partial v_i}{\partial n} dl - \int_{\Upsilon_i \cap \partial\Omega} v_i \frac{\partial \phi_j}{\partial n} dl \quad (5.89)$$

and the components of the vector ${}^p \mathbf{h}$ are

$${}^p h_i = - \int_{\Upsilon_i \cap \partial\Omega} e^{-jp\varphi} \frac{\partial v_i}{\partial n} dl \quad (5.90)$$

So in order to find the $2P + 1$ modal solutions ψ_p , we need to apply the MLPG process $2P + 1$ times:

$$\forall p \in \{-P, \dots, P\} \left({}^p\hat{\mathbf{u}} = {}^p\mathbf{K}^{-1} {}^p\mathbf{h} \right) \quad (5.91)$$

For each set of nodal parameters ${}^p\hat{\mathbf{u}}$, ψ_p is calculated at a point \vec{x} through (5.85). This is not a strong drawback as it could appear. If the nodal distributions are the same for all $2P + 1$ problems, the stiffness matrices ${}^p\mathbf{K}$ will all be equal to each other. Only the vectors ${}^p\mathbf{h}$ will undergo a change, as each one of them depends on a different Dirichlet condition.

Observation #1: The normal derivative of the shape functions that appears in the last line integral of (5.89) is easily calculated for a circular boundary $\partial\Omega$. We can form the gradient $\nabla\phi_j$ through the derivatives in rectangular coordinates that have been given us through the black box procedure described in Chapter 3. The unit normal to $\partial\Omega$ is $\hat{\mathbf{n}} = \hat{\mathbf{x}} \cos \varphi + \hat{\mathbf{y}} \sin \varphi$. So what we are looking for is no more than a simple directional derivative:

$$\frac{\partial\phi_j}{\partial n} = \nabla\phi_j \cdot \hat{\mathbf{n}} = \left(\hat{\mathbf{x}} \frac{\partial\phi_j}{\partial x} + \hat{\mathbf{y}} \frac{\partial\phi_j}{\partial y} \right) \cdot (\hat{\mathbf{x}} \cos \varphi + \hat{\mathbf{y}} \sin \varphi) \quad (5.92)$$

In order to verify the precision of the method, we applied it to the analysis of the scattering of a plane wave by a dielectric circular cylinder, a problem which is known to possess analytical solution [Balanis, 1989]. The results obtained are shown in Figs.5.11 and 5.12, which show the amplitude and phase for the scattering of a TM^z plane wave of unit amplitude by a cylinder with radius $\lambda/2\pi$ and relative permittivity $\varepsilon_r = 3$. Approximately 340 nodes have been spread over the domain Ω (although coarser results begin to appear when only 91 nodes are spread).

Observation #2: The implementation of the meshless variant of the Unimoment method is the only time in this work where the RPIM-PR process for constructing the shape functions has been employed (details in [Liu, 2003]).

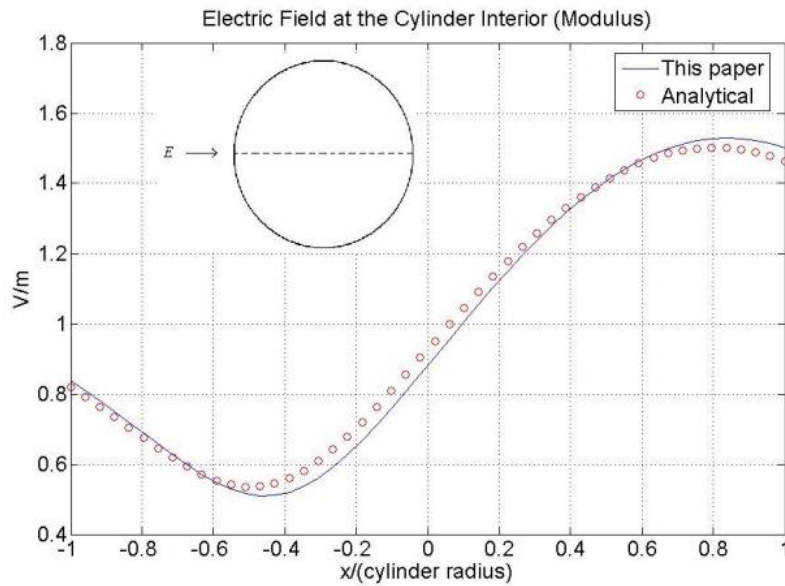


Fig.5.11. Electric field calculated along the dashed line (modulus). Dimension x is normalized with respect to the cylinder radius. Figure taken from reference [7] (see page Chapter 1, page 5).

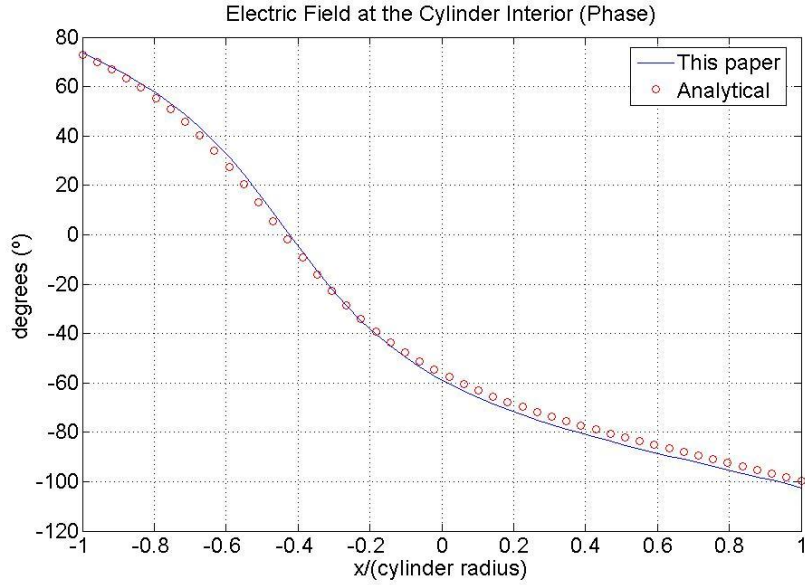


Fig.5.12. Electric field calculated along the dashed line (phase). Dimension x is normalized with respect to the cylinder radius. Figure taken from reference [7] (see page Chapter 1, page 5).

5.5 The Collocation Method

In the discussion of the MLPG exposed in the last two sections, we saw that the weak forms are integrated in a local domain around each node i :

$$R = \Upsilon_i \cap \Omega \quad \text{and} \quad \partial R = (\partial \Upsilon_i \cap \Omega) \cup (\Upsilon_i \cap \partial \Omega) \quad (5.93)$$

Although the method proved to be successful, no one could deny the extra difficulty provided by the task of finding the intersections between Υ_i and Ω . As the situations studied thus far these domains happened to be simple circles, the procedure employed to determine (5.93) was relatively easy. By just resorting to polar angle solved the issue.

However, this problem gets serious when the computational domains have forms different from the circle. For example, if $\partial \Omega$ were a square, than the region R for a node i situated close to $\partial \Omega$ would look like the figure depicted in Fig.5.13.

It has now become clear how cumbersome this task would be. Furthermore, such a procedure would have to be performed for all nodes whose test domains intersect the global boundary $\partial \Omega$. As the boundary conditions come into the problem through the data specified on $\partial \Omega$, we must find a way to deal with these conditions without the boring procedures of finding intersections between Υ_i and Ω .

The solution we have found to solve this issue is commonly used in FEM. It is called *collocation method*, and the boundary conditions are imposed at the nodes directly, without relying on weak forms. In order to implement this method, the test domains shall not cross the global boundary $\partial \Omega$.

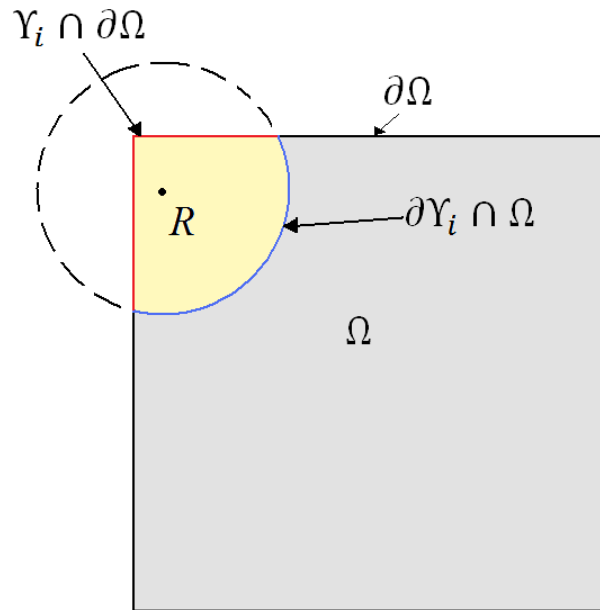


Fig.5.13. If the computational domain $\partial\Omega$ were a square, then for a node like that one depicted close to the upper left corner, the associated weak form would have to be integrated in the region R (yellow). However, there seems to be no advantage in dealing with integrations carried out in non-regular regions such as this one depicted here. Trying to solve this issue is the main motivation behind the collocation method.

Although for a node i we usually took the same value for the radii of the influence and test domains (i.e., $r_i = s_i$), things must be different now: *as the location of a node gets closer and closer to the global boundary $\partial\Omega$, its corresponding test domain is gradually diminished, until it eventually vanishes when the node is located exactly on $\partial\Omega$. The influence domains remain the same.* This is so important in the implementation of the collocation method that it deserves to be stated as a proposition:

Proposition 4.1 *As the location of a node i gets closer and closer to the global boundary $\partial\Omega$, the radius s_i of its corresponding test domain Y_i is gradually diminished, until it eventually vanishes when the node is located exactly on $\partial\Omega$. The influence domains Λ_i remain the same. The radius of the test domain i is calculated as*

$$s_i = \min\{r_i, d_i\} \quad (5.94)$$

where d_i is the distance from the node i (located at \vec{x}_i) to the global boundary $\partial\Omega$.

Figure 5.14 illustrates the meaning of this proposition. Node i is located relatively far from $\partial\Omega$ ($d_i > r_i$), and the radii of its associated influence and test domains are equal ($r_i = s_i$). Node j is closer to the global boundary ($d_j < r_j$). Therefore, we choose $s_j = d_j$, i.e., the test domain Y_j just touches $\partial\Omega$. Node k lies exactly on the global boundary, and then $d_k = 0$. So we choose $s_k = 0$. Note that although the test domains of the nodes j and k had their test domains diminished, *their influence domains remained unaltered*, i.e., they are able to influence (through their associated shape functions ϕ_j and ϕ_k) any point within the dashed circumferences.

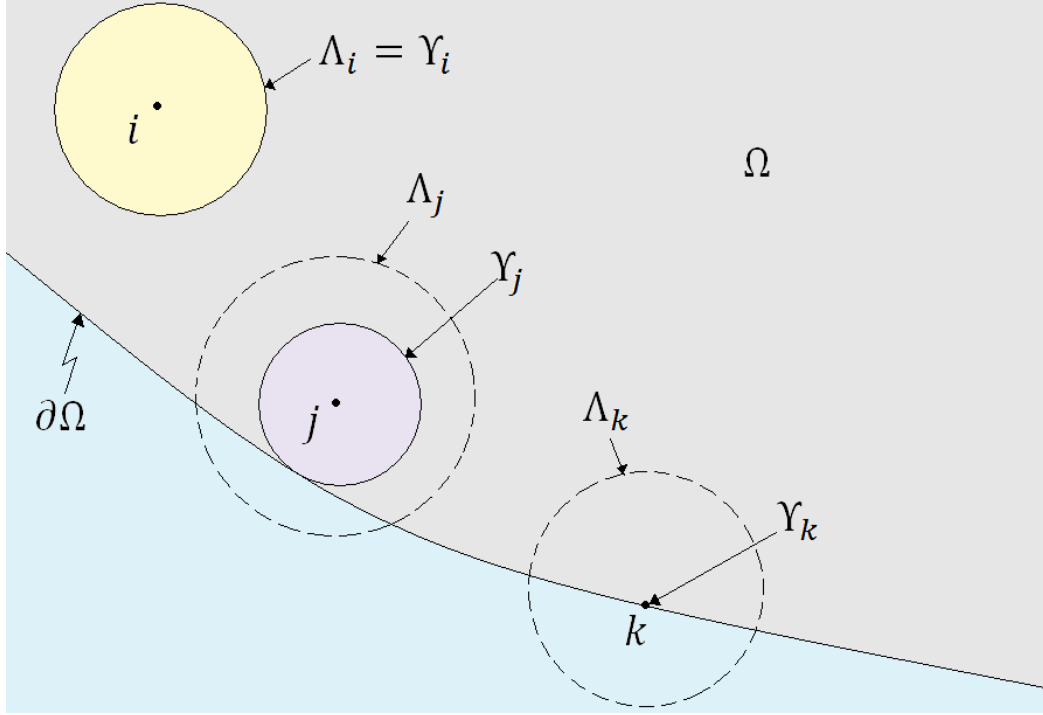


Fig.5.14. Nodes i, j, k and their associated influence ($\Lambda_i, \Lambda_j, \Lambda_k$) and test domains ($\Upsilon_i, \Upsilon_j, \Upsilon_k$). The influence domains of nodes j and k extend throughout the regions inside the dashed circumferences.

Observation #1: To recapitulate, we scattered N nodes throughout our region of interest Ω . The indices vary from 1 to N :

$$I = \{1, 2, 3, 4, \dots, i, \dots, N\} \quad (5.95)$$

Each node i is located at a point \vec{x}_i

$$\mathcal{N} = \{\vec{x} \in \bar{\Omega} \mid \exists i \in I (\vec{x} = \vec{x}_i)\} = \{\vec{x}_i \mid i \in I\} \quad (5.96)$$

and has an associated influence domain Λ_i (radius r_i)

$$\Lambda_i = \{\vec{x} \in \bar{\Omega} \mid \|\vec{x} - \vec{x}_i\| \leq r_i\} \quad (5.97)$$

along with a test domain Υ_i (radius s_i)

$$\Upsilon_i = \{\vec{x} \in \bar{\Omega} \mid \|\vec{x} - \vec{x}_i\| \leq s_i\} \quad (5.98)$$

We can then speak of a family \mathcal{L} of N influence domains

$$\mathcal{L} = \{\Lambda \mid \exists i \in I (\Lambda = \Lambda_i)\} = \{\Lambda_1, \Lambda_2, \dots, \Lambda_i, \dots, \Lambda_N\} \quad (5.99)$$

and of a family \mathcal{Y} of N test domains

$$\mathcal{Y} = \{\Upsilon \mid \exists i \in I (\Upsilon = \Upsilon_i)\} = \{\Upsilon_1, \Upsilon_2, \dots, \Upsilon_i, \dots, \Upsilon_N\} \quad (5.100)$$

The test domains must cover the whole computational domain $\bar{\Omega}$; it is a requirement that

$$\bar{\Omega} \subseteq \bigcup \mathcal{L} = \bigcup_{i \in I} \Lambda_i \quad (5.101)$$

In the method outlined in sections 4.2 and 4.3, as the influence and test domains had the same radii, then, by extension (5.101) above was satisfied by the family of test domains

$$\bar{\Omega} \subseteq \bigcup \mathcal{Y} = \bigcup_{i \in I} Y_i \quad (5.102)$$

However, because in the collocation procedure the test domains are diminished and even disappear (reduce to a point for nodes lying on $\partial\Omega$), (5.102) no longer remains true. Working out the symbols that appear in (5.102), it can be restated as

$$\forall \vec{x} \left(\vec{x} \in \bar{\Omega} \rightarrow \vec{x} \in \bigcup_{i \in I} Y_i \right) \quad (5.103)$$

i.e., if \vec{x} is a point of the set $\bar{\Omega}$, then it is a point of the set formed by the union of test domains from the family \mathcal{Y} . This means that there is at least one test domain Y_j from the family \mathcal{Y} of which \vec{x} is an element:

$$\forall \vec{x} \left(\vec{x} \in \bar{\Omega} \rightarrow \exists Y_j \in \mathcal{Y} (\vec{x} \in Y_j) \right) \quad (5.104)$$

As this proposition does not hold true for the collocation method, it must be false:

$$\neg \forall \vec{x} \left(\vec{x} \in \bar{\Omega} \rightarrow \exists Y_j \in \mathcal{Y} (\vec{x} \in Y_j) \right) \quad (5.105)$$

From the equivalence relations between the negations of the universal and existential quantifiers \forall and \exists :

$$\neg \forall w P(w) = \exists w \neg P(w) \quad (5.106)$$

where P is a proposition that depends on the variable w , (5.105) can be rewritten as

$$\exists \vec{x} \neg \left(\vec{x} \in \bar{\Omega} \rightarrow \exists Y_j \in \mathcal{Y} (\vec{x} \in Y_j) \right) \quad (5.107)$$

From the equivalent expression of implication

$$\exists \vec{x} \neg \left(\neg \vec{x} \in \bar{\Omega} \vee \exists Y_j \in \mathcal{Y} (\vec{x} \in Y_j) \right) \quad (5.108)$$

where \vee is the disjunction (OR) connective. Moving the negation sign inside the parentheses, and recalling DeMorgan's law (\wedge is the conjunction (AND) connective)

$$\exists \vec{x} \left(\neg \neg \vec{x} \in \bar{\Omega} \wedge \neg \exists Y_j \in \mathcal{Y} (\vec{x} \in Y_j) \right) \quad (5.109)$$

Finally

$$\exists \vec{x} \left(\vec{x} \in \bar{\Omega} \wedge \neg \exists Y_j \in \mathcal{Y} (\vec{x} \in Y_j) \right) \quad (5.110)$$

Proposition (5.110) above means that, when using the collocation method, there could be a point \vec{x} in the computational domain $\bar{\Omega}$ for which there is not any test domain from the family \mathcal{Y} that contains \vec{x} . This generally occurs for points that happen to be located close to the global

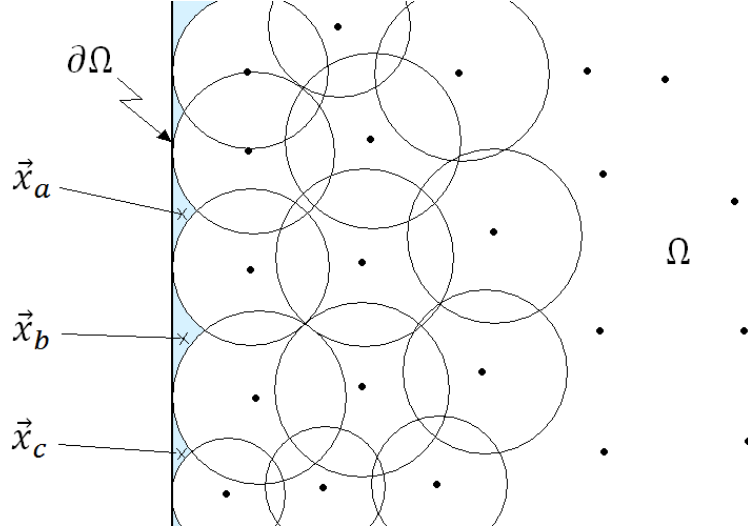


Fig.5.15. A domain Ω and some nodes scattered throughout it. The test domains associated to each node are represented by the circles (those of the interior nodes located farther to the right are not shown). When the collocation method is employed, some regions close to the global boundary $\partial\Omega$ (light blue) remain outside of any test domain in the family \mathcal{Y} . The interior of the domain is entirely covered by the test domains, but points like \vec{x}_a , \vec{x}_b and \vec{x}_c are not. Despite the tiny regions uncovered by the test domains, the results we have got are actually quite precise.

boundary. Figure 5.15 illustrates this. There it can be seen that there is no test domain including a points such as \vec{x}_a , \vec{x}_b and \vec{x}_c . As more and more nodes are added to the problem, the set of points that are outside any test domain gets smaller and smaller.

The collocation method represents an advantage, rather than a drawback, because it releases the analyst from the tedious task of finding intersections between domains. The method we are illustrating in this section is actually a hybrid MLPG method. The MLPG4 employs test domains for all nodes and therefore has to deal with the issue of intersections. The MLPG2 uses collocation for all nodes, dismissing any kind of test domain [Atluri and Shen, 2002]. However, it is generally less precise than MLPG4. What we have done here was to use the good characteristics of both methods. In interior nodes, where its precision is better, we employed MLPG4. In the other hand, for nodes located on the global boundary, where MLPG4 ceases to be attractive, we resorted to MLPG2 (collocation scheme).

We are again to deal with Helmholtz equation (5.29), restated for convenience:

$$\forall \vec{x} \in \Omega \quad \nabla \cdot \left(\frac{1}{p} \nabla u \right) + k^2 q u = f \quad (5.111)$$

In order to find the weak forms for (5.111), we take the weighted residual method instead of Green's second identity. However, when dealing with the collocation scheme, only the nodes situated in the interior of Ω are considered (nodes whose test domains at most touch the global boundary). If there are N nodes, and if N^i are interior and N^b lie on $\partial\Omega$ (such that $N^i + N^b = N$) then

$$\forall i \leq N^i \quad \iint_{Y_i} \nabla \cdot \left(\frac{1}{p} \nabla u \right) v_i dA + \iint_{Y_i} k_0^2 q u v_i dA = \iint_{Y_i} f v_i dA \quad (5.112)$$

Applying the following vector identity (where g is a scalar function and \vec{A} a vector function)

$$\nabla \cdot (g\vec{A}) = \nabla g \cdot \vec{A} + g\nabla \cdot \vec{A} \quad (5.113)$$

to the first term at the left side of (5.112), and then the two-dimensional version of the Divergence Theorem we arrive at

$$\forall i \leq N^i \quad \oint_{\partial Y_i} \frac{1}{p} v_i \frac{\partial u}{\partial n} dl - \iint_{Y_i} \frac{1}{p} \nabla v_i \cdot \nabla u dA + \iint_{Y_i} k_0^2 q u v_i dA = \iint_{Y_i} f v_i dA \quad (5.114)$$

Because the test function v_i vanishes at the boundary of the test domain ∂Y_i [according to (5.35)], the term involving the line integral is disregarded. The weak form then reads:

$$\forall i \leq N^i \quad \iint_{Y_i} \frac{1}{p} \nabla v_i \cdot \nabla u dA - \iint_{Y_i} k_0^2 q u v_i dA = - \iint_{Y_i} f v_i dA \quad (5.115)$$

We already know how to discretize (5.115), i.e., we take

$$\forall \vec{x} \in \bar{\Omega} \quad u(\vec{x}) = \sum_{m \in \text{Neigh}(\vec{x})} \phi_m(\vec{x}) \hat{u}_m \quad (5.116)$$

Numbering the nodes differently (as explained in Section 3.1):

$$\forall \vec{x} \in \bar{\Omega} \quad u(\vec{x}) = \sum_{j=1}^n \phi_j(\vec{x}) \hat{u}_j \quad (5.117)$$

Substituting (5.117) in (5.115)

$$\forall i \leq N^i \quad \sum_{j=1}^n \left(\iint_{Y_i} \frac{1}{p} \nabla v_i \cdot \nabla \phi_j dA - \iint_{Y_i} k_0^2 q \phi_j v_i dA \right) \hat{u}_j = - \iint_{Y_i} f v_i dA \quad (5.118)$$

From (5.118), we can extract the form of the linear system:

$$\mathbf{K}^i \hat{\mathbf{u}} = \mathbf{h}^i \quad (5.119)$$

where the elements of the matrix \mathbf{K}^i are given by

$$K_{ij}^i = \iint_{Y_i} \frac{1}{p} \nabla v_i \cdot \nabla \phi_j dA - \iint_{Y_i} k_0^2 q \phi_j v_i dA \quad (5.120)$$

and the elements of the vector \mathbf{h}^i are

$$h_i^i = - \iint_{Y_i} f v_i dA \quad (5.121)$$

Because the points inside Y_i (those used for the numerical integration) can be influenced by nodes from the interior of the domain and from those lying at the global boundary as well, any one of the N nodes can theoretically contribute to the integrals in (5.120) and (5.121) (of course that the contribution from the distant nodes would be zero). Therefore, each one of the expressions in (5.118) gives rise to a linear equation in N unknowns (the coefficients are listed in (5.120) and (5.121)). It does not take much effort to realize that the linear system (5.119) is

incomplete, i.e., it has N^i equations and $N = N^i + N^b$ unknowns. \mathbf{K}^i is a $N^i \times N$ matrix, and \mathbf{h}^i is a $N^i \times 1$ vector. The extra N^b relations come from the boundary nodes.

The information concerning the boundary conditions at $\partial\Omega$ comes into the problem through the boundary nodes. But, as we have just seen, these nodes are not assigned any kind of test domain. A simple scheme that requires no integration whatsoever is a *meshless collocation* scheme, based on the approximation described by (5.116). Let us suppose that a node m (the index m counts the number of boundary nodes, i.e., $1 \leq m \leq N^b$) whose coordinates are $\vec{x}_m = (x_m, y_m)$, lies at a portion of the global boundary $\partial\Omega$ where the boundary conditions are (expressed in general form):

$$a(\vec{x})u(\vec{x}) + b(\vec{x})\frac{\partial u(\vec{x})}{\partial n} = g(\vec{x}) \quad (5.122)$$

where the coefficients $a(\vec{x})$ and $b(\vec{x})$ are given functions of the position \vec{x} along $\partial\Omega$, and $g(\vec{x})$ is a known function of \vec{x} . In (5.122) three types of boundary conditions are embedded: if Dirichlet conditions are assumed, then $a(\vec{x}) = 1$ and $b(\vec{x}) = 0$; otherwise, if Neumann conditions are assumed, then $a(\vec{x}) = 0$ and $b(\vec{x}) = 1$. In treating Robin conditions, $a(\vec{x}) \neq 0$ and $b(\vec{x}) \neq 0$. Thence based on (5.116) and for each node m located at $\vec{x} = \vec{x}_m$, there follows:

$$\forall m \leq N^b \quad a(\vec{x}_m)u^h(\vec{x}_m) + b(\vec{x}_m)\frac{\partial u^h(\vec{x}_m)}{\partial n} = g(\vec{x}_m) \quad (5.123)$$

Expanding (5.123) we have N^b nodal equations:

$$\forall m \leq N^b \quad a(\vec{x}_m) \sum_{k \in Neigh(\vec{x}_m)} \phi_k(\vec{x}_m)\hat{u}_k + b(\vec{x}_m) \sum_{k \in Neigh(\vec{x}_m)} \frac{\partial \phi_k(\vec{x}_m)}{\partial n} \hat{u}_k = g(\vec{x}_m) \quad (5.124)$$

where the global index k runs through all nodes whose influence domains include point \vec{x}_m . In Fig.5.27 (page 110), there are 5 influencing nodes whose global indices are 2, 5, 21, 30 and m (since the distance from node m to \vec{x}_m is zero, the window function w centered at \vec{x}_m is exactly 1 at \vec{x}_m). The $\phi_k(\vec{x}_m)$ is the shape function associated to the influencing node k evaluated at the point \vec{x}_m , $\partial\phi_k(\vec{x}_m)/\partial n$ is the normal derivative of the shape function associated to node k evaluated at \vec{x}_m , and \hat{u}_k is the nodal parameter associated to the influencing node k (unknown). This meshless collocation procedure renders the imposition of boundary conditions elegant and fairly simple; neither finding intersections between domains nor performing numerical integrations is necessary.

As theoretically all nodes (from the interior and from the boundary as well) are able to extend their influence domain until \vec{x}_m , each expression in (5.124) is actually a linear equation in N unknowns. They can be written in a linear system as

$$\mathbf{K}^b \hat{\mathbf{u}} = \mathbf{h}^b \quad (5.125)$$

The element in line m and column k (as long as $k \in Neigh(\vec{x}_m)$) of the matrix \mathbf{K}^b is given by the left side of (5.124). All other elements are zero. The m th component of the vector \mathbf{h}^b is the right side of (5.124).

Because the matrix \mathbf{K}^b is $N^b \times N$, and the vector \mathbf{h}^b is $N^b \times 1$, the linear systems (5.119) and (5.125) can be assembled together into a $N \times N$ system:

$$\begin{bmatrix} K^i \\ K^b \end{bmatrix} \hat{\mathbf{u}} = \begin{bmatrix} \mathbf{h}^i \\ \mathbf{h}^b \end{bmatrix} \quad (5.126)$$

From (5.126), the nodal parameters $\hat{\mathbf{u}}$ are finally retrieved. Let us proceed and take a look at some worked examples. Just for the sake of developing further insight on the application of MLPG with the collocation method, the next three figures (Figs. 5.16, 5.17 and 5.18) illustrate, in this order: A circular computational domain $\bar{\Omega}$ with some nodes, the same domain covered by the influence domains and $\bar{\Omega}$ again packed with test domains associated to the nodes.

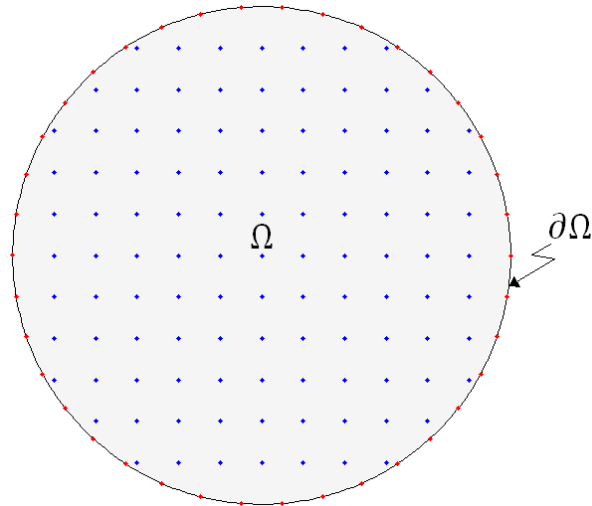


Fig.5.16. The sequence of steps in the implementation of MLPG4 and the collocation method. *First:* The nodes are spread throughout the computational domain Ω and its boundary $\partial\Omega$.

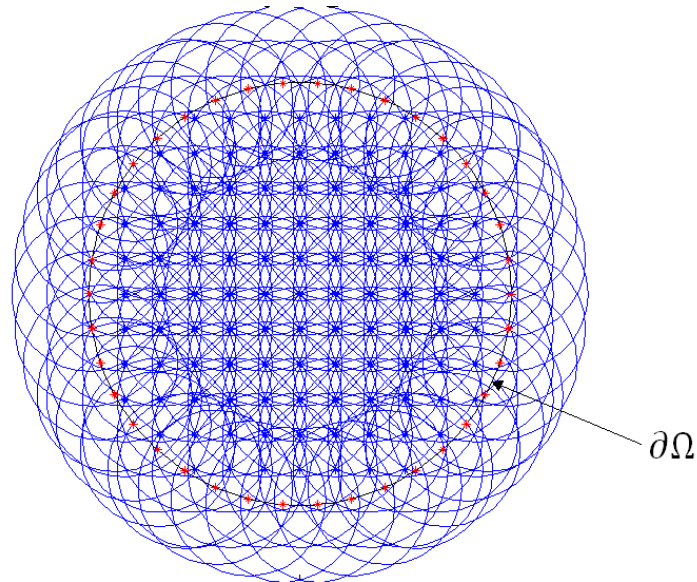


Fig.5.17. *Second:* The influence domains Λ are associated to each node so that they cover the domain $\bar{\Omega}$ entirely (the ‘no-hole’ condition).

The first example deals with the task of finding the electric field E_z inside a cavity excited by a line of current, i.e., one is interested in Green’s problem:

$$\nabla^2 E_z + k_0^2 E_z = -\delta(x - \xi)\delta(y - \eta) \quad (5.127)$$

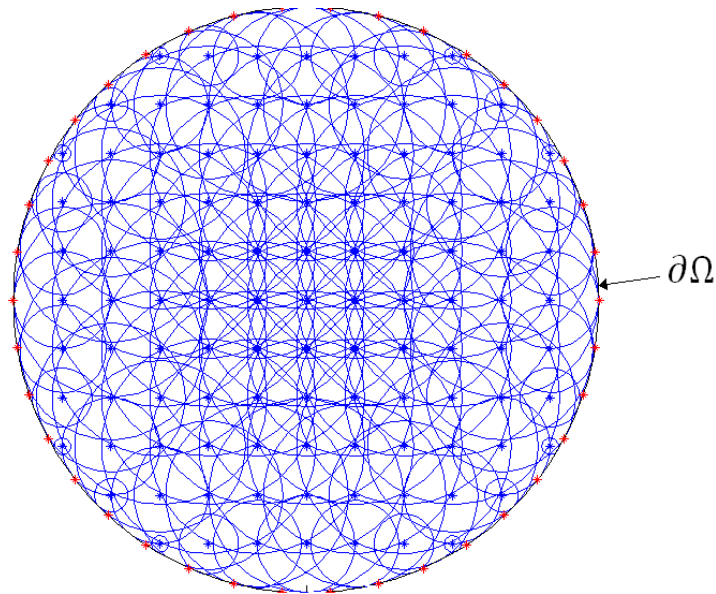


Fig.5.18. *Third*: The family of test domains Y ascribed to the nodes. They are arranged in such a way that they just touch the global boundary $\partial\Omega$, thus avoiding any kind of intersection. The boundary conditions are imposed through the collocation scheme, and the weak forms are ready to be enforced at the circular test domains. It is really far easier to perform numerical integrations in simple circles rather than in regions like that depicted in Fig.5.5.

Equation (5.127) is to be solved inside a square region $\Omega = (0,1) \times (0,1)$ where $k_0 = 10$ and the condition $E_z = 0$ is imposed along the global boundary $\partial\Omega$. The current source (the Dirac delta function) is located at $(\xi, \eta) = (0.35, 0.35)$. A total of 1796 nodes have been spread across the computational domain, and each node influences, approximately, 16 other nodes. Figures 5.19 and 5.20 compare the analytical solution (Fig. 5.19) (which can be found in the chapter 5 of [Duffy, 2001]) to the numerical (Fig. 5.20) one provided by MLPG4/LBIE.

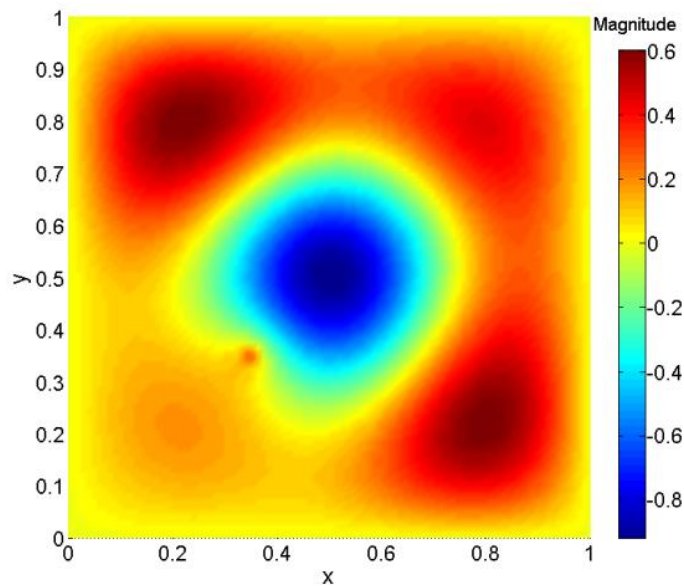


Fig.5.19. Analytical solution to Green's problem (5.127). The whole domain Ω is shown.

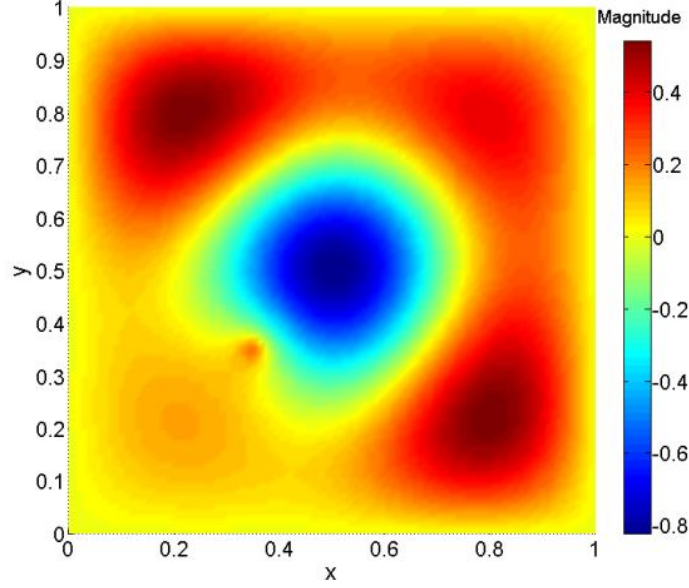


Fig.5.20. MLPG4/LBIE numerical solution to Green's problem (5.127). The whole domain Ω is shown.

The second problem addresses the TM^z scattering of a plane wave by a dielectric circular cylinder. The incident field is $E_z^i = e^{-jk_0 x}$, and the frequency is 1 GHz. The scatterer is modeled by circle S (boundary ∂S) of a given radius, within which the relative electric permittivity has a given value. In order to deal with scattered fields, a first order Bayliss-Turkel radiation boundary condition (RBC) [Jin, 1993] is imposed at a circumference placed away from the scatterer. As explained earlier, there is an air (or free space) layer between the scatterer surface ∂S and the circumference where the RBC conditions are imposed, i.e., the global boundary $\partial\Omega$ ($\partial\Omega$ and ∂S are concentric circumferences).

Because we employ a first order RBC, the radius of $\partial\Omega$ was chosen three times larger than the radius of the scatterer. According to (5.13), the function $p(\vec{x}) = \mu_r(\vec{x}) = 1$ everywhere, whereas $q(\vec{x}) = \varepsilon_r = 1$ between $\partial\Omega$ and ∂S , and $q(\vec{x}) = \varepsilon_r$ within ∂S . Besides that, the excitation term $f(\vec{x})$ (i.e., the current J_z) is zero everywhere. The first order RBC employed is [Jin, 1993]:

$$\frac{\partial E_z^s}{\partial n} + \left(jk_0 + \frac{1}{2\rho_b} \right) E_z^s = 0 \quad (5.128)$$

where E_z^s is the scattered field and ρ_b is the radius of $\partial\Omega$. As we are interested in the total field E_z , we substitute $E_z = E_z^i + E_z^s$ in (5.128) and thus find a boundary condition for E_z :

$$\frac{\partial E_z}{\partial n} + \left(jk_0 + \frac{1}{2\rho_b} \right) E_z = \frac{\partial E_z^i}{\partial n} + \left(jk_0 + \frac{1}{2\rho_b} \right) E_z^i \quad (5.129)$$

A comparison with (5.122) then reveals that $a(\vec{x}) = jk_0 + 1/2\rho_b$, $b(\vec{x}) = 1$, and $g(\vec{x}) = \partial E_z^i / \partial n + (jk_0 + 1/2\rho_b) E_z^i$, which is a known expression, since the incident field E_z^i is given. We performed two simulations, in each one of which we compared the numerical results regarding the modulus and the phase of the electric field to the analytical solutions [Balanis, 1989]. In simulation 1, the scatterer's radius is $\lambda_0/2\pi$ and its relative permittivity is $\varepsilon_r = 1 - j4$; the total number of nodes spread across the computational domain is 189. In simulation 2, the scatterer's radius is $0.8\lambda_0/\pi$ and its relative permittivity is $\varepsilon_r = 2.75$, whereas the total

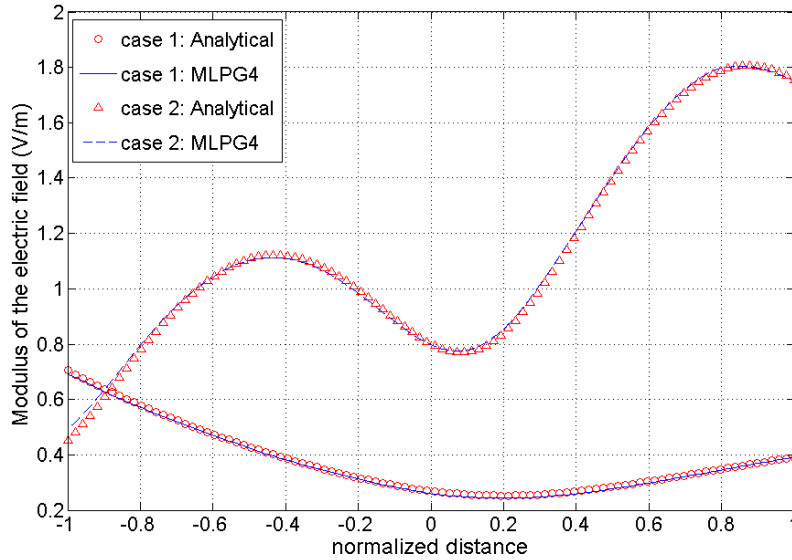


Fig.5.21. The electric field phasor (modulus). The abscissa x is measured along a horizontal line passing through the center of the cylinder. This value is then normalized to the cylinder radius a (i.e., normalized distance = x/a).

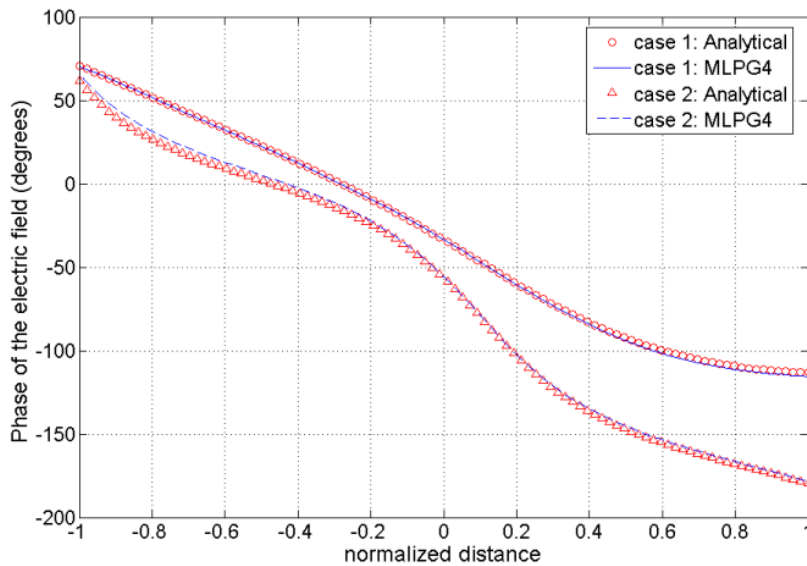


Fig.5.22. The electric field phasor (phase). The abscissa x is measured along a horizontal line passing through the center of the cylinder. This value is then normalized to the cylinder radius a (i.e., normalized distance = x/a).

number of nodes is 626. These simulations show good concordance when compared to the analytical solutions, as shown in Figures 5.21 and 5.22, which plot the solutions along a horizontal line passing through the center of the cylinder.

The third problem deals with the flow of light down a photonic crystal. A two-dimensional photonic bandgap crystal is a periodic array of dielectric structures, the most remarkable property of which is that it is able to select what wavelengths can actually propagate through it. This phenomenon can be verified if one sketches the crystal's dispersion curve, where it is seen that certain wavelengths inside an interval cannot propagate (there are no modes supporting these wavelengths). The 'forbidden' wavelengths form a bandgap, i.e., every incoming wave whose wavelength falls inside the bandgap is unable to propagate through the crystal. There is a

wide range of applications concerning these photonic bandgap crystals; details about the theory underlying them can be found in [Joannopoulos *et al.*, 2008] and [Skorobogaty and Yang, 2009].

Let it be a periodic array of dielectric circular rods, whose relative electric permittivity is $\varepsilon_r = 9$. The relative permittivity of the medium surrounding these rods is 1. Each of these rods has a radius r , here normalized to 1. Besides that, the distance between a rod and its neighbor is also r . (It should be kept in mind that this structure is three-dimensional; it is a collection of cylindrical dielectric rods placed side by side, forming a kind of ‘forest’ immersed in a medium where $\varepsilon_r = 1$. Because no magnitude depends upon z , we are concerned here only with the cross section of this structure.) Simulations show that a wave whose wavenumber k_0 is 1 ($k_0 = 2\pi/\lambda_0$) falls within a bandgap, and then is unable to propagate along this structure [Tsukerman, 2005]. Now, given a photonic crystal and an incoming wave unable to propagate through it, *if some rods are removed from the structure*, forming a path, then this incoming wave will be able to propagate only within the ‘carved’ path. Thus the incoming wave (usually light) can be guided along a path through the crystal.

The photonic crystal studied in this work has also been analyzed in [Tsukerman, 2005], which employed FEM and another technique (FLAME) in order to get the numerical results. Given a periodic structure, we removed some rods, forming a L-shaped path as it can be seen in Fig. 5.23, which shows the whole computational domain Ω .

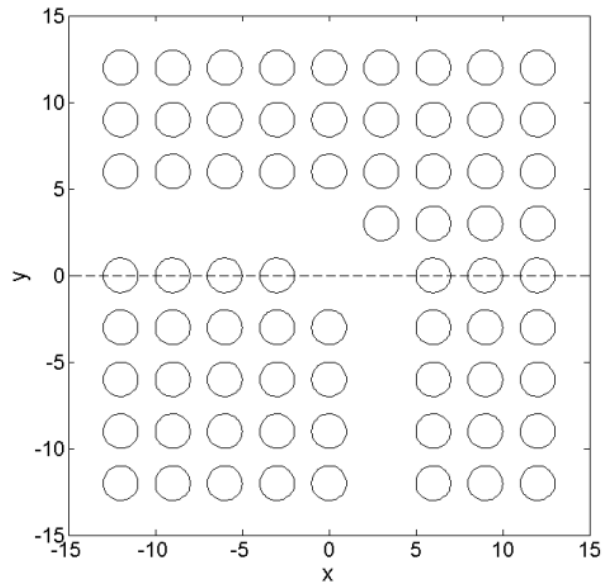


Fig.5.23. The photonic crystal, with some removed rods, forming an L-shaped path.

We have studied what happens to an incident TM^z plane wave $E_z^i = e^{-jk_0x}$, where $k_0 = 1$, as it impinges upon this structure. The differential equation to be solved is (5.111), where $p(\vec{x}) = \mu_r = 1$ everywhere, and $q(\vec{x}) = \varepsilon_r = 1$ outside the rods and $q(\vec{x}) = \varepsilon_r = 9$ inside each rod. There is no current density (excitation term f). According to [Tsukerman, 2005] and [Tsukerman, 2008], for bandgap operation and in order to eliminate errors due to imperfect absorbing boundary conditions, Dirichlet conditions corresponding to the incident field have been imposed on the whole global boundary (i.e., $E_z(x, y) = E_z^i(x, y) = e^{-jk_0x}$ on $\partial\Omega$). Figure 5.24 shows the real part of the electric field along the dashed line in Fig. 5.23. The concordance between the results provided by LBIE/MLPG4 and FEM is excellent. However, according to

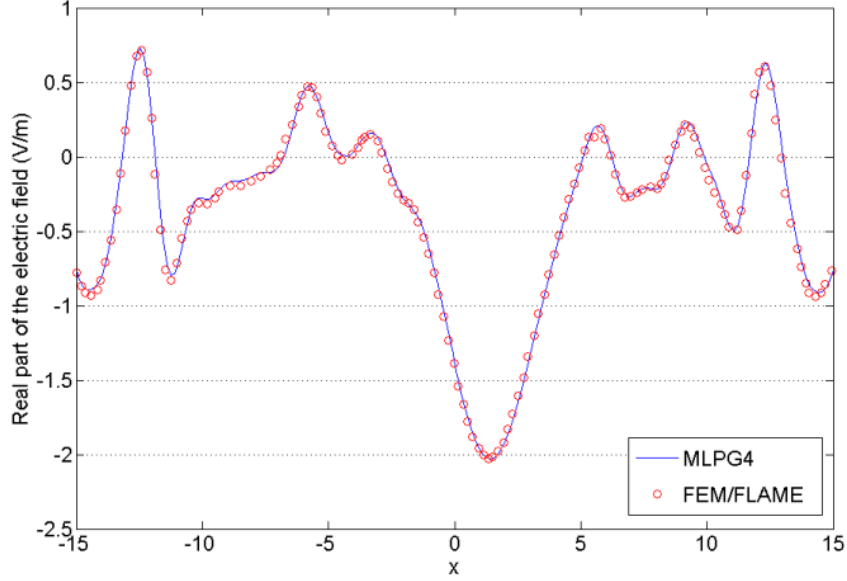


Fig.5.24. The real part of the electric field along the line $y = 0$, ($-15 \leq x \leq 15$).

[Tsukerman, 2005], while FEM uses more than 100 000 degrees of freedom (DoF) to attain this result (in addition to the task of setting up a mesh), our meshless method uses 2700 DoF (1 DoF per node).

Figures 5.25 and 5.26 show the real and imaginary parts of the electric field across the whole computational domain, where the bending of the flow of light can be clearly observed. The incoming wave whose wavenumber $k_0 = 1$ enters the crystal through the ‘carved’ path formed by the removed rods. Once there, the only way available for this wave is to follow this path until the end, as it cannot ‘leak’ into the bulk of the crystal, because in this region there are no conditions for propagation (the wavenumber $k_0 = 1$ falls within a bandgap). Thus the photonic crystal herein described is able to bend the flow of light in 90° , in a completely lossless way (the dielectric rods do not absorb radiation, since they are lossless). There is a great concordance between Fig.5.26 and the figure 17 of [Tsukerman, 2005], both depicting the imaginary part of E_z throughout the computational domain.

Through this example the MLPG4/LBIE has proven to be an efficient method. This problem actually deals with the scattering of a plane wave by dozen of objects. If the integral approach from chapter 3 had been employed here, we would have to find equivalent currents flowing at the boundary of each scatterer in Fig. 5.23. Needless to say that the amount of required work would be formidable.

5.5.1 Interface conditions and the TE^z polarization

Care must be taken when dealing with problems in which some material property [described by the function $p(\vec{x})$ in (5.111)] is discontinuous across an interface. This is so because the shape functions are smooth (i.e., the functions themselves and their derivatives are continuous). Shape functions inherit the order of continuity from the window function w (in this

work, a $C^4(\Theta)$ function, Θ being the nodal influence domain). In electromagnetic wave scattering analysis,

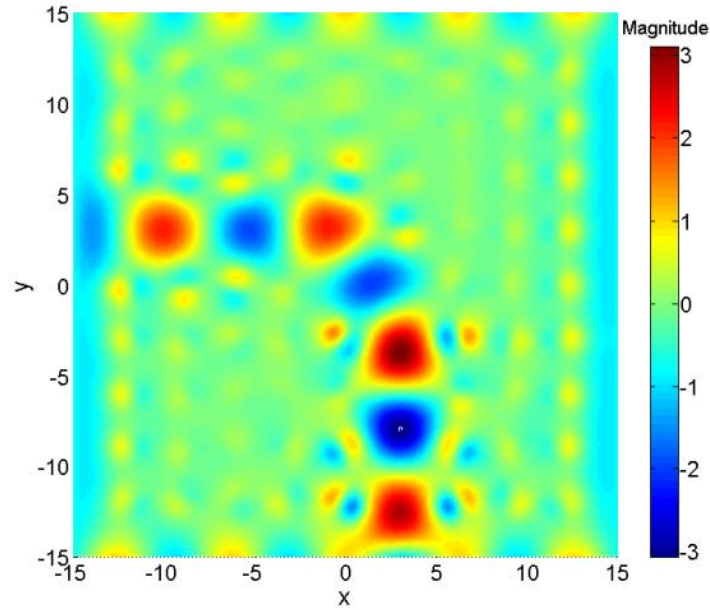


Fig.5.25. The MLPG4 numerical result for the electric field across the whole computational domain Ω : The real part.

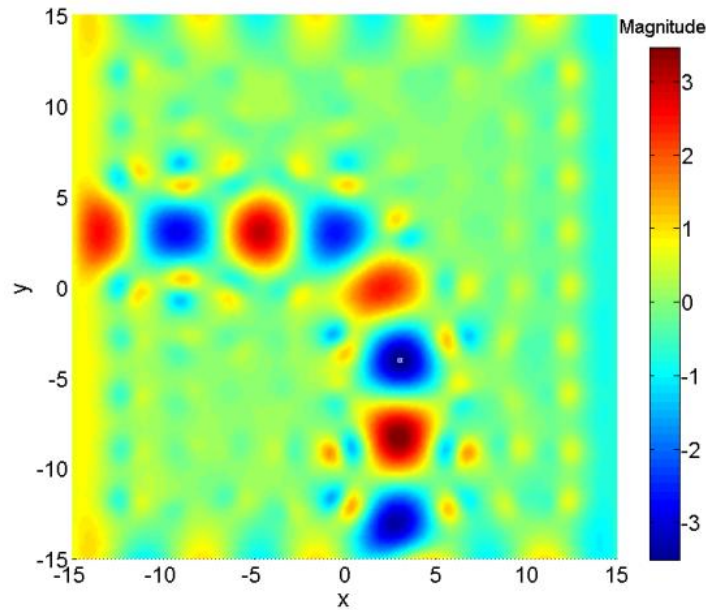


Fig.5.26. The MLPG4 numerical result for the electric field across the whole computational domain Ω : The imaginary part. It can be verified from the last two figures (this one and Fig.5.25) that the light propagates only within the path formed by the removed rods.

when the unknown function u is the electric field E_z (TM^z polarization) and when there are no magnetic materials inside the domain Ω ($p(\vec{x}) = \mu_r(\vec{x}) = 1$ everywhere), one knows that E_z must be continuous across the interface between two dielectric media ($q(\vec{x}) = \epsilon_r^-$ at one side and $q(\vec{x}) = \epsilon_r^+$ at the other side). This poses no problem when expressing the electric field as an expansion like (5.116) (u replaced by E_z), because the shape functions are known to be smooth and thus able to reproduce the continuity of E^z . But there is a small issue when it comes to TE^z

polarization: the magnetic field H_z experiences a discontinuity in its normal derivative across the interface between two dielectric media:

$$\frac{1}{\varepsilon_r^-} \frac{\partial H_z^-}{\partial n} = \frac{1}{\varepsilon_r^+} \frac{\partial H_z^+}{\partial n} \quad (5.130)$$

where H_z^- is the magnetic field at one side of the interface and H_z^+ is the field at the other side. The function $p(\vec{x}) = \varepsilon_r(\vec{x})$ (in (5.111), where u now represents H_z , as in (5.20)) is discontinuous across an interface, and there is not a direct way of inserting (5.130) at the governing equation (5.20). If one tries to solve (5.111) without giving this issue its due attention, only an approximate solution for H_z will be attained (i.e., smoother than the real one), since the shape functions used to represent the magnetic field are smooth, and thus unable to reproduce a discontinuity such as (5.130) by themselves. In order to deal with this issue concerning material discontinuities in TE^z polarization, we employ a technique described in [Li *et al.*, 2003].

Let us assume that the problem in question is characterized by a relative permittivity ε_r which is piecewise homogeneous: each sub-region i has a relative permittivity ε_{r_i} . In Fig. 5.27, there are two such sub-regions, each one with its value for the relative permittivity, separated by an interface τ .

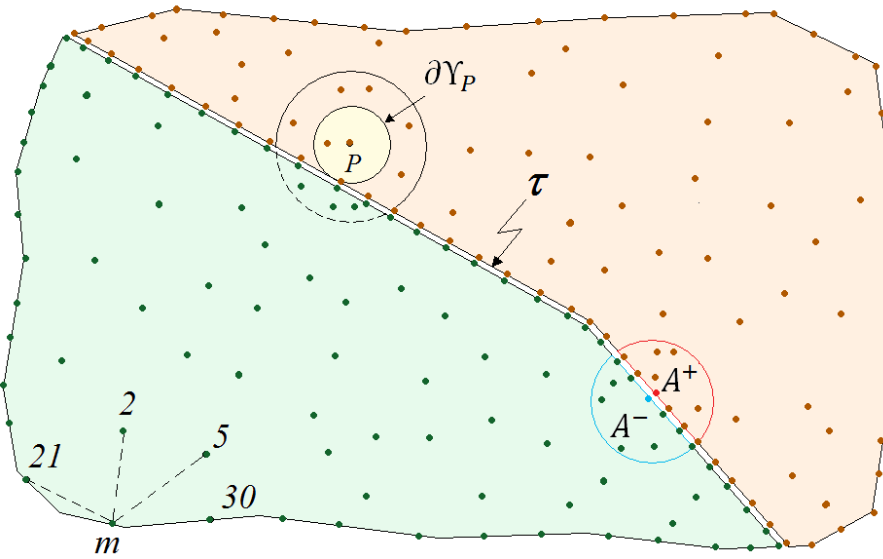


Fig.5.27. A computational domain wherein there is a material discontinuity at the interface τ , which divides Ω in two regions: R_1 (green) and R_2 (orange). A double layer of nodes is placed along τ . A^- and A^+ are dual nodes. The boundary ∂Y_P of test domain associated to node P just touches the interface τ . The nodes inside its influence domain and located at the other side of τ (inside the dashed portion of the larger circumference centered at P) are not influenced by P .

Nodes from one region do not influence the other, even if their influence domains extend over there (in Fig. 5.27, node P lies in region 2; so, nodes from region 1 lying inside the dashed curve are not influenced by this node, even if they are located theoretically within the influence domain of P). Moreover, the test domains assigned to interior nodes from one region just touches the interface τ (interior circle associated to node P). Now, in addition to interior nodes and to boundary nodes, this situation demands a new kind of node: an *interface node*. Along the interface τ a double layer of nodes is placed, i.e., nodes lying at the interface are doubled: each

interface node is actually considered equivalent to two nodes, one belonging to region 1 and the other to region 2. *Each interface node has its dual; they are placed at exactly the same location, but are two distinct entities, to each one being assigned a nodal parameter and thus a row in the global stiffness matrix* (Fig. 5.27, nodes A^- and A^+). A restriction is then imposed: node A^- influences (and is influenced by) only nodes from region 1; and node A^+ influences (and is influenced by) only nodes from region 2. No test domains are assigned to interface nodes at all: a meshless collocation scheme, like the one described earlier, is enforced at each dual interface node, one dealing with interface conditions on the function itself (H_z) and the other with conditions on the normal derivative ($\partial H_z / \partial n$).

After we spread N^d (where the ‘d’ stands for discontinuity) nodes along the interface τ (which actually gives rise to $2N^d$ unknowns, since the nodes at τ are doubled) we must apply a collocation method (related to TE^z interface conditions) to each one of the “double nodes”.

For each interface double node i lying at \vec{x}_i , we have

$$\forall i \leq N^d \quad H_z^- = H_z(\vec{x}_i^-) = H_z(\vec{x}_i^+) = H_z^+ \quad (5.131)$$

$$\forall i \leq N^d \quad \frac{1}{\varepsilon_r^-} \frac{\partial H_z^-}{\partial n} = \frac{1}{\varepsilon_r^-} \frac{\partial H_z(\vec{x}_i^-)}{\partial n} = \frac{1}{\varepsilon_r^+} \frac{\partial H_z(\vec{x}_i^+)}{\partial n} = \frac{1}{\varepsilon_r^+} \frac{\partial H_z^+}{\partial n} \quad (5.132)$$

The nodes influencing \vec{x}_i^- are actually those ones that influence location \vec{x}_i and lie in region 1 (R_1), i.e., they are the nodes whose indices are elements of the set

$$S_1 = \{j \in I \mid j \in \text{Neigh}(\vec{x}_i) \text{ and } \vec{x}_j \in R_1\} \quad (5.133)$$

where $\vec{x}_j \in R_1$ actually means that $\varepsilon_r(\vec{x}_j) = \varepsilon_1$ (relative permittivity of the material constituting region 1). Analogously,

$$S_2 = \{k \in I \mid k \in \text{Neigh}(\vec{x}_i) \text{ and } \vec{x}_k \in R_2\} \quad (5.134)$$

In (5.133) and (5.134), the set I is given by (5.23).

Expression (5.131) therefore means

$$\forall i \leq N^d \quad \sum_{j \in S_1} \phi_j(\vec{x}_i) \hat{u}_j = \sum_{k \in S_2} \phi_k(\vec{x}_i) \hat{u}_k \quad (5.135)$$

whereas (5.132) means

$$\forall i \leq N^d \quad \frac{1}{\varepsilon_r^-} \sum_{j \in S_1} \frac{\partial \phi_j(\vec{x}_i)}{\partial n} \hat{u}_j = \frac{1}{\varepsilon_r^+} \sum_{k \in S_2} \frac{\partial \phi_k(\vec{x}_i)}{\partial n} \hat{u}_k \quad (5.136)$$

The index j runs through all nodes from region 1 whose influence domains include point \vec{x}_i (in Fig.5.27, they are depicted inside the semicircle surrounding \vec{x}_i), and k through all nodes from region 2 whose influence domains include point \vec{x}_i (nodes inside the semicircle surrounding \vec{x}_i). So, through the collocation scheme, that small issue concerning interface conditions in TE^z polarization has been solved. To each double node lying on the interface τ , we get two linearly independent equations (in the nodal parameters \hat{u}), provided by (5.135) and (5.136). Numerical

integrations do not need to be used at all: Simple nodal equations such as (5.135) and (5.136) are able to impose the discontinuity condition expressed by (5.130).

The fourth problem studied is similar to the second, but takes the TE^z polarization into account. The incident magnetic field is $H_z^i = e^{-jk_0x}$, and the frequency is also 1 GHz. As far as

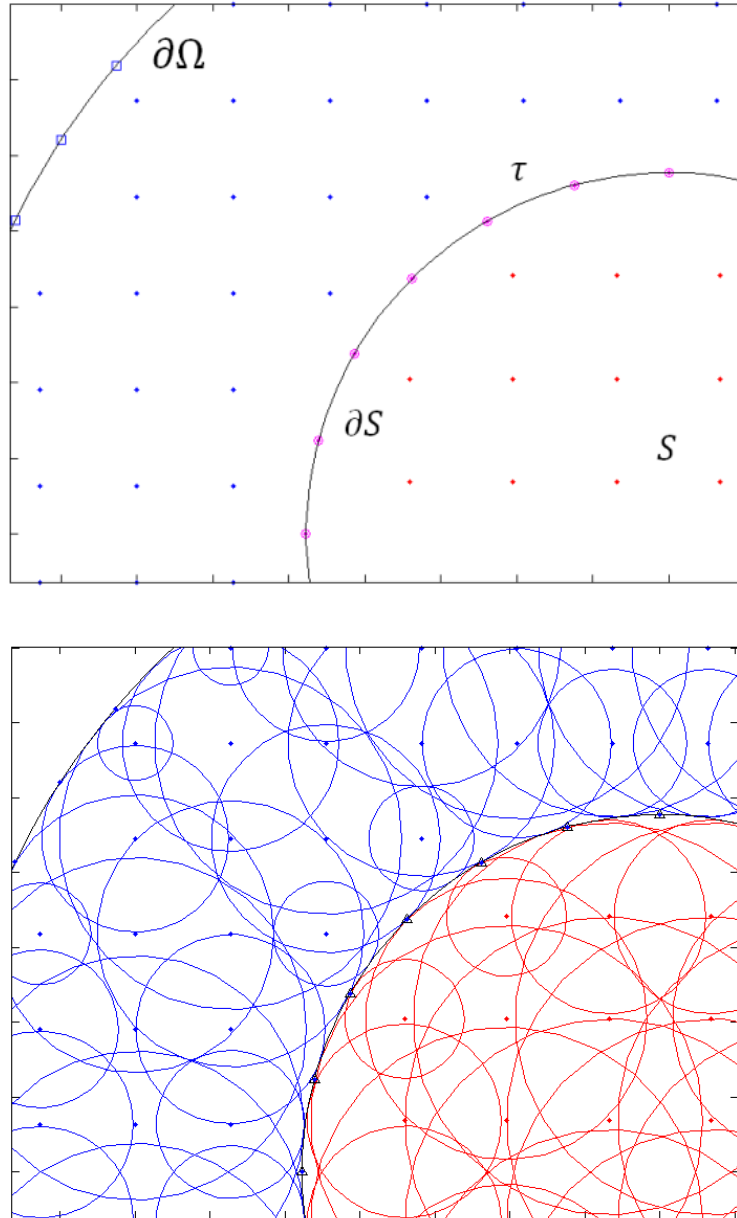


Fig.5.28. A portion of the computational domain. *First figure:* The global boundary $\partial\Omega$, the scatterer S , and the scatterer's boundary ∂S , which coincides with the air-dielectric interface τ . Some interior nodes, boundary nodes (three little squares at $\partial\Omega$) and also the double layer of interface nodes (small points at τ) are shown. *Second figure:* A profusion of test domains covering the computational domain. The problem is broken up into two sub-regions: one between $\partial\Omega$ and ∂S , and the other within the scatterer S . Only the interior nodes of both sub-regions are assigned test domains, which can be seen just touching the interface τ or the global boundary $\partial\Omega$ (if this is the case).

boundary conditions are concerned, the same treatment dispensed to TM^z polarization is employed here; (5.129) is still valid, but the electric field is substituted by the magnetic field, i.e., E_z has been substituted by H_z and E_z^i by H_z^i . The difference between the two polarizations lies in the fact that there is a discontinuity in the normal derivative of H_z , as explained earlier.

This issue is solved through a subdivision of the computational domain, wherein the nodes from one sub-region do not influence the nodes from the other, and through a double layer of nodes placed along the interface between these sub-regions. In this problem, one sub-region is the air layer between $\partial\Omega$ and ∂S , where [according to (5.111)] $p(\vec{x}) = \varepsilon_r(\vec{x}) = 1$, whereas the other sub-region is the interior of the scatterer (circular region S), where $p(\vec{x}) = \varepsilon_r$. The function $q(\vec{x}) = \mu_r(\vec{x}) = 1$ everywhere (as there are no magnetic materials). Figure 5.28 illustrates the test domains from both regions; it is clearly seen that nodes from one side of ∂S do not extend their test domains to the other side.

We performed two simulations: in simulation 1, the scatterer's radius is $\lambda_0/2\pi$ and its relative permittivity is $\varepsilon_r = 4$; the total number of nodes spread throughout the computational domain amounts to 494. In simulation 2, the scatterer's radius is $5\lambda_0/8\pi$ and its relative permittivity is $\varepsilon_r = 0.25 - j1.75$, whereas the total number of nodes is 759. The concordance between numerical and analytical solutions is again very good, as Figures 5.29 and 5.30 indicate. These simulations show that the meshless collocation procedure proved to be quite handy in treating the interface conditions.

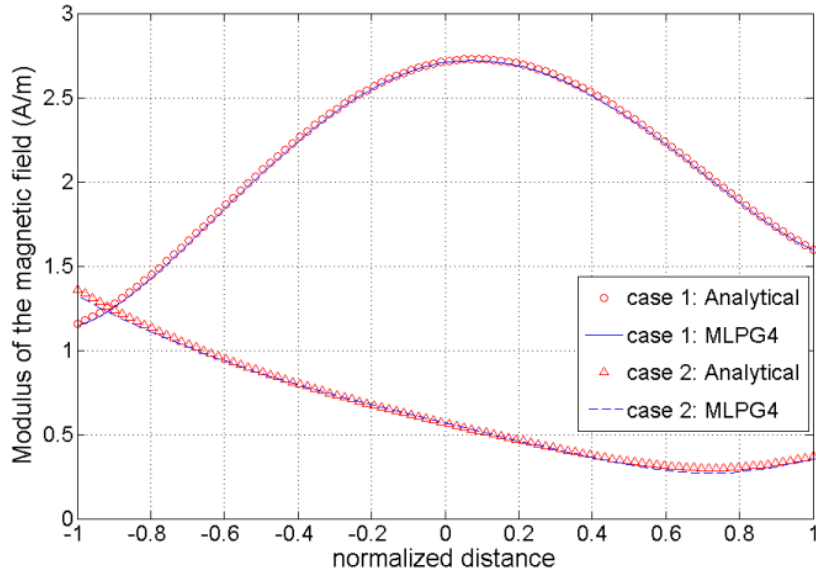


Fig.5.29. The magnetic Field phasor (modulus). The abscissa x is measured along a horizontal line passing through the center of the cylinder. This value is then normalized to the cylinder radius a (i.e., normalized distance = x/a).

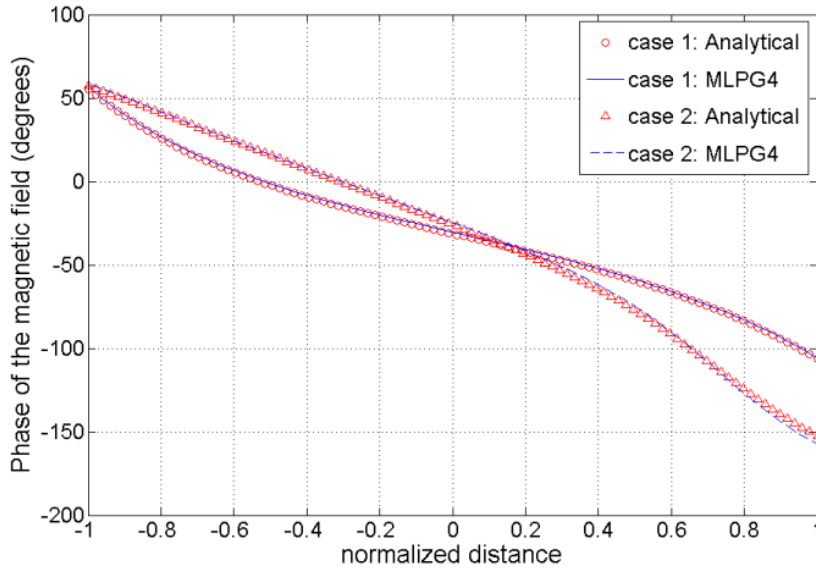


Fig.5.30. The magnetic Field phasor (phase). The abscissa x is measured along a horizontal line passing through the center of the cylinder. This value is then normalized to the cylinder radius a (i.e., normalized distance = x/a).

Concluding Remarks

This chapter illustrated the whole procedure one has to go through in order to solve a differential equation employing the MLPG method. Although the examples are concerned to electromagnetic wave scattering, the same approach can be extended to differential equations modeling other kinds of phenomena. Our table describing the overall process thus can be completed:

THE MESHLESS PROCEDURE IN A NUTSHELL

Given a differential equation and a domain where it shall be solved:

First Step	Set up the domain Ω and its boundary $\partial\Omega$.
Second Step	Spread N nodes throughout the domain Ω and at its boundary $\partial\Omega$ as well.
Third Step	<ul style="list-style-type: none"> • To each node i, define the radius of its influence domain Λ_i; • Make sure the influence domains cover the computational domain entirely.
Fourth Step	Numerical construction of the shape functions.
Fifth Step	<ul style="list-style-type: none"> • For each node i, define the test domains Y_i (radius s_i); • Define the test functions accordingly.
Sixth Step	Choose the way boundary conditions shall be dealt with: either through intersecting domains or through the collocation scheme.
Seventh Step	State the weak forms (Green's second identity or weighted residual method).
Eighth Step	<ul style="list-style-type: none"> • Numerical integration of the weak forms; • Assembling of the final linear system.
Ninth Step	Solution of the final linear system and determination of the nodal parameters $\hat{\mathbf{u}}$.

Chapter 6

The MLPG Method and other Applications: Three-Dimensional Electrostatics and Photonic Bandgap Crystals

THIS short chapter deals with other applications of MLPG relevant to Electrical Engineering that have not been included in the last chapter (which focused exclusively on scattering). We explore two different areas: 3D Electrostatics and photonic crystals. The reason behind such a choice is given by the fact that both aforementioned areas provide problems mathematically distinct from what was discussed in the last chapter.

In what concerns Electrostatics, we deal with Poisson's equation stated in three-dimensional domains $\bar{\Omega}$. The main difference is that the test domains are now spheres instead of circles. The true efficacy of imposing boundary conditions through the collocation method is verified, as the issue of finding intersections between three-dimensional domains would render the implementation of MLPG ridiculously difficult.

The photonic crystals actually comprise too large an area of study, and we therefore highlight here only the most basic problem of finding their band structure. The true interest is in the application of MLPG to eigenvalue problems arising from the analysis of which frequencies can propagate through a given crystal.

As the main concepts associated with shape functions and the whole structure of MLPG have been laid down in earlier chapters, we now take a more direct approach to the subject, without delving too much on details.

6.1 Electrostatics

We are interested in the solutions to Poisson's equation

$$\nabla \cdot (\varepsilon(\vec{x})\nabla u(\vec{x})) = -\rho(\vec{x}) \quad (6.1)$$

where the function u represents the *electrostatic scalar potential* (volts), ε is the electric permittivity (farads/meter) and ρ is the electric charge density (coulombs/cubic meter). Equation (6.1) is stated in a three-dimensional domain Ω and the quantities ε and ρ are both allowed to vary with position $\vec{x} = (x, y, z)$.

After spreading nodes and defining the influence and test domains, we proceed to find the weak form for (6.1). As the boundary conditions are dealt with by the collocation scheme, all test domains are those associated to interior nodes and therefore are simple spheres (according to Section 5.5). So if N nodes have been spread throughout the computational domain, and N^i of which are located in the interior of $\bar{\Omega}$, the weighted residual method gives us

$$\forall i \leq N^i \quad \iiint_{Y_i} (\varepsilon \nabla u) v_i dV = - \iiint_{Y_i} \rho v_i dV \quad (6.2)$$

If we take the vector identity

$$\nabla \cdot (f \vec{A}) = \nabla f \cdot \vec{A} + f \nabla \cdot \vec{A} \quad (6.3)$$

where f is a scalar-valued and \vec{A} a vector-valued function, and associate f with the test function v_i and \vec{A} with $\varepsilon \nabla u$, we get

$$\forall i \leq N^i \quad \iiint_{Y_i} \nabla \cdot (v_i \varepsilon \nabla u) dV - \iiint_{Y_i} \varepsilon \nabla v_i \cdot \nabla u dV = - \iiint_{Y_i} \rho v_i dV \quad (6.4)$$

From the Divergence Theorem

$$\iiint_R \nabla \cdot \vec{F} dV = \oiint_{\partial R} \vec{F} \cdot \hat{\mathbf{n}} dS \quad (6.5)$$

where \vec{F} is a vector-valued function and $\hat{\mathbf{n}}$ is the outward unit normal to the closed three-dimensional surface ∂R , the first volume integral is rewritten as

$$\forall i \leq N^i \quad \oiint_{\partial Y_i} v_i \varepsilon \nabla u \cdot \hat{\mathbf{n}} dS - \iiint_{Y_i} \varepsilon \nabla v_i \cdot \nabla u dV = - \iiint_{Y_i} \rho v_i dV \quad (6.6)$$

However, the test function v_i is zero at any point located in the boundary of the test domain Y_i . Therefore, we get the weak form (for each interior node i):

$$\forall i \leq N^i \quad \iiint_{Y_i} \varepsilon \nabla v_i \cdot \nabla u dV = \iiint_{Y_i} \rho v_i dV \quad (6.7)$$

Expressing the electrostatic potential u as a sum of shape functions:

$$\forall \vec{x} \in \bar{\Omega} \quad u(\vec{x}) = \sum_{k \in \text{Neigh}(\vec{x})} \phi_k(\vec{x}) \hat{u}_k \quad (6.8)$$

or (according to a new numbering scheme, as explained earlier in Section 3.1):

$$\forall \vec{x} \in \bar{\Omega} \quad u(\vec{x}) = \sum_{j=1}^n \phi_j(\vec{x}) \hat{u}_j \quad (6.9)$$

Substituting (6.9) in (6.7)

$$\forall i \leq N^i \quad \sum_{j=1}^n \left(\iiint_{Y_i} \varepsilon \nabla v_i \cdot \nabla \phi_j dV \right) \hat{u}_j = \iiint_{Y_i} \rho v_i dV \quad (6.10)$$

The form of the (still incomplete) linear system is retrieved from (6.10) as $\mathbf{K}^i \hat{\mathbf{u}} = \mathbf{h}^i$, where

$$K_{ij}^i = \iiint_{Y_i} \varepsilon \nabla v_i \cdot \nabla \phi_j dV \quad (6.11)$$

and

$$h_i^i = \iiint_{Y_i} \rho v_i dV \quad (6.12)$$

If the medium is homogeneous (ε is constant throughout the computational domain), we write (6.1) as

$$\nabla^2 u(\vec{x}) = -\frac{\rho(\vec{x})}{\varepsilon} \quad (6.13)$$

This is also the case if ε is piecewise constant, i.e., the computational domain $\bar{\Omega}$ is divided in regions R_i each one of the which is characterized by a constant permittivity ε_i . Therefore, we can employ Green's second identity for scalar fields

$$\iiint_R (u \nabla^2 v - v \nabla^2 u) dV = \iint_{\partial R} \left(u \frac{\partial v}{\partial n} - v \frac{\partial u}{\partial n} \right) dS \quad (6.14)$$

in order to get the weak forms. By associating u with the electrostatic potential and v with the test function v_i we get

$$\forall i \leq N^i \quad \iiint_{Y_i} u(-\delta(\vec{x} - \vec{x}_i)) dV - \iiint_{Y_i} v_i \left(-\frac{\rho}{\varepsilon} \right) dV = \iint_{\partial Y_i} u \frac{\partial v_i}{\partial n} dS - \iint_{\partial Y_i} v_i \frac{\partial u}{\partial n} \quad (6.15)$$

where we used $\nabla^2 v_i = -\delta(\vec{x} - \vec{x}_i)$ (from the definition of v_i) and $\nabla^2 v_i = -\rho/\varepsilon$ [from (6.13)]. The last surface integral in (6.15) is zero, because it depends on v_i evaluated on the surface ∂Y_i , which by definition is zero. The weak form then reads

$$\forall i \leq N^i \quad u(\vec{x}_i) + \iint_{\partial Y_i} u \frac{\partial v_i}{\partial n} dS = \iiint_{Y_i} v_i \frac{\rho}{\varepsilon} dV \quad (6.16)$$

The linear system based on the weak form above is described by [after the same reasoning described in (6.11) and (6.12)]

$$K_{ij}^i = \phi_j(\vec{x}_i) + \iint_{\partial Y_i} \phi_j \frac{\partial v_i}{\partial n} dS \quad (6.17)$$

$$h_i^i = \iiint_{Y_i} v_i \frac{\rho}{\varepsilon} dV \quad (6.18)$$

When the incomplete $N^i \times N$ linear system [(6.11) - (6.12) or (6.17) - (6.18)] is formed, we now turn to the boundary conditions. We must apply the collocation scheme to each one of the N^b nodes spread throughout $\partial\Omega$. If a node m lies in a portion of $\partial\Omega$ where a Dirichlet condition $u = \bar{u}$ is to be imposed, we have

$$\sum_{k \in \text{Neigh}(\vec{x}_m)} \phi_k(\vec{x}_m) \hat{u}_k = \bar{u}(\vec{x}_m) \quad (6.19)$$

Otherwise, if a Neumann condition \bar{h} is imposed:

$$\sum_{k \in \text{Neigh}(\vec{x}_m)} \frac{\partial \phi_k}{\partial n}(\vec{x}_m) \hat{u}_k = \sum_{k \in \text{Neigh}(\vec{x}_m)} \nabla \phi_k(\vec{x}_m) \cdot \hat{n} \hat{u}_k = \bar{h}(\vec{x}_m) \quad (6.20)$$

Figure 1 illustrates this. Had the node $m = 40$ been located in a part of $\partial\Omega$ where a Dirichlet condition is imposed, then, from $\text{Neigh}(\vec{x}_{40}) = \{20, 25, 30, 39, 40, 41\}$ we have a linear equation on the nodal parameters

$$\begin{aligned} \phi_{20}(\vec{x}_{40}) \hat{u}_{20} + \phi_{25}(\vec{x}_{40}) \hat{u}_{25} + \phi_{30}(\vec{x}_{40}) \hat{u}_{30} + \phi_{39}(\vec{x}_{40}) \hat{u}_{39} + \phi_{40}(\vec{x}_{40}) \hat{u}_{40} + \phi_{41}(\vec{x}_{40}) \hat{u}_{41} \\ = \bar{u}(\vec{x}_{40}) \end{aligned} \quad (6.21)$$

In the case a Neumann condition is imposed

$$\begin{aligned} \frac{\partial \phi_{20}}{\partial n}(\vec{x}_{40}) \hat{u}_{20} + \frac{\partial \phi_{25}}{\partial n}(\vec{x}_{40}) \hat{u}_{25} + \frac{\partial \phi_{30}}{\partial n}(\vec{x}_{40}) \hat{u}_{30} + \frac{\partial \phi_{39}}{\partial n}(\vec{x}_{40}) \hat{u}_{39} + \frac{\partial \phi_{40}}{\partial n}(\vec{x}_{40}) \hat{u}_{40} \\ + \frac{\partial \phi_{41}}{\partial n}(\vec{x}_{40}) \hat{u}_{41} = \bar{h}(\vec{x}_{40}) \end{aligned} \quad (6.22)$$

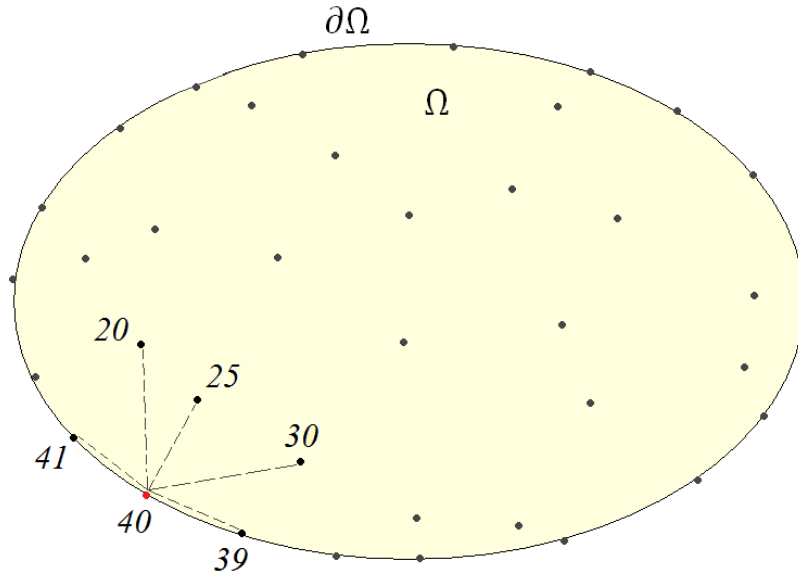


Fig.6.1. Node 40 located on $\partial\Omega$ is influenced by a set of other nodes.

Observation: As the MLS shape functions do not satisfy Kronecker's delta property, the row in the global matrix \mathbf{K} that equation (6.21) gives rise to contains values different from zero at elements outside the main diagonal (for example, because $\phi_{20}(\vec{x}_{40})$ is different from zero, so is $K_{40,20}$). Had RPIM-PR been used, then (6.21) would be substituted by a single term: $\hat{u}_{40} = \bar{u}(\vec{x}_{40})$ (because these shape functions interpolate the solution).

So from the N^b boundary nodes we get N^b linear equations like (6.21) (Dirichlet) or (6.22) (Neumann), which are assembled in a $N^b \times N$ matrix

$$\mathbf{K}^b \hat{\mathbf{u}} = \mathbf{h}^b \quad (6.23)$$

Equations (6.11) and (6.23) are finally assembled into the final $N \times N$ linear system:

$$\begin{bmatrix} \mathbf{K}^i \\ \mathbf{K}^b \end{bmatrix} \hat{\mathbf{u}} = \begin{bmatrix} \mathbf{h}^i \\ \mathbf{h}^b \end{bmatrix} \quad (6.24)$$

From (6.24), one retrieves the nodal parameters $\hat{\mathbf{u}}$. The solution is then expressed for every \vec{x} in $\partial\Omega$ through (6.8).

The first problem analyzed is that of a homogeneous dielectric sphere ($\varepsilon_r = 1$) with unit radius ($a = 1$) and no charge density inside ($\rho = 0$, which reduces to solving Laplace's equation), subject to the Dirichlet condition $\bar{u} = 3\cos^2\theta + 3\cos\theta + 1$ V on $\partial\Omega$. Figure 6.2 shows the potential along a path C defined in spherical coordinates as $r = 0.5$ m; $0 \leq \theta \leq 180^\circ$; $\varphi = 0$. The analytical solution is

$$u(\vec{x}) = u(r, \theta) = 2 \left(\frac{r}{a}\right)^2 P_2(\cos\theta) + 3 \left(\frac{r}{a}\right) P_1(\cos\theta) + 2P_0(\cos\theta) \quad (6.25)$$

where P_0, P_1 and P_2 are the Legendre polynomials.

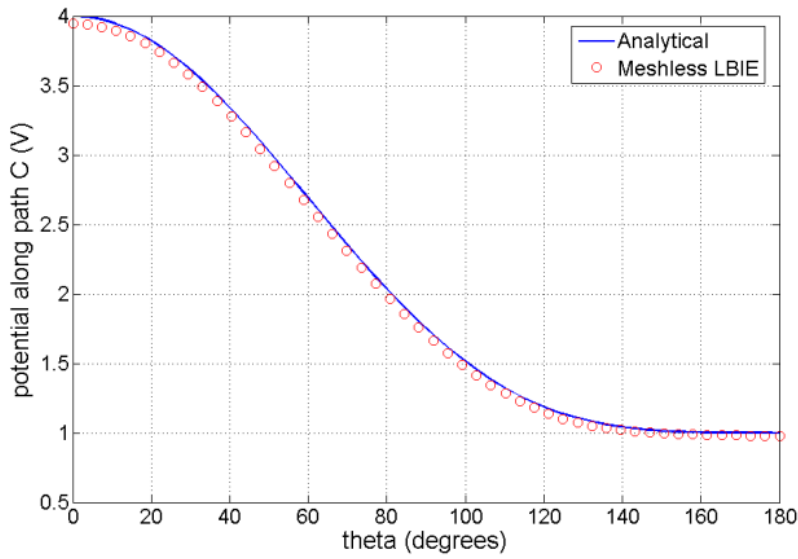


Fig.6.2. Solution to Laplace's equation stated in a spherical domain.

The second problem investigated takes a non-homogeneous unit cube ($x \in [0,1], y \in [0,1]$ and $z \in [0,1]$), whose relative permittivity is 1.5 in the inferior half and 15 in the superior half (Figure 6.3). A charge density ρ is present in the inferior half ($\rho/\varepsilon_1 = -6$ V/m²) and a surface charge density $\sigma_s = 3$ C/m² at the interface.

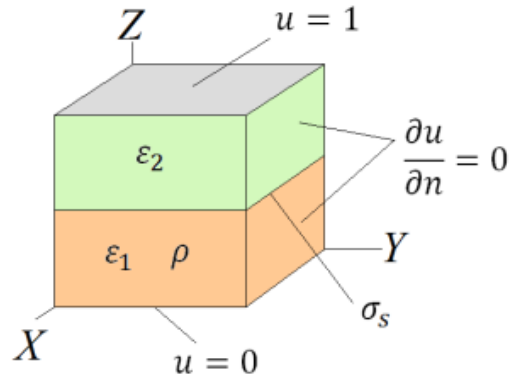


Fig.6.3.A non-homogeneous cube. The permittivities are different for both halves of the cube. Dirichlet conditions are imposed at top and bottom faces, whereas Neumann conditions are stated at the lateral faces. There is a volumetric charge density ρ in the lower half, in addition to a surface charge density σ_s at the interface separating both regions.

Homogeneous Neumann conditions ($\bar{h} = \partial u / \partial n = 0$) were imposed at lateral faces, while Dirichlet conditions $\bar{u} = 1V$ and $\bar{u} = 0$ were imposed at top and bottom faces, respectively. Figure 6.4 shows the potential along a path defined as $x = 0.5m; y = 0.5m; 0 \leq z \leq 1m$.

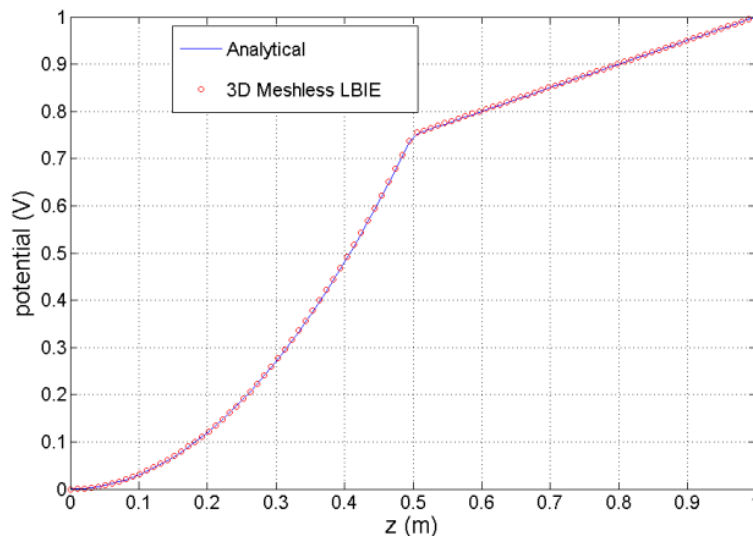


Fig.6.4.Electrostatic potential for a non-homogeneous unit cube.

When solving this problem, in addition to interior and boundary nodes, a layer of interface double nodes had to be placed along the plane that separates the regions of different permittivities, i.e., the portion of the plane $z = 0.5$ that lies inside the computational domain Ω ($0 < x < 1$, $0 < y < 1$ and $z = 0.5$). These nodes are treated exactly in the same way as described in Section 5.5.1. The only difference is that now there is a surface \mathcal{S} (plane) of discontinuity instead of a curve (line) τ . Each dual node generates a new linear equation to the system, and nodes from one side of the discontinuity do not influence points in the other side. So for each double interface node i (supposing there are N^d of them, which generates $2N^d$ unknowns) the interface conditions for the electrostatic problem are:

- The continuity condition:

$$\forall \vec{x} \in \mathcal{S} \quad u^-(\vec{x}) = u^+(\vec{x}) \quad (6.26)$$

When expressed for each interface node, (6.26) becomes

$$\forall i \leq N^d \quad u(\vec{x}_i^-) = u(\vec{x}_i^+) \quad (6.27)$$

- The condition on the normal derivative (normal to the interface \mathcal{S} , which in this example happens to be $\partial/\partial z$):

$$\forall \vec{x} \in \mathcal{S} \quad \varepsilon_2 \frac{\partial u^+}{\partial n} - \varepsilon_1 \frac{\partial u^-}{\partial n} = \sigma_S \quad (6.28)$$

For each interface node:

$$\forall i \leq N^d \quad \varepsilon_2 \frac{\partial u(\vec{x}_i^+)}{\partial n} - \varepsilon_1 \frac{\partial u(\vec{x}_i^-)}{\partial n} = \sigma_S(\vec{x}_i) \quad (6.29)$$

The nodes influencing \vec{x}_i^- are actually those ones that influence location \vec{x}_i and lie in region 1 ($R_1 =$ lower half of the cube), i.e., they are the nodes whose indices are elements of the set

$$S_1 = \{j \in I \mid j \in Neigh(\vec{x}_i) \wedge \vec{x}_j \in R_1\} \quad (6.30)$$

Analogously,

$$S_2 = \{k \in I \mid k \in Neigh(\vec{x}_i) \wedge \vec{x}_k \in R_2\} \quad (6.31)$$

where $I = \{1, 2, 3, 4, \dots, i, \dots, N\}$ (ranges from 1 to the number of nodes in the problem). Equations (6.27) and (6.29) then become

$$\forall i \leq N^d \quad \sum_{j \in S_1} \phi_j(\vec{x}_i) \hat{u}_j = \sum_{k \in S_2} \phi_k(\vec{x}_i) \hat{u}_k \quad (6.32)$$

$$\forall i \leq N^d \quad \varepsilon_2 \sum_{j \in S_1} \frac{\partial \phi_j(\vec{x}_i)}{\partial n} \hat{u}_j - \varepsilon_1 \sum_{k \in S_2} \frac{\partial \phi_k(\vec{x}_i)}{\partial n} \hat{u}_k = \sigma_S(\vec{x}_i) \quad (6.33)$$

6.2 Eigenvalue Problems and Photonic Crystals

We now turn our attention to eigenvalue problems. The examples to which we are going to apply the MLPG method come from the field of photonic bandgap crystals.

A two-dimensional crystal is an array of dielectric structures, periodic in the x and y directions. Given a pattern, which stands for a two-dimensional region characterized by a permittivity $\varepsilon(x, y)$, it is replicated indefinitely (for the purposes of analysis) throughout the plane XY , as illustrated by Fig.6.5.

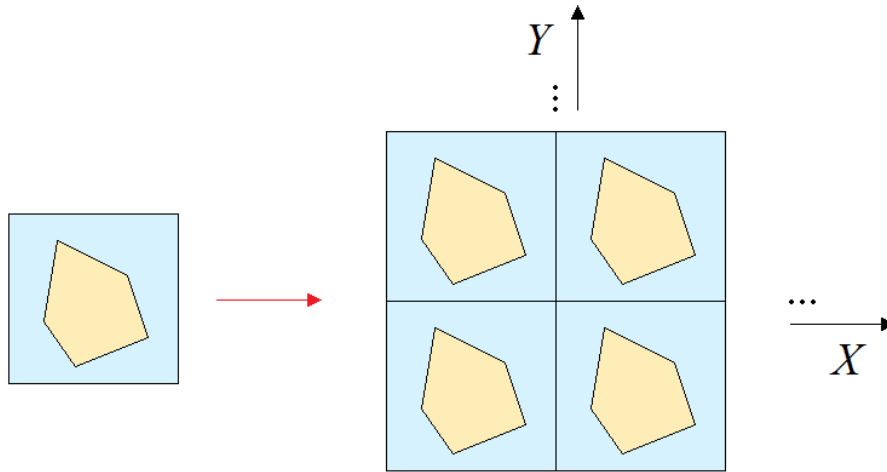


Fig.6.5. A single cell (in the left) is characterized by a permittivity $\varepsilon(x, y)$, which generally is 1 in the blue region and assumes a different value inside the light orange region. This region (in this case a pentagon) actually stands for the cross-section of a dielectric cylinder. The cell is replicated indefinitely along directions X and Y , which generates a periodic array (i.e., the crystal).

One of the main characteristic these structures exhibit is that they allow only radiation with certain wavelengths to propagate through it. Waves whose wavelength falls off certain “bands” are blocked. This characteristic and others make them attractive for a myriad of applications in modern technology. A beam of light can even be bent in 90 degrees within a crystal, as we were able to show in Section 5.5.

The theoretical treatment of the photonic crystals is vast and complex, and it constitutes an area of research by its own. But because in this work we are dealing with the numerical implementation of MLPG, we are not going to go deep into the theory behind these crystals. Further information on the theoretical underpinnings of photonic crystals can be found in [Joannopoulos *et al.*, 2008] and [Skorobogaty and Yang, 2009].

The objective of our analysis is to find out what wavelengths are actually ‘forbidden’. In order to do so, we begin from the differential equation describing the phenomenon, find a suitable weak form and solve the resultant generalized eigenvalue problem of the type $A\hat{u} = \lambda B\hat{u}$, where A and B are square matrices. The eigenvalues are represented by λ . In this kind of problem, we deal with two matrices, instead of a matrix K and a vector \mathbf{h} , as in the case for boundary value problems. However, the greatest novelty to be employed in the solution of these problems is a set of periodic shape functions. The boundary conditions for this sort of problems are periodic ones; so we found a way to build periodic shape functions. If we discretize the weak forms through these periodic shape functions, the boundary conditions do not need to be imposed anymore. Let us take a look at how such a process is carried out.

According to Fig.6.5, the unit cell (a single two-dimensional pattern) generates the crystal as it is translated indefinitely. Because this structure is periodic, the analysis amounts to a single cell. So for the purposes of eigenvalue analysis, the computational domain Ω is the unit cell (Fig.6.5).

Observation: We are dealing with two-dimensional problems (no quantity depends on the z -direction), and therefore, Fig.6.5 actually represents the cross section of the structure. The dielectric body S is a cylinder whose cross section is that one depicted in Fig.6.5. So the whole crystal resembles a ‘forest’ of dielectric bars (or cylinders). We are concerned with what

happens in a cut only, i.e., in a plane $z = \text{constant}$. This problem is quite like that one describing the scattering of a wave by many cylinders (it really can be seen as a scattering problem).

For TM^z polarization, the PDE describing the z -component of the electric field is (assuming no magnetic materials anywhere)

$$\nabla^2 E_z(\vec{x}) + k_0^2 \varepsilon_r(\vec{x}) E_z(\vec{x}) = 0 \quad (6.34)$$

Because the wavenumber k_0 in free space is $k_0^2 = \omega^2 \mu_0 \varepsilon_0$ and the velocity of light is given by $1/\sqrt{\mu_0 \varepsilon_0}$ (also in free space), (6.34) can be rewritten as

$$\nabla^2 E_z(\vec{x}) + \left(\frac{\omega}{c}\right)^2 \varepsilon_r(\vec{x}) E_z(\vec{x}) = 0 \quad (6.35)$$

Equation (6.35) holds true in every point of the computational domain Ω . The boundary conditions stated in the boundary of the unit cell $\partial\Omega$ are

$$E_z(\vec{x} + \vec{L}) = e^{-j\vec{K}\cdot\vec{L}} E_z(\vec{x}) \quad (6.36)$$

$$\frac{\partial E_z}{\partial n}(\vec{x} + \vec{L}) = e^{-j\vec{K}\cdot\vec{L}} \frac{\partial E_z}{\partial n}(\vec{x}) \quad (6.37)$$

where \vec{L} is the lattice vector. Expressions (6.36) and (6.37) mean that the value of the field (and its derivatives) in a given point \vec{x} of the crystal translated by \vec{L} (resulting in the point $\vec{x} + \vec{L}$) is equal to the field at \vec{x} multiplied by an exponential factor. When it comes to a single cell Ω only, they mean that the field at one side is equal to the field at the opposite side multiplied by an exponential factor (the same holds for the derivatives). The vector $\vec{K} = [K_x, K_y]$ is the Bloch vector. If the unit cell Ω is a square whose side is a , the components of the Bloch vector vary as $-\pi/a \leq K_x \leq \pi/a$ and $-\pi/a \leq K_y \leq \pi/a$. Under these conditions, the cell is assumed to be the square domain $\Omega = [-0.5a, 0.5a] \times [-0.5a, 0.5a]$ and the lattice vector is $\vec{L} = \hat{x}a + \hat{y}a$. The boundary conditions (6.36) and (6.37) therefore read as

$$E_z(0.5a, y) = e^{-jK_x a} E_z(-0.5a, y) \quad (6.38)$$

$$E_z(x, 0.5a) = e^{-jK_y a} E_z(x, -0.5a)$$

$$\frac{\partial E_z}{\partial x}(0.5a, y) = e^{-jK_x a} \frac{\partial E_z}{\partial x}(-0.5a, y)$$

$$\frac{\partial E_z}{\partial y}(x, 0.5a) = e^{-jK_y a} \frac{\partial E_z}{\partial y}(x, -0.5a)$$

In order to avoid working with the Bloch-periodic boundary conditions (6.36)-(6.38), the Bloch theorem [Tsukerman, 2008] is employed

$$E_z(\vec{x}) = e^{-j\vec{K}\cdot\vec{x}} u(\vec{x}) \quad (6.39)$$

where $u(\vec{x})$ is a periodic function

$$u(\vec{x} + \vec{L}) = u(\vec{x}) \quad (6.40)$$

$$\frac{\partial u}{\partial n}(\vec{x} + \vec{L}) = \frac{\partial u}{\partial n}(\vec{x}) \quad (6.41)$$

When (6.39) is substituted back in (6.36)-(6.37), the dependency on the exponential factor has been dropped. We are now left with a problem on $u(\vec{x})$. After the function u is found, the original electric field is recovered through (6.39). The periodic boundary conditions for u are

$$u(0.5a, y) = u(-0.5a, y) \quad (6.42)$$

$$u(x, 0.5a) = u(x, -0.5a)$$

$$\frac{\partial u}{\partial x}(0.5a, y) = \frac{\partial u}{\partial x}(-0.5a, y)$$

$$\frac{\partial u}{\partial y}(x, 0.5a) = \frac{\partial u}{\partial y}(x, -0.5a)$$

From the viewpoint of numerical implementation, it seems that the boundary conditions (6.42) are easier to deal with than conditions (6.38). Looking for the partial differential equation that governs u , it is derived from the substitution of (6.39) in (6.35). The result is equivalent to changing the ∇ operator by $\nabla - j\vec{K}$ [Tsukerman, 2008]. Therefore we get

$$-\nabla^2 u + j2\vec{K} \cdot \nabla u + \|\vec{K}\|^2 u = \left(\frac{\omega}{c}\right)^2 \varepsilon_r u \quad (6.43)$$

This is the PDE we are going to solve through MLPG.

At this point, we turn to the standard procedure of spreading nodes, defining the domains and the shape functions (in addition to the test functions). The weak form for (6.43) is obtained through the weighted residual method (explained earlier). For each node i (out of N), we multiply (6.43) by the test function v_i and integrate over the test domain Y_i :

$$\begin{aligned} \forall i \leq N \quad & - \iint_{Y_i} v_i \nabla^2 u \, dA + \iint_{Y_i} v_i (j2\vec{K} \cdot \nabla u + \|\vec{K}\|^2 u) \, dA \\ & = \left(\frac{\omega}{c}\right)^2 \iint_{Y_i} \varepsilon_r v_i u \, dA \quad (6.44) \end{aligned}$$

Employing (6.3), the two-dimensional analogue of (6.5) and the fact that the test function $v_i = 0$ in at ∂Y_i , we arrive at the weak form

$$\forall i \leq N \quad \iint_{Y_i} \nabla v_i \cdot \nabla u \, dA + \iint_{Y_i} v_i (j2\vec{K} \cdot \nabla u + \|\vec{K}\|^2 u) \, dA = \left(\frac{\omega}{c}\right)^2 \iint_{Y_i} \varepsilon_r v_i u \, dA \quad (6.45)$$

Given the line of reasoning we have been following, one may think there is something wrong with expression (6.45). The index i ranges from 1 to N , which means that the (6.45) are imposed for all nodes, for those located in the interior of Ω and for those lying in the boundary as well. And the boundary conditions, how do they come into the problem?

We have found a way of dealing with periodic boundary conditions such as (6.42) that allows them *not to be imposed at all*. Furthermore, besides not imposing any kind of boundary conditions (neither intersecting domains or collocation schemes are ever considered), the

integrations are carried out in simple circular domains Y_i . There is a manner of constructing periodic shape functions we have come across [Jun *et al.*, 2003] which modifies the MLS procedure a little bit. However, in this work we try another way of building them. The approach we develop here is somehow naïve, and it is based on operations regarding the indices of the nodes. In this naïve approach, the MLS procedure is left untouched. The same black box procedure described in Chapter 3 is applied here.

Let us clarify the reason why periodic shape functions can dismiss the imposition of boundary conditions. Bearing in mind the conditions (6.42) u must satisfy, if we find a shape function ϕ_m satisfying the same conditions, then we write

$$\begin{aligned}\phi_m(0.5a, y) &= \phi_m(-0.5a, y) \\ \phi_m(x, 0.5a) &= \phi_m(x, -0.5a) \\ \frac{\partial \phi_m(0.5a, y)}{\partial x} &= \frac{\partial \phi_m(-0.5a, y)}{\partial x} \\ \frac{\partial \phi_m(x, 0.5a)}{\partial y} &= \frac{\partial \phi_m(x, -0.5a)}{\partial y}\end{aligned}\tag{6.46}$$

If we find other shape function ϕ_n satisfying (6.42):

$$\begin{aligned}\phi_n(0.5a, y) &= \phi_n(-0.5a, y) \\ \phi_n(x, 0.5a) &= \phi_n(x, -0.5a) \\ \frac{\partial \phi_n(0.5a, y)}{\partial x} &= \frac{\partial \phi_n(-0.5a, y)}{\partial x} \\ \frac{\partial \phi_n(x, 0.5a)}{\partial y} &= \frac{\partial \phi_n(x, -0.5a)}{\partial y}\end{aligned}\tag{6.47}$$

It does not take much effort to realize that a linear combination of shape functions $\alpha_m \phi_m + \alpha_n \phi_n$ also will satisfy conditions (6.42):

$$\begin{aligned}\alpha_m \phi_m(0.5a, y) + \alpha_n \phi_n(0.5a, y) &= \alpha_m \phi_m(-0.5a, y) + \alpha_n \phi_n(-0.5a, y) \\ \alpha_m \phi_m(x, 0.5a) + \alpha_n \phi_n(x, 0.5a) &= \alpha_m \phi_m(x, -0.5a) + \alpha_n \phi_n(x, -0.5a) \\ \alpha_m \frac{\partial \phi_m(0.5a, y)}{\partial x} + \alpha_n \frac{\partial \phi_n(0.5a, y)}{\partial x} &= \alpha_m \frac{\partial \phi_m(-0.5a, y)}{\partial x} + \alpha_n \frac{\partial \phi_n(-0.5a, y)}{\partial x} \\ \alpha_m \frac{\partial \phi_m(x, 0.5a)}{\partial y} + \alpha_n \frac{\partial \phi_n(x, 0.5a)}{\partial y} &= \alpha_m \frac{\partial \phi_m(x, -0.5a)}{\partial y} + \alpha_n \frac{\partial \phi_n(x, -0.5a)}{\partial y}\end{aligned}\tag{6.48}$$

A linear combination of n shape functions therefore also satisfies (6.42). This is the fundamental result we have been expecting for. Let us write it as

$$\sum_j \phi_j(0.5a, y) \alpha_j = \sum_j \phi_j(-0.5a, y) \alpha_j\tag{6.49}$$

$$\sum_j \phi_j(x, 0.5a)\alpha_j = \sum_j \phi_j(x, -0.5a)\alpha_j$$

$$\sum_j \frac{\partial \phi_j(0.5a, y)}{\partial x} \alpha_j = \sum_j \frac{\partial \phi_j(-0.5a, y)}{\partial x} \alpha_j$$

$$\sum_j \frac{\partial \phi_j(x, 0.5a)}{\partial y} \alpha_j = \sum_j \frac{\partial \phi_j(x, -0.5a)}{\partial y} \alpha_j$$

Expressions (6.49) mean that a linear combination of periodic shape functions will also be periodic. Because in MLPG we approximate the function u by a linear combination of shape functions, we can therefore rest assured that the approximated solution u will satisfy (6.42) as well. This little explanation served the purpose of showing that the periodicity of the solution required by the problem has been transferred to the shape functions (building blocks) used to approximate it. Once we guarantee the shape functions are periodic, so will be a linear combination of them. Let us now verify how these special shape functions are constructed.

Given a unit cell (which is our computational domain) Ω , we spread N nodes throughout it. To each node we ascribe an index from the set I

$$I = \{1, 2, 3, 4, \dots, i, \dots, N\} \quad (6.50)$$

To each node we also associate an influence domain Λ_i (satisfying the no-hole condition, as said in the last chapters). In addition to the influence domains, we associate test domains to all nodes, but now with a difference. They are equal to the influence domains, i.e., they are all circles:

$$\forall i \in I (Y_i = \Lambda_i) \quad (6.51)$$

In this approach, there is no need to worry either about the intersections $Y_i \cap \Omega$ or about collocation schemes. However, if we take a node close to $\partial\Omega$ in such a way that there are points in Λ_i that lie outside Ω , how are they to be treated? The next step is to exactly replicate the unit cell and its nodal distribution 8 times, so that our domain Ω is now surrounded by other 8 cells (Fig.6.6), forming an extended domain Π :

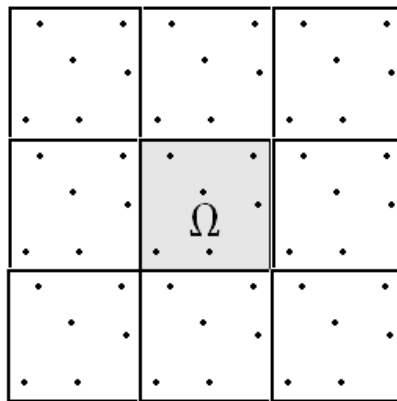


Fig.6.6. The extended domain Π , which is no more than a layer of 8 extra cells around the unit cell Ω . The nodal distributions inside each one of the 9 cells must be exactly the same.

In order to deal with the extra nodes, an extended numbering scheme is required. Because there are now $9N$ nodes, the indices are elements of the set

$$E = \{1, 2, 3, 4, \dots, i, \dots, N, N + 1, \dots, 2N, \dots, 3N, \dots, 9N\} \quad (6.52)$$

Each node in the extended domain Π has its associated influence and test domains:

$$\forall i \in E (Y_i = \Lambda_i) \quad (6.53)$$

However, although the problem seems to have become larger, it actually has not. Even with $9N$ nodes in Π , we use them only for the construction of the shape functions. We are concerned only with the N nodes lying in Ω . In the extended domain of Fig.6.7, the nodes in the upper left cell are to be numbered from 1 to N ; those in the cell in its right from $N + 1$ to $2N$; the nodes in the upper right cell from $2N + 1$ to $3N$, and so on, until the lower right cell, whose nodes are numbered from $8N + 1$ to $9N$. In this scheme, the nodes in the innermost cell (which happens to be our true computational domain Ω) are numbered from $4N + 1$ to $5N$. In order to build the periodic shape functions for the nodes in Ω (those which really interest us), we just take their influence domains (eventually they extend to regions outside Ω , but the purpose of the extra layer of cells surrounding Ω is to precisely allow this to occur naturally) and apply the normal MLS procedure, but *taking into account all nodes in Π , not only those in Ω* . The final step is to map the indices back to the unit cell Ω . Let us restate all that was said hitherto concerning these periodic shape functions through an example.

Just to remember, in the MLS approximation, if one wants to calculate the shape functions at a point \vec{x} , what one has to do amounts to finding out which nodes influence \vec{x} (nodes from the set $Neigh(\vec{x})$) and to plugging their coordinates (together with those of \vec{x}) in certain matrices. After some calculations (the black box procedure), one ends up with a vector Φ whose elements are the shape functions associated to the influencing nodes evaluated at the desired point \vec{x} .

Let us suppose that the problem is stated in a cell Ω . In this cell, we set up a nodal distribution. We then surround this cell with other 8 cells, and in each one of these extra cells, we assume a nodal distribution *identical* to that set up in Ω (i.e., we replicate it throughout). The situation is depicted in Fig.6.7: nine cells, each one with the same nodal distribution within. This array of nine cells form an extended domain Π , in the middle of which our original cell is situated. We then proceed to ascribe a global index i to each one of the nodes in Π . If there are, say, 100 nodes in the original cell Ω , then in Π the nodes in the first cell (top left) vary from 1 to 100; in the second cell (top middle), from 101 to 200, in the third (top right), from 201 to 300, and so on. The nodes in the innermost cell Ω vary from 401 to 500. Just to note: we use this bunch of extra nodes only when calculating the shape functions; as far as the problem (6.42)-(6.43) is concerned, only the innermost cell Ω and its nodes are considered.

Now in order to produce the periodic shape functions, *nodes that occupy the same position within each cell throughout the 9 cells are considered equivalent*. For example, nodes 2 (top left cell), 102 (top middle cell), 202 (top right cell), and so on, amounts to the same entity. It is as if the 9 nodes with global indices (2, 102, 202, ..., 802) were all equivalent to each other. As a result of the equivalence, each node in the extended domain Π can be mapped to a node inside Ω . This is carried out through a new index scheme:

$$\forall i \in E \quad j = i \bmod N \quad (6.54)$$

where i is a node's global index (in Π), N is the number of nodes inside a cell, and j is the node's global index mapped to the innermost cell Ω . Clearly

$$1 \leq j \leq N \quad (6.55)$$

Observation: When i is some multiple of N , in order to avoid $j = 0$, we ascribe i the correct value N whenever this occurs. So we guarantee the original range (from 1 to N).

Figure 6.7 illustrates this: suppose we want to calculate ϕ associated to node 431 (located close to the left edge) at \vec{x} .

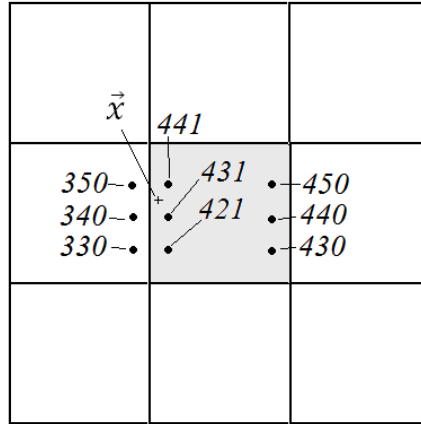


Fig.6.7. The extended domain of Fig.6. We are interested in the shape function associated to the node 431, located close to the left edge of the unit cell Ω . The value of ϕ calculated for node 330 (outside Ω) is transferred to its equivalent node inside Ω , node 430. Nodes 330 and 430 (global indices in Π) both have index 30 in the new index scheme (Fig.6.8).

Given \vec{x} , we apply the MLS procedure considering also nodes from neighbor cells. This is accounted for by the global index scheme. For example, in the global scheme, the nodes influencing \vec{x} are

$$Neigh(\vec{x}) = \{330, 340, 350, 421, 431, 441\} \quad (6.56)$$

Nodes 330, 340 and 350 come from a neighbor cell. So information concerning these 6 nodes is fed into the matrices of the MLS approximation (black box procedure), and we get a vector whose elements are the shape functions $(\phi_{330}, \phi_{340}, \phi_{350}, \phi_{421}, \phi_{431}, \phi_{441})$ evaluated at \vec{x} . Now it is time to find the equivalent indices: the influencing nodes at \vec{x} are then (30, 40, 50, 21, 31, 41). They are obtained through (6.54):

$$\forall i \in Neigh(\vec{x}) \quad j = i \bmod 100 \quad (6.57)$$

The equivalent scenario is illustrated in Fig.6.8.

A subtlety should be noticed: in Fig.6.7, nodes 340 and 440 are both equivalent (equivalent index $j = 40$), but the correct distance to be taken is the shorter distance from \vec{x} to node 340, and not from \vec{x} to 440. Just manipulating indices in this way avoids the issue of having to figure out the correct distance between points and nodes. In this way, the correct node 340 has been taken into account, and not 440.

The desired ϕ can be seen throughout Ω by taking a set of points \vec{x} covering Ω , and subsequently applying the procedure we have just described to each \vec{x} . The result is shown in

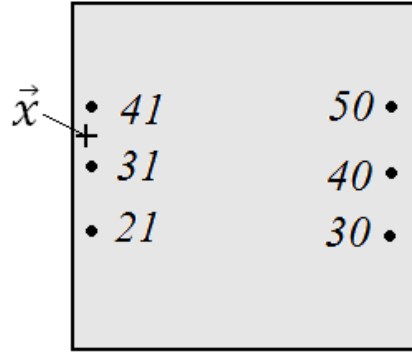


Fig.6.8. The indices referred back to the unit cell Ω . The indices now range from 1 to 100, as required.

Fig.6.9, where it can be seen that we indeed got a periodic shape function. The same profile is obtained at the left and right edges, i.e., $\phi(\vec{x} + \vec{L}) = \phi(\vec{x})$ and $\partial\phi(\vec{x} + \vec{L})/\partial n = \partial\phi(\vec{x})/\partial n$.

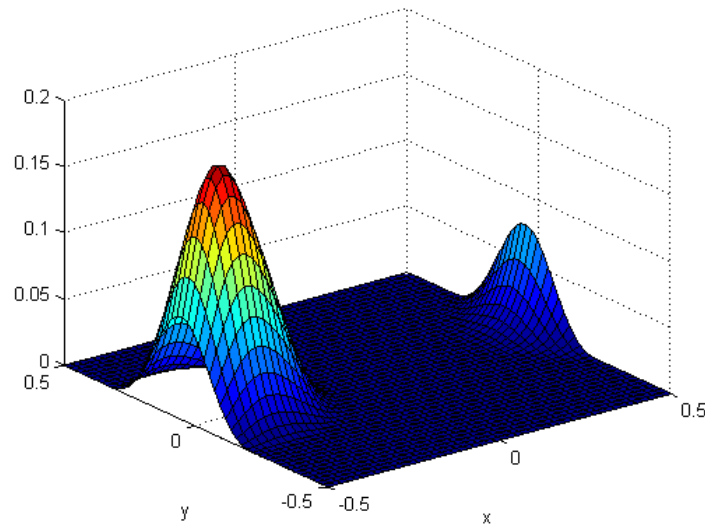


Fig.6.9. A periodic shape function (in Ω) associated to a node close to the left edge of Ω (431 in the global scheme, equivalent to 31 in the new scheme).

More periodic shape functions (associated to different nodes of the unit cell Ω) are shown in Figures 6.10 and 6.11.

Figures 6.9, 6.10 and 6.11 reveal that according to expected, besides being periodic, the shape functions are also compactly supported (the domain of influence is somewhat more complicated than just a circular region around a node), which gives rise to sparse matrices. Now that we know how to numerically construct periodic shape functions, let us return to the weak forms (6.45).

The weak forms (6.45) are stated for each node i in the computational domain Ω . Because $1 \leq i \leq N$, we can just replace it by i (as it actually stands for a dummy variable). Rewriting the weak forms:

$$\forall i \leq N \quad \iint_{Y_i} \nabla v_i \cdot \nabla u \, dA + \iint_{Y_i} v_i (j2\vec{K} \cdot \nabla u + \|\vec{K}\|^2 u) \, dA = \left(\frac{\omega}{c}\right)^2 \iint_{Y_i} \varepsilon_r v_i u \, dA \quad (6.58)$$

Representing the function u by an expansion in periodic shape functions:

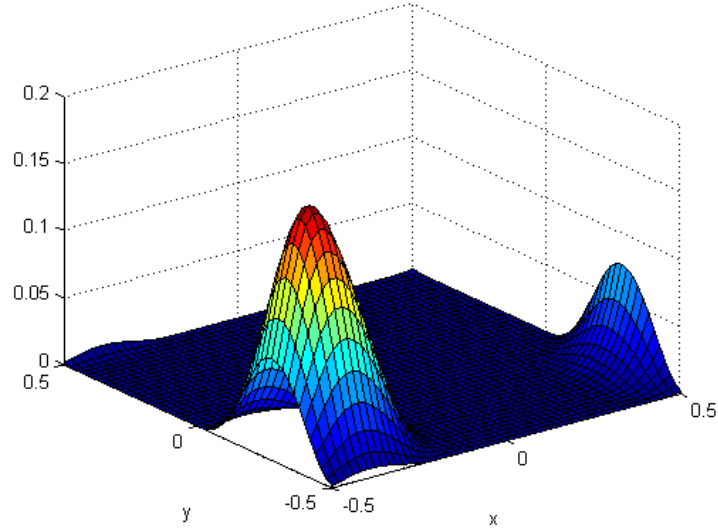


Fig.6.10. A shape function associated to a node located close to the left bottom vertex of Ω . It is beginning to extend its influence to regions opposed to the bottom line ($y = -0.5$).

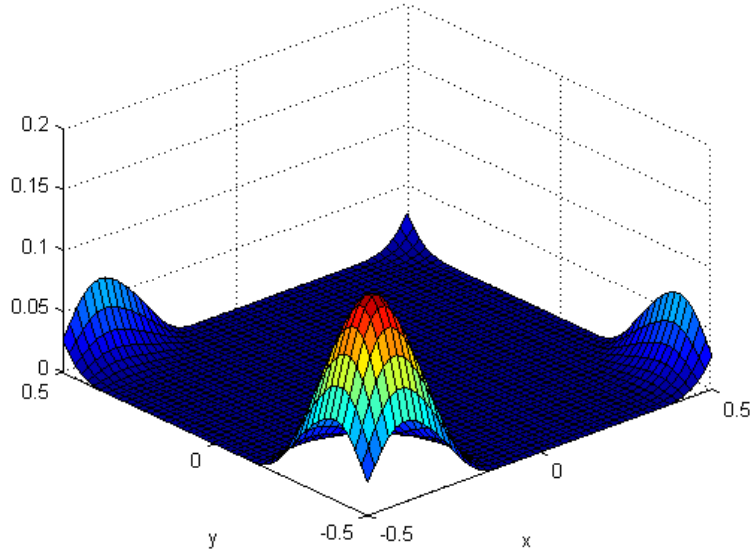


Fig.6.11. A shape function associated to a node located close to $(-0.5, -0.5)$. It extends its influence across the 4 vertices of Ω .

$$\forall \vec{x} \in \Omega \quad u(\vec{x}) = \sum_j \phi_j(\vec{x}) \hat{u}_j \quad (6.59)$$

where the indices j are obtained from the set $Neigh(\vec{x})$ considered in the context of the extended domain (all $9N$ nodes) and from the subsequent application of (6.54). Substituting (6.59) in (6.58) we get

$$\forall i \leq N \quad \sum_j \left(\iint_{\gamma_i} \nabla v_i \cdot \nabla \phi_j dA + \iint_{\gamma_i} v_i (j2\vec{K} \cdot \nabla \phi_j + \|\vec{K}\|^2 \phi_j) dA \right) \hat{u}_j = \quad (6.60)$$

$$= \left(\frac{\omega}{c}\right)^2 \sum_i \left(\iint_{\gamma_i} \varepsilon_r v_i \phi_i dA \right) \hat{u}_i$$

So we can retrieve the matrix system

$$\mathbf{A}\hat{\mathbf{u}} = \xi\mathbf{B}\hat{\mathbf{u}} \quad (6.61)$$

where the sparse $N \times N$ matrices \mathbf{A} and \mathbf{B} have their elements specified by

$$A_{ij} = \iint_{\gamma_i} \nabla v_i \cdot \nabla \phi_j dA + \iint_{\gamma_i} v_i \left(j2\vec{K} \cdot \nabla \phi_j + \|\vec{K}\|^2 \phi_j \right) dA \quad (6.62)$$

$$B_{ij} = \iint_{\gamma_i} \varepsilon_r v_i \phi_j dA \quad (6.63)$$

Expression (6.61) is a generalized eigenvalue problem. The eigenvalues $(\xi_1, \xi_2, \dots, \xi_n, \dots)$ are

$$\xi_n = \left(\frac{\omega_n}{c}\right)^2 \quad (6.64)$$

Once the eigenvalues are calculated, the frequencies f_n of the propagating modes $\omega_n = 2\pi f_n$ are finally obtained.

Thus far, the values for the Bloch vectors \vec{K} are unknown. We know that its components vary according to $-\pi/a \leq K_x \leq \pi/a$ and $-\pi/a \leq K_y \leq \pi/a$. In order to verify the propagating modes for a given Bloch vector, we pick up a value for \vec{K} (both components), plug it into (6.62), solve (6.61) and retrieve the eigenvalues (6.64). If we are dealing with a range of Bloch vectors, then we pick up another value for \vec{K} and repeat the procedure. We must do this for all values of \vec{K} we are interested in. In solid-state physics, there are some values for \vec{K} that receive special names. They are

$$\Gamma: \vec{K} = [K_x, K_y] = [0, 0] \quad (6.65)$$

$$X: \vec{K} = [K_x, K_y] = [\pi/a, 0]$$

$$M: \vec{K} = [K_x, K_y] = [\pi/a, \pi/a]$$

In our simulations, we considered three ranges of values for \vec{K} . The first links Γ to X , i.e., the component K_x ranges from 0 to π/a and $K_y = 0$. The second links X to M , i.e., $K_x = \pi/a$ and K_y ranges from 0 to π/a . The third links M back to Γ , i.e., K_x and K_y both range from π/a to 0. More on these values can be found in [Joannopoulos *et al.*, 2008].

The unit cell is normalized with respect to a , i.e., $a = 1$. We performed simulations for many different permittivity profiles, i.e., for crystals whose dielectric bars have different cross sections (both in the value of ε and in the geometric shape). When we considered circles, we obtained the correct prediction that waves with $k = 1$ would be unable to propagate through a crystal. We used this result in the example dealing with the propagation of light down photonic crystals shown in the last chapter. So the MLPG can be used in at least two stages in the analysis of photonic crystals: in the determination of the band structure (eigenvalue problem)

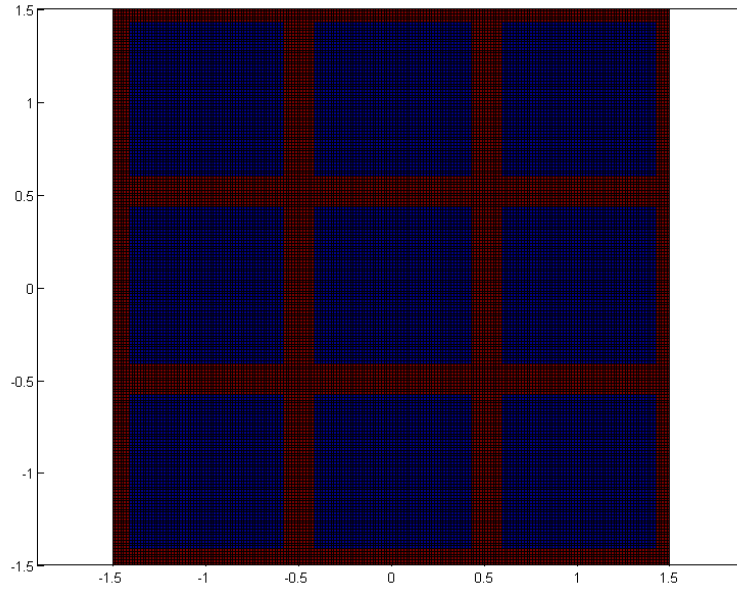


Fig.6.12. The profile of a crystal formed by dielectric veins (red). There are 9 cells in this figure.

and in the propagation of light when some bars are removed (boundary value problem). We considered also the profile of dielectric veins illustrated by Fig.6.12.

Figure 6.12 shows the extended domain Π for this problem. That figure actually illustrates 9 cells. The computational domain Ω refers only to the innermost cell (as discussed earlier). The blue regions are characterized by $\epsilon_r = 1$, whereas the red grating (veins) has $\epsilon_r = 8.9$ and thickness equivalent to $0.165a$. Figure 6.13 shows the resulting band structure (frequencies normalized to $\omega a/2\pi c$) for this crystal calculated through MLPG and compared to results in [Joannopoulos *et al.*, 2008].

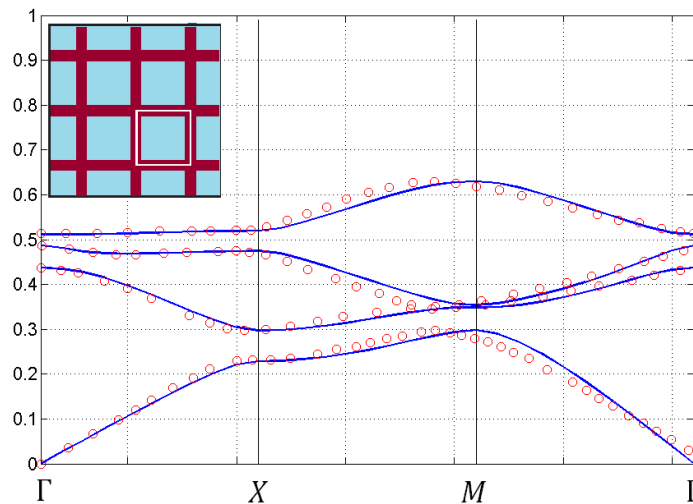


Fig.6.13. Band structure (frequencies normalized to $\omega a/2\pi c$) for the crystal formed by dielectric veins. Blue lines: MLPG4, Red balls: [Joannopoulos *et al.*, 2008]. At the inset, the light blue regions are characterized by $\epsilon_r = 1$, whereas the grating (veins) has $\epsilon_r = 8.9$. The region inside the white square is the unit cell Ω .

Concluding Remarks

Through the examples studied in this chapter, MLPG has proved to work well for three-dimensional and eigenvalue problems. Because the overall procedure has remained unchanged, with only some slight modifications concerning the calculation of periodic shape functions, we therefore just repeat here our table describing the implementation of MLPG method.

THE MESHLESS PROCEDURE IN A NUTSHELL

Given a differential equation and a domain where it shall be solved:

First Step	Set up the domain Ω and its boundary $\partial\Omega$.
Second Step	Spread N nodes throughout the domain Ω and at its boundary $\partial\Omega$ as well.
Third Step	<ul style="list-style-type: none"> • To each node i, define the radius of its influence domain Λ_i; • Make sure the influence domains cover the computational domain entirely.
Fourth Step	Numerical construction of the shape functions.
Fifth Step	<ul style="list-style-type: none"> • For each node i, define the test domains Y_i (radius s_i); • Define the test functions accordingly.
Sixth Step	Choose the way boundary conditions shall be dealt with: either through intersecting domains or through the collocation scheme.
Seventh Step	State the weak forms (Green's second identity or weighted residual method).
Eighth Step	<ul style="list-style-type: none"> • Numerical integration of the weak forms; • Assembling of the final linear system.
Ninth Step	Solution of the final linear system and determination of the nodal parameters $\hat{\mathbf{u}}$.

Chapter 7

Some Extensions of MLPG to Quantum Mechanics

IN this last chapter, we investigate the extension of MLPG to problems arising in quantum mechanics, particularly those related to computing the energy of quantum states. The PDE that MLPG will be applied to is Schrödinger's equation. The procedures used to solve this equation are the same as those illustrated in the last chapter. After the discretization process is completed, we arrive at a generalized eigenvalue problem (like that which appeared in the problems concerned to the photonic crystals), which is readily solved. This is the case for the majority of situations studied here, except for the last, which deals with a boundary value problem. Schrödinger's equation is solved in two and three-dimensional domains, and we compare the results to analytical solutions (benchmark) whenever possible. Everything described in this chapter is the result of the initial studies made by the author regarding numerical methods and quantum mechanics, a theme he intends to explore further in the future.

Although this is a work which deals with the numerical solution of PDE's, it is important to lay down some theoretical concepts, just for the sake of gaining some insight into the subject. There are many good books on quantum mechanics, some of which are those listed by the references: [Philips, 2003], [Zettili, 2009] and [Shankar, 1994].

7.1 Theoretical Motivation

7.1.1 Overview

A quantum system is described by a mathematical entity called the *wavefunction* Ψ . For example, particles with a given mass moving in a region of space where there is some potential energy distribution (caused by whatever agent, like electric fields, magnetic fields, etc.) form a quantum system, described by a certain wavefunction Ψ . This is so powerful a concept that everything in the small scale seems to fall under its influence, e.g., the behavior of molecules, the movement of electrons inside a nanoelectronic device, atomic and subatomic particles, are all described by a suitable wavefunction Ψ . It is actually one of the postulates of quantum mechanics: The state of a quantum system is specified by an entity like Ψ (sometimes called the state vector, which lives in a Hilbert space \mathcal{H}), which contains all information about the system. How this information is retrieved is stated in another postulate: A physically observable quantity A is associated to an operator \hat{A} (Hermitian) whose eigenvectors (Ψ_n) (or eigenfunctions) form a complete basis (for the space \mathcal{H}). If someone tries to measure the value for the quantity A in a system described by Ψ , he will get one of the eigenvalues a_n of the operator \hat{A} :

$$\hat{A}\Psi_n = a_n\Psi_n \quad (7.1)$$

Immediately after the measurement, the state of the system changes from Ψ (which could be a linear combination of the eigenvectors Ψ_i) to the state Ψ_n (associated to the eigenvalue a_n) with

a certain probability p_n . There are much more to be said about eigenvectors, eigenvalues and probabilities, but let us restrict the discussion to the lines above, otherwise we are in risk of being led too far away from the main topic (the numerical solution of PDE's).

We have not yet made explicit what the wavefunction Ψ depends on. It actually depends on the space (coordinates x , y and z) and on the time t . Such dependence is usually written as $\Psi(\vec{r}, t)$, where $\vec{r} = \hat{x}x + \hat{y}y + \hat{z}z$.

The energy E of the system is an observable, and therefore is associated to an operator \hat{E} . Actually, it is represented by \hat{H} , and it is called the *Hamiltonian operator*:

$$\hat{H} = -\frac{\hbar^2}{2m}\nabla^2 + V(\vec{r}, t) \quad (7.2)$$

where $\hbar = h/2\pi$, h is the Planck's constant (6.626068×10^{-34} J.s), m is the mass of the particle and V is the potential energy distribution. In (7.2), the quantum system described by Ψ is composed of a single particle. In the cases that shall be studied, the potential energy does not vary with time. So we write (7.2) as

$$\hat{H} = -\frac{\hbar^2}{2m}\nabla^2 + V(\vec{r}) \quad (7.3)$$

However, in order to retrieve the energy of the quantum system, we do not apply \hat{H} to $\Psi(\vec{r}, t)$. In quantum mechanics, there is a fundamental connection between the energy and the evolution of a quantum state. This relation is expressed as:

$$\hat{H} \Psi(\vec{r}, t) = i\hbar \frac{\partial \Psi(\vec{r}, t)}{\partial t} \quad (7.4)$$

Expression (7.4) is the celebrated *time-dependent Schrödinger's equation*, where i is the imaginary number $\sqrt{-1}$. This equation is so important that it is expressed as another postulate of quantum mechanics. In order to find the energy states, we begin by rewriting (7.4) as

$$-\frac{\hbar^2}{2m}\nabla^2\Psi(\vec{r}, t) + V(\vec{r})\Psi(\vec{r}, t) = i\hbar \frac{\partial \Psi(\vec{r}, t)}{\partial t} \quad (7.5)$$

We look for separable solutions of the type $\Psi(\vec{r}, t) = \psi(\vec{r})T(t)$. Substituting this in (7.5) and dividing by $\psi(\vec{r})T(t)$, we find

$$\frac{1}{\psi(\vec{r})} \left(-\frac{\hbar^2}{2m}\nabla^2\psi(\vec{r}) + V(\vec{r})\psi(\vec{r}) \right) = i\hbar \frac{1}{T(t)} \frac{dT(t)}{dt} \quad (7.6)$$

Equation (7.6) is true only if both sides are equal to a constant (because one depends on \vec{r} only and the other on t only). Let this constant be called W . So we arrive at two equations

$$\frac{dT(t)}{dt} = \frac{1}{i\hbar}WT(t) = -\frac{i}{\hbar}WT(t) \quad (7.7)$$

$$-\frac{\hbar^2}{2m}\nabla^2\psi(\vec{r}) + V(\vec{r})\psi(\vec{r}) = W\psi(\vec{r}) \quad (7.8)$$

The solution to (7.7) is easily found as

$$T(t) = T_0 e^{-\frac{iWt}{\hbar}} \quad (7.9)$$

However, from the inspection of the units appearing in the exponential, we verify that W must have the units of energy (the reduced Planck's constant in the denominator has units of joule \times second, the term t is the time in seconds and the imaginary unit is dimensionless; therefore, as the whole term in the exponential must also be dimensionless, W is measured in joules). W is actually the value of energy we are looking for. Making $W = E$, (7.8) is rewritten as

$$-\frac{\hbar^2}{2m} \nabla^2 \psi(\vec{r}) + V(\vec{r})\psi(\vec{r}) = E \psi(\vec{r}) \quad (7.10)$$

or

$$\left[-\frac{\hbar^2}{2m} \nabla^2 + V(\vec{r}) \right] \psi(\vec{r}) = \hat{H}\psi(\vec{r}) = E \psi(\vec{r}) \quad (7.11)$$

which is an eigenvalue equation. This is the energy eigenvalue equation or *time-independent Schrödinger equation*. There are many eigenfunctions $\psi_n(\vec{r})$ and eigenvalues E_n which satisfy (7.11). When (7.11) is solved, we can express the original wavefunction as

$$\Psi_n(\vec{r}, t) = \psi_n(\vec{r}) e^{-iE_n t/\hbar} \quad (7.12)$$

It can be found that wavefunctions corresponding to states of different energy are orthogonal to each other, i.e., for $m \neq n$, we have $E_m \neq E_n$ and $\langle \psi_m | \psi_n \rangle = 0$, where the brackets correspond to an inner product defined in \mathcal{H} :

$$\langle \psi_m | \psi_n \rangle = \iiint \psi_m^*(\vec{r}) \psi_n(\vec{r}) dV = 0 \quad \text{if } m \neq n \quad (7.13)$$

The integration in (7.13) is to be carried out over all space. If (7.13) is satisfied, then $\langle \Psi_m | \Psi_n \rangle$ also will (the exponential terms involving the time are taken out of the integral, which is carried out in regard to the spatial coordinates; we are then left with an integral like (7.13), which is zero). The wavefunctions Ψ_n (eigenfunctions of \hat{H}) usually are normalized, which means that one makes

$$\langle \psi_n | \psi_n \rangle = \iiint \psi_n^*(\vec{r}) \psi_n(\vec{r}) dV = 1 \quad (7.14)$$

(Again, if (7.14) is satisfied, then $\langle \Psi_n | \Psi_n \rangle = 1$ holds true as well). Because the function $|\Psi|^2 = \Psi^* \Psi$ actually stands for a probability density, the expectation value of the energy is

$$\langle E \rangle = \iiint \Psi^*(\vec{r}, t) \hat{H} \Psi(\vec{r}, t) dV = \langle \Psi | \hat{H} | \Psi \rangle \quad (7.15)$$

i.e., if our state is described by Ψ , the expected, or average value of the energy we get from the measurement process is given by (7.15). The actual, or real value someone gets is an eigenvalue E_n of \hat{H} , which can be measured with a probability p_n . When we consider all possible outcomes E_n together with their probabilities p_n , we perform a weighted sum (or integration) and obtain an expression like (7.15). The result $\langle E \rangle$ is not measured, it is just some kind of average.

If the quantum system is described by a wavefunction $\Psi = \Psi_n$ which is an eigenfunction of \hat{H} , we say it is in a state of definite energy, i.e., the result of the measurement process is certain to be E_n when Ψ is an eigenfunction of \hat{H} . To see this, we first take (7.15) with $\Psi = \Psi_n$:

$$\begin{aligned}\langle E \rangle &= \iiint \Psi_n^*(\vec{r}, t) \hat{H} \Psi_n(\vec{r}, t) dV = \iiint (\psi_n(\vec{r})e^{-iE_n t/\hbar})^* \hat{H} (\psi_n(\vec{r})e^{-iE_n t/\hbar}) dV = \quad (7.16) \\ &= \iiint \psi_n^*(\vec{r}) e^{iE_n t/\hbar} (\hat{H} \psi_n(\vec{r})) e^{-iE_n t/\hbar} dV = \iiint \psi_n^*(\vec{r}) E_n \psi_n(\vec{r}) dV = \\ &= E_n \iiint \psi_n^*(\vec{r}) \psi_n(\vec{r}) dV = E_n\end{aligned}$$

after considering expressions (7.11) (applied to ψ_n), (7.12) and (7.14).

The expectation value of the energy squared (E^2) is given by the application of the Hamiltonian twice:

$$\begin{aligned}\langle E^2 \rangle &= \iiint \Psi_n^*(\vec{r}, t) \hat{H}^2 \Psi_n(\vec{r}, t) dV = \iiint (\psi_n(\vec{r})e^{-iE_n t/\hbar})^* \hat{H}^2 (\psi_n(\vec{r})e^{-iE_n t/\hbar}) dV = \quad (7.17) \\ &= \iiint \psi_n^*(\vec{r}) e^{iE_n t/\hbar} (\hat{H}^2 \psi_n(\vec{r})) e^{-iE_n t/\hbar} dV = \iiint \psi_n^*(\vec{r}) \hat{H} (\hat{H} \psi_n(\vec{r})) dV = \\ &E_n \iiint \psi_n^*(\vec{r}) \hat{H} \psi_n(\vec{r}) dV = E_n^2 \iiint \psi_n^*(\vec{r}) \psi_n(\vec{r}) dV = E_n^2\end{aligned}$$

So when measuring the energy the variance is $\langle E^2 \rangle - \langle E \rangle^2 = E_n^2 - E_n^2 = 0$. The uncertainty ΔE (in this case the standard deviation) is also zero. Therefore, when $\Psi = \Psi_n$, the outcome of measurement process would be E_n .

So far, so good. More complicated solutions arise when the system is in a state described by more than one eigenfunction of \hat{H} , for example, a state characterized by 2 eigenfunctions

$$\Psi(\vec{r}, t) = \frac{1}{\sqrt{2}} \psi_1(\vec{r}) e^{-iE_1 t/\hbar} + \frac{1}{\sqrt{2}} \psi_2(\vec{r}) e^{-iE_2 t/\hbar} \quad (7.18)$$

or, more generally, when there are many eigenfunctions involved

$$\Psi(\vec{r}, t) = \sum_{n=1,2,\dots} c_n \psi_n(\vec{r}) e^{-iE_n t/\hbar} \quad (7.19)$$

States described by linear combinations of eigenfunctions like (7.18) and (7.19) usually have an uncertainty ΔE associated to the process of measuring the energy E . However, we are not going to consider such issues in this work.

From the brief discussion above it became clear that much information can be retrieved from the quantum system through the eigenvalues and eigenfunctions of \hat{H} . The analysis of a quantum system usually involves steps such as the solution of time-independent Schrödinger equation (7.11), the construction of an orthonormal basis for \mathcal{H} , the incorporation of time-dependent terms like in (7.12) and the application of many operators to Ψ in order to retrieve some properties from the system under study. In addition to \hat{H} , there are operators for position,

momentum of a particle, angular momentum, etc., which sometimes are combined in such a way to provide a means to retrieve a myriad of information regarding the quantum system. There are other formalisms in which quantum mechanics is developed, but in that one exposed here the solution of time-independent Schrödinger equation (7.11) is really fundamental. And it is precisely this equation that we intend to solve numerically through MLPG. Before we move on and begin to consider the details of the implementation, lets us take a look at the analytical solution to a particular problem that will be used as a basis for comparison with some of the MLPG numerical solutions.

7.1.2 Analytical solution to the harmonic oscillator potential

This problem is concerned to a particle of mass m under the action of a potential energy distribution of the type

$$V(\vec{r}) = \frac{1}{2} m \omega^2 \vec{r} \cdot \vec{r} \quad (7.20)$$

where ω is the angular frequency (radians/second). If we insert (20) in time-independent Schrödinger equation (7.10) we get

$$-\frac{\hbar^2}{2m} \nabla^2 \psi(\vec{r}) + \frac{1}{2} m \omega^2 \vec{r} \cdot \vec{r} \psi(\vec{r}) = E \psi(\vec{r}) \quad (7.21)$$

The boundary condition ψ must satisfy is

$$\lim_{|\vec{r}| \rightarrow \infty} \psi(\vec{r}) = 0 \quad (7.22)$$

We begin by analyzing the one-dimensional case

$$-\frac{\hbar^2}{2m} \frac{d^2 \psi(x)}{dx^2} + \frac{1}{2} m \omega^2 x^2 \psi(x) = E \psi(x) \quad (7.23)$$

From (7.9) we learned that Et/\hbar must be dimensionless. So the unit of energy is proportional to the units of \hbar divided by the units of t . Because ω is given by rad/s (time in the denominator), we express the energy as

$$E = \epsilon \hbar \omega \quad (7.24)$$

in units of joules, as expected. ϵ is just a dimensionless real number. From the traditional formula for the kinetic energy $K = mv^2/2$ (or from the famous Einstein's equation $E = mc^2$) we can play with the units

$$[J] = [kg][m/s]^2 = [kg] \frac{[m]^2}{[s]^2} \quad (7.25)$$

From which we see that

$$[m]^2 = [J] \frac{[s]^2}{[kg]} = \frac{[J \cdot s]}{[kg][1/s]} \quad (7.26)$$

or

$$[m] = \sqrt{\frac{[J \cdot s]}{[kg][1/s]}} \quad (7.27)$$

The rationalized Planck's constant \hbar has the dimensions of $J \cdot s$, the mass m is measured in kg and the angular frequency ω has the dimensions of rad/s . Therefore, we can express the distance x (in meters) as

$$x = s \sqrt{\frac{\hbar}{m\omega}} \quad (7.28)$$

where s is a dimensionless real number. Substituting (7.22) and (7.26) in (7.21) we find

$$-\frac{d^2\psi(s)}{ds^2} + s^2\psi(s) = 2\epsilon\psi(s) \quad (7.29)$$

where ψ is now a function of s .

We shall now deal with the some manipulation of operators. We begin by finding out what $\left[s + \frac{d}{ds}\right]\left[s - \frac{d}{ds}\right]\psi$ stands for:

$$\begin{aligned} \left[s + \frac{d}{ds}\right]\left[s - \frac{d}{ds}\right]\psi &= \left[s + \frac{d}{ds}\right]\left(s\psi - \frac{d\psi}{ds}\right) = \\ &= s^2\psi - s\frac{d\psi}{ds} + \frac{d(s\psi)}{ds} - \frac{d^2\psi}{ds^2} = -\frac{d^2\psi}{ds^2} + s^2\psi - s\frac{d\psi}{ds} + \frac{d(s\psi)}{ds} \end{aligned} \quad (7.30)$$

The first two terms in the right side of (7.28) is actually (7.27), and from

$$\frac{d(s\psi)}{ds} = \psi + s\frac{d\psi}{ds} \quad (7.31)$$

So we can write (7.28) as

$$\left[s + \frac{d}{ds}\right]\left[s - \frac{d}{ds}\right]\psi = (2\epsilon + 1)\psi \quad (7.32)$$

Now we investigate $\left[s - \frac{d}{ds}\right]\left[s + \frac{d}{ds}\right]\psi$:

$$\begin{aligned} \left[s - \frac{d}{ds}\right]\left[s + \frac{d}{ds}\right]\psi &= \left[s - \frac{d}{ds}\right]\left(s\psi + \frac{d\psi}{ds}\right) = \\ &= s^2\psi + s\frac{d\psi}{ds} - \frac{d(s\psi)}{ds} - \frac{d^2\psi}{ds^2} = -\frac{d^2\psi}{ds^2} + s^2\psi + s\frac{d\psi}{ds} - \frac{d(s\psi)}{ds} \end{aligned} \quad (7.33)$$

From (7.27) and (7.29) we arrive at

$$\left[s - \frac{d}{ds}\right]\left[s + \frac{d}{ds}\right]\psi = (2\epsilon - 1)\psi \quad (7.34)$$

We can verify that (7.30) is true if $\epsilon = -1/2$ and $\left[s - \frac{d}{ds}\right]\psi = 0$. However, this implies that

$$\frac{d\psi}{ds} = s\psi \quad (7.35)$$

which produces a solution of the type $\psi(s) = Ae^{s^2/2}$ (where A is just an integration constant), which does not go to zero when s (and therefore x) assumes large values. So we try (7.32). It is satisfied if $\epsilon = 1/2$ and $\left[s + \frac{d}{ds}\right]\psi = 0$. This implies that

$$\frac{d\psi}{ds} = -s\psi \quad (7.36)$$

which gives rise to an acceptable solution $\psi(s) = Ae^{-s^2/2}$. So our first eigenvalue is $\epsilon_0 = 1/2$ and our first eigenfunction is $\psi_0(s) = Ae^{-s^2/2}$. To find the second eigenvalue, we take (7.30) (restated below and regarding the first pair eigenvalue-eigenfunction)

$$\left[s + \frac{d}{ds}\right]\left[s - \frac{d}{ds}\right]\psi_0 = (2\epsilon_0 + 1)\psi_0 \quad (7.37)$$

and apply the operator $\left[s - \frac{d}{ds}\right]$ to both sides of it:

$$\left[s - \frac{d}{ds}\right]\left[s + \frac{d}{ds}\right]\left[s - \frac{d}{ds}\right]\psi_0 = (2\epsilon + 1)\left[s - \frac{d}{ds}\right]\psi_0 \quad (7.38)$$

which we rewrite as

$$\left[s - \frac{d}{ds}\right]\left[s + \frac{d}{ds}\right]\left(\left[s - \frac{d}{ds}\right]\psi_0\right) = (2\epsilon_0 + 1)\left(\left[s - \frac{d}{ds}\right]\psi_0\right) \quad (7.39)$$

Let us represent the function expressed within parentheses of u (i.e., $\left[s - \frac{d}{ds}\right]\left[s + \frac{d}{ds}\right]u = (2\epsilon_0 + 1)u$). But this is quite similar to (7.32) applied to a function u , i.e., the function u is an eigenfunction of $\left[s - \frac{d}{ds}\right]\left[s + \frac{d}{ds}\right]$ and must have its associated eigenvalue ϵ :

$$\left[s - \frac{d}{ds}\right]\left[s + \frac{d}{ds}\right]u = (2\epsilon - 1)u \quad (7.40)$$

Comparing (7.37) and (7.38), we find that $\epsilon = \epsilon_0 + 1$. So we have found our second eigenvalue $\epsilon_1 = \epsilon_0 + 1$ together with our second eigenfunction $\psi_1 = u = \left[s - \frac{d}{ds}\right]\psi_0$. To find the third eigenvalue, we take (7.30) again (now restated for the second eigenvalue-eigenfunction pair)

$$\left[s + \frac{d}{ds}\right]\left[s - \frac{d}{ds}\right]\psi_1 = (2\epsilon_1 + 1)\psi_1 \quad (7.41)$$

Operating with $\left[s - \frac{d}{ds}\right]$:

$$\left[s - \frac{d}{ds}\right]\left[s + \frac{d}{ds}\right]\left(\left[s - \frac{d}{ds}\right]\psi_1\right) = (2\epsilon_1 + 1)\left(\left[s - \frac{d}{ds}\right]\psi_1\right) \quad (7.42)$$

If we represent the term inside the parameters by w :

$$\left[s - \frac{d}{ds} \right] \left[s + \frac{d}{ds} \right] w = (2\epsilon_1 + 1)w \quad (7.43)$$

which again resembles (7.32). So w is also an eigenfunction of (7.32):

$$\left[s - \frac{d}{ds} \right] \left[s + \frac{d}{ds} \right] w = (2\epsilon - 1)w \quad (7.44)$$

Comparing (7.41) and (7.42) we retrieve the third eigenvalue as $\epsilon_2 = \epsilon = \epsilon_1 + 1$, and the third eigenfunction as $\psi_2 = w = \left[s - \frac{d}{ds} \right] \psi_1$. The process goes on indefinitely, and more eigenvalues and eigenfunctions can be obtained. There is a remaining issue concerning the fact if ϵ_0 is really the lowest eigenvalue. It is. This can be proved either from physical grounds (Heisenberg's uncertainty principle implies that the energy of an oscillator cannot be less than $E_0 = \hbar\omega/2$, which by its turn implies that ϵ_0 cannot be less than $1/2$) or from mathematical arguments (through the application of other operator that takes an eigenfunction ψ_n and returns ψ_{n-1} , and that returns 0 when applied to ψ_0). The eigenvalues and eigenfunctions for the harmonic oscillator are summarized in the table I below.

TABLE I
EIGENVALUES AND EIGENFUNCTIONS FOR THE ONE-DIMENSIONAL HARMONIC OSCILLATOR

Energy (dimensionless)	Energy (J)	Eigenfunction ($s = x\sqrt{m\omega/\hbar}$)
$\epsilon_0 = 1/2$	$E_0 = \hbar\omega/2$	$\psi_0(s) = Ae^{-s^2/2}$
$\epsilon_1 = \epsilon_0 + 1 = 3/2$	$E_1 = 3\hbar\omega/2$	$\psi_1 = \left[s - \frac{d}{ds} \right] \psi_0$
$\epsilon_2 = \epsilon_1 + 1 = 5/2$	$E_2 = 5\hbar\omega/2$	$\psi_2 = \left[s - \frac{d}{ds} \right] \psi_1 = \left[s - \frac{d}{ds} \right]^2 \psi_0$
$\epsilon_N = N + 1/2$	$E_N = (N + 1/2) \hbar\omega$	$\psi_N = \left[s - \frac{d}{ds} \right]^N \psi_0$

We now turn to (7.21) stated in higher dimensions. In two-dimensions, we have (for a level N)

$$-\frac{\hbar^2}{2m} \left(\frac{\partial^2}{\partial x^2} + \frac{\partial^2}{\partial y^2} \right) \psi_N(\vec{r}) + \frac{1}{2} m\omega^2(x^2 + y^2) \psi_N(\vec{r}) = E_N \psi_N(\vec{r}) \quad (7.45)$$

We can rewrite (7.43) as

$$\hat{H}\psi_N(\vec{r}) = [\hat{H}_x + \hat{H}_y]\psi_N(\vec{r}) = E_N\psi_N(\vec{r}) \quad (7.46)$$

where

$$\hat{H}_x = -\frac{\hbar^2}{2m} \frac{\partial^2}{\partial x^2} + \frac{1}{2} m\omega^2 x^2 \quad (7.47)$$

$$\hat{H}_y = -\frac{\hbar^2}{2m} \frac{\partial^2}{\partial y^2} + \frac{1}{2} m \omega^2 y^2 \quad (7.48)$$

Expressions (7.45) and (7.46) are one-dimensional Hamiltonians. If we seek for separable solutions, i.e., solutions of the form

$$\psi_N(\vec{r}) = \psi_N(x, y) = \psi_{n_x}(x) \psi_{n_y}(y) \quad (7.49)$$

where $\psi_{n_x}(x)$ is an eigenfunction of \hat{H}_x and $\psi_{n_y}(y)$ is an eigenfunction of \hat{H}_y , i.e.,

$$\hat{H}_x \psi_{n_x}(x) = E_{n_x} \psi_{n_x}(x) \quad (7.50)$$

$$\hat{H}_y \psi_{n_y}(y) = E_{n_y} \psi_{n_y}(y) \quad (7.51)$$

we have

$$\begin{aligned} [\hat{H}_x + \hat{H}_y] \psi_N(\vec{r}) &= [\hat{H}_x + \hat{H}_y] \psi_{n_x}(x) \psi_{n_y}(y) = E_{n_x} \psi_{n_x}(x) \psi_{n_y}(y) + E_{n_y} \psi_{n_x}(x) \psi_{n_y}(y) \\ &= (E_{n_x} + E_{n_y}) \psi_{n_x}(x) \psi_{n_y}(y) = E_N \psi_N(\vec{r}) \end{aligned} \quad (7.52)$$

So the eigenvalues for the two-dimensional harmonic oscillator in a level N are

$$E_N = E_{n_x} + E_{n_y} \quad (7.53)$$

For one-dimensional problems, the energies for an oscillator in level n_x are given by the last line of table I:

$$E_{n_x} = \left(n_x + \frac{1}{2} \right) \hbar \omega \quad (7.54)$$

$$E_{n_y} = \left(n_y + \frac{1}{2} \right) \hbar \omega \quad (7.55)$$

Therefore

$$E_N = (n_x + n_y + 1) \hbar \omega \quad (7.56)$$

where $n_x + n_y = N$. The energy levels for the two-dimensional oscillator, i.e., there are more than one configuration corresponding to the same energy. This does not happen for the first level $N = 0$ (because the only way for N to be zero occurs if $n_x = n_y = 0$). The degeneracies begin to show up in the second level $N = 1$ (either $(n_x, n_y) = (1, 0)$ or $(n_x, n_y) = (0, 1)$). For $N = 2$, there are 3 degenerate states $((n_x, n_y) = (2, 0), (n_x, n_y) = (1, 1)$ or $(n_x, n_y) = (0, 2))$, and so on.

The situation for three-dimensional oscillators is similar, with the exception that there is an extra term

$$\hat{H}_z = -\frac{\hbar^2}{2m} \frac{\partial^2}{\partial z^2} + \frac{1}{2} m \omega^2 z^2 \quad (7.57)$$

in the Hamiltonian \hat{H} which is now represented by

$$\hat{H} = \hat{H}_x + \hat{H}_y + \hat{H}_z \quad (7.58)$$

The energy levels are now given by the addition of (7.52), (7.53) and a similar term coming from \hat{H}_z ($E_{n_z} = (n_z + 1/2)\hbar\omega$):

$$E_N = \left(n_x + n_y + n_z + \frac{3}{2} \right) \hbar\omega \quad (7.59)$$

The number of degenerate states for a level N (three-dimensional oscillator) is $(n + 1)(n + 2)/2$.

Now that we have gained some insight into the basics of quantum mechanics and have discovered the analytical expressions for the eigenvalues of the Hamiltonian corresponding to the harmonic oscillator, let us proceed and verify if MLPG is able to provide the same results.

7.2 Two-dimensional examples

We are interested in the problem described by the two-dimensional time-independent Schrödinger equation stated in the infinite domain $\Omega = [-\infty < x < \infty] \times [-\infty < y < \infty]$:

$$-\frac{\hbar^2}{2m} \left(\frac{\partial^2}{\partial x^2} + \frac{\partial^2}{\partial y^2} \right) \psi(x, y) + \frac{1}{2} m \omega^2 (x^2 + y^2) \psi(x, y) = E \psi(x, y) \quad (7.60)$$

The boundary condition is

$$\lim_{x, y \rightarrow \pm\infty} \psi(x, y) = 0 \quad (7.61)$$

i.e., the wavefunction ψ must vanish when the independent variables x and y assume large values. Schrödinger's equation (7.58) is stated in SI units. However, as the reduced Planck's constant \hbar is so small a quantity, we rewrite (7.58) in Hartree atomic units, which is suitable for numerical simulation. In this new system of units, the mass of the electron m and reduced Planck's constant \hbar take on the value 1:

$$-\frac{1}{2} \left(\frac{\partial^2}{\partial x^2} + \frac{\partial^2}{\partial y^2} \right) \psi(x, y) + \frac{1}{2} \omega^2 (x^2 + y^2) \psi(x, y) = E \psi(x, y) \quad (7.62)$$

The unit of time in Hartree atomic units is $t_H = 2.418884 \times 10^{-7}$ s. If we consider a particle (electron) oscillating with a frequency 1 in Hartree atomic units, i.e., if $\omega = 1$ (which actually corresponds to $2\pi/t_H$ radians per second) our equation becomes

$$-\frac{1}{2} \left(\frac{\partial^2}{\partial x^2} + \frac{\partial^2}{\partial y^2} \right) \psi(x, y) + \frac{1}{2} (x^2 + y^2) \psi(x, y) = E \psi(x, y) \quad (7.63)$$

or

$$-\nabla^2 \psi + 2V\psi = 2E\psi \quad (7.64)$$

where $V = (x^2 + y^2)/2$. When solving this problem numerically, we cannot consider the domain Ω as an infinite region such as $[-\infty < x < \infty] \times [-\infty < y < \infty]$. We therefore restrict the computational domain Ω to a finite square region $[-R < x < R] \times [-R < y < R]$, and impose homogeneous Dirichlet boundary conditions on it:

$$\forall \vec{r} \in \partial\Omega \quad \psi(\vec{r}) = 0 \quad (7.65)$$

We are now at the point to apply the already familiar MLPG process to the problem (7.62) - (7.63). First, N nodes are spread throughout the computational domain $\bar{\Omega}$ (square region). Second, we find the weak forms associated to the PDE (7.62), through Green's second identity. Lastly, we discretize the weak forms, assemble everything in a matrix system and solve it.

We solved this problem in the two different ways: by considering the intersection of the test domains Y_i with Ω and by imposing the boundary conditions (7.63) through the collocation method. Taking Green's second identity

$$\iint_R (u\nabla^2 v - v\nabla^2 u) dA = \oint_{\partial R} \left(u \frac{\partial v}{\partial n} - v \frac{\partial u}{\partial n} \right) dl \quad (7.66)$$

we substitute u by ψ , v by the test function v_i and the region R by

$$R = Y_i \cap \Omega \quad \text{and} \quad \partial R = (\partial Y_i \cap \Omega) \cup (Y_i \cap \partial\Omega) \quad (7.67)$$

where we assume the most difficult case of a node whose test domain intersects the boundary $\partial\Omega$. Because $\nabla^2 v_i = -(\vec{r} - \vec{r}_i)$ (from the definition) we get

$$\begin{aligned} \forall i \in I \quad & -\alpha(\vec{r}_i)\psi(\vec{r}_i) - \iint_{Y_i \cap \Omega} 2V\psi v_i dA + E \iint_{Y_i \cap \Omega} 2\psi v_i dA = \\ & = \oint_{(\partial Y_i \cap \Omega) \cup (Y_i \cap \partial\Omega)} \psi \frac{\partial v_i}{\partial n} dl - \oint_{(\partial Y_i \cap \Omega) \cup (Y_i \cap \partial\Omega)} v_i \frac{\partial \psi}{\partial n} dl \end{aligned} \quad (7.68)$$

Working out the domains in the line integrals at the right side of (7.66):

$$\begin{aligned} \forall i \in I \quad & -\alpha(\vec{r}_i)\psi(\vec{r}_i) - \iint_{Y_i \cap \Omega} 2V\psi v_i dA + E \iint_{Y_i \cap \Omega} 2\psi v_i dA = \\ & = \int_{\partial Y_i \cap \Omega} \psi \frac{\partial v_i}{\partial n} dl + \int_{Y_i \cap \partial\Omega} \psi \frac{\partial v_i}{\partial n} dl - \int_{\partial Y_i \cap \Omega} v_i \frac{\partial \psi}{\partial n} dl - \int_{Y_i \cap \partial\Omega} v_i \frac{\partial \psi}{\partial n} dl \end{aligned} \quad (7.69)$$

The second line integral is zero, as it depends on ψ evaluated at a portion of $\partial\Omega$, which is zero [by (7.63)]. The third line integral also vanishes, because it depends on v_i evaluated at ∂Y_i (which is zero, according to the definition of a test function v_i). So our weak form becomes

$$\forall i \in I \quad \alpha(\vec{r}_i)\psi(\vec{r}_i) + \int_{\partial Y_i \cap \Omega} \psi \frac{\partial v_i}{\partial n} dl - \int_{Y_i \cap \partial\Omega} v_i \frac{\partial \psi}{\partial n} dl + \iint_{Y_i \cap \Omega} 2V\psi v_i dA = E \iint_{Y_i \cap \Omega} 2\psi v_i dA \quad (7.70)$$

Approximating the wavefunction by an expansion in shape functions

$$\forall \vec{r} \in \bar{\Omega} \quad \psi(\vec{r}) = \sum_{m \in \text{Neigh}(\vec{r})} \phi_m(\vec{r}) \hat{u}_m \quad (7.71)$$

If we number the nodes differently (as explained in Chapter 3):

$$\forall \vec{r} \in \bar{\Omega} \quad \psi(\vec{r}) = \sum_{j=1}^n \phi_j(\vec{r}) \hat{u}_j \quad (7.72)$$

we get

$$\begin{aligned} \forall i \in I \quad \sum_{j=1}^n \left(\alpha(\vec{r}_i) \phi_j(\vec{r}_i) + \int_{\partial Y_i \cap \Omega} \phi_j \frac{\partial v_i}{\partial n} dl - \int_{Y_i \cap \partial \Omega} v_i \frac{\partial \phi_j}{\partial n} + \iint_{Y_i \cap \Omega} 2V \phi_j v_i dA \right) \hat{u}_j = \\ = E \sum_{j=1}^n \left(\iint_{Y_i \cap \Omega} 2\phi_j v_i dA \right) \hat{u}_j \end{aligned} \quad (7.1)$$

From (7.71) we retrieve the matrix system

$$\mathbf{A}\hat{\mathbf{u}} = \xi \mathbf{B}\hat{\mathbf{u}} \quad (7.73)$$

where the coefficients of the $N \times N$ matrices \mathbf{A} and \mathbf{B} are

$$A_{ij} = \alpha(\vec{r}_i) \phi_j(\vec{r}_i) + \int_{\partial Y_i \cap \Omega} \phi_j \frac{\partial v_i}{\partial n} dl - \int_{Y_i \cap \partial \Omega} v_i \frac{\partial \phi_j}{\partial n} + \iint_{Y_i \cap \Omega} 2V \phi_j v_i dA \quad (7.74)$$

$$B_{ij} = \iint_{Y_i \cap \Omega} 2\phi_j v_i dA \quad (7.75)$$

Expression (7.72) is a generalized eigenvalue problem. The eigenvalues $(\xi_1, \xi_2, \dots, \xi_n, \dots)$ are the energies E_n , which are readily available after (7.72) is solved.

Observation: As we used an approach in which the intersections of the test domains with Ω have to be found (7.65), the radii of test domains Y_i were assumed to be equal to the radii of the influence domains Λ_i . In the collocation method, the radii of the test domain gets smaller the closer they are to the boundary $\partial \Omega$ (as explained in Chapter 3).

When imposing the boundary conditions through the collocation method, we proceed as follows. Supposing the N nodes are numbered in such a way that the first N^i correspond to interior nodes and the last $N^b = N - N^i$ to nodes lying on $\partial \Omega$, we impose the weak form (7.68) to each one of them. Because there are no intersections, the matrices are somehow simplified:

$$A_{ij} = \alpha(\vec{r}_i) \phi_j(\vec{r}_i) + \int_{\partial Y_i} \phi_j \frac{\partial v_i}{\partial n} dl + \iint_{Y_i \cap \Omega} 2V \phi_j v_i dA \quad (7.76)$$

$$B_{ij} = \iint_{Y_i} 2\phi_j v_i dA \quad (7.77)$$

Matrices \mathbf{A} and \mathbf{B} are $N^i \times N$. As they are not square matrices, the problem

$$\mathbf{A}\hat{\mathbf{u}} = \mathbf{E}\mathbf{B}\hat{\mathbf{u}} \quad (7.78)$$

is incomplete. Then we take each one of the N^b boundary nodes (indices ranging from $N^i + 1$ to N) and apply the collocation procedure. This returns N^b linear relations of the type

$$\forall i \in \{m \mid m \geq N^i + 1 \text{ and } m \leq N\} \quad \sum_{j=1}^N \phi_j(\vec{r}_i) \hat{u}_j = 0 \quad (7.79)$$

The index j runs from 1 to N just to make explicit that potentially any node can influence \vec{r}_i . However, the majority of the terms $\phi_j(\vec{r}_i)$ are zero, only the nodes close to \vec{r}_i (whose indices are elements of the set $Neigh(\vec{r}_i)$) are actually different from zero. If each node in the boundary gives rise to a relation like (7.78), and because any shape function ϕ_i (associated to node i located at \vec{r}_i) calculated exactly at \vec{r}_i is different from zero, we can express the nodal parameter \hat{u}_i of a boundary node i as a function of the other nodes:

$$\forall i \in \{m \mid m \geq N^i + 1 \text{ and } m \leq N\} \quad \hat{u}_i = \frac{1}{\phi_i(\vec{r}_i)} \sum_{\substack{j=1 \\ j \neq i}}^N \phi_j(\vec{r}_i) \hat{u}_j \quad (7.80)$$

We take expression (7.79) associated to node $N^i + 1$ (first boundary node) and substitute in matrices \mathbf{A} and \mathbf{B} . We get $N - 1 \times N - 1$ matrices \mathbf{A}' and \mathbf{B}' in which the nodal parameter \hat{u}_{N^i+1} is absent. We now take (7.79) associated to node $N^i + 2$ (second boundary node) and substitute in matrices \mathbf{A}' and \mathbf{B}' , getting $N - 2 \times N - 2$ matrices \mathbf{A}'' and \mathbf{B}'' in which the nodal parameter \hat{u}_{N^i+2} is absent. This process is repeated for all boundary nodes, until the nodal parameter associated to them are eliminated from \mathbf{A} and \mathbf{B} . We finally get two square $N^i \times N^i$ matrices \mathcal{A} and \mathcal{B} which allow our eigenvalue problem to be written as

$$\mathcal{A}\hat{\mathbf{u}} = \mathbf{E}\mathcal{B}\hat{\mathbf{u}} \quad (7.81)$$

The matrix system (7.80) is readily solved and the energies are retrieved.

The next table illustrates the results we have obtained from both implementations of MLPG4, compared to the analytical solutions.

According to (7.54), the energies for the two-dimensional harmonic oscillator at level N given by are $(N + 1)\hbar\omega$ in SI units. Because in Hartree atomic units $\hbar = 1$ and $\omega = 1$ (in the case studied), the energy levels are therefore given by $E_N = N + 1$. From table II, we conclude that both implementations of MLPG method provided correct values. MLPG were able even to account for the degenerate levels.

TABLE II
ENERGY LEVELS FOR THE TWO-DIMENSIONAL HARMONIC OSCILLATOR. COMPARISON BETWEEN
THE ANALYTICAL VALUES AND THOSE PROVIDED BY MLPG METHOD (BOTH
IMPLEMENTATIONS)

Level N	Analytical	Intersecting domains	Collocation
0	1	0.9993	0.9993
1	2	1.9985, 1.9985	1.9986, 1.9986
2	3	2.9976, 2.9978, 2.9979	2.9977, 2.9978, 2.9979
3	4	3.9970, 3.9970, 3.9988 3.9988	3.9968, 3.9968, 3.9970 3.9970
4	5	4.9955, 4.9988, 4.9998 5.0045, 5.0046	4.9957, 4.9957, 4.9957 4.9960, 4.9960
5	6	5.9961, 5.9961, 6.0100 6.0100, 6.0211, 6.0211	5.9944, 5.9944, 5.9947 5.9947, 5.9950, 5.9950

It is really interesting, and even beautiful, the fact that things derived from highly abstract grounds (or ‘theoretical’) like the manipulation of operators described in earlier pages actually coincide with others arrived at by purely numerical (or ‘practical’) means.

After the problem for the two-dimensional harmonic oscillator has been solved, we applied the same procedure to another case, the Henon-Heiles potential

$$V(x, y) = \frac{1}{2}(x^2 + y^2) + (0.0125)^{1/2} \left(x^2 y - \frac{y^3}{3} \right) \quad (7.82)$$

TABLE III
ENERGY LEVELS FOR THE HENON-HEILES POTENTIAL

Energy	Method 1*	Method 2*	Intersecting MLPG	Collocation MLPG
E_0	0.9978	0.9986	0.9979	0.9979
E_1	1.9879	1.9901	1.9886, 1.9886	1.9887, 1.9887
E_2	2.9512	2.9562	2.9541	2.9541
E_2	2.9815	2.9853	2.9830, 2.9833	2.9831, 2.9832
E_3	3.9176	3.9259	3.9239, 3.9242	3.9229, 3.9229
E_3	3.9749	3.9822	3.9801	3.9794
E_3	3.9783	3.9856	3.9833	3.9827
E_4	4.8572	4.8700	4.8714	4.8663
E_4	4.8880	4.8986	4.8973, 4.9016	4.8946, 4.8948
E_4	4.9749	4.9860	4.9842, 4.9861	4.9823, 4.9823
E_5	5.7993	5.8174	5.8236, 5.8286	5.8124, 5.8139
E_5	5.8497	5.8679	5.8767	5.8632
E_5	5.8642	5.8812	5.8887	5.8765
E_5	5.9753	5.9912	5.9946, 5.9948	5.9864, 5.9866

Table III shows the results of both implementations of MLPG4 and those provided by other numerical methods (the asterisk* refers to results taken from [Kalogiratou *et al.*, 2005]). From this, it becomes apparent that MLPG worked well when applied to this particular case also.

7.3 Three-dimensional examples

We are again interested in time-independent Schrödinger equation expressed in Hartree atomic units

$$-\frac{1}{2}\nabla^2\psi(\vec{r}) + V(\vec{r})\psi(\vec{r}) = E\psi(\vec{r}) \quad (7.83)$$

together with homogeneous Dirichlet conditions

$$\forall \vec{r} \in \partial\Omega \quad \psi(\vec{r}) = 0 \quad (7.84)$$

As the problems are now stated in three dimensions, we shall not deal with the issue concerning the intersection between test domains and Ω . We enforce the weak forms at the test domains for interior nodes only. The boundary conditions are treated through the same collocation scheme as that illustrated in the last section. In order to get the weak forms, we apply the weighted residual method, i.e., We take each interior node i (there are N^i of them, out of N), multiply the residual of (7.82) by the test function v_i and integrate over the test domain Y_i :

$$\forall i \in \{m \mid m \leq N^i\} \quad \iiint_{Y_i} [\nabla v_i \cdot \nabla \psi + 2Vv_i\psi] dV = E \iiint_{Y_i} 2v_i\psi dV \quad (7.85)$$

In deriving (7.84), we had in mind the property that $v_i = 0$ at ∂Y_i , what allows us to get rid of a surface integral appearing in the process. Other weak forms for (7.84) could be obtained through Green's second identity for the two functions ψ and v_i . Experience teaches us that (7.84) gives rise to an incomplete linear system of the type $\mathbf{A}\hat{\mathbf{u}} = \mathbf{E}\mathbf{B}\hat{\mathbf{u}}$ whose $N^i \times N$ matrices \mathbf{A} and \mathbf{B} have their coefficients given by

$$A_{ij} = \iiint_{Y_i} [\nabla v_i \cdot \nabla \phi_j + 2Vv_i\phi_j] dV \quad (7.86)$$

$$B_{ij} = \iiint_{Y_i} 2v_i\phi_j dV \quad (7.87)$$

From now on everything is now quite akin to what has been done in the last section. The collocation procedure is enforced at each one of the N^b boundary nodes, which generates N^b relations among N variables. These relations are substituted back in \mathbf{A} and \mathbf{B} , and through some eliminations, new $N^i \times N^i$ square matrices \mathcal{A} and \mathcal{B} are obtained. Finally, we get a generalized eigenvalue problem $\mathcal{A}\hat{\mathbf{u}} = \mathbf{E}\mathcal{B}\hat{\mathbf{u}}$, which is solved for the E 's.

The first example is the quantum harmonic oscillator. The sides of the cubic domain have been set to 9 a.u., and the potential energy is $V(\vec{r}) = \|\vec{r}\|^2/2$. The level N has energy given by (7.57)

$$E_N = E_{n_x+n_y+n_z} = N + 3/2 \quad (7.88)$$

Multiple values for E_N account for degenerate states. The nodal distribution is depicted in Fig. 7.1, and the results are shown in table IV.

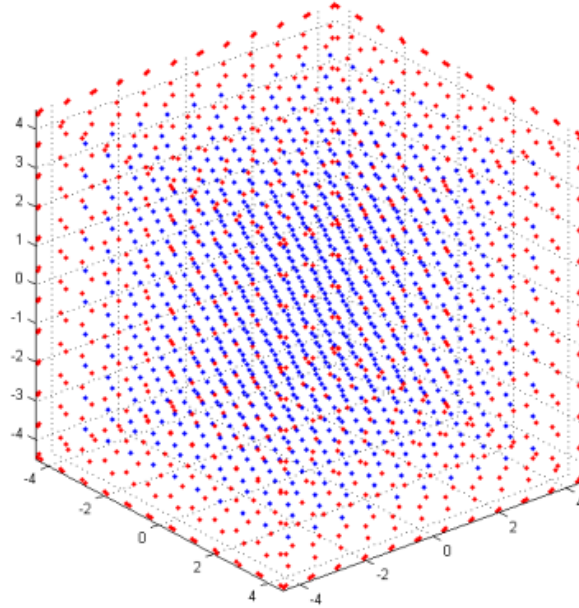


Fig.7.1. 1864 nodes in the cubic domain Ω concerned to the three-dimensional harmonic oscillator problem. Each interior node (blue) is ascribed a test domain Y where the weak forms are integrated. The boundary nodes (red) contribute with extra relations through the collocation procedure.

TABLE IV
FIRST EIGENVALUES FOR THE THREE-DIMENSIONAL HARMONIC OSCILLATOR

Level N	Analytical	MLPG4/LBIE
0	1.5	1.4962
1	2.5	2.4934; 2.4956; 2.4956
2	3.5	3.4902; 3.4902; 3.4949; 3.4984; 3.5029; 3.5035
3	4.5	4.4856; 4.4911; 4.4927; 4.4958; 4.4958; 4.5031; 4.5031; 4.5151; 4.5257; 4.5257
4	5.5	5.4867; 5.4867; 5.4900; 5.4907; 5.4953; 5.5053; 5.5053; 5.5087; 5.5242; 5.5242; 5.5295; 5.5301; 5.5722; 5.5932; 5.5939

The second example is concerned to those levels that can exist inside a spherical infinite square well, i.e., $V(\vec{r}) = 0$ for $\|\vec{x}\| \leq R$ and ∞ otherwise. The radius R of the spherical region has been set to 5 a.u. and homogeneous Dirichlet conditions have also been employed on $\partial\Gamma$. The allowed energy levels (in a.u.) are given by $E = u_{np}^2/2R^2$, where u_{np} are the p -th zeros of the spherical Bessel functions j_n . The nodal distribution is depicted in Fig.7.2, and the results are shown in table V.

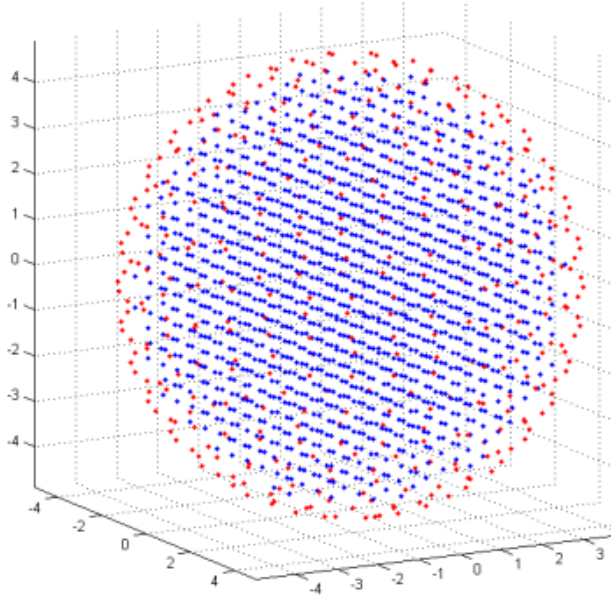


Fig.7.2. 1868 nodes for the spherical domain of the second example.

TABLE V
FIRST EIGENVALUES FOR THE SPHERICAL INFINITE SQUARE WELL

n	p	Analytical	MLPG4/LBIE
0	0	0.1974	0.1966
1	0	0.4038	0.4018; 0.4023; 0.4025
2	0	0.6643	0.6606; 0.6607; 0.6614; 0.6623; 0.6632
0	1	0.7896	0.7864
3	0	0.9766	0.9687; 0.9725; 0.9728; 0.9730; 0.9730; 0.9733; 0.9747
1	1	1.1936	1.1878; 1.1890; 1.1895
4	0	1.3391	1.3294; 1.3301; 1.3314; 1.3333; 1.3349 1.3350; 1.3355; 1.3355; 1.3379

The third example comes from solid-state physics, and deals with the calculation of the electronic band structure of solids. The potential energy $V(\vec{r})$ is periodic in the three-dimensional space, i.e., it replicates itself within each region called a *unit cell*.

For the purposes of analysis, if this array of cells is taken to be infinite, the problems need to be solved only for a unique cell. The strong form is then imposed at a cell Ω as:

$$-\nabla^2\psi(\vec{r}) + V(\vec{r})\psi(\vec{r}) = E\psi(\vec{r}) \quad (7.89)$$

In (7.88), Schrödinger's equation (7.6) has been written using Rydberg atomic units (this system differs from Hartree's in what regards the mass of the electron; $2m$ is taken as 1). The boundary conditions at $\partial\Omega$ are

$$\psi(\vec{r} + \vec{L}) = e^{j\vec{k}\cdot\vec{L}}\psi(\vec{r}) \quad (7.90)$$

$$\frac{\partial\psi(\vec{r} + \vec{L})}{\partial n} = e^{j\vec{k}\cdot\vec{L}} \frac{\partial\psi(\vec{r})}{\partial n} \quad (7.91)$$

\vec{K} is a vector called the Bloch vector, and \vec{L} is the lattice vector. For a cubic cell, the boundary conditions expressed in (7.89)-(7.90) mean that ψ at a face is equal to ψ at the opposite face multiplied by an exponential term. If we invoke Bloch theorem:

$$\psi(\vec{x}) = e^{j\vec{K}\cdot\vec{x}}u(\vec{x}) \quad (7.92)$$

where $u(\vec{x})$ is a periodic function over a cell, we get a new strong form on $u(\vec{x})$:

$$-\nabla^2 u(\vec{r}) - 2j\vec{K} \cdot \nabla u(\vec{r}) + (V(\vec{r}) + \vec{K} \cdot \vec{K})u(\vec{r}) = Eu(\vec{r}) \quad (7.93)$$

The boundary conditions now are given by

$$u(\vec{r} + \vec{L}) = u(\vec{r}) \quad (7.94)$$

$$\frac{\partial u(\vec{r} + \vec{L})}{\partial n} = \frac{\partial u(\vec{r})}{\partial n} \quad (7.95)$$

The boundary conditions stated in (7.93)-(7.94) mean that for a cubic cell, $u(\vec{r})$ at a face equals $u(\vec{r})$ at the opposite face. As the function u will be expanded in shape functions, it is interesting if this periodicity were transferred to the ϕ 's: boundary conditions would be unnecessary. From what we have been discussing so far it is evident that this problem is the three-dimensional equivalent to that one related to the calculation of band structure of photonic crystals. The extension of the procedure employed in chapter 5 to three-dimensional problems is: We take a cubic cell Ω , set up a nodal distribution and replicate it throughout the 26 cells surrounding Ω . We form a global numbering scheme, do all the MLS calculations as if we were dealing with a larger problem and then map the global indices back to Ω . These new periodic shape functions behave in such a way that a linear combination of them will also be periodic in a cell. Then the approximated u will also be periodic. Conclusion: The boundary conditions need not be imposed. Just take a cell Ω , spread some nodes, attach a spherical test domain Y_i to each node i and enforce the weak form at them:

$$\forall i \in \{m \mid m \geq 1 \text{ and } m \leq N\} \quad \iiint_{Y_i} \nabla v_i \cdot \nabla u \, dV + \iiint_{Y_i} (-2j\vec{K} \cdot \nabla u + (V + \vec{K} \cdot \vec{K})u) \, dV \quad (7.96)$$

$$= E \iiint_{Y_i} v_i u \, dV$$

The weak forms (7.95) came from the weighted residual method. After substituting u by an expansion in shape functions, one gets a generalized eigenvalue problem of the form $\mathbf{A}\hat{\mathbf{u}} = \mathbf{E}\mathbf{B}\hat{\mathbf{u}}$, where

$$A_{ij} = \iiint_{Y_i} \nabla v_i \cdot \nabla \phi_j \, dV + \iiint_{Y_i} (-2j\vec{K} \cdot \nabla \phi_j + (V + \vec{K} \cdot \vec{K})\phi_j) \, dV \quad (7.97)$$

$$B_{ij} = \iiint_{Y_i} v_i u \, dV \quad (7.98)$$

In this example, Ω is a cube whose side b is 3 a.u., and the potential energy $V(\vec{r})$ is the three-dimensional Kronig-Penney potential:

$$V(\vec{r}) = V(x, y, z) = \bar{V}(x) + \bar{V}(y) + \bar{V}(z) \quad (7.99)$$

$$\bar{V}(x) = \begin{cases} 0, & 0 \leq x \leq a \\ V_0, & a \leq x \leq b \end{cases}$$

where $a = 2$ a.u. and $V_0 = 6.5$ Ry. The eigenvalues (Rydberg a.u.) calculated as functions of \vec{K} are shown in Fig.7.3. The Bloch vector \vec{K} varies from $[0; 0; 0]$ (point Γ) to $(\pi/b)[1; 0; 0]$ (point X). A total of 729 ($9 \times 9 \times 9$) nodes has been employed in the analysis, and a good concordance can be verified when the LBIE solutions are compared to the results provided by another numerical method [Jun, 2004].

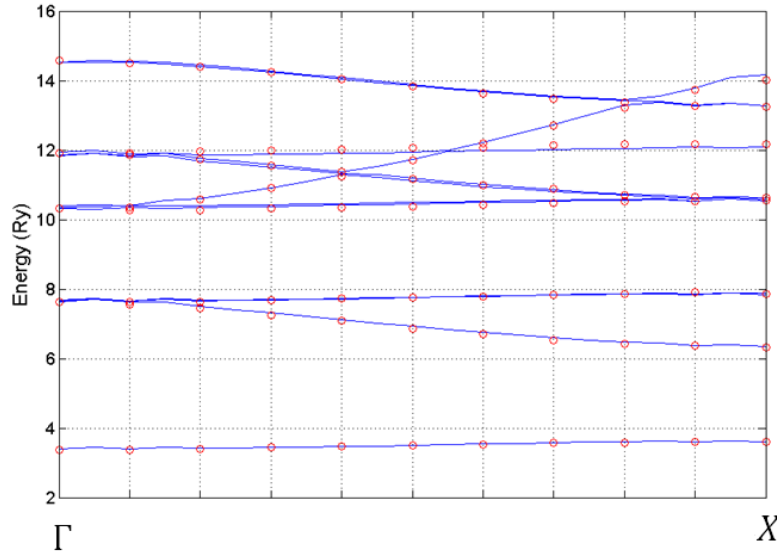


Fig.7.3. The electronic band structure for the third example (Kronig-Penney model). Blue line: MLPG4/LBIE method. Red balls: results taken from [Jun, 2004].

7.4 A nonlinear boundary value problem

We now turn our attention to boundary value problems, here illustrated by the two-dimensional nonlinear Schrödinger (NLS) equation. This equation appears in some contexts of quantum theory, and in other areas as well, as in the propagation of electromagnetic waves in nonlinear media. We employ a time-difference approximation and a predictor-corrector scheme (to deal with the nonlinearity) in conjunction with MLPG4 in order to find the numerical solutions.

Let Ω be the computational domain. The NLS reads as

$$i \frac{\partial \psi(\vec{x}, t)}{\partial t} + \nabla^2 \psi(\vec{x}, t) = \alpha(\vec{x}, t) + \beta(\vec{x}) |\psi(\vec{x}, t)|^p \psi(\vec{x}, t) \quad (7.100)$$

The initial and boundary conditions are

$$\forall \vec{x} \in \Omega \quad \psi(\vec{x}, 0) = f(\vec{x}) \quad (7.101)$$

$$\forall \vec{x} \in \partial\Omega_g \quad \psi(\vec{x}, t) = g(\vec{x}, t) \quad (\text{Dirichlet}) \quad (7.102)$$

$$\forall \vec{x} \in \partial\Omega_h \quad \frac{\partial\psi}{\partial n}(\vec{x}, t) = h(\vec{x}, t) \quad (\text{Neumann}) \quad (7.103)$$

where $\vec{x} = (x, y) \in \bar{\Omega}$, $i = \sqrt{-1}$, α, β, f, g and h are known functions, $\partial\Omega = \partial\Omega_g \cup \partial\Omega_h$, and p is a positive real number. The time interval is

$$\mathfrak{T} = \{t \in \mathbb{R} \mid t \geq 0 \text{ and } t \leq T\} \quad (7.104)$$

[Dehgan and Mirzaei, 2008] solve this problem through MLPG5, a meshless method whose test function v is a Heaviside step function instead of a function like

$$v_i(\vec{x}) = \frac{1}{2\pi} \ln\left(\frac{s_i}{\|\vec{x} - \vec{x}_i\|}\right) \quad (7.105)$$

and having the properties

$$\forall \vec{x} \in Y_i \quad \nabla^2 v_i = -\delta(\vec{x} - \vec{x}_i) \quad (7.106)$$

and

$$\forall \vec{x} \in \partial Y_i \quad v_i = 0 \quad (7.107)$$

which characterizes MLPG4. Furthermore, [Dehgan and Mirzaei, 2008] do not use the collocation method when treating Neumann boundary conditions; intersections have to be found there. In order to solve (7.99), we must take some approximations.

First, a discretization in time. \mathfrak{T} is no longer represented by (7.104), but by

$$\mathfrak{T} = \{t \in \mathbb{R} \mid t = k\Delta t, k \in \mathbb{N}, \Delta t \in \mathbb{R}\} \quad (7.108)$$

i.e., $\mathfrak{T} = \{0, \Delta t, 2\Delta t, \dots, k\Delta t, \dots\}$, and Δt is the time step. We then use the shorthand $\psi^{(k)}(\vec{x}) = \psi(\vec{x}, k\Delta t)$ to denote the wavefunction calculated at the instant $k\Delta t$.

Second, whenever the wavefunction in continuous time ψ appears in (7.99), it is substituted by

$$\psi(\vec{x}, t) \sim \eta\psi^{(k+1)}(\vec{x}) + (1 - \eta)\psi^{(k)}(\vec{x}) \quad (7.109)$$

where $0 < \eta \leq 1$.

Third, the time derivative is approximated by

$$\frac{\partial\psi(\vec{x}, t)}{\partial t} \sim \frac{\psi^{(k+1)}(\vec{x}) - \psi^{(k)}(\vec{x})}{\Delta t} \quad (7.110)$$

Fourth, the function $\alpha(\vec{x}, t)$ in (7.99) is taken at the instant $(k + 1)\Delta t$:

$$\alpha(\vec{x}, t) \sim \alpha^{(k+1)}(\vec{x}) \quad (7.111)$$

Fifth, in order to apply a predictor-corrector scheme (to be explained later), the nonlinearity is “approximated”, i.e., the ψ inside the nonlinear term is approximated by ψ_{ap} :

$$\beta(\vec{x})|\psi(\vec{x}, t)|^p \psi(\vec{x}, t) \rightarrow \beta(\vec{x})|\psi_{ap}(\vec{x}, t)|^p \psi(\vec{x}, t) \quad (7.112)$$

Inserting all these approximations at (7.99), we get a strong form:

$$\begin{aligned} \eta \nabla^2 \psi^{(k+1)} + \frac{i}{\Delta t} \psi^{(k+1)} - \eta \alpha^{(k+1)} \psi^{(k+1)} - \eta \beta |\psi_{ap}|^p \psi^{(k+1)} &= \\ &= -(1-\eta) \nabla^2 \psi^{(k)} + \frac{i}{\Delta t} \psi^{(k)} + (1-\eta) \alpha^{(k)} \psi^{(k)} + (1-\eta) \beta |\psi_{ap}|^p \psi^{(k)} \end{aligned} \quad (7.113)$$

Expression (7.112) is organized in such a way that, if we know ψ at time step k , then ψ at time step $k+1$ can be known. After spreading N^i interior nodes throughout Ω and N^b at $\partial\Omega$, we proceed to get a weak form for (7.112). We take each interior node i , its test function v_i and its test domain Y_i (these test domains cannot intersect the global boundary: $Y_i \cap \partial\Omega = \emptyset$). A weak form coming from Green's second identity is:

$$\begin{aligned} \forall i \in \{m \mid m \geq 1 \text{ and } m \leq N^i\} \quad -\eta \psi^{(k+1)}(\vec{x}_i) - \eta \oint_{\partial Y_i} \frac{\partial v_i}{\partial n} \psi^{(k+1)} dl + \\ + \iint_{Y_i} \left(\frac{i}{\Delta t} - \eta \alpha^{(k+1)} - \eta \beta |\psi_{ap}|^p \right) v_i \psi^{(k+1)} dA = (1-\eta) \psi^{(k)}(\vec{x}_i) + (1-\eta) \oint_{\partial Y_i} \frac{\partial v_i}{\partial n} \psi^{(k)} dl \\ + \iint_{Y_i} \left(\frac{i}{\Delta t} + (1-\eta) \alpha^{(k+1)} + (1-\eta) \beta |\psi_{ap}|^p \right) v_i \psi^{(k)} dA \end{aligned} \quad (7.114)$$

After substituting

$$\psi^{(k+1)} = \sum_j \phi_j(\vec{x}) \hat{u}_j^{(k+1)} \quad (7.115)$$

we get a matrix \mathbf{G} (N^i rows and N columns) and a vector \mathbf{Q} (N^i elements) whose elements are

$$G_{ij} = -\eta \phi_j(\vec{x}_i) - \eta \oint_{\partial Y_i} \frac{\partial v_i}{\partial n} \phi_j dl + \iint_{Y_i} \left(\frac{i}{\Delta t} - \eta \alpha^{(k+1)} - \eta \beta |\psi_{ap}|^p \right) v_i \phi_j dA \quad (7.116)$$

$$\begin{aligned} Q_i = (1-\eta) \psi^{(k)}(\vec{x}_i) + (1-\eta) \oint_{\partial Y_i} \frac{\partial v_i}{\partial n} \psi^{(k)} dl + \\ + \iint_{Y_i} \left(\frac{i}{\Delta t} + (1-\eta) \alpha^{(k+1)} + (1-\eta) \beta |\psi_{ap}|^p \right) v_i \psi^{(k)} dA \end{aligned} \quad (7.117)$$

The nodal parameters from the previous iteration $\hat{u}_j^{(k)}$ are known, so whenever $\psi^{(k)}$ needs to be calculated in (7.116), we just employ

$$\psi^{(k)} = \sum_j \phi_j(\vec{x}) \hat{u}_j^{(k)} \quad (7.118)$$

The other N^b equations come from the collocation at each boundary node. This information can be assembled in a matrix \mathbf{H} (N^b rows and N columns) and a vector \mathbf{R} (N^b rows). If the boundary conditions are expressed in a general way as

$$\forall \vec{x} \in \partial\Omega \quad a(\vec{x}, t)\psi(\vec{x}, t) + b(\vec{x}, t)\frac{\partial\psi(\vec{x}, t)}{\partial n} = q(\vec{x}, t) \quad (7.119)$$

then we have, for each boundary node i (there being N^b of them) the time step $k + 1$:

$$\forall i \in \{m \mid m \geq N^i + 1 \text{ and } m \leq N\} \quad (7.120)$$

$$\begin{aligned} a(\vec{x}_i, (k+1)\Delta t) \sum_j \phi_j(\vec{x}_i) \hat{u}_j^{(k+1)} + b(\vec{x}_i, (k+1)\Delta t) \sum_j \frac{\partial\phi_j(\vec{x}_i)}{\partial n} \hat{u}_j^{(k+1)} = \\ = q(\vec{x}_i, (k+1)\Delta t) \end{aligned}$$

The elements of \mathbf{H} and \mathbf{R} are therefore given by

$$H_{ij} = a(\vec{x}_i, (k+1)\Delta t)\phi_j(\vec{x}_i) + b(\vec{x}_i, (k+1)\Delta t)\frac{\partial\phi_j(\vec{x}_i)}{\partial n} \quad (7.121)$$

$$R_i = q(\vec{x}_i, (k+1)\Delta t) \quad (7.122)$$

Assembling the matrices \mathbf{G} and \mathbf{H} together into a $N \times N$ matrix \mathbf{M}

$$\mathbf{M} = \begin{bmatrix} \mathbf{G} \\ \mathbf{H} \end{bmatrix} \quad (7.123)$$

and the vectors \mathbf{Q} and \mathbf{R} into a $N \times 1$ vector \mathbf{F}

$$\mathbf{F} = \begin{bmatrix} \mathbf{Q} \\ \mathbf{R} \end{bmatrix} \quad (7.124)$$

we form a system:

$$\mathbf{M}(t, \psi_{ap})\hat{\mathbf{u}}^{(k+1)} = \mathbf{F}(t, \psi_{ap}) \quad (7.125)$$

where the matrix \mathbf{M} and the vector \mathbf{F} depends on the time t and on the ‘‘approximated’’ term ψ_{ap} . The predictor-corrector scheme works as follows, assuming that the nodal parameters for the last iteration $\hat{\mathbf{u}}^{(k)}$ are known:

First estimate for $\hat{\mathbf{u}}^{(k+1)}$: $\hat{\mathbf{u}}^{(k+1),0} = \hat{\mathbf{u}}^{(k)}$

First estimate for $\hat{\mathbf{u}}_{ap}$: $\hat{\mathbf{u}}_{ap} = \hat{\mathbf{u}}^{(k)}$

Calculate \mathbf{M} and \mathbf{F} .

Next estimate for $\hat{\mathbf{u}}^{(k+1)}$: $\hat{\mathbf{u}}^{(k+1),1} = \mathbf{M}^{-1}\mathbf{F}$

Next estimate for $\hat{\mathbf{u}}_{ap}$: $\hat{\mathbf{u}}_{ap} = 0.5[\hat{\mathbf{u}}^{(k+1),1} + \hat{\mathbf{u}}^{(k)}]$

Calculate \mathbf{M} and \mathbf{F} (with new $\hat{\mathbf{u}}_{ap}$)

Next estimate for $\hat{\mathbf{u}}^{(k+1)}$: $\hat{\mathbf{u}}^{(k+1),2} = \mathbf{M}^{-1}\mathbf{F}$

Next estimate for $\hat{\mathbf{u}}_{ap}$: $\hat{\mathbf{u}}_{ap} = 0.5[\hat{\mathbf{u}}^{(k+1),2} + \hat{\mathbf{u}}^{(k)}]$

Calculate \mathbf{M} e \mathbf{F} (with new $\hat{\mathbf{u}}_{ap}$)

Next estimate for $\hat{\mathbf{u}}^{(k+1)}$: $\hat{\mathbf{u}}^{(k+1),3} = \mathbf{M}^{-1}\mathbf{F}$

⋮

Repeat m times until

$$\|\hat{\mathbf{u}}^{(k+1),m} - \hat{\mathbf{u}}^{(k+1),m-1}\| \leq \varepsilon$$

So

$$\hat{\mathbf{u}}^{(k+1)} = \hat{\mathbf{u}}^{(k+1),m}$$

where ε is some established error.

We applied this time-domain LBIE to the NLS problem (7.99) in which

$$\begin{aligned}\Omega &= [0,1] \times [0,1] \\ \alpha(x,y) &= (1 - 2\pi^2)(1 - \cos^2\pi x \cos^2\pi y) \\ \beta(x,y) &= 1 - 2\pi^2 \\ p &= 2 \\ \psi(x,y,0) &= \cos\pi x \cos\pi y \\ \partial\psi/\partial n &= 0 \text{ at } \partial\Omega \\ \Delta t &= 0.05\end{aligned}$$

The analytical solution to this problem is

$$\psi(x,y,t) = e^{-it} \cos\pi x \cos\pi y \quad (7.126)$$

In the simulations, the index k varies from 1 to 20 (20 time steps), and we have got again a good concordance between the numerical and analytical solutions. Figure 7.4 shows the nodes spread throughout $\bar{\Omega}$, Fig.7.5 illustrates the set of influence domains Λ covering the computational domain entirely, and Fig.7.6 depicts the set of test domains Y ascribed to the interior nodes only. The results of the simulation are shown in Fig.7.7 (real and imaginary parts).

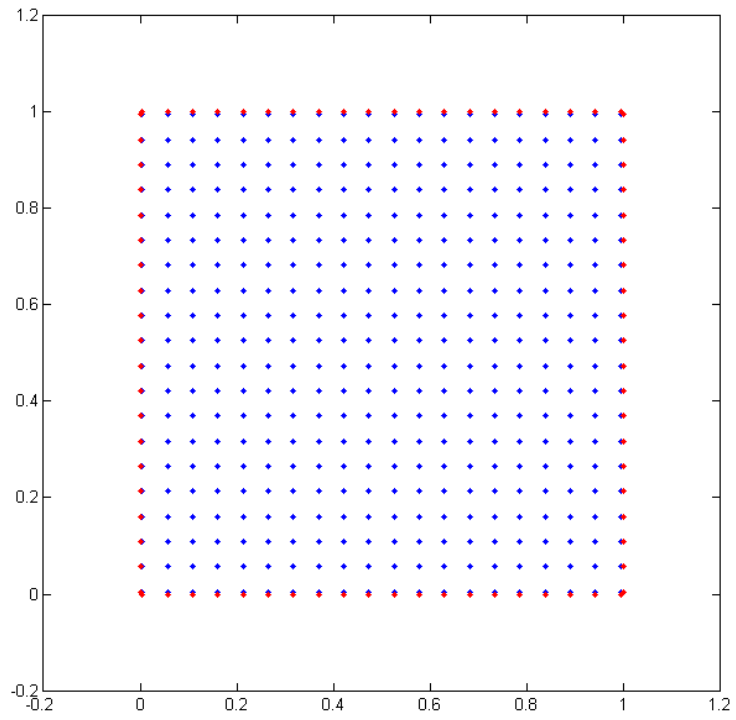


Fig.7.4. Nodes spread throughout the computational domain $\bar{\Omega}$.

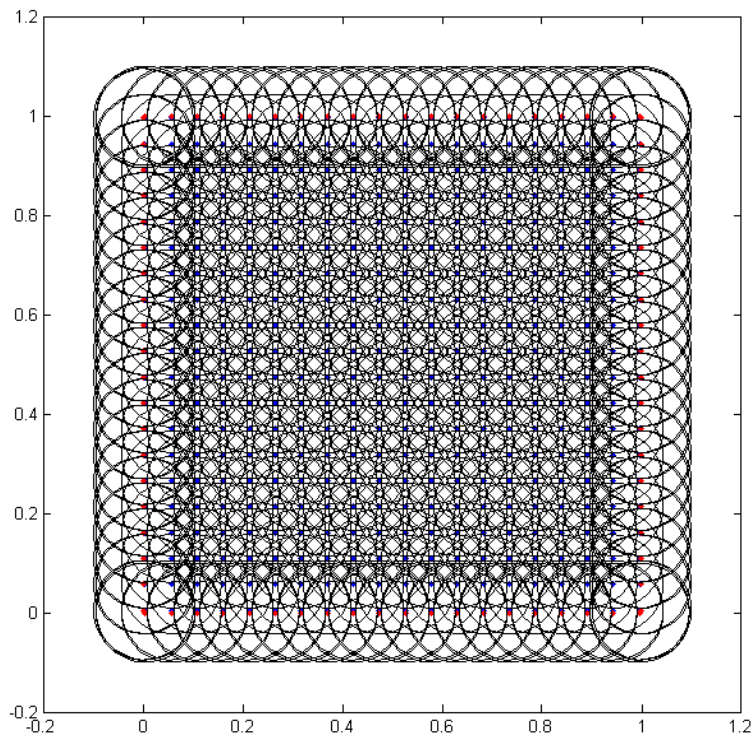


Fig.7.5. The domain covered by the circular influence domains Λ .

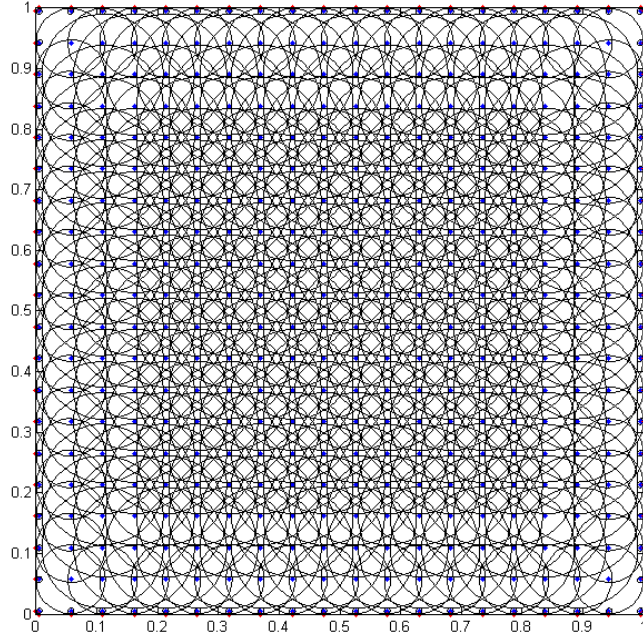


Fig.7.6. A collection of test domains Y (ascribed to the interior nodes only).

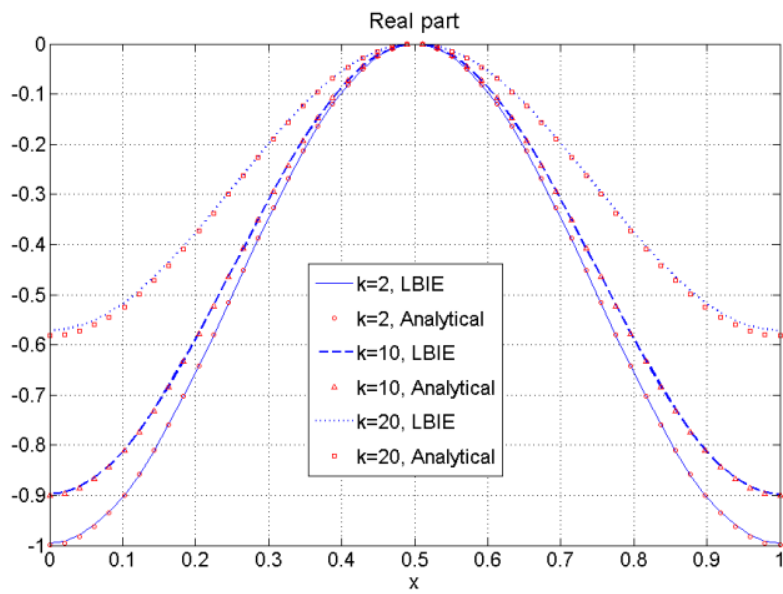


Fig.7.7.(a). Real part of the solution to NLS at 3 time steps (out of 20) along the line $x + y = 1$. 285 nodes have been scattered throughout Ω .

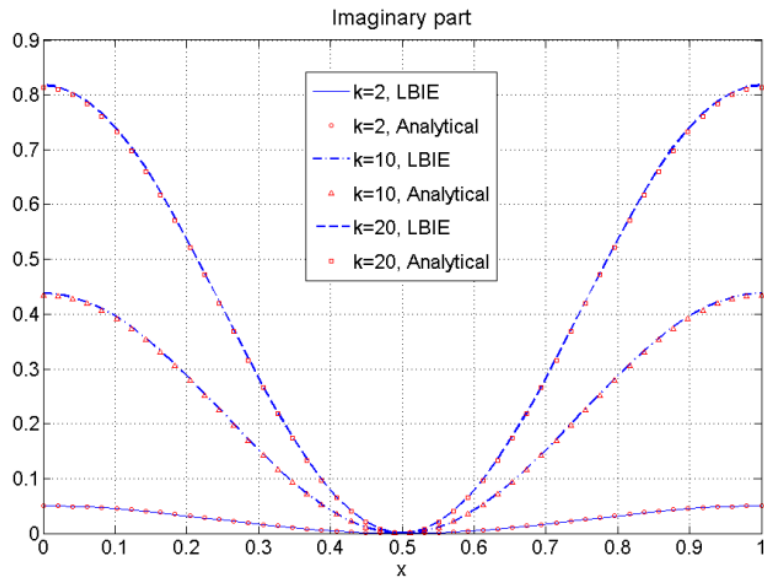


Fig.7.7.(b) Imaginary part of the solution to NLS at 3 time steps (out of 20) along the line $x + y = 1$. 285 nodes have been scattered throughout Ω .

Concluding Remarks

This chapter focused on applications of MLPG to some problems in quantum mechanics. The same ideas from earlier chapters have been successfully employed here. The collocation procedure developed in Chapter 5 is an excellent tool in the solution of three-dimensional Schrödinger's equation, and the scheme we devised for constructing periodic shape functions for photonic crystals is able to be extended to three dimensions with ease. The novelty is the treatment of time-dependent and nonlinear problems which, as these preliminary studies make clear, could also be solved by MLPG4/LBIE. The solution did not deviate from the analytical results as the time steps evolved. It therefore shows that, at least for the example studied in Section 7.4, MLPG4/LBIE is stable. Further studies dealing with the stability and other ways of approaching the nonlinear term will be the theme for future works.

Chapter 8

Conclusions

8.1 Summary

This dissertation has fulfilled its purpose of demonstrating the applicability of meshfree methods to many problems relevant to electrical engineering. I sought to demonstrate with as much detail as possible how the methods work. The cost of such a job is reflected in rather long expositions, particularly in those relative to the construction of weak forms.

We began from the definition of differential equations, and from what a domain represents. From this point on, the whole idea (or philosophy) permeating the meshless methods is exposed in an instructive way, through an analogy with electrostatics (in which the charges are represented by the nodes, and the electrostatic potentials by the shape functions). Once the basics have been presented, the rest of the work is dedicated to the refinement of the ideas shown here in Chapter 2.

The construction of the shape functions is the theme of Chapter 3. The MLS approximation is dissected in a particularly incisive way, with pages and more pages showing the process behind the MLS shape functions. Despite the fact it could be seen as a black box procedure, much insight can be gained if one knows how these shape functions are calculated. Chapter 3 also makes a brief reference to the RPIM shape functions, since they are employed only once in the entire work.

Once the shape functions – basic components in the approximation of the fields – have been defined, the following pages proceeded in the application of these functions to the discretization of the integral equations arising in electromagnetic wave scattering. The results are very good, outperforming the method of moments (traditionally employed in this category of problems) in precision. Moreover, Chapter 4 discusses the main drawbacks from MLS in the construction of shape functions for ‘flat-sided’ objects. After much discussion, an extremely simple way of solving the problems from the MLS approach is presented by the end of the chapter.

Chapter 5, which deals with the development of MLPG applied to scattering problems, is the central point in this work. Different strategies for treating the imposition of boundary conditions are exposed here with detail. Particular attention is paid to the method of collocation, because of the ease with which it can be employed to effectively enforce boundary conditions.

Equipped with the experience of the previous chapters, one now proceeds to new areas of application of MLPG to three-dimensional problems (in which the collocation method once more reveals its force) and to eigenvalue problems coming from the analysis of photonic crystals and quantum mechanics. This material, which comprises the last two chapters, concludes the dissertation.

8.2 Future Work

The original intent of this work was to show how MLPG could be applied to problems in electromagnetic wave scattering. All the rest is a kind of ‘byproduct’ (an invaluable source of experience, by the way), that was obtained as one gradually advanced along the lines of the main theme. Many topics have been treated here for the first time, and particular attention has been paid to the detailed exposition of the methods. Such an approach led, as said earlier, to somehow long discussions and to deductions that at first sight could be deemed unnecessary. However, this was predicted from the outset; one of the intentions I had in producing this work is that it could also serve as some kind of reference, in which everything (or almost everything) I had explored concerning meshfree is collected.

Once the applicability of the meshless methods has been successfully demonstrated, the next step is the refinement of these methods. Results concerning errors, convergence rates, and above all, extensive comparisons with finite element methods, must be addressed in future works. The frontier has been opened, and now one can see at a glance many themes to be approached, like:

- Problems involving vector quantities;
- Non-linear problems (mainly those related to the non-linearity of certain photonic crystals);
- Different ways of solving time-dependent problems;
- The use of PML’s (Perfectly Matched Layers) instead of boundary radiation conditions (RBC’s);
- More efficient schemes in the numerical integration of weak forms (fundamental in large problems, dealing with hundreds of thousands of nodes);
- A more rigorous mathematical treatment (detailed description of the function spaces and operators appearing in meshless methods). That would inevitably lead to works more mathematical in character.

The future of meshfree methods in electrical engineering seems to be promising. In view of the huge area that still needs to be explored, the actual state of affairs indicates that the next years will bring a mouthful of pleasant surprises.

Bibliography

- [Atluri and Shen, 2002] S. Atluri and S. Shen, “The Meshless Local Petrov-Galerkin Method: A simple & less-costly alternative to the finite-element and boundary element methods”, *CMES*, vol. 3, no 1, pp. 11-51, 2002.
- [Balanis, 1989] C. Balanis, *Advanced Engineering Electromagnetics*, John Wiley & Sons, 1989.
- [Bottauscio *et al.*, 2006] O. Bottauscio, M. Chiampi, and A. Manzin, “Element-free Galerkin method in eddy-current problems with ferromagnetic media”, *IEEE Trans. Magn.*, vol. 42, no 5, pp. 1577-1584, 2006.
- [Brezis and Browder, 1998] Haïm Brezis and Felix Browder, “Partial Differential Equations in the 20th Century”, *Advances in Mathematics*, v.135, pp. 76-144.
- [Chang and Mei, 1976] S. K. Chang and K. K. Mei, “Application of the Unimoment Method to Electromagnetic Scattering of Dielectric Cylinders”, *IEEE Transactions on Antennas and Propagation*, vol. AP-24, no 1, 99. 35-42, 1976.
- [Cingoski *et al.*, 1998] V. Cingoski, N. Miyamoto and H. Yamashita, “Element-Free Galerkin Method for Electromagnetic Field Computations”, *IEEE Trans. Magn.*, vol. 34, no 5, pp. 3236-3239, 1998.
- [Dehghan and Mirzaei, 2008] M. Dehghan and D. Mirzaei, “The Meshless Local Petrov-Galerkin (MLPG) method for the generalized two-dimensional nonlinear Schrödinger equation”, *Engineering Analysis with Boundary Elements*, v. 32, pp. 747-756, 2008.
- [Duffy, 2001] D. G. Duffy, *Green's Functions with Applications*. Chapman & Hall/CRC, 2001.
- [Fonseca *et al.*, 2008] A. Fonseca, S. Viana, E. Silva and R. Mesquita, “Imposing boundary conditions in the meshless local Petrov-Galerkin method”, *IET Science Measurement & Technology*, v. 2, p. 387, 2008.
- [Harrington, 1968] Roger F. Harrington, *Field Computation by Moment Methods*, Macmillan, New York, 1968.
- [Harrington, 2001] Roger F. Harrington, *Time-Harmonic Electromagnetic Fields*, IEEE Press Series on Electromagnetic Wave Theory, IEEE Press Classic Reissue 2001, Wiley-Interscience, John Wiley & Sons, Inc.
- [Jackson, 1998] John D. Jackson, *Classical Electrodynamics*, 3rd Edition, Wiley, 1998.
- [Jin, 1993] Jianming Jin, *The Finite Element Method in Electromagnetics*, John Wiley & Sons, 1993.

- [Joannopoulos *et al.*, 2008] J. D. Joannopoulos, S.G. Johnson, J. N. Winn and R. D. Meade, *Photonic Crystals: Molding the Flow of Light*, Princeton University Press, 2008.
- [Jun *et al.*, 2003] Sukky Jun, Young-Sam Cho, and Seyoung Im, “Moving least-square method for the band-structure calculation of 2D photonic crystals”, *Optics Express*, vol 11, no 6, pp. 541-551, 2003.
- [Jun, 2004] S. Jun, “Meshfree implementation for the real-space electronic-structure calculation of crystalline solids”, *International Journal for Numerical Methods in Engineering*, v. 59, pp. 1909-1923, 2004.
- [Kalogiratou *et al.*, 2005] Z. Kalogiratou, T. Monovasilis and T. Simos, “Numerical solution of the two-dimensional time independent Schrödinger equation with Numerov-type methods”, *Journal of Mathematical Chemistry*, vol. 37, no. 3, pp. 271-279, 2005.
- [Li *et al.*, 2003] Q. Li, S. Shen, Z. Han, and S. Atluri, “Application of Meshless Petrov-Galerkin (MLPG) to Problems with Singularities, and Material Discontinuities, in 3-D Elasticity”, *CMES*, vol. 4, no 5, pp. 571-585, 2003.
- [Liu, 2003] G. R. Liu, *Mesh Free Methods: Moving Beyond the Finite Element Method*. CRC Press, 2003.
- [Manzin and Bottauscio, 2008] A. Manzin, and O. Bottauscio, “Element-free Galerkin method for the analysis of electromagnetic-wave scattering”, *IEEE Trans. Magn.*, vol. 44, no 6, pp. 1366-1369, 2008.
- [Maréchal, 1998] Y. Maréchal, “Some Meshless Methods for Electromagnetic Field Computations”, *IEEE Trans. Magn.*, vol. 34, no 5, pp. 3351-3354, 1998.
- [Parreira *et al.*, 2006] G. Parreira, E. Silva, A. Fonseca, and R. Mesquita, “The Element-free Galerkin Method in 3-Dimensional Electromagnetic Problems”, *IEEE Trans. Magn.*, vol. 42, no. 4, pp. 711-714, 2006.
- [Parreira² *et al.*, 2006] G. Parreira, A. Fonseca, A. Lisboa, E. Silva, and R. Mesquita, “Efficient Algorithms and Data Structures for Element-Free Galerkin Method”, *IEEE Trans. Magn.*, vol. 42, no 4, pp. 659-662, 2006.
- [Peng and Cheng, 2009] Peng M, Cheng Y. “A boundary element-free method (BEFM) for two-dimensional potential problems”, *Engineering Analysis with Boundary Elements*, vol. 33, no 1, pp. 77-82, 2009.
- [Peterson *et al.*, 1998] A. Peterson, S. Ray, and R. Mittra, *Computational Methods for Electromagnetics*, IEEE Press, 1998.
- [Philips, 2003] A. C. Philips, *Introduction to Quantum Mechanics*, John Wiley and Sons, 2003.
- [Rothwell and Cloud, 2001] Edward J. Rothwell and Michael J. Cloud, *Electromagnetics*, CRC Press, 2001.

- [Shankar, 1994] R. Shankar, *Principles of Quantum Mechanics*, 2nd Edition, Kluwer Academic/Plenum Publishers, 1994.
- [Skorobogaty and Yang, 2009] M. Skorobogaty and J. Yang, *Fundamentals of Photonic Crystal Guiding*, Cambridge University Press, 2009.
- [Soares, 2009] D. Soares Jr., “Numerical Modeling of Electromagnetic Wave Propagation by Meshless Local Petrov-Galerkin Formulations”, *CMES*, vol. 50, no. 2, pp. 97-114, 2009.
- [Tsukerman, 2005] I. Tsukerman, “Electromagnetic Applications of a New Finite Difference Calculus”, *IEEE Transactions on Magnetics*, vol. 41, no 7, pp. 2206 – 2225, July 2005.
- [Tsukerman, 2008] I. Tsukerman, *Computational Methods for Nanoscale Applications*, Nanostructure Science and Technology Series, Springer, 2008.
- [Viana and Mesquita, 1999] S. A. Viana and R. C. Mesquita, “Moving Least Square Reproducing Kernel Method for Electromagnetic Field Computation”, *IEEE Trans. Magn.*, vol. 35, no 3, pp. 1372 – 1375, 1999.
- [Yavari *et al.*, 2001] A. Yavari, A. Kaveh, S. Sarkani and H. Bondarabady, “Topological aspects of meshless methods and nodal ordering for meshless discretizations”, *International Journal for Numerical Methods in Engineering*, v.52, pp.921-938, 2001.
- [Yu and Chen, 2009] Y. Yu and Z. Chen, “A 3D Radial Point Interpolation Method for Meshless Time-Domain Modeling”, *IEEE Trans. Microw. Theory Tech.*, vol. 57, no 8, pp. 2015-2020, August 2009.
- [Yu and Chen, 2010] Y. Yu and Z. Chen, “Towards the Development of an Unconditionally Stable Time-Domain Meshless Method”, *IEEE Trans. Microw. Theory Tech.*, vol. 58, no 3, pp. 578-586, March 2010.
- [Zettili, 2009] N. Zettili, *Quantum Mechanics – Concepts and Applications*, John Wiley & Sons, 2009.